ЖУРНАЛ
ПРИКЛАДНОЙ ХИМИИ

Vol. 31 No. 4

April 1958

JOURNAL OF
APPLIED CHEMISTRY
OF THE USSR

(ZHURNAL PRIKLADNOI KHIMII)

IN ENGLISH TRANSLATION

CONSULTANTS BUREAU, INC.

Chemistry Collection No. 2

SOVIET RESEARCH IN

GLASS and CERAMICS

(1949-1955)

One hundred and forty six reports, in complete English translation, with all tabular material and diagrams integral with the text. Selection and Preface by W. G. Lawrence, Chmn., Dept. of Ceramic Research, State University of New York College of Ceramics at Alfred University.

The complete collection.....$150.00

The one hundred and forty six reports included in this collection originally appeared in the Soviet Journals of General and Applied Chemistry and the Bulletin of the Academy of Sciences of the USSR, beginning with 1949. The collection comprises over 900 pages, more than 400,000 words of recent research on glass and ceramics by Soviet scientists, in complete English translation.

The Collection is divided into sections, which may be purchased separately, as follows:

Basic Science: (70 reports)	$90.00
Glass, glazes and enamels (32 reports)	40.00
Refractories (12 reports)	20.00
Cements, limes and plasters (28 reports)	35.00
Miscellaneous (4 reports)	7.50

C/b

CONSULTANTS BUREAU, INC.

227 W. 17th St., NEW YORK 11, N. Y.

Vol. 31 No. 4

April 1958

JOURNAL OF
APPLIED CHEMISTRY
OF THE USSR

(ZHURNAL PRIKLADNOI KHIMII)

A publication of the Academy of Sciences of the USSR

IN ENGLISH TRANSLATION

Year and issue of first translation:
vol. 23, no. 1 January 1950

	U. S. and Canada	*Foreign*
Annual subscription	*$60.00*	*$65.00*
Annual subscription for libraries of non-profit academic institutions	*20.00*	*25.00*
Single issue	*7.50*	*7.50*

Printed in the United States

JOURNAL OF APPLIED CHEMISTRY OF THE USSR

Volume 31, Number 4 April 1958

CONTENTS

CONTENTS (continued)

ALEKSEI ALEKSANDROVICH VANSHEIDT

January 8, 1958 marked the 70th birthday and the completion of 50 years of scientific and teaching activity of Doctor of Chemical Sciences, Professor Aleksei Aleksandrovich Vansheidt, one of the most eminent Soviet scientists in the fields of organic and polymer chemistry.

A.A. Vansheidt was born in Batumi in 1888. He received his higher education in the University of Peterburg, where he graduated in 1910 in the Faculty of Chemistry; he was a pupil of Academician A.E. Favorskii and of Professor of the University of Strassburg J. Thiele. Up to 1930 Vansheidt worked as Assistant Professor in the First Leningrad Medical Institute, where he performed a series of researches in the field of naphtho derivatives of fluorene, which led to the discovery of new relationships between structure and color, and to the discovery of new reactions, including the autooxidation of fluorene derivatives. For this work Vansheidt was awarded the prize "For Best Research in Chemistry" by the Committee of Chemical Industry of the USSR in 1930.

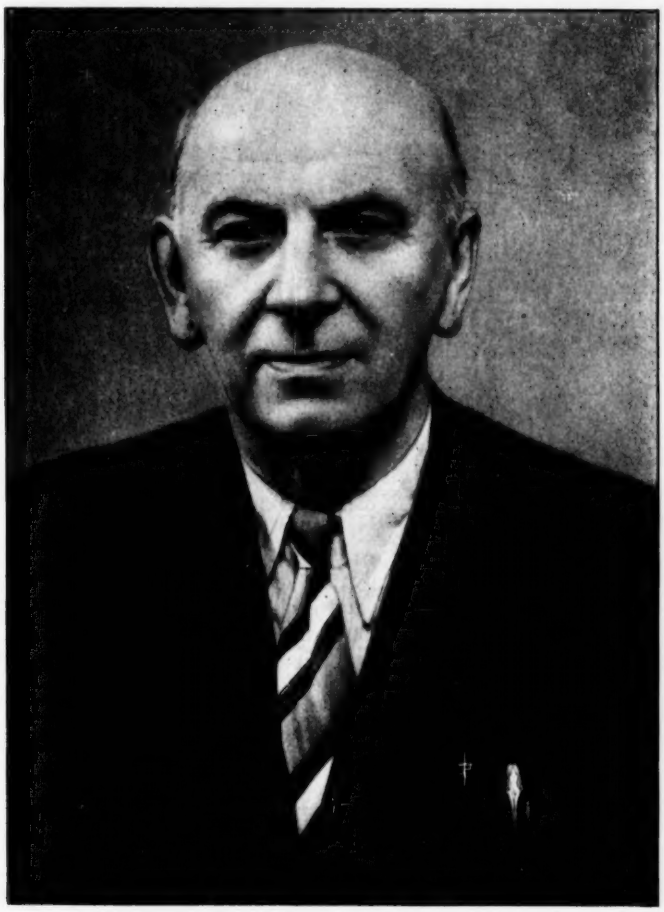

A.A. Vansheidt

Since 1931 Vansheidt has been Professor of the Chair of Plastics Technology of the Lensoviet Technological Institute, Leningrad. Here he is presenting a course of polymer chemistry which he was the first to give in the Soviet Union. Between 1930 and 1941 he also worked in the State Institute of High Pressures and in the Plastics Institute.

Since 1949, while continuing his work in the Lensoviet Technological Institute, Leningrad, he has been the head of the laboratory of polycondensation processes in the Institute of High Polymers (IVS) of the Academy of Sciences USSR.

Prominent among his work over many years are his classic researches into the mechanism of formation and the structure of phenol-aldehyde resins.

The process developed by him jointly with E.M. Kaganova in the State Institute of High Pressures for the production of ethyl alcohol by direct hydration of ethylene without expenditure of sulfuric acid is of great economic importance, The industrial adoption of this method had a significant economic effect and made it possible to release large amounts of grain for direct use. Vansheidt and Kaganova, and the workers of the industry who took part in the development of the process, were awarded a First-Class Stalin Prize for this work in 1952. Vansheidt's work in the field of urea- and melamine-formaldehyde resins led to the development of a very efficient technological process for the production of amino plastics, which has been utilized in our industry for many years.

During recent years Vansheidt, in his work in the IVS of the Academy of Sciences USSR, has prepared a number of high-quality ion exchangers; as the result of joint work with Prof. S.E. Bresler and G.V. Samsonov, these resins have been adopted in the antibiotics industry and are used with great success for the isolation and purification of streptomycin and other substances. Among other work carried out by Vansheidt at different stages of his activity, mention must be made of his research into methods of synthesis and polymerization of styrene, polymerization of vinyl formate, kinetics and mechanism of polymerization and copolymerization processes, synthesis of unsaturated polyesters, improvement of the heat and light resistance of polyvinyl chloride, and many others. Vansheidt's published papers number a hundred.

A.A. Vansheidt is also an outstanding teacher, who has trained many hundreds of engineers and research workers employed in industry and in the scientific institutions of our country. The scientific and practical activity of A.A. Vansheidt has been highly valued by the party and government; he has been awarded the Order of Lenin and various medals.

The workers of science and industry wish him, on his seventieth birthday, many years of life, health, and further fruitful activity devoted to the work of Soviet science for the good of our country.

SOME DATA ON THE DESORPTION OF A LIQUID FROM THE SURFACE OF A FLUIDIZED LAYER

Ia. Tsiborovskii and A. Seletskii

Chair of Processes and Equipment of Chemical Technology, the Warsaw Polytechnic Institute

The desorption of liquids from the surfaces of fluidized layers has not been discussed in the literature (apart from brief descriptions in certain patents [1]).

It seems likely that investigators devoted their attention primarily to the simplest processes, not complicated by subsidiary or secondary effects. Therefore, despite many years of research, many fundamental problems of heat and mass transfer in fluidized layers still remain insufficiently studied.

The desorption of liquid from the surface of a fluidized layer is much more complex than the periodic process of mass transfer in a fluidized layer, which is the process usually studied. The simultaneous continuous humidification and drying of the grains in the fluidized material are superposed on each other, and complicate the mechanism of the process.

In periodic drying or humidification of a fluidized layer, we are dealing mainly with a homogeneous material which is in dynamic equilibrium with a gas stream in a definite thermodynamic state.

When a liquid evaporates from the surface of a fluidized layer, simultaneously with its humidification, the parameters measured in practice, such as the moisture content and temperature, are average values for the different grains of the layer.

In such cases it may be assumed that the entire surface of some of the grains (directly after contact with the moistening liquid) is moist, and their temperature is equal or close to the reading of the wet-bulb thermometer in the gas stream. The evaporation of liquid from the surface of such grains is analogous to the drying process in the first stage (period of constant rate of drying). Other grains, with moisture contents below the critical value, may have temperatures above the wet-bulb reading and evaporation of liquid from their surface corresponds to the second stage (period of decreasing rate of drying). The temperatures and moisture contents of such grains differ, and depend mainly on the time which elapses from the end of the period of constant drying rate. In a third group of grains the temperature and moisture content may correspond to equilibrium relative to the gas stream.

Because of the different states of the individual grains in a fluidized layer, heat and mass transfer may take place between them, complicating the whole effect still further.

The purpose of the present investigation was to make a preliminary study of the course of evaporation of a liquid from the surface of a fluidized layer. The published results must be regarded as approximate only, and as presenting a general outline of the process. The results refer to the effects of spraying with water a fluidized layer of granular material through which air was blown at temperatures between 91 and 162° at gravimetric rates from 1760 to 2650 kg/m^2·hour. The rate of spraying of the layer with water was varied from 14 to 208 kg/m^2·hour, and in some instances reached 300 kg/m^2·hour. The layer, 10 cm thick, consisted of porous ceramic grains of equivalent diameter 0.71 mm, with shape factor 1.92. A column 7 cm in diameter was used for the experiments. Qualitative observations were made on the behavior of layers consisting of ceramic grains with reduced diameters of 0.55 and 0.346 mm, and also of sand grains 0.45 mm in diameter with shape factor 1.15.

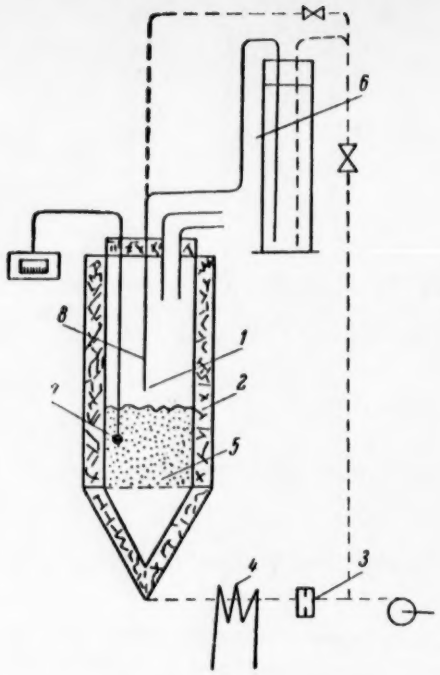

Fig. 1. Diagram of experimental unit. Explanation in text.

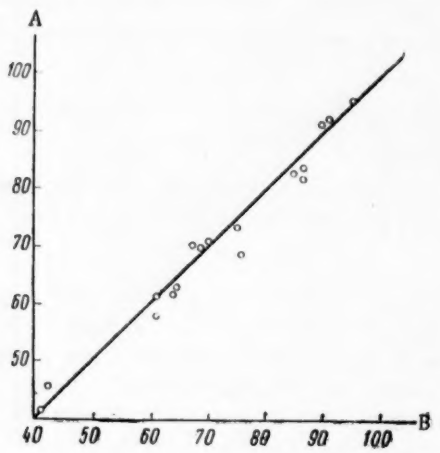

Fig. 2. Correlation of calculated and measured temperatures in the fluidized layer. Temperature (°C): A) calculated; B) measured.

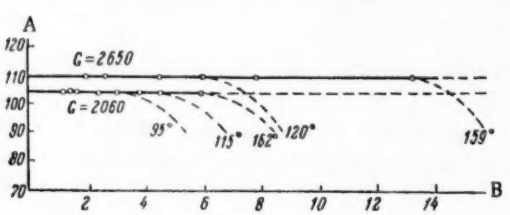

Fig. 3. Variation of the pressure Δp with the water rate L in the column. A) Δp (in mm H_2O); B) L (g/minute).

Apparatus and Method

The main part of the experimental unit was the glass column 1 (Figure 1). A porous glass plate was fixed in its lower end. It was surrounded by a layer of cork for heat insulation. A slit 2 cut in the cork, normally closed by a cork insert, was used for observation of the layer.

After passing through the calibrated diaphragm meter 3 and the electric heater 4, compressed air passed through the porous plate 5 into the column, fluidized the layer of porous material, and emerged through the top opening of the column.

A jet for spraying the grains passed through the same opening. Water entered the jet from the measuring cylinder 6. The grains were moistened either by means of a spray of water injected from the cylinder, or by drops of water at constant pressure. The thermocouple 7 was used to measure the temperature in the layer. To compensate for heat losses (which may be considerable, despite the heat insulation of the column) a procedure similar to that described by Hamsley and Johanson [2] was used for calculation of the heat balance; the initial temperature of the incoming air was the same as the temperature which became established when the air passed through a dry layer. The difference in the balance calculated by this method did not exceed 5%.

The spraying method and the grain size of the fluidized material were determined after many visual observations. It was found that the use of a spray is essential if the fluidized layer consists of fine nonporous grains (for example, sand with grains 0.4 mm and smaller) at low air rates and moderate temperature. In such cases moistening of the layer with drops of normal size caused agglomeration of the grains at the points of contact of the drops with the layer. The agglomerates fell to the bottom of the column and took no part on the motion of the layer.

Agglomeration of the particles did not occur in the fluidization of layers consisting of porous ceramic grains over 0.35 mm in diameter. When air was passed at moderate rates and low temperature through fractions of small grain size, a few agglomerates were formed, but these disintegrated rapidly without settling to the bottom of the column.

If a spray is used, it is necessary to take into account the influence of the additional air introduced for spraying the water. For steady operation of the jet, the air velocity must be high. The air stream formed vortices on the surface of the layer and disturbed the hydrodynamic conditions in the column. It was therefore found that it is more conveneint from the experi-

mental standpoint to fluidize layers consisting of relatively large ceramic grains, and to wet their surface by drops of water emerging from the capillary 8, situated in the center of the column above the surface of the layer.

It may be noted that the course of the experiment was not affected if the opening of the capillary was within the layer. However, this method was inconvenient owing to the frequent clogging of the capillary.

The temperature was measured by means of a thermocouple, the junction of which was 5 cm from the bottom of the column and half way between the vertical axis and the wall, in the constant-temperature region.

In agreement with the results of our experiments and those of other workers, it was assumed that the temperature of the exit gas was equal to the grain temperature in the fluidized layer as measured by the thermocouple. This assumption is justified by the fact that the temperature of the gas calculated from the thermal and material balance coincides, within the limits of experimental error, with the measured temperature of the fluidized layer (Figure 2).

Preliminary experiments were performed in order to study the behavior of a fluidized layer of granular material, usually heated to above 100°, when moistened with different amounts of water at a constant gas rate and constant gas temperature.

The motion of the particles in the fluidized layer is not visibly influenced when a layer consisting of porous ceramic grains is moistened by means of water drops at moderate rates.

However, the layer "becomes heavy" with increase of the water rate, the intensity of circulation of the individual particles decreases, and at a definite water rate "dead spaces" form, small at first, but gradually increasing in size. The grains are motionless and agglomerated in these spaces. At the same time one or two channels are formed in the layer, through which the gas passes. Finally, the motion of the layer ceases, and all the gas escapes through the channels. Sometimes (when fine grains were used) the whole layer of material was ejected in the form of a plug.

The pressure on the floor of the column remained unchanged with variations of the water rate up to the moment when the motion of the layer ceased. The pressure then fell sharply. This decrease was not constant, but depended on the size of the channels formed, and was not reproducible (Figure 3).

When the column contained sand, the results were the same at first. However, "flooding" usually occurred suddenly, with a short transitional period, and very often the whole layer of sand was ejected.

The moisture content of the layer of the "flooding" point varied, and depended mainly on the parameters of the gas stream. For limiting cases, at gravimetric gas rate G equal to 3500 kg/m^2·hour, t = 128°, and at the critical water rate, the moisture content of sand with grain size (equivalent diameter) d_e = 0.35 mm was 1.65%. At G = 2650 kg/m^2·hour and t = 129°, ceramic grains of d_e = 0.71 mm contained 2.78% moisture at the "flooding" point. However, the moisture-content data showed poor reproducibility, and more precise relationships could not be established.

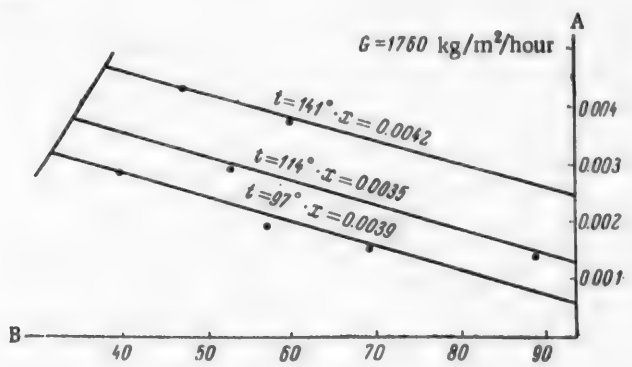

Fig. 4. Humidity diagram for air: A) x (kg/kg); B) temperature (°C).

The temperature of the layer, equal (by our assumption) to the temperature of the exit gas, decreased with increasing water rate, as the temperature of the exit gas decreased in accordance with the air humidity diagram.

A general characteristic feature of the desorption (evaporation) region studied is the analogy of the course of the process with the humidity diagram for air, up to the point when fluidization ceases. This point – "flooding" – is always reached at 100% saturation.

Figure 4 is a portion of the humidity diagram for air (after Garber), on which are plotted the points for the state of the air in one series of experiments (Table 1). The temperatures of the moist air simultaneously determine the corresponding temperatures established in the layer under given process conditions.

It follows from Figure 4 and Table 1 that, as the water rate increases, the temperature of the gas and the equal temperature of the fluidized layer move to the left along the adiabatic line which determines the initial state of the air.

TABLE 1

$G = 1760$ kg/m^2·hour

Initial state of the air		Water rate	State of the exit air	
t (°C)	x (kg/kg)	L (g/min)	t (°C)	x (kg/kg)
97	0.0039	1.25	69.5	0.015
97	0.0039	1.70	57	0.019
97	0.0039	2.70	40	0.028
114	0.0035	1.80	70	0.019
114.5	0.0035	2.66	53	0.028
114.5	0.0035	1.13	88.5	0.014
141	0.0042	3.40	60	0.037
141	0.0042	4.40	50	0.043

The limits of the water and evaporation rates are reached at the flooding point, when fluidization ceases.

Since there are at present no objective criteria whereby the instant at which fluidization ends may be determined, it was necessary to determine it visually. Of course, this introduces a subjective element into the results of the determinations, and is the probable reason for the considerable scatter of the experimental points in Figure 5, which represents the variations of the maximum water rate (at which fluidization ceases) with the initial temperature of the air and with its gravimetric rate.

Despite the extensive scattering of the experimental points, the general character of the dependence of the limiting water rate with the temperature and feed rate of the gas is quite distinct.

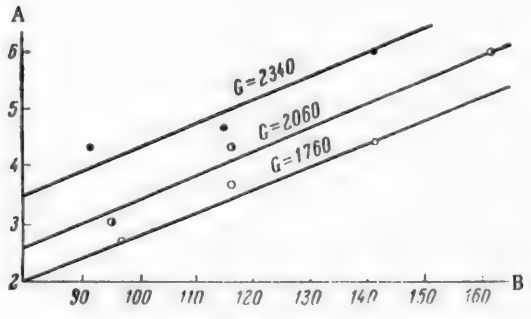

Fig. 5. Variations of the maximum water rate with the initial temperature and the gravimetric rate of the air. A) L_{max} (g/min); B) temperature (°C).

The limiting water rate depends also on the initial humidity of the gas. Since the humidity of the gas stream varied little during the experiments, the influence of this parameter is not revealed in Figure 5. For practical utilization of evaporation from the surface of a fluidized layer, the technologist must be able to calculate the limiting rates of water feed and evaporation under various hydrodynamic and thermodynamic conditions, because if these rates are exceeded the course of the process is inevitably disturbed owing to cessation of fluidization.

It may be concluded from the foregoing that the parameters of the process at water rates below the limiting value can be calculated from the thermal and material balance equations. The limiting water rate for definite gas flow parameters can be calculated if the

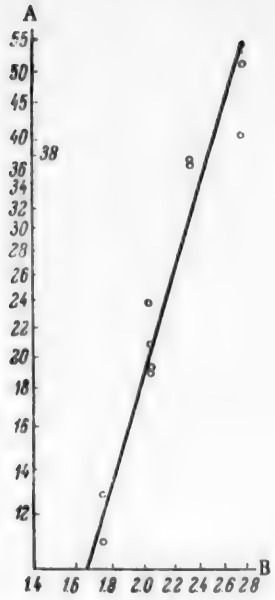

Fig. 6. Experimental coefficients of mass transfer at different air rates. A) $k_g a$ (kg/m³ · mm Hg · hour); B) $G \cdot 10^{-3}$ (kg/m² · hour).

volumetric coefficient of mass transfer at the instant when fluidization ceases is known.

By the fundamental laws of mass transfer, the amount of evaporating water at the point of cessation of fluidization can be found from the equation

$$L_{max} \cdot 60 = (k_g a)_{L_{max}} v \Delta p, \qquad (1)$$

where Δp is the reduced difference of water vapor partial pressures (nominally taken as the logarithmic mean difference between the vapor pressures at the beginning and end of the process)•

$$\Delta p = \frac{p_f - p_1}{\ln \frac{p_{sat} - p_1}{p_{sat} - p_f}}$$

This method of calculating the logarithmic pressure difference is analogous to the methods used in thermal calculations. Calculation of the reduced pressure difference as the integral mean is not free from arbitrary factors and, moreover, involves considerable experimental difficulties.

If the gravimetric feed rate of the dry air is denoted by W, the amount of moisture taken away with it can be determined from the balance expression

$$L_{max} = \frac{18W}{29}\left(\frac{p_f}{P - p_f} - \frac{p_1}{P - p_1}\right), \qquad (2)$$

where 18 and 29 represent the molecular weights of water and air respectively.

Since $p_1 < p_f \ll P$, the preceding expression can be written

$$L_{max} = \frac{18}{29}\frac{W}{P}(p_f - p_1). \qquad (3)$$

From the equation for the heat balance of the process we have

$$L_{max} r = W c_x (t_1 - t_{sat}). \qquad (4)$$

If a high degree of accuracy is not required, it may be assumed that $c_x \cong c_p$, and then

$$L_{max} r = W c_p (t_1 - t_{sat}). \qquad (5)$$

Finally, from the Clausius-Clapeyron equation in the form

•A is a constant ($A = 18CW/R$); B is an exponent $B = \frac{29}{18 \cdot 60} \times \frac{v(k_g a)_{L_{max}} P}{W}$; C is the integration constant; d_e is the equivalent grain diameter (in mm); e is the base of natural logarithms; c_p is the heat capacity of air (kcal/kg · °C); c_x is the heat capacity of moist air (kcal/kg · °C); G is the gravimetric gas rate (kg/m² · · hour); x is the moisture content of the air (kg/kg); $(k_g a)_{L_{max}}$ is the coefficient of mass transfer at the limiting evaporation rate (kg/m³ · mm Hg · hour); L is the water rate (kg/min); L_{max} is the limiting water rate (kg/min); p_1 is the initial partial pressure of water vapor in the gas stream (mm Hg); p_f is the final partial pressure of water vapor in the exit gas (mm Hg); p_{sat} is the saturated water-vapor pressure at the surface of the grains in the fluidized layer (mm Hg); Δp_{av} is the reduced pressure difference (mm Hg); P is the atmospheric pressure (mm Hg); r is the latent heat of evaporation (kcal/kg); R is the gas constant (kcal/mole · °K); t_{sat} is the temperature of the fluidized layer (°C); t_1 is the initial air temperature (°C); T is the temperature (°K); T_1 is the initial air temperature (°K); v is the volume of the fluidized layer (m³); and W is the gravimetric air rate (kg/min).

$$dp/dT = 18rp/RT^2$$

we have, after integration over a narrow temperature range, with constant heat of evaporation r

$$\ln p_{sat} = -\frac{A}{t_{sat} + 273} + C. \tag{6}$$

The constants A and C are easily calculated for a definite range of temperature. For example, for the range $40° < t < 80°C$, assuming that $r = 562$ kcal/kg and $R = 1.98$ kcal/mole · °K, we find $A = 5100$ and $C = 20.25$.

By solving the system of Equations (1), (3), (5) and (6), we can find the limiting water rate L_{max}. This solution gives

$$C - \frac{A}{T_1 - \frac{L_{max}r}{Wc_p}} = \ln\left(p_1 - \frac{29}{18} \cdot \frac{L_{max}P}{W} \cdot \frac{e^B}{1 - e^B}\right), \tag{7}$$

where the index $B = \frac{29}{60 \cdot 18} \cdot \frac{v(k_g a)_{L_{max}} P}{W}$.

This equation is used to find L_{max} by the method of successive approximations, from the known parameters for the air stream and the limiting volume coefficients of mass transfer at the instant when fluidization ceases.

It is quite obvious that the limiting volume coefficients of mass transfer and their dependence on the air rate must be determined experimentally. The air rate varied over a narrow range. It was limited by the critical fluidization rate on the one hand, and by the grain velocity on the other. Equation (1) was used for calculation of the coefficients.

Despite the lack of an objective method for determination of the point at which fluidization ceases, the difference between the determinations does not exceed 25%, so that their practical use is admissible.

TABLE 2

Volume Coefficients of Mass Transfer at the Instant When Fluidization Ceases

t_1 (°C)	P_{sat} (mm Hg)	P_1 (mm Hg)	P_f (mm Hg)	$L_{max} \cdot 10^3$ (kg/min)	G (kg/m² · hr)	$(k_g a)_{L_{max}}$ (kg/m³ · mm Hg · hour)
120	52.4	5.2	44.0	5.95	2650	41.5
129	55.3	4.8	49.5	6.85	2650	52.0
91	42.2	8.0	35.0	4.3	2340	37.6
115	47.1	4.8	40.0	4.6	2340	36.4
115	50.2	4.2	40.0	4.6	2340	31.4
141	61.5	4.3	48.4	6.0	2340	31.0
116	58.3	5.4	45.0	4.4	2060	23.8
116	49.6	5.4	38.5	3.7	2060	19.2
94.5	42.2	4.9	31.4	2.95	2060	21.6
162	83.7	5.0	56.0	6.0	2060	19.0
97	55.3	4.7	32.5	2.7	1760	13.2
141	92.5	5.0	48.5	4.4	1760	11.0

The results of the experimental determinations of the limiting mass transfer coefficients are summarized in Table 2 and plotted in Figure 6. The plot of the points in logarithmic coordinates gives a straight line represented by the equation

$$(k_g a)_{L_{max}} = 5.3 \cdot 10^{-11} G^{3.5} \text{ kg/m}^3 \cdot \text{mm Hg} \cdot \text{hour}. \tag{8}$$

SUMMARY

1. The limit of the rate of water feed and evaporation from the surface of a fluidized layer is reached at the rate at which the granular layer ceases to be fluidized, owing to agglomeration of the particles.

2. The limiting water rate is a function of the thermodynamic state and the velocity of the gas stream.

3. The limiting volume coefficients of mass transfer are proportional to the gravimetric gas rate to the power 3.5.

4. Desorption (evaporation) of liquid from a moist fluidized granular material can be used as a simple method of air humidification (with great potentialities for acceleration of the process).

The evaporation rate attained in some instances, of the order of 200-300 kg of water per hour per square meter of column cross section, had not previously been reached in equipment for evaporation of water and humidification of air.

LITERATURE CITED

[1] U.S. Patent 2,579,944; German Patent 883,591.

[2] W.W. Hamsley and L.N. Johanson, Chem. Engr. Progr. 50, 7, 347 (1954).

[3] P.M. Heertjes, H.G.J. de Boer and A.H. de Haas van Dorsser, Chem. Eng. Sc. Genie Chim. 2, 3, 97 (1953).

[4] K.N. Kettenring, E.L. Manderfield and J.M. Smith, Chem. Eng. Progr. 46, 3, 139 (1950).

Received November 14, 1957

APPROXIMATE CALCULATION METHOD FOR BATCH-RECTIFICATION COLUMNS

Fu Tsziui-fu

Chair of Chemical Fuel Technology, Tientsin Polytechnic Institute

The previous communication [1] contained the principal equations for calculations of the average reflux ratio, the amount and average concentration of the distillate, and the duration of batch rectification at constant concentration of distillate or constant reflux ratio, and also gave the derivation of analytical equations used for calculations in cases when the distillate concentration is close to unity and the $y = f(x)$ equilibrium curve is a straight line. A critical examination of Kasatkin's methods of algebraic integration [2] was also given.

Despite the defects of Kasatkin's methods, some of his concepts can be used for approximate algebraic integration of the principal equations for ideal binary mixtures for cases in which the plate holdup can be neglected (if there is a sufficient number of plates in the column).

Since

$$R_{\min} = \frac{x_p - y}{y - x} \text{ and } R = \frac{x_p - y_0}{y_0 - x} ,$$

where R_{min} is the minimum reflux ratio, R is the operating reflux ratio, $\underline{y}$ is the equilibrium molar concentration of the more volatile component in the vapor over the mixture at concentration $\underline{x}$ in the still, $\underline{x}$ is the molar concentration of the more volatile component in the liquid phase in the still, y_0 is the ordinate corresponding to the abscissa $\underline{x}$ of the point at which the operating reflux ratio is equal to R, and x_p is the molar concentration of the distillate (all the above values are instantaneous), then with an infinite number of plates R is equal to R_{min} and y_0 is equal to $\underline{y}$.

In practice, although the number of plates is limited, when the number of plates reaches a certain value the lower end of the operating line is very close to the equilibrium curve. Within the limits of the calculation accuracy we can assume that $y_0 = y$, and thereby simplify the calculation. In this instance, the relationship between the instantaneous values of R, x_p, $\underline{x}$, and relative volatility α can be approximately represented as follows

$$R = \frac{x_p - [\alpha - (\alpha - 1)x_p]x}{x(\alpha - 1) - (\alpha - 1)x^2} . \quad (1)$$

Equation (1) is valid on the assumption that the instantaneous quantity of vapor ascending in the column is constant for any section of the column. The number of plates for which Equation (1) is valid depends on the limits of the values of α, R, and $\underline{x}$; this can be seen on examination of Figure 1 in the article by Rose [3].

It follows from Figure 1a that when $\alpha = 1.25$, $R = 1$ and $n > 5$, for $x = 0\text{-}1$, increase of the number of plates does not lead to any appreciable change of the concentration $\underline{x}$ of the liquid phase in the still, corresponding to a definite concentration x_p of the distillate. In other words, the lower end of the operating line in this case is very close to the equilibrium curve. Therefore, if $n > 5$, Equation (1) is sufficiently accurate.

Analogously, it follows from Figure 1b with $\alpha = 1.25$, $R = 19$ and $x = 0\text{-}1$, the relationships between x_p and $\underline{x}$ are almost the same for two cases: when $n = 50$, and $n = 100$. Equation (1) is also applicable if $n > 50$, and also, within the ranges $x = 0\text{-}0.15$ and $0.35\text{-}1$, when $n > 30$, and when $n > 20$, if $x = 0.6\text{-}1$.

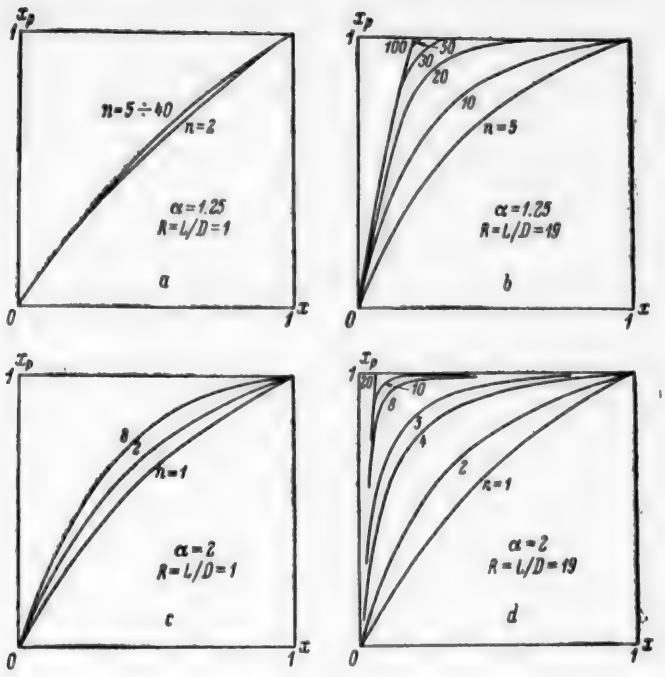

Fig. 1. Relationship between x_p and $\underline{x}$ (for different values of α, R and $\underline{n}$).

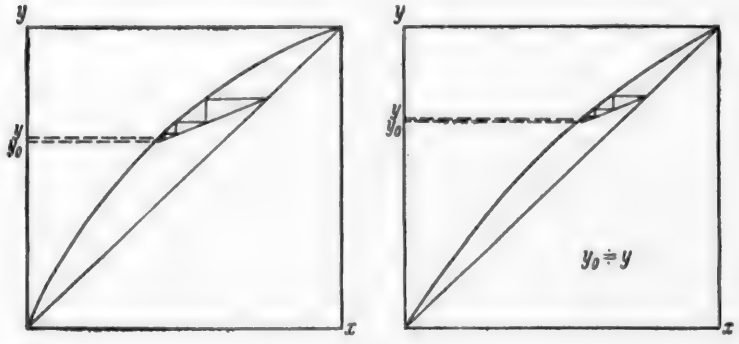

Fig. 2. Variations of y_0 and $\underline{y}$ with α (with constant values of $\underline{n}$ and R).

It follows that the smaller the value of R, the smaller is the number of plates at which Equation (1) is applicable.

Comparison of Figure 1c with Figure 1a shows that the number of plates $\underline{n}$ at which Equation (1) is applicable decreases with decreasing α.

When $\alpha = 1$, $y_0 = y$ with any number of plates. Figure 2 shows that y_0 approaches $\underline{y}$ as α decreases, while Figure 3 for $n = 4$ shows that y_0 approaches $\underline{y}$ with decrease of R.

Since R gradually increases to infinity in the course of distillation with constant distillate composition, if Equation (1) is used it is necessary to have a larger number of plates than in distillation at constant reflux ratio. However, Equation (1) may be applied both in calculations for distillation at constant reflux ratio, and for distillation with constant distillate composition (within appropriate limits of the concentration $\underline{x}$), as a small number of plates is required in either case.

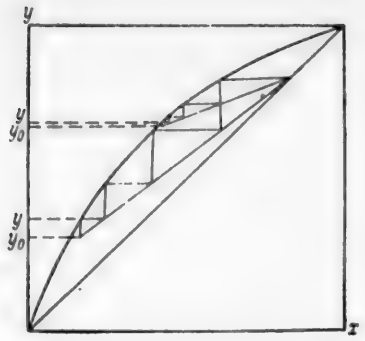

Fig. 3. Variations of y_0 and y with R (with constant values of n and α).

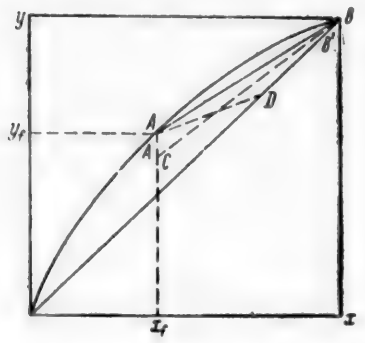

Fig. 4. Determination of the critical reflux ratio R_{cr}.

Calculation of the Rectification Process at Constant Reflux Ratio

In this case the Rayleigh equation [4] may be used to determine the amount of distillate

$$\ln \frac{F}{W} = \int_{x_w}^{x_f} \frac{dx}{x_p - x} \qquad (2)$$

in conjunction with the relationship

$$P = F - W,$$

where F is the amount of initial mixture (in kg-moles), W is the amount of residue in the still (in kg-moles), x_p is the distillate concentration (in mole fractions of the more volatile component), x_f is the concentration of the initial mixture (in mole fractions of the more volatile component), and x_w is the concentration of the residue (in mole fractions of the more volatile component).

Substitution of Equation (1) into (2) followed by integration gives

$$\ln \frac{F}{W} = \frac{1}{R+1}\left[\frac{1}{\alpha - 1} \ln \frac{x_f (1 - x_w)}{x_w (1 - x_f)} + \ln \frac{1 - x_w}{1 - x_f}\right], \qquad (3)$$

It should be noted that Equation (3) is the same as the Gilliland equation [5] for calculation of the minimum amount of vapor in rectification at constant R, although they are intended for different calculation purposes.

It follows from Equation (3) that, for the same values of x_f, x_w, n and R, F/W decreases when α increases, while the average concentration of the distillate $(x_p)_{av}$ increases. This means that mixtures of higher relative volatility are separated more easily. In other words, for the same values of x_f, x_w, n and α, F/W decreases and $(x_p)_{av}$ increases with increase of R.

It must be pointed out that when $R > R_{cr}$ (R_{cr} is the critical reflux ratio) Equation (3) cannot be used. Although in practice it is possible to operate at reflux ratios above R_{cr}, in such cases the lower end of the operating line is a long way from the equilibrium curve, and in such conditions Equation (1) is not applicable.

The value of R_{cr} can be determined graphically.

In Figure 4, y_f is the equilibrium concentration of the vapor phase over the initial mixture of concentration x_f; the coordinates of the point A are (x_f, y_f); the coordinates of the point B are (x = 1, y = 1); AB is a straight line. It is seen that if the slope of the operating line CB is greater than the slope of the equilibrium line AB, the lower end of the operating line is a long way from the equilibrium curve (while the upper end of the operating line is close to the equilibrium line if the number of plates is considerable).

If the slope of the operating line A'D is less than the slope of AB, the lower end of the operating line is very close to the equilibrium curve. We thus find the tangent of the angle of inclination of the line AB

$$m = \frac{R_{cr}}{R_{cr} + 1} = \frac{1 - y_f}{1 - x_f} = \frac{1 - \dfrac{\alpha x_f}{1 + (\alpha - 1) x_f}}{1 - x_f} = \frac{1}{1 + (\alpha - 1) x_f}.$$

Hence

$$R_{cr} = \frac{1}{(\alpha - 1) x_f} \qquad (4)$$

When the value of (F/W) has been calculated by means of Equation (3), we can calculate the average concentration of the distillate $(x_p)_{av}$ and the rectifiction time t from the following equations:

$$(x_p)_{av} = \frac{Fx_f - Wx_w}{F - W} = \frac{\frac{F}{W}x_f - x_w}{\frac{F}{W} - 1}, \tag{5}$$

$$t = \frac{(F - W)(R + 1)}{V}, \tag{6}$$

where V is the quantity of vapor ascending in the column, in kg-moles per unit time.

Calculation of the Rectification Process With Constant Concentration of the Distillate

The amount of distillate can be calculated by means of the material-balance equation for the rectification column.

From Equation (1) and the author's formula [1] for determination of the average reflux ratio R_{av} we have

$$R_{av} = \frac{(x_f - x_p)(x_p - x_w)}{x_f - x_w} \int_{x_f}^{x_p} \frac{Rdx}{(x_p - x)^2}, \tag{7}$$

where

$$\int \frac{Rdx}{(x_p - x)^2} = \int \frac{x_p - [\alpha - (\alpha - 1)x_p]x}{\frac{x(\alpha - 1) - (\alpha - 1)x^2}{(x_p - x)^2}} dx = \int \frac{x_p(1 - x) + \alpha x(x_p - 1)}{(x_p - x)^2(\alpha - 1)(1 - x)x} dx =$$

$$= \int \frac{x_p dx}{(x_p - x)^2(\alpha - 1)x} + \int \frac{\alpha(x_p - 1)}{(x_p - x)^2(\alpha - 1)(1 - x)} dx.$$

For the first term

$$\int \frac{x_p dx}{(x_p - x)^2(\alpha - 1)x} = \frac{1}{\alpha - 1}\left[\frac{1}{x_p - x} - \frac{1}{x_p}\ln\frac{x_p - x}{x}\right] + C.$$

For the second term we put $x_p - x = y$, then $-dx = dy$ and

$$\int \frac{\alpha(x_p - 1)\,dx}{(x_p - x)^2(\alpha - 1)(1 - x)} = \frac{\alpha(x_p - 1)}{\alpha - 1}\int \frac{-dy}{y^2(1 + y - x_p)} =$$

$$= \frac{-\alpha(x_p - 1)}{\alpha - 1}\left[-\frac{1}{(1 - x_p)y} + \frac{1}{(1 - x_p)^2}\ln\frac{1 - x_p + y}{y}\right] + C =$$

$$= \frac{\alpha(x_p - 1)}{\alpha - 1}\left[\frac{1}{(1 - x_p)(x_p - x)} - \frac{1}{(1 - x_p)^2}\ln\frac{1 - x}{x_p - x}\right] + C.$$

Integration gives (7) in the following form:

$$R_{av} = \frac{(x_f - x_p)(x_p - x_w)}{(x_f - x_w)(\alpha - 1)}\left[\frac{\alpha}{1 - x_p}\ln\frac{(1 - x_w)(x_p - x_f)}{(1 - x_f)(x_p - x_w)} - \right.$$

$$\left. - \frac{1}{x_p}\ln\frac{(x_p - x_w)x_f}{(x_p - x_f)x_w}\right] - 1. \tag{8}$$

We now compare Equation (8) with the Gilliland equation [5] for calculation of the minimum amount of vapor in rectification with constant concentration of the distillate

$$\frac{V_{min}}{F} = \frac{x_f - x_p}{\alpha(\alpha-1)}\left[\frac{\alpha(\alpha-1)+(1-x_p)}{x_p-1}\ln\frac{(1-x_w)(x_f-x_p)}{(1-x_f)(x_w-x_p)}\right] -$$

$$-\ln\frac{x_w^2(x_f-x_p)(1-x_f)}{x_f^2(x_w-x_p)(1-x_w)}, \qquad (9)$$

where V_{min} is the minimum number of kg-moles of vapor evaporating from the still in the course of rectification.

If the number of plates is infinite, $V = V_{min}$, where V is the actual number of kg-moles of vapor evaporating from the still in the course of rectification. Then

$$V_{min} = V = P(R_{av} + 1).$$

If Equations (8) and (9) are put into similar form, Equation (9) becomes:

$$R_{av}+1 = \frac{(x_f-x_p)(x_p-x_w)}{(x_f-x_w)(\alpha-1)}\left[\frac{\alpha}{x_p-1}\ln\frac{(1-x_w)(x_p-x_f)}{(1-x_f)(x_p-x_w)} + \ln\frac{(1-x_w)x_f}{(1-x_f)x_w}\right]. \qquad (10)$$

Comparison of Equations (8) and (10) shows that they are not identical. Since the derivation of Equation (8) was strict and mathematically exact, it follows that there must be errors in Gilliland's mathematical derivation.

Examination of Equation (8) shows that, for the same values of x_f, x_p, x_w, and $\underline{n}$, R_{av} decreases when α increases. Therefore, the mixture is more easily separated. In the limiting cases, when $\alpha = 1$, R_{av} tends to ∞, and when $\alpha = \infty$, R_{av} is zero.

Using Equation (1) and integrating the Bogart equation [6], we obtain a formula for calculation of the rectification time $\underline{t}$

$$t = \frac{-F(x_p-x_f)}{V(\alpha-1)}\left[\frac{\alpha}{(1-x_p)}\ln\frac{(1-x_w)(x_p-x_f)}{(1-x_f)(x_p-x_w)} - \frac{1}{x_p}\ln\frac{(x_p-x_w)x_f}{(x_p-x_f)x_w}\right]. \qquad (11)$$

As in the case of Equation (8), it follows from Equation (11) that, for the same values of x_f, x_p, x_W, and $\underline{n}$, $\underline{t}$ decreases with increase of α. In the limiting cases, when $\alpha = 1$, $\underline{t}$ tends to ∞, and when $\alpha = \infty$, $\underline{t}$ is zero.

Comparison of the Two Variants of the Rectification Process

For a given average distillate concentration $(x_p)_{av}$, the ratio of the rectification times and of the average reflux ratios in rectification at constant reflux ratio and at constant distillate concentration should show which of these variants is the more advantageous.

Since the consumption of heating steam, the consumption of condenser cooling water, and $P(R_{av} + 1)$ increase proportionately, we can suitably compare the values of $(R_{av} + 1)$ for the two variants.

In rectification at constant reflux ratio

$$(x_p)_{av} = \frac{\frac{F}{W}x_f - x_w}{\frac{F}{W} - 1}$$

Hence

$$\frac{F}{W} = \frac{(x_p)_{av} - x_w}{(x_p)_{av} - x_f}.$$

With the aid of Equation (3) we have

$$R+1=\frac{\frac{1}{\alpha-1}\ln\frac{x_f(1-x_w)}{x_w(1-x_f)}+\ln\frac{1-x_w}{1-x_f}}{\frac{(x_p)_{av}-x_w}{(x_p)_{av}-x_f}}. \tag{12}$$

Comparison of Equation (8) with Equation (12) gives the ratio for the two variants

$$\frac{(R+1)_p}{(R_{av}+1)_R}=$$

$$=\frac{(x_f-x_w)\left[\ln\frac{x_f}{x_w}+\alpha\ln\frac{1-x_w}{1-x_f}\right]}{(x_f-x_p)(x_p-x_w)\ln\left(\frac{x_p-x_w}{x_p-x_f}\right)\left[\frac{\alpha}{1-x_p}\ln\frac{(1-x_w)(x_p-x_f)}{(1-x_f)(x_p-x_w)}-\frac{1}{x_p}\ln\frac{(x_p-x_w)x_f}{(x_p-x_f)x_w}\right]}. \tag{13}$$

Comparison of Equations (6) and (11) gives the following ratio of the rectification times for the two variants:

$$\frac{t_R}{t_p}=\frac{(R+1)_R}{(R_{av}+1)_p}, \tag{14}$$

where the subscript p refers to operation at constant distillate concentration, and R, to operation at constant reflux ratio. This time ratio is clearly a function of the variables x_f, x_w, x_p and α.

Consider the following example of the rectification of an ideal binary mixture. The composition of the mixture $x_f = 0.5$, the relative volatility $\alpha = 2$. A batch column in which the number of theoretical plates $n = 20$ is used. In operation at constant reflux ratio $R = 1.8$, the final concentration of the mixture in the still $x_w = 0.1$. We have to determine the average distillate concentration $(x_p)_{av}$.

First, examination of Figure 1d shows that Equation (1) may be used when $R = 19$ and $n = 20$; in this instance $R = 1.8$, or much less than 19, so that this equation is all the more applicable.

From Equation (4) we have:

$$R_{cr}=\frac{1}{(\alpha-1)x_f}=2.$$

Since R is less than R_{cr}, Equation (3) is fully applicable. Substitution of the values of x_f, x_w, α, R into Equation (3) gives $F/W = 2.72$. Then, from Equation (5) we have

$$(x_p)_{av}=0.773.$$

We now find the average reflux ratio R_{av} if the same column is used for rectification of the same mixture in operation with constant concentration of the distillate, the value of $x_p = 0.773$ being reached [in other words, when x_p is equal to $(x_p)_{av}$] and with $x_w = 0.1$.

In this instance when the concentration of the mixture in the still falls to 0.1, the final reflux ratio will be greatest. We denote this final reflux ratio by R_w; then, approximately

$$\frac{R_w}{R_w+1}=\frac{x_p-y_w}{x_p-x_w},$$

where y_w is the equilibrium concentration of the vapor phase over the final mixture of concentration x_w.

Putting $x_p = 0.773$, $x_w = 0.1$ and $y_w=\frac{\alpha x_w}{1+(\alpha-1)x_w}$ into this expression, we have $R_w = 9.05$. This is much smaller than the value of R ($R = 19$) shown in Figure 1d. Therefore, when the number of plates is 20 the end of the operating line is close to the equilibrium curve and Equation (8) may be used for the calculation. Substitution of the values of x_f, x_w, x_p and α into Equation (8) gives $R_{av} = 1.47$.

We thus find the following ratios of the steam and cooling water consumptions for the two variants of the rectification process:

$$\frac{1+1.8}{1+1.47}=1.43.$$

Analogously, the ratio of the rectification times is

$$t_R/t_p = 1.43.$$

Therefore, rectification at constant distillate concentration is more economical under the conditions of the example considered.

SUMMARY

1. The proposed analytical method for calculations relating to the separation of an ideal binary mixture in a batch-rectification column with a sufficient number of plates is simpler than the graphical method.

2. At certain values of α, R and $\underline{x}$ the proposed method is applicable even with a small number of plates (sometimes a few plates are sufficient).

3. The greater the number of plates, the more accurate is the result given by this calculation method. If the number of plates is small and the terminal point of the operating line is at some distance from the equilibrium curve, Equations (13) and (14) can still be used for rough calculations of the ratios of the rectification times and average reflux ratios for operation by the two variants giving distillates of the same average concentration, as the errors in the determinations of t_p and $(R + 1)_p$, and of t_R and $(R_{av} + 1)_R$ more or less cancel each other out.

4. The Gilliland formula for calculations of the rectification process at constant distillate concentration is incidentally shown to be erroneous.

LITERATURE CITED

[1] Fu Tziui-fu, J. Appl. Chem. (USSR) 30, 6, 862 (1957).*

[2] A.G. Kasatkin, Principal Processes and Equipment of Chemical Technology** (Goskhimizdat, 1950), p. 533.

[3] A. Rose and E. Rose, Technique of Organic Chemistry, IV, Distillation 60-61 (Interscience Publishing Inc., New York, 1951).

[4] Rayleigh, Phil. Mag. 524, 521 (1902).

[5] C.S. Robinson and E.R. Gilliland, Elements of Fractional Distillation (McGraw Hill Book Co., New York, 1950), p. 377.

[6] M.T.P. Bogart, Trans. Amer. Inst. Chem. Engrs. 33, 139 (1931).

Received November 21, 1957

*Original Russian pagination. See C.B. Translation.

**In Russian.

KINETIC RELATIONSHIPS IN ABSORPTION BY THE BUBBLING METHOD

L.A. Mochalova and M.Kh. Kishinevskii

Laboratory of Physical Chemistry, the Kishinev State University

There have been many investigations of the mechanism of gas-liquid interaction on bubble-cap and sieve plates, and interest in this subject has increased considerably during recent years.

Theoretical calculations of plate efficiency are hindered by inadequate information on the mechanism of mass transfer from the gas stream-bubble interface into the liquid phase.

In the great majority of experimental investigations the systems chosen, in order to avoid difficulties in interpretation of the experimental results, are such that there is no chemical interaction between the gas and liquid. Indeed, if the mechanism and kinetics of the reactions superposed on the diffusion processes are not understood, interpretation of the experimental data is very difficult. However, if definite information on the mechanism and kinetics of the chemical process is available, and if the order, and the value of the rate constant and its temperature coefficient, of the slowest reaction are known, then data on the rate of absorption accompanied by chemical reaction can even assist in elucidation of the nature of the liquid-phase mass transfer coefficient, i.e., of the mechanism of mass transfer. An attempt in this direction is described in this paper.

It is now widely held that the coefficient of mass transfer in the liquid phase under bubbling conditions is proportional to the square root of the ratio of the diffusion coefficient and the phase contact time, or the time of renewal of the surface layer

$$k_L = 1.13\sqrt{\frac{D}{\Delta\tau}}. \qquad (1)$$

This equation is derived on the assumption that the diffusion of gas molecules from the interface into the volume does not reach equilibrium during the time of phase contact, and that the region through which the molecules diffuse is very large. Higbie [1] considered that $\Delta\tau$ is approximately equal to the time required for a bubble to traverse the horizontal plane, but that $\Delta\tau$ decreases with increasing agitation in the liquid phase. According to Higbie, the removal of gas molecules from the interface into the liquid phase during the time of contact is determined by a molecular-diffusion mechanism only, and D is therefore the coefficient of molecular diffusion.

West, Gilbert and Shimizu [2], who studied the mechanism of mass transfer on sieve plates, held similar views.

These authors define $\Delta\tau$ as

$$\Delta\tau = 2r\epsilon/V, \qquad (2)$$

where r is the effective bubble radius; V is the linear gas velocity, equal to the ratio of the volume flow rate to the total plate cross section; ϵ is the gas volume fraction.

Calderbank [3] also accepts Higbie's equation, and assumes that $k_L \sim \sqrt{DV/r}$, where V is the linear velocity of ascent of the bubble.

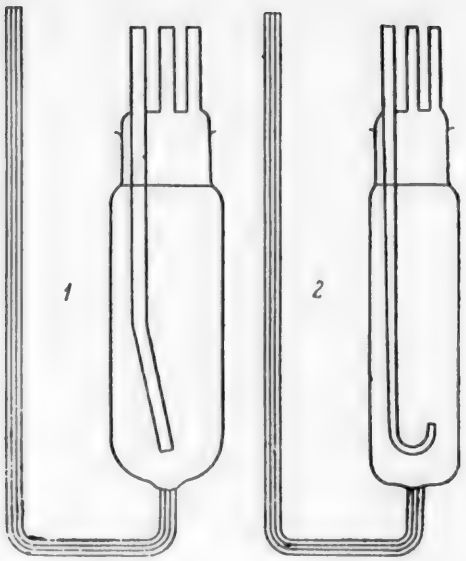

Fig. 1. Bubblers. The diameter of the bubbling tube is 5 mm in bubbler 1, and 2 mm in bubbler 2; the diameter of bubbler 1 is 50 mm, and of bubbler 2, 35 mm.

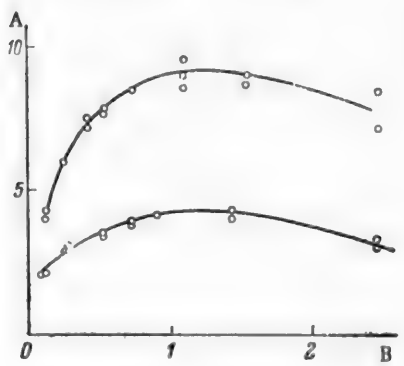

Fig. 2. Rate of absorption of CO_2 by NaOH solutions in bubbler 1. Partial pressure of CO_2 at the entry into the absorber 0.52 atmos. A) Absorption rate · 10^5 (moles/min); B) NaOH concentration (M). Temperature (°C): 1) 5; 2) 45. Curves (in Figs 1-8): 1) lower; 2) upper.

This author analyzed the experimental data available in the literature on the rate of bubble formation, and concluded that this rate is almost constant in the range of bubbling rates used in practice. The effective bubble radius is proportional to the cube root of the volumetric gas rate per orifice.

Under streaming conditions, when chains of closely adjoining bubbles emerge from each orifice, the ascent velocity of each is equal to the product of the frequency of formation and the diameter, i.e., it is again proportional to the cube root of the volume rate. Hence it is concluded that k_L in all cases of bubbling absorption is determined only by the coefficient of molecular diffusion.

It is difficult to agree with this conclusion. It is difficult to accept that the degree of turbulence of the liquid phase has no effect on the liquid-phase coefficient of mass transfer. The viewpoints of Higbie and of West, et al. are more flexible in this respect, as according to these authors intensification of the bubbling rate results in a decrease of the renewal time of the surface layer. Nevertheless, Calderbank's conclusion that $\Delta\tau$ is independent of the bubbling rate is justified if it is taken into account that the rate of bubble formation is constant in the practical range of bubbling rates. In our opinion this contradiction can be resolved if it is assumed that the transfer of gas molecules from the interface into the liquid phase is effected not only by molecular but also by turbulent diffusion, i.e., if in Equation (1) the coefficient of molecular diffusion is replaced by the effective diffusion coefficient, equal to the sum of the molecular and turbulent diffusion coefficients. This concept is quite compatible with Calderbank's conclusion that $\Delta\tau$ is constant over a wide range of bubbling rates, and at the same time it is not contrary to the idea that the mass-transfer coefficient increases with increasing turbulence of the liquid phase. It should be noted that available experimental data indicate that k_L increases with intensified agitation of the liquid phase. We carried out experiments under mass-bubbling conditions at various linear velocities of the liquid on the plate, with the same bubbling depth in all cases. The results showed that $k_L \cdot F^*$ increases approximately linearly with the liquid velocity on the plate. Similar results were obtained by Bonnet et al., whose data are presented in the monograph by Sherwood and Pigford [4]. For example, it follows from Bonnet's data that when the linear gas velocity (for the full section of the column) is 2.2 feet per hour, the height of a transfer unit in the liquid phase increases roughly 2 to 2.5-fold with a nearly 10-fold variation of the volumetric liquid rate. The only possible explanation for this is a considerable increase of $k_L \cdot a$,** but since $\underline{a}$ is constant at a constant volumetric gas rate, it follows that k_L increases with increase of the liquid velocity.

The purpose of the present investigation was to analyze experimental data on the kinetics of absorption accompanied by chemical reactions in order to determine: 1) the dependence of $\Delta\tau$ on the bubbling conditions,

*F is the total interfacial area, constant in all our experiments.

**$\underline{a}$ is the interfacial area in unit volume of liquid.

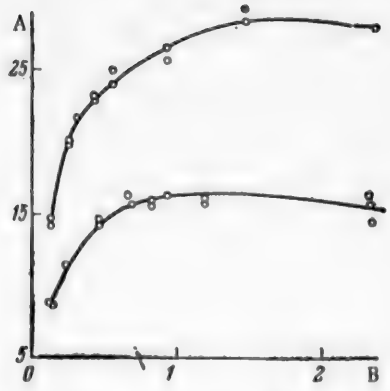

Fig. 3. Rate of absorption of CO_2 by NaOH solutions in bubbler 2. Partial pressure of CO_2 at the entry into the absorber 0.52 atmos. A) Absorption rate · 10^3 (moles/min); B) NaOH concentration (M). Temperature (°C): 1) 5; 2) 45.

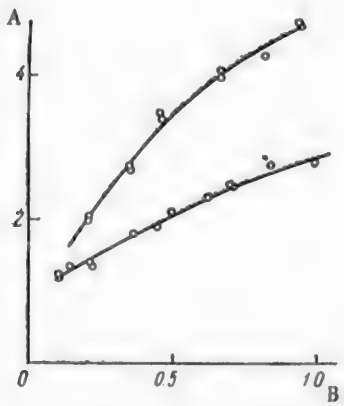

Fig. 4. Rate of absorption of CO_2 by aqueous NH_3 solutions in bubbler 1. Partial pressure of CO_2 at the entry into the absorber 0.515 atmos. A) Absorption rate · 10^3 (moles/min); B) NH_4OH concentration (M). Temperature (°C): 1) 5; 2) 45.

2) the dependence of the mass-transfer coefficient in the liquid phase on the viscosity, and 3) the dependence of $\Delta\tau$ on viscosity.

EXPERIMENTAL

The following systems were used in the experiments: CO_2 – aqueous NaOH solutions, CO_2 – aqueous Na_2CO_3 solutions, and CO_2 – aqueous ammonia solutions. Since the purpose of the work was to determine the influence of viscosity on the kinetic relationships in bubbling absorption, the method of coordinated selection of temperatures and concentrations [5] was not used.

The influence of the concentration of the active component of the absorbent on the absorption rate was studied at 5 and 45°. The form and dimensions of the bubblers used are shown in Figure 1. The gas rate was 0.6 liter/minute in the experiments with bubbler 1, and 3.12 liters/minute in the experiments with bubbler 2. The same volume of absorbent (60 ml) was used in all the experiments, corresponding to a bubbling depth of 17 mm in bubbler 1 and 45 mm in bubbler 2. The bubbles were formed singly in bubbler 1, and in streams in bubbler 2. In the latter case there was considerable foaming. To the lower end of each bubbler there was sealed a capillary tube which emerged from the thermostat containing the bubblers. This tube was used for removal of the liquid after each experiment; a rubber bulb was used to create a slight increase of pressure in the bubbler for this purpose. The middle portions of liquid were taken for analysis. The vessels were thoroughly washed after each experiment. The duration of each individual experiment was short, as it was the intention, in order to avoid complication of the chemical kinetics, to stop at the initial stages of carbonation. Otherwise, the experimental procedure was the same as that described in the previous paper. The experimental data are presented in Figs. 2-7.

DISCUSSION OF RESULTS

Comparison of the experimental curves shows that caustic soda solutions absorb carbon dioxide at the greatest rate. The absorption rate reaches its maximum value at NaOH concentrations of about 1-1.5 mole/liter at both the temperatures. This form of the curves cannot be attributed to the small increase in the viscosity of caustic soda solutions in the range from 0 to 1-1.5 mole/liter. The more likely explanation is that the gas-phase resistance increases rapidly with increasing NaOH concentration, since the partial pressure P^* of CO_2 at the interface decreases with increasing gas-phase resistance, and the absorption rate, expressed in terms of the driving force in the gas phase

$$\frac{d\omega}{d\tau} = k_G \cdot F \cdot (P - P^*), \tag{3}$$

tends to its limiting value

$$\frac{d\omega}{d\tau} = k_G \cdot F \cdot P. \tag{4}$$

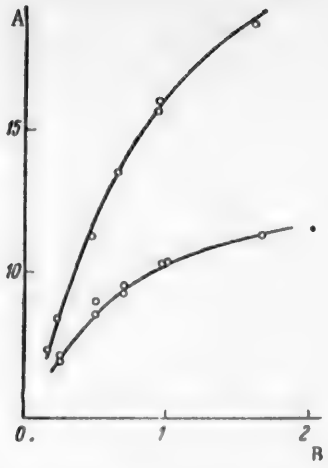

Fig. 5. Rate of absorption of CO_2 by aqueous ammonia solutions in bubbler 2. Partial pressure of CO_2 at the entry into the absorber 0.52 atmos. A) Absorption rate $\cdot 10^3$ (moles/min); B) NH_4OH concentration (M). Temperature (°C): 1) 5; 2) 45.

The decrease of the absorption rate with increase of NaOH concentration above 1-1.5 M is probably due to the influence of viscosity on $k_G \cdot F$.

The values of $k_G \cdot F$ were calculated from the limiting rates of absorption of CO_2 by NaOH solutions, with the aid of Equation (4). The data are presented in Table 1. It is seen that the temperature has a significant influence on $k_G \cdot F$; this influence may either be direct, or indirect in consequence of changes in the viscosity of the absorbent.

The experimental curves for Na_2CO_3 were used for determination of the liquid-phase mass transfer coefficient $k_L F$. For this, the curves were extrapolated to zero concentration of Na_2CO_3. When $C_{Na_2CO_3} = 0$, the absorption rate is

$$\frac{d\omega}{d\tau} = \frac{HP}{\frac{1}{k_L F} + \frac{H}{k_G F}}, \qquad (5)$$

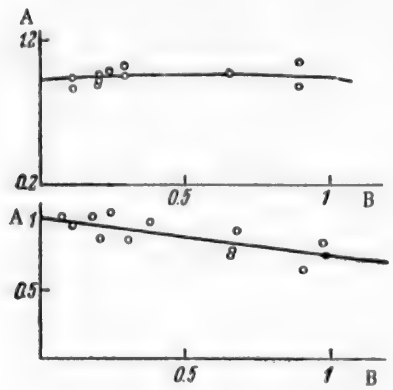

Fig. 6. Rate of absorption of CO_2 by Na_2CO_3 solutions in bubbler 1. Partial pressure of CO_2 at the entry into the absorber 0.48 atmos. A) Absorption rate $\cdot 10^3$ (moles/min); B) Na_2CO_3 concentration (g-equiv/liter). Temperature (°C) 1) 5; 2) 45.

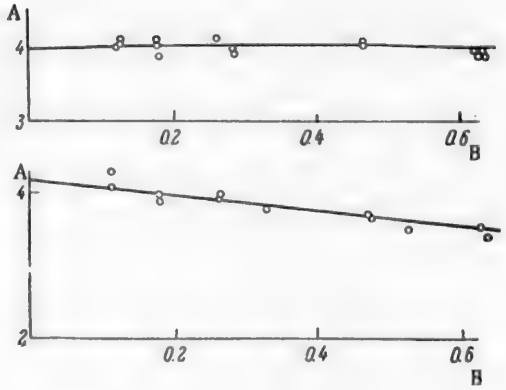

Fig. 7. Rate of absorption of CO_2 by Na_2CO_3 solutions in bubbler 2. Partial pressure of CO_2 at the entry into the absorber 0.515 atmos. A) Absorption rate $\cdot 10^3$ (moles/min); B) Na_2CO_3 concentration (g-equiv/liter). Temperature (°C): 1) 5; 2) 45.

TABLE 1

Calculation of Gas-Phase Mass-Transfer Coefficient

Bubbler	Temperature (°C)	Gas rate (liters/min)	Absorption rate (moles/min)	Average partial pressure of CO_2 (atmos)	$k_G F$ (moles/min·atm)
2	5	3.12	$16.5 \cdot 10^{-3}$	0.48	$35 \cdot 10^{-3}$
2	45	3.12	$28.5 \cdot 10^{-3}$	0.40	$71 \cdot 10^{-3}$
1	5	0.60	$4.25 \cdot 10^{-3}$	0.47	$9.0 \cdot 10^{-3}$
1	45	0.60	$9.2 \cdot 10^{-3}$	0.325	$28 \cdot 10^{-3}$

TABLE 2

Calculation of Liquid-Phase Resistance

Bubbler	Na_2CO_3 concentration (M)	Temperature (°C)	Viscosity (centipoises)	Solubility coefficient (moles/liter · atm)	Gas rate (liters/min)	Gas-phase mass-transfer coefficient k_GF (moles/min · atm)	Average partial pressure of CO_2 (atm)	Absorption rate (moles · min · 10^3)	Total resistance $\frac{1}{k_LF}+\frac{H}{k_GF}$	Liquid-phase resistance $1/k_LF$ (min/liter)
2	0.00	5.0	1.52	0.064	3.12	$35 \cdot 10^{-3}$	0.50	4.2	7.6	5.8
2	0.00	45.0	0.596	0.0216	3.12	$71 \cdot 10^{-3}$	0.46	4.0	2.5	2.2
1	0.00	5.0	1.52	0.064	0.60	$9.0 \cdot 10^{-3}$	0.47	0.98	30.7	23.5
1	0.00	45.0	0.596	0.0216	0.60	$28 \cdot 10^{-3}$	0.42	0.95	9.6	8.8

where H is the coefficient of solubility of CO_2 in water (in moles/liter · atmos).

The calculation of $k_L \cdot F$ is given in Table 2. The variation of $1/k_LF$ with the viscosity of the absorbent is plotted in Figure 8. In both cases the liquid-phase resistance $1/k_LF$ was directly proportional to the viscosity.

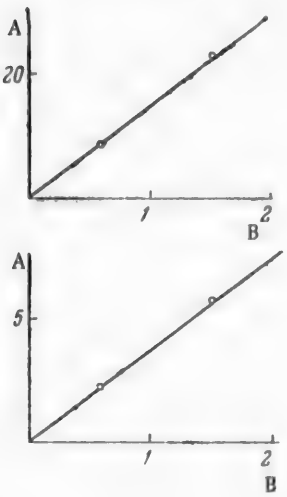

Fig. 8. Variation of $1/k_LF$ with viscosity: A) values of $1/k_LF$ (min/liter); B) viscosity (centipoises).

The influence of viscosity on the liquid-phase transfer coefficient in bubbling absorption was also studied by Walter and Sherwood [6] for the system CO_2-water. The viscosity of the absorbent was varied by two methods: by addition of glycerol at constant temperature, and by changes of the temperature of pure water. In the first case the reciprocal of k_La was proportional to the viscosity to the power 0.43, and in the second, to the power 1.35.

In our opinion, the second method for studying the influence of viscosity is the more reliable, as glycerol may influence foaming. The discrepancy between our results and those of Walter and Sherwood in experiments in which the viscosity was varied by changes of temperature cannot be attributed to the fact that in our experiments a single bubbling orifice was used, whereas they used a bubble tower. We obtained similar results in experiments with mass bubbling. Our results approximate to those of Kuz'minykh and Koval' [7], who studied the influence of viscosity on the mass-transfer coefficient on sieve plates. In their studies of the kinetics of CO_2 desorption from aqueous glycerol solutions they found that the reciprocal of k_La is proportional to the viscosity to the power 0.85.

For determination of the influence of bubbling conditions on $\Delta\tau$, the equation [5]

$$\frac{d\omega}{d\tau}=\frac{\frac{C}{m}(1-A)+HP}{\frac{1}{k_LF}+\frac{H}{k_GF}}, \qquad (6)$$

where

$$A=\frac{e^{-mHK_C\Delta\tau P^*}}{\sqrt{mHK_C\Delta\tau P^*}}\int_0^{\sqrt{mHK_C\Delta\tau P^*}} e^{y^2}dy,$$

was used to calculate $K_C\Delta\tau$ for all the systems studied. These calculations are given in Tables 3 and 4.*

*It was assumed that the solubility coefficient H was the same for NaOH solutions as for NaCl solutions; the same for Na_2CO_3 solutions as for $NaHCO_3$ solutions; and the same for NH_4OH solutions as for pure water.

The average partial pressure of CO_2 was calculated with a correction for the vapor pressures of the solutions.

TABLE 3

Calculation of $K_C\Delta\tau$ for the Systems CO_2-NaOH, CO_2-NH_4OH, $CO_2-Na_2CO_3$. Gas Rate 3.12 liters/min, Volume of Absorbent 60 ml, Bubbler 2

System	Temperature (°C)	Initial concentration (M)	Average concentration (M)	Average partial pressure of CO_2 (atm)	Viscosity of absorbent (centipoises)	Solubility coefficient (moles/liter · atm)	Absorption rate (moles/min · 10^3)	Liquid-phase resistance $1/k_LF$ (min/liter)	Gas-phase transfer coefficient k_GF (moles/min · atm)	$\frac{H}{k_GF}$	$\frac{H}{k_GF}+\frac{1}{k_LF}$	Partial pressure P^* of CO_2 at the interface (atm)	A	$\sqrt{mHP^*K_C\Delta\tau}$	$K_C\Delta\tau$
CO_2—NaOH	5	0.404	0.300	0.49	1.64	0.058	12.5	6.2	$35 \cdot 10^{-3}$	1.7	7.9	0.134	0.530	1.01	65
		0.513	0.400	0.49	1.68	0.056	13.5	6.3	$35 \cdot 10^{-3}$	1.6	7.9	0.103	0.607	0.88	67
	45	0.435	0.310	0.42	0.65	0.020	21.5	2.5	$71 \cdot 10^{-3}$	0.28	2.78	0.117	0.657	0.81	140
		0.631	0.500	0.415	0.67	0.019	23.8	2.5	$71 \cdot 10^{-3}$	0.27	2.77	0.079	0.768	0.64	135
CO_2—NH_4OH	5	0.572	0.500	0.50	1.52	0.064	8.6	5.8	$35 \cdot 10^{-3}$	1.8	7.6	0.255	0.866	0.47	6.8
		1.087	1.00	0.495	1.52	0.064	10.4	5.8	$35 \cdot 10^{-3}$	1.8	7.6	0.197	0.905	0.385	5.9
	45	0.599	0.500	0.43	0.596	0.0216	11.9	2.25	$71 \cdot 10^{-3}$	0.30	2.55	0.26	0.915	0.37	12
		1.136	1.00	0.41	0.596	0.0216	16.3	2.25	$71 \cdot 10^{-3}$	0.30	2.55	0.18	0.934	0.32	13
CO_2—Na_2CO_3	5	1.182	0.150	0.50	1.66	0.055	3.90	6.3	$35 \cdot 10^{-3}$	1.6	7.9	0.39	0.977	0.19	1.7
		0.280	0.250	0.50	1.78	0.050	3.64	6.8	$35 \cdot 10^{-3}$	1.4	8.2	0.40	0.980	0.18	1.6
	45	0.183	0.150	0.46	0.63	0.018	4.06	2.4	$71 \cdot 10^{-3}$	0.30	2.7	0.40	0.982	0.17	4.0
		0.283	0.250	0.46	0.67	0.0167	4.04	2.6	$71 \cdot 10^{-3}$	0.23	2.8	0.40	0.985	0.15	3.4

TABLE 4

Calculation of $K_c\Delta\tau$ for the Systems CO_2-NaOH, CO_2-NH_4OH, $CO_2-Na_2CO_3$. Gas Rate 0.600 liter/min, Volume of Adsorbent 60 ml, Bubbler 1

System	Temperature (°C)	Initial concentration (M)	Average concentration (M)	Average partial pressure of CO_2 (atm)	Viscosity of absorbent (centipoises)	Solubility coefficient (moles/liter · atm)	Absorption rate (moles/min · 10^3)	Liquid-phase resistance $1/k_LF$ (min/liter)	Gas-phase transfer coefficient k_GF (moles/min · atm)	$\frac{H}{k_GF}$	$\frac{1}{k_LF}+\frac{H}{k_GF}$	Partial pressure P^* of CO_2 at the interface (atm)	A	$\sqrt{mHP^*K_c\Delta\tau}$	$K_c\Delta\tau$
CO_2-NaOH	45	0.290	0.260	0.40	0.63	0.020	6.0	9.6	$28\cdot10^{-3}$	0.7	10.3	0.185	0.597	0.91	112
		0.562	0.500	0.37	0.67	0.019	7.5	10.2	$28\cdot10^{-3}$	0.7	10.9	0.102	0.700	0.74	141
	5	0.350	0.300	0.48	1.62	0.059	3.0	24.6	$9.0\cdot10^{-3}$	6.5	31.1	0.15	0.565	0.95	51
		0.557	0.500	0.48	1.70	0.055	3.4	26.0	$9.0\cdot10^{-3}$	6.1	32.1	0.10	0.670	0.79	56
CO_2-NH_4OH	45	0.675	0.500	0.42	0.596	0.0216	3.5	9.0	$28\cdot10^{-3}$	2.4	11.4	0.30	0.877	0.44	15.0
		1.237	1.000	0.395	0.596	0.0216	4.74	9.0	$28\cdot10^{-3}$	2.4	11.4	0.225	0.909	0.37	14.0
	5	0.636	0.500	0.49	1.52	0.064	2.05	23.0	$9.0\cdot10^{-3}$	7.0	30.2	0.26	0.877	0.44	5.8
		1.188	1.000	0.49	1.52	0.064	2.82	23.0	$9.0\cdot10^{-3}$	7.0	30.2	0.18	0.893	0.41	7.3
$CO_2-Na_2CO_3$	45	0.182	0.150	0.42	0.63	0.0184	0.97	9.6	$28\cdot10^{-3}$	0.7	10.3	0.39	0.983	0.16	3.6
		0.282	0.250	0.42	0.67	0.0168	0.98	10.2	$28\cdot10^{-3}$	0.6	10.8	0.39	0.985	0.15	3.4
	5	0.180	0.150	0.47	1.66	0.055	0.91	25.2	$9.0\cdot10^{-3}$	6.1	31.3	0.37	0.982	0.16	1.3
		0.278	0.250	0.47	1.77	0.050	0.86	27.0	$9.0\cdot10^{-3}$	5.6	32.6	0.38	0 982	0.16	1.4

The first interesting result is that the values of $K_c\Delta\tau$ for a given chemical system are approximately the same under totally different bubbling conditions. These conditions are different in bubblers 1 and 2, not only because of the different gas rates, but also because the tubes through which the gas passes differ in diameter and direction: in bubbler 1 the gas stream is directed down into the liquid, and in bubbler 2 it is directed toward the interface. A second interesting result is the ratio of the values of $K_c\Delta\tau$ for different chemical systems at the same temperature. For example, the $K_c\Delta\tau$ ratio for the systems CO_2-NaOH and CO_2-NH_4OH is approximately 10 (in good agreement with direct kinetic measurements). Our values of $K_c\Delta\tau$ from the system $CO_2-Na_2CO_3$ also seem consistent, although because of the low rate of the chemical reaction in this case these calculations are less reliable than the others. The $K_c\Delta\tau$ ratio for the caustic soda and sodium carbonate systems respectively at 45° is approximately 36. This result is satisfactorily explained on the following considerations.

According to the literature [8, 9], the rate of reaction of CO_2 with sodium carbonate is determined by the reaction between CO_2 and the hydroxyl ions in the sodium carbonate solution. In the kinetic Equation (6) applied to the system $CO_2-Na_2CO_3$, K_c was taken to be a constant formally defined by the equation

$$-\frac{d[CO_2]}{d\tau} = K_c[Na_2CO_3][CO_2].$$

It is therefore natural that K_c for the system $CO_2-Na_2CO_3$, calculated by means of Equation (6) should be less than K_c for the system CO_2-NaOH in the same ratio as the concentration (molar) of Na_2CO_3 is greater than the corresponding concentration of hydroxyl ions or, as a rough approximation, in the ratio of their activities in these solutions.

Comparison of the values of $K_c\Delta\tau$ for the system CO_2-NaOH at various temperatures gave results which differed considerably from the results in our experiments with coordinated selection of temperatures and concentrations. In the latter case it was found that the temperature coefficient of the reaction between CO_2 and hydroxyl ions is approximately 2. Hence the rate constant should increase 16-fold with a 40° rise of temperature. However, $K_c\Delta\tau$ increased only 2.2-fold. It follows that the time of renewal of the surface layer $\Delta\tau$ decreased 7-fold between 5 and 45°, owing to the considerable decrease of viscosity, i.e.,

$$\Delta\tau \propto \eta^2.$$

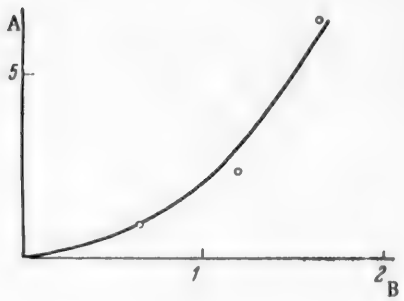

Fig. 9. Variation of $\Delta\tau$ with viscosity. A) $\Delta\tau \cdot 10^4$ (in min); B) viscosity (centipoises)

According to Van Krevelen's data [10], the interfacial area in bubbling absorption is virtually independent of viscosity. Therefore, the variation of k_LF, which is given by

$$k_L F = F\sqrt{\frac{4D_{eff}}{\pi\Delta\tau}}, \qquad (7)$$

with viscosity can be caused only by variations of the effective diffusion coefficient D_{eff} and the renewal time $\Delta\tau$. However, since experimental results show that k_LF is inversely proportional to the viscosity, and $\Delta\tau \propto \eta^2$, it follows that D_{eff} is independent of viscosity, at least for practical purposes. This may seem an improbable result at first sight. However, more careful consideration provides an explanation which, in our opinion, does not contradict the physical picture. Suppose that the effective diffusion coefficient is six times the molecular diffusion coefficient at 5°.* Between 5 and 45° the molecular diffusion coefficient increases approximately three-fold. Since at 5° it is only 1/6 of the effective diffusion coefficient, the latter changes by a factor of only 1.3 for the same change of viscosity, if it is assumed that the coefficient of turbulent diffusion is independent of viscosity. Under bubbling conditions, turbulent diffusion near the interface is associated with transfer of turbulence between the phases, and it may decrease somewhat, or, in any event, remain almost unchanged, with decrease of the viscosity of the liquid phase over a definite range.

*In reality, it may be either larger or smaller than this value.

The results of the present investigation are in agreement with those of our previous study [5], where the viscosity of the absorbent was 1.2 centipoises. The value $\Delta\tau = 2.5 \cdot 10^{-4}$ minute was found in that study. In the present investigation, with viscosities of 0.65 and 1.65 centipoises, we found $\Delta\tau$ to be $0.92 \cdot 10^{-4}$ min.and $6.6 \cdot 10^{-4}$ min.respectively. In a graphical plot of these data (Figure 9), the points lie close to a curve of the form

$$\Delta\tau = B\eta^2. \tag{8}$$

If $\Delta\tau$ is expressed in minutes and the viscosity in centipoises, B is approximately 2.2.

This result requires additional experimental verification and probably some modification. Preliminary experiments on mass bubbling showed that this relationship may be applicable there also. It remains uncertain whether the equation is applicable to sieve plates on which the foaming regime predominates.

SUMMARY

The following conclusions with regard to bubbling absorption may be drawn from the experimental results of this investigation.

1. The time of renewal of the surface layer is independent of the diameter and shape of the orifice through which the gas enters.

2. The time of renewal of the surface layer is independent of the volumetric gas rate per orifice.

3. The coefficient of mass transfer through the liquid phase is inversely proportional to the first power of the viscosity of the absorbent.

4. The time of renewal of the surface layer is proportional to the square of the absorbent viscosity.

LITERATURE CITED

[1] R. Higbie, Trans. Am. Inst. Chem. Engrs. 31, 365 (1935).

[2] F.B. West, W.D. Gilbert and T. Shimizu, Ind.Eng. Ch. 44, 2470 (1952).

[3] P.H. Calderbank, Trans. Am. Inst. Chem. Engrs. 34, 79 (1956).

[4] T.K. Sherwood and R.L. Pigford, Absorption and Extraction (New York, 1952).

[5] M.Kh. Kishinevskii and L.A. Mochalova, J. Appl. Chem. 29, 2, 170 (1956).*

[6] J.F. Walter and T.K. Sherwood, Ind. Eng. Ch. 33, 493 (1941).

[7] I.N. Kuz'minykh and Zh.A. Koval', J. Appl. Chem. 28, 1, 21 (1955).*

[8] B.R.W. Pinsent and F.J.W. Roughton, Trans. Faraday Soc. 47, 3 (1951).

[9] C. Fourholt, J. Chim. Phys. 21, 400 (1924).

[10] D.W. Van Krevelen and P.S. Hoftijzer, Chem. Eng. Progress 46, 29 (1950).

Received May 24, 1957

*Original Russian pagination. See C.B. translation.

THE HYDRAULIC RESISTANCE OF GRIDS

I.P. Mukhlenov and E.Ia. Tarat

The Lensoviet Technological Institute, Leningrad

Sieve-plate equipment is widely used for processes of gas-liquid interaction. The hydraulic resistance of the tray is one of the determining quantities in analysis of the performance of existing equipment and in the design of new apparatus. Therefore, the hydraulic resistance of sieve plates has been studied by numerous investigators [1-13].

Detailed studies of the determination of hydraulic resistance were carried out by Zhavoronkov and Furmer [4], Usiukin and Aksel'rod [5], and by Romankov, Noskov and Sokolov [11]. The results of other workers are also presented and critically analyzed in these papers. These investigations revealed the factors which influence the hydraulic resistance of a grid and of a gas-liquid layer on the grid. Several empirical formulas have been proposed for calculation of the hydraulic resistance of the whole tray, but these formulas are somewhat contradictory.

Most investigators consider the pressure drop in the dry grid ΔP_1, and in the gas-liquid layer, ΔP_2, separately. The total resistance of the tray is given by the formula

$$\Delta P = \Delta P_1 + \Delta P_2. \tag{1}$$

This formula is somewhat mechanistic, and does not reflect the fact that some of the orifices in an operating grid are usually more or less filled with liquid. However, Equation (1) is convenient because it separates a complex effect into simpler components, more amenable to study.

An attempt to derive an equation for calculation of the hydraulic resistance, with partial filling of the orifices with liquid taken into account, yielded equations [13] which can be only of partial value, since many parameters which influence the filling of the orifices with liquid [14, 15] were not taken into consideration.

We studied, consecutively, the hydraulic resistance of a dry grid and then the hydraulic resistance of a tray, i.e., a grid together with the gas-liquid layer, in foaming conditions. The present communication is concerned with the resistance of dry grids.

The criterial equation derived earlier [14-16] for the hydrodynamics of a tray of the foam apparatus under foaming conditions:

$$Eu = B \cdot Re_G^a \cdot Rq_L^b \cdot We^c \cdot \left(\frac{\nu_G}{\nu_L}\right)^d \cdot \Gamma_1^e \cdot \Gamma_2^f \cdot \Gamma_3^g \tag{2}$$

or

$$\frac{\Delta P g}{\gamma_G w_G^2} = B \cdot \left(\frac{w_G D_e}{\nu_G}\right)^a \cdot \left(\frac{i}{\nu_L}\right)^b \cdot \left(\frac{\sigma}{\gamma_L h_0^2}\right)^c \cdot \left(\frac{\nu_2}{\nu_L}\right)^d \cdot \left(\frac{D_e}{h_0}\right)^e \times$$
$$\times \left(\frac{m}{d_0}\right)^f \cdot \left(\frac{H_0 b}{S_0}\right)^g \tag{2a}$$

is much simplified for a dry grid, since all the liquid-phase criteria vanish; as a result we have

$$Eu = \zeta' \cdot Re_G^a \cdot \Gamma_2^f, \tag{3}$$

analogous to the equation for pipes [17].

The following symbols are used in Equations (2, 2a, and 3): g, the acceleration due to gravity (in m/sec^2); w_G, the linear gas velocity in the apparatus (m/sec); $\gamma = \rho g$, the density of the gas or liquid (kg/m^3); $\nu = \mu/\rho$, the kinematic viscosity coefficient of the gas or liquid (m^2/sec or m^2/hour); σ, the coefficient of surface tension of the liquid at the gas interface (kg/m); i, the liquid flow rate per 1 m of weir length (m^3/m · hour); h_0, the height of the original (unfoamed) layer of liquid on the grid (m); D_e, the equivalent diameter of the apparatus (it is assumed in the criteria that $D_e = 1.13$ m); b, the width of the grid (m); m, the spacing between the orifice centers (m); d_0, the diameter of an orifice (m); S_0, the cross section of the overflow orifice (m^2); H_p, the pressure head, i.e., the height of the foam layer above the center of the overflow orifice (m); B is a coefficient; ζ, the coefficient of local resistance of the dry grid; Eu, the Euler number (in the cross section of the apparatus); Re, the Reynolds number for gas and liquid; We, the Weber number; Γ, the geometrical criterion.

The criteria Eu and Re_G in Equation (3) include the gas velocity in the full section of the apparatus, W_G. In calculations of the resistance ΔP_1 of dry grids it is usual [4-14] and expedient to take into account the relationship between ΔP_1 and the gas velocity W_0 in the orifices. When W_G is replaced by W_0, D_e in Re_G should be replaced by d_0. Equation (3), referred to the grid orifices (subscript 0) is therefore expanded as follows:

$$Eu_0 = \frac{\Delta P_1 g}{\gamma_G w_0^2} = \zeta' \cdot \left(\frac{w_0 d_0 \gamma_G}{g \mu_G}\right)^a \cdot \left(\frac{m}{d_0}\right)^f \tag{3a}$$

or

$$\Delta P_1 = \zeta' \cdot w_0^{2+a} \cdot \gamma_G^{1+a} \cdot g^{-1-a} \cdot \mu^{-a} \cdot d_0^{a-f} \cdot m^f. \tag{3b}$$

It is known [15] that the open section of the grid is

$$S = A \cdot \frac{d_0^2}{m^2} = 100A \cdot \frac{w_G}{w_0} \tag{4}$$

where A is a coefficient which characterizes the method of orifice spacing; for circular orifices spaced in equilateral triangles, A = 0.91. Therefore, in Equation (3a) m/d_0 can be replaced by the ratio w_0/w_G or by the dimensionless quantity S.

Our determinations of the hydraulic resistance of grids were performed in the models of foam equipment described previously [14-16, 18], with cross sections (equal to the grid areas) of 24 to 400 cm^2; the results were also confirmed in plant equipment. The gas velocity w_G in the full section of the apparatus varied from 0.5 to 4.0 m/sec, and the velocity w_0 in the grid orifices, from 3 to 50 m/sec. Manometers were placed at the entry and exit of the apparatus; these were used to determine, first, the hydraulic resistance of the empty apparatus, and second, the resistance of the apparatus with a dry grid inserted in it. The difference between the first and second determinations gave ΔP_1.

The results of experiments with grids of thickness $\delta = 5$ mm are given in Tables 1 and 2.

The experimental data show that increase of the gas velocity in the full section of the apparatus (if S = = constant) or decrease of the open section of the grid leads to a regular increase of the dry grid resistance (Fig. 1), owing to the increase of the gas velocity in the grid orifices. It follows from Fig. 1 that the resistance of the dry grids increases greatly when the gas velocity in the apparatus and the open section of the grid reach values corresponding to gas velocities of over 20 m/sec in the orifices. The curves representing the resistance of dry grids begin to ascend steeply at this stage.

The experimental results are plotted in Fig. 2 (in logarithmic coordinates) in the form

$$\Delta P_1 = \alpha w_0^n. \tag{5}$$

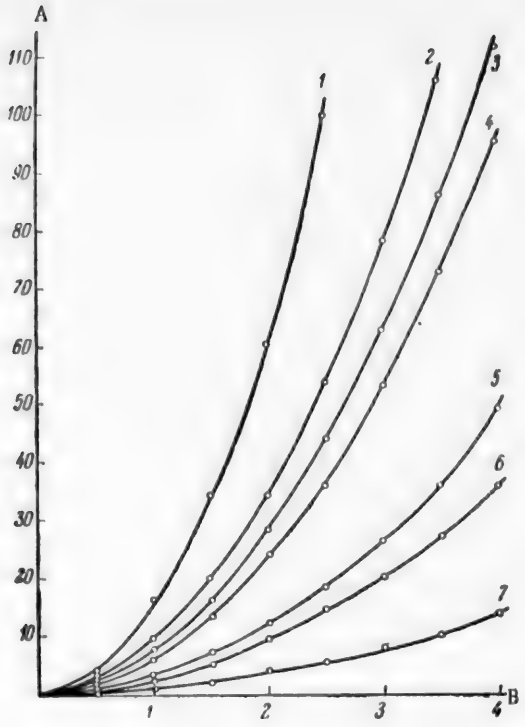

Fig. 1. Variation of the resistance of dry grids with the gas velocity in the apparatus: A) dry grid resistance ΔP_1 (mm H_2O); B) gas velocity w_G in apparatus (m/sec). Open section S of the grid (%): 1) 7.5; 2) 10.2; 3) 11.3; 4) 12.3; 5) 17.6; 6) 20.1; 7) 31.5. Model of foam apparatus with 86 x 86 mm grid.

This graph shows the measured values of the resistance of dry grids with orifices from 2 to 8 mm in diameter, open section S from 5 to 40%, grid thickness $\delta = 5$ mm, to air blown through at 16-18°, for different models of the foam apparatus.

The average straight line in Fig. 2 fits the equation

$$\Delta P_1 = 0.09 w_0^2, \tag{5a}$$

i.e., in Equation (5) the resistance coefficient $\alpha = 0.09$, and the index $n = 2$.

It must be noted that the value $n = 2$ was adopted for convenience in the use of the equation. In fact the index in Equation (5) varied between $n = 1.8$ to $n = 2.1$ for different grids, but these variations are largely balanced by simultaneous variations of the coefficient α in the opposite direction. The difference between the quadratic relationship (5a) and the actual relationship between the resistance and the gas velocity, for the usual values of $w_0 = 7$-20 m/sec is slight, and may be ignored in technical calculations. This difference, of course, increases with increase of w_0 and may reach 4-5 mm H_2O at $w_0 = 30$ m/sec.

The fact that the values of the resistance determined for different d_0, S, and cross sections of the equipment fit on one straight line in Fig. 2 shows, despite the views of a number of investigators [2, 4, 11, 19], that ΔP_1 is independent of D_{app} and d_0 in the range of d_0 from 2 to 8 mm. Therefore, in Equations (3, 3a, 3b) $f = 0$, but, since ΔP_1 is independent of d_0, in Equation (3b) $a - f = 0$, i.e., $\underline{a}$ is also 0.

Thus, Equation (3) reduces to a form normal for the second self-modeling region:

$$Eu_0 = \text{const} = \zeta'. \tag{6}$$

Usually [5, 9-11, 20] the hydraulic resistance of grids is represented by an equation which is general for all forms of local resistances in turbulent motion

$$\Delta P_1 = \zeta (\gamma_G/2g) w_0^n, \tag{7}$$

where it is assumed that the index $n = 2$. The results of our experiments, expressed in the form of Equation (5a), show that when air at 18° is blown through the grids ($\gamma_G = 1.22$), $\underline{n}$ is again 2, and $\alpha = \zeta \cdot \gamma_G/2g = 0.09$, and hence $\zeta = 1.45$. From Equations (3, 6 and 7) we find that the coefficient of local resistance of the grids is

$$\zeta = 2Eu_0. \tag{8}$$

It is clear from the foregoing that the main object of the experiments is determination of the values of Eu_0 or of the coefficient of local resistance ζ, as the other parameters in the right-hand side of Equation (7) are very easily found.

In most determinations of the resistance of dry grids, air was blown through the grids at room temperature. The values of the coefficient α in Equation (5) differ considerably in such determinations. For example, Usiukin

TABLE 1

Resistance ΔP_1 of Dry Grids, for a Model 86 x 86 mm in Section (With Air Blow, t = = 18°).

Grid characteristics			Dry grid resistance ΔP_1 (in mm H_2O) with gas velocity w_G in the apparatus (m/second)						
m/d_0 (mm)	number of orifices	open section S (%)	1.0	1.5	2.0	2.5	3.0	3.5	4.0
10/3	80	7.5	16	34	60	100	144	196	255
12/4	52	8.7	12	26	48	74	108	146	190
6/2	217	9.1	10	24	44	68	98	134	174
14/5	39	10.2	9	19	35	55	80	106	140
8/3	120	11.3	7	16	28	44	63	86	112
5/2	294	12.3	6	13	24	36	53	73	96
10/4	80	13.4	5	12	18	32	45	61	77
12/5	52	13.6	5	11	18	30	43	59	77
14/6	39	14.7	5	10	17	27	39	52	68
4/2	421	17.6	3	7	12	18	26	36	46
6/3	188	17.7	2	6	11	17	26	35	45
8/4	120	20.1	2	5	9	14	20	27	36
5/3	294	27.8	1	3	4	7	10	14	19
6/4	188	31.5	—	2	3	6	8	10	14

TABLE 2

Resistance ΔP_1 of Dry Grids, for a Model 200 x 60 mm in Section (With Air Blow, t = = 18°).

Grid characteristics			Dry grid resistance ΔP_1 (in mm H_2O) with gas velocity w_G in the apparatus (m/second)						
m/d_0 (mm)	number of orifices	open section S (%)	1.0	1.5	2.0	2.5	3.0	3.5	4.0
6/2	244	6.4	22	50	85	138	196	270	—
14/5	54	8.8	11	26	46	75	106	140	185
8/3	158	9.3	10	23	41	65	93	127	166
12/5	58	9.5	10	22	39	62	90	120	158
5/2	365	9.6	10	22	39	61	88	120	156
16/7	35	11.2	7	16	28	44	64	86	112
14/6	54	12.7	6	12	22	35	51	69	90
18/8	31	13.0	6	12	22	34	50	65	85
12/6	58	13.7	5	11	19	30	43	58	77
8/4	135	14.1	5	10	18	28	41	56	72
6/3	244	14.4	4	10	17	27	38	53	69
5/2.5	365	14.9	4	9	16	25	36	49	65
10/5	92	15.1	4	9	16	25	35	48	63
4/2	592	15.5	4	9	15	23	34	46	60
10/6	92	21.7	2	4	8	11	17	22	30
8/5	135	22.1	2	4	7	10	17	21	29
6/4	244	25.5	1	3	5	9	11	16	22

and Aksel'rod [5] and Sobchuk and Surkov [8] found $\alpha = 0.12$, whereas Romankov, Noskov and Sokolov [11], and Mayfield, Church, et al. [10] found $\alpha = 0.086$. Our experiments gave $\alpha = 0.09$, the experiments of Kuz'minykh and Rodionov [12] (with $\gamma_G = 1.2$) and of Arnold, et al. [9] gave $\alpha = 0.109$, etc. In an attempt to find the causes of these differences, we studied the influence of various factors on α or ζ. The view advanced by some authors [3, 4, 19] that α and ζ depend on D_{app}, d_0, and the distance between grids was not confirmed by our experiments, for variations of D_{app} from 36 to 2700 mm, of d_0 from 2 to 8 mm, and of the distance between grids from 400 to 800 mm. Analysis of Equation (3b) shows that a = 0, and the gas viscosity μ should also be without any influence on α and ζ.

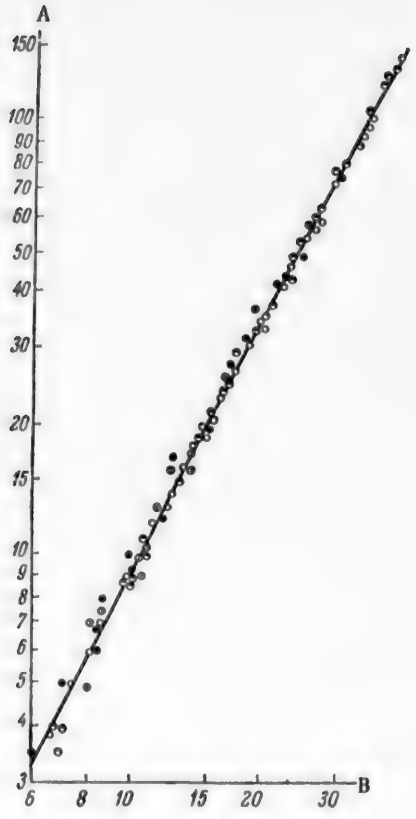

Fig. 2. Variation of the resistance of dry grids with the gas velocity in the orifices: A) dry grid resistance ΔP_1 (in mm H_2O); B) gas velocity in orifices, w_0 (m/sec). Different points correspond to the following grid dimensions in model foam apparatus: 86 x 86, 60 x 40, 120 x 60 mm and d = 96 mm.

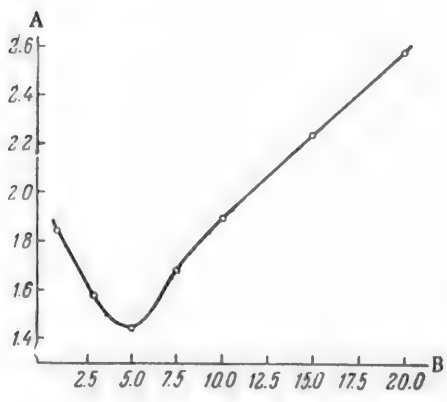

Fig. 3. Variation of the coefficient of local resistance ζ with the grid thickness: A) coefficient of local resistance ζ; B) grid thickness δ (mm).

The resistance coefficient of slotted grids with notched slots 1, 2, and 3 mm wide may be assumed equal to the coefficient for grids with circular drilled orifices, although there is some tendency for the resistance of slotted grids to be lower than that of the usual type of grid.

The experimental data show that at $d_0 = 2$ mm the gas remains in turbulent motion ($Eu_0 = const$) with decrease of Re_G in the grid orifices to 400 (i.e., $w_0 = 3$ m/sec) and in the full section of the apparatus to 930, whereas in smooth circular pipes the transition to laminar flow occurs at $Re_{cr} \sim 2100$. It was noticed that for grids with large orifices of $d_0 = 6$-8 mm and S > 30%, ζ and Eu_0 begin to decrease at $w_0 = 3$ m/sec; therefore, the value of Re_{cr} for the transition from laminar to turbulent motion increases with increase of d_0.

The friction of the gas against the orifice walls depends on the orifice outline, wall roughness, and edge finish. The influence of orifice finish was studied by Usiukin and Aksel'rod, and is confirmed by the results of our experiments. Decrease of roughness as the result of application of bakelite varnish to the grid leads to a decrease of $\alpha(\zeta)$. For example, the resistance coefficient of a steel grid of thickness $\delta = 5$ mm, with drilled orifices of $d_0 = 2$ mm and S = 10%, decreased by 25% after application of a thin layer of bakelite varnish (the decrease of d_0 caused by the bakelite film was not taken into account in the calculation).

In earlier investigations the grid thickness was ignored, and experimental data for grids of different thickness were compared. In some cases [9, 10] it was even erroneously concluded that the grid resistance does not depend on the grid thickness δ. However, we had shown [15, 18] that the grid thickness has a significant influence on the value of the resistance coefficient ζ.

The relationship between ζ and δ is plotted in Fig. 3. The lowest resistance is found for grids of thickness $\delta = 5$ mm, for which the resistance coefficient $\zeta = 1.45$. The grid resistance increases both with decrease and with increase of δ. If the resistance of a grid 5 mm thick is taken as unity, the factor K by which the resistance is increased has the following values for different grid thicknesses:

Grid thickness (mm)	1	3	5	7.5	10	15	20
Increase factor K	1.25	1.1	1.0	1.15	1.3	1.5	1.7

Analysis of the numerical values of α found by different workers, and of their experimental conditions, showed that the main cause of the apparent contradictions mentioned earlier is the difference of grid thickness, the influence of which was not taken into account.

In our experiments the resistance coefficient of a grid 5 mm thick was $\alpha = 0.09$. Usiukin and Aksel'rod [5] found that $\alpha = 0.12$ for $\delta = 0.8$ mm. Extrapolation of the values of the increase factor gives K = 1.27. Therefore, for $\delta = 5$ mm, by Usiukin's data, $\alpha = 0.094$. The data of Mayfield et al. [10],

calculated in metric units, give $\alpha = 0.086$ for an average grid thickness of ~6 mm. The results of Kuz'minykh et al. [12], and of Arnold et al. [9], obtained with grids of average thickness $\delta = 2$ mm, give $\alpha = 0.093$ for $\delta = 5$ mm. Romankov, Noskov and Sokolov [11] found $\alpha = 0.087$ for $\delta = 3$ mm (i.e., for the optimum region of grid thickness). It is seen that the experimental data obtained by different workers, when reduced to the same optimum grid thickness, are in very close agreement, and the average value of $\alpha = 0.09$ ($\zeta = 1.45$) agrees with our value.

However, values of α obtained under different conditions are sometimes unjustifiably equated in the literature. For example, Sobchuk and Surkov [8], in confirmation of their value for $\alpha = 0.12$ at $\delta = 5$ mm, refer to the agreement of this result with Usiukin and Aksel'rod's data ($\alpha = 0.12$ for $\delta = 0.8$ mm). In reality, Sobchuk's data contradict rather than are confirmed by the values of α obtained by others.

Thus, experimental data show that the optimum grid thickness with regard to hydraulic resistance is 5 mm. This explains why Mayfield, Church et al. [10] did not find that δ had any influence on ΔP_1. The reason is that they compared the resistance of grids from 3 to 9 mm thick, i.e., with values of δ differing little from the optimum thickness in either direction; the usual experimental errors therefore masked the influence of grid thickness on the resistance.

The hydraulic resistance of dry grids can be calculated by means of the formula:

$$\Delta P_1 = 1.45K\,(\gamma_G w_0^2/2g)\ \text{mm } H_2O \tag{9}$$

or

$$Eu_0 = 0.725K, \tag{9a}$$

where K is found from the data presented above.

The influence of γ_G in Equation (9) was verified by experiments with air at different temperatures. For air at room temperature (15-20°), and for other gases with $\gamma_G \sim 1.2$ kg/m^3, Equation (9) becomes

$$\Delta P_1 = 0.09Kw_0^2\ \text{mm } H_2O\ (\text{kg/m}^2). \tag{9b}$$

When grid apparatus is used in foaming conditions – in foam apparatus – it is not necessary to use gas velocities greater than 20 m/sec in the orifices, as foaming is not improved thereby. In industrial foam equipment w_0 is usually between 7 and 15 m/sec, and the hydraulic resistance of the grid is only 5-20 mm H_2O.

SUMMARY

1. Analysis of the criterial equation for hydrodynamic similarity of shelves of the sieve apparatus yielded Equations (3) and (3a), characterizing hydrodynamic similarity for the flow of gas through the orifices of a dry grid.

2. It was shown experimentally that, contrary to the views of a number of workers, the hydraulic resistance of the grid is independent of the diameter of the apparatus or the diameter of the grid orifices, over a wide range of these diameters.

3. It is confirmed that the grid resistance is proportional to the square of the gas velocity; i.e., that the Euler criterion, characteristic of the second self-modeling region, is constant.

4. Equation (9) for calculation of the hydraulic resistance of dry grids was derived from the results of experimental determinations of the coefficient of local resistance for different grid thicknesses.

5. It is shown that the apparent discrepancies between the resistance coefficients determined by different workers are largely due to the fact that the grid thickness was not taken into account.

LITERATURE CITED

[1] I.L. Peisakhov and V.I. Kuznetskii, J. Chem. Ind. 8, 21 (1938).

[2] V.N. Stabnikov, Trans. Voronezh. Chem. Tech. Inst. 3-4, 177 (1939); Chemical Machine Construction 2, 9 (1940).

[3] E. Kirschbaum, Destillier- und Rektifiziertechnik (Berlin, 1940).

[4] N.M. Zhavoronkov and I.E. Furmer, Oxygen 5, 9 (1947).

[5] I.P. Usiukin and L.S. Aksel'rod, Oxygen 1, 1 and 2, 5 (1949).

[6] L.S. Aksel'rod and V.V. Dil'man, Oxygen 6, 9 (1950).

[7] V.N. Stabnikov and S.E. Kharin, Theoretical Principles of the Distillation and Rectification of Alcohol (Food Industry Press, 1951).•

[8] Iu.I. Sobchuk and E.I. Surkov, J. Chem. Ind. 6, 165 (1952).

[9] D.S. Arnold, S.A. Plank and E.M. Schoenborn, Chem. Eng. Progr. 48, 12, 633 (1952).

[10] F.D. Mayfield, W.Z. Church, A.C. Green and Lee, Ind. Eng. Chem. 44, 9, 2238 (1952).

[11] V.N. Sokolov, Candidate's Dissertation (Lensoviet Tech. Inst., Leningrad, 1953).•

[12] I.N. Kuz'minykh and A.I. Rodionov, Trans. MKhTI 18, 109 (1954).

[13] V.V. Dil'man, E.P. Darovskikh, M.E. Aerov and L.S. Aksel'rod, J. Chem. Ind. 3, 156 (1956).

[14] I.P. Mukhlenov, Doctorate Dissertation (Lensoviet Tech. Inst., Leningrad, 1955).•

[15] M.E. Pozin, I.P. Mukhlenov, E.S. Tumarkina and E.Ia. Tarat, The Foam Method for Treatment of Gases and Liquids (Goskhimizdat, 1955).•

[16] I.P. Mukhlenov, J. Appl. Chem. 30, 12, 1750 (1957).••

[17] P.G. Romankov, Hydraulic Processes in Chemical Technology (Goskhimizdat, 1948).•

[18] M.E. Pozin, I.P. Mukhlenov and E.Ia. Tarat, The Foam Method for Removal of Dust, Smoke, and Mist from Gases (Goskhimizdat, 1953).•

[19] A.A. Grigor'ev, Chemical Machine Construction 7, 6, 3 (1938); 8, 7, 8 (1939).

[20] A.G. Kasatkin, Principal Processes and Equipment of Chemical Technology (Goskhimizdat, 1955).•

Received October 23, 1956

•In Russian.

••Original Russian pagination. See C.B. translation.

THE HYDRAULIC REGIMES WHICH ARISE IN SIEVE AND BUBBLE-CAP EQUIPMENT

R.A. Melikian

The S.M. Kirov Works Central Scientific Research Laboratory, Erevan

Investigation of the hydrodynamic regimes arising in sieve and bubble-cap equipment is an important and very urgent task. Numerous investigations of Soviet authors, including that of Pozin, Mukhlenov and Tarat [1], are devoted to this problem. Their paper is also particularly valuable because it goes outside the scope of the usual scientific paper and raises a discussion on the topic in question.

The present paper is published in order to develop this discussion, as in our opinion a number of essential questions are wrongly interpreted by these authors.

The equipment does not determine the nature of the hydrodynamic regime. In sieve and bubble-cap equipment used in industry, gas bubbles usually ascend in large numbers through a liquid medium. We have shown [2] that several different hydrodynamic regimes may arise in the process, depending on the velocity of the gas and the physicochemical nature of the liquid; the first regime to be established is always free ascent of the bubbles in the liquid layer, generally described as the bubbling regime. With increase of the gas velocity above a definite critical value, this passes into the streaming or the foam regime, depending on the nature of the liquid and the process conditions. A bubbling-streaming or mixed regime, or a mixed-foam regime may exist within certain limits of gas velocity. Thus, different hydrodynamic regimes may arise in the same sieve or bubble-cap tower at different gas velocities and with different liquids. Therefore, expressions such as "the hydrodynamics of sieve and bubble-cap equipment" or "the hydrodynamics of gas lifts" are erroneous in form and meaning.

Three streams coexist in the bubbling process, regardless of the design of the equipment. The authors cited [1] write: "Melikian's assumption of the presence of three coexisting streams, in general valid with reference to narrow gas lifts, is inappropriately used by him to explain the hydrodynamics in bubbling and foam equipment."

We showed by thermodynamic analysis that the phenomenon of bubble ascent involves the action of three coexisting flows [2]. It is true that this was based on a consideration of the ascent of a single bubble, but a similar analysis for groups of bubbles should lead to an analogous result for bubbling conditions. A repetition of the previous thermodynamic analysis would be superfluous in this paper; we will attempt to prove this point more clearly by logical analysis.

Consider a vessel of any cross section F, filled with liquid to any level h. When gas bubbles are introduced into the lower part of the vessel, the formation of an ascending flow (the first flow) of liquid in the vessel is inevitable, as the liquid displaced by the gas must move upward from below. The intensity of this liquid flow is independent of the number of bubbles; it depends on the volume of gas only. In this case the action of the bubbles is analogous to the action of a piston placed in the bottom of the vessel, which displaces the whole column h of liquid upward by a distance Δh (Fig. 1).

If n is the number of bubbles, V the total volume of the gas, and F the cross section of the vessel, then $\Delta h = V/F$ and is independent of n. It is clear that if the gas is introduced continuously into the vessel, the ascending liquid flow in the vessel is also continuous, and has the velocity

$$V_{sec}/F = w_{cm}, \qquad (1)$$

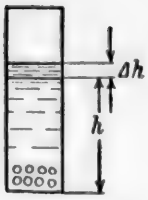

Fig. 1. Vessel with liquid after introduction of gas bubbles: h) initial liquid level; Δh) change of level after introduction of gas bubbles in the lower part of the vessel.

where V_{sec} is the volume of gas entering the vessel per second. It must be pointed out that if the bubbles are introduced continuously the ascending flow does not consist of liquid only, as after a certain time the bubbles will occupy a definite fraction of the volume of the liquid column, and will move together with it. It is seen that the authors' assertion that "the hydrodynamics of sieve and bubble-cap equipment used in industry differs in principle from the hydrodynamics of gas lifts, primarily by the absence of a stream of ascending gas-liquid mixture" is entirely unfounded. The principle of action of sieve and bubble-cap apparatus is the introduction of gas bubbles into a liquid layer; this inevitably results in an upward flow of the mixture, irrespective of the cross section and design of the apparatus. The gas bubbles present in the liquid medium immediately cause the formation, by the action of Archimedes' forces, of a second flow – a flow of ascending bubbles in a rising liquid stream. Only the flow of ascending bubbles is observed visually, while the flow of ascending liquid remains unnoticed. This often leads to errors, as the displacement of the bubbles relative to the walls of the vessel in unit time is taken to be the ascent velocity of the bubbles, whereas it is the sum of two velocities – the velocity of bubble ascent and the velocity of flow of the ascending mixture. The velocities of individual bubbles cannot be determined in mass ascent of bubbles. Moreover, this quantity is not characteristic, as the velocities of individual bubbles alter during ascent owing to changes in the crowding conditions and in bubble size. The average ascending velocity of the bubbles over a given region is the most characteristic magnitude in the process, and is the value which should be used.

The average ascent velocity of bubbles over a given region is given by the equation

$$w_s = V_{sec}/F_G, \tag{2}$$

i.e., the ratio of the volume of gas entering per second (V_{sec}) to the fraction of the cross section of the vessel (F_G) occupied by the gas in this vertical region.

The third flow is the flow of descending liquid. The existence of this flow in bubbling can be easily proved by means of the argument used [1] to deny the existence of this flow. The authors state: "The statistical average speed of the liquid is such that the projection of its vector on the vertical axis is zero, i.e., all the vertical pulsations of the liquid mutually cancel each other." It was demonstrated above that an ascending flow of gas-liquid mixture is inevitable in the bubbling process, and therefore, if the argument is valid, the liquid displaced upward by this flow should return downward completely in order that "all the vertical pulsations of the liquid [should] mutually cancel each other." The validity of the authors' argument with respect to the bubbling process is obvious, as in the steady process the level of the gas-liquid mixture remains unchanged. How and why the descending flow of liquid originates is discussed in adequate detail in our preceding communications [2, 3]. The velocity of this flow (w_L) also varies along the height of the layer of mixture. Its average value for a definite region of the layer can be expressed as the ratio of the volume of liquid flowing down per second (which is equal to V_{sec}) to the fraction of the cross section of the vessel occupied by the liquid.

$$w_L = V_{sec}/(F - F_G). \tag{3}$$

On the foregoing considerations, the hydrodynamics of the bubbling process can be represented as a continuous ascending flow of liquid in which gas bubbles float up freely, surrounded by a flow of descending liquid; i.e., as a combination of three coexisting flows. The velocities of these flows are interrelated [3] as follows:

$$w_L = w_{cm}/(1 - w_{cm}/w_s). \tag{4}$$

The views of Aksel'rod and Dil'man on the hydrodynamics of the bubbling process [4] are in principle similar to ours; they consider that a descending and an ascending flow of liquid are formed in the process, and that these flows are equal in each layer. In confirmation, they cite the experimental fact that the liquid is displaced both upward from below and downward from above in the process. However, their concept contains certain inaccuracies. They write: "The liquid drawn up from the bottom of the bubbler by the newly formed bub-

Fig. 2. Velocity distribution in the descending liquid flow.

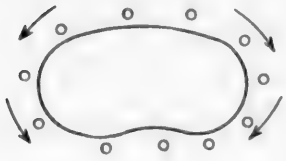

Fig. 3. Direction of the liquid flow around an ascending bubble.

bles is transferred upward in the layers between the consecutive bubbles." We cannot agree with this. First, it is seen that the bubbles do not draw up liquid from the bottom of the vessel but displace it; second, the whole column of liquid with ascending bubbles, around which the returning liquid flows, is displaced upward. Moreover, the velocity distributions assumed by Aksel'rod and Dil'man for the descending liquid require correction.

In accordance with the action of gravitational forces, the maximum velocities are found at the boundaries between the bubbles and the liquid, while the velocities decrease within the depth of the liquid film situated vertically between two neighboring bubbles (Fig. 2).

The accuracy of the quantitative equations for the flow velocities is indubitable. Pozin, Mukhlenov and Tarat state in their paper [1] that "The speed of the descending liquid stream is incorrectly referred to the whole cross section occupied by the liquid, as part of the cross section should be referred to the ascending liquid stream entrained by the gas bubbles as the result of friction."

We consider that the forces of viscous friction between a freely ascending gas bubble and the liquid flowing around it are far from sufficient for inversion of the boundary liquid film, and therefore there can be no question of the existence of an ascending stream of liquid drawn up by the gas bubble by friction.

This is easily demonstrated by a simple experiment. If a viscous liquid (glycerol) is shaken vigorously with air, a stable dispersion of very fine air bubbles in the liquid can be obtained. If large gas bubbles are passed through the disperse system, the behavior of the liquid at the interface can be studied visually. It was found in such an experiment that when a bubble ascends the boundary liquid layer is displaced downward only, flowing around the bubble from above (Fig. 3).

Moreover, Semenov [5] demonstrated in a study of the behavior of the boundary film of a freely descending liquid in presence of a countercurrent stream of gas that for inversion of the boundary liquid film under these conditions the velocity of the countercurrent gas must exceed 7.5 m/sec. In the free ascent of gas bubbles, the liquid film in contact with the ascending bubble meets a gas stream with a velocity less than 0.5 m/sec. The velocity of free ascent of the gas is therefore very much less than the velocity at which the boundary liquid film can be drawn upward. Finally, the free descent of liquid drops in a gas has been observed frequently, but upward inversion of the boundary liquid film has never been observed under such conditions.

In our opinion, all the foregoing shows quite convincingly that a gas bubble under the action of gravitational forces is incapable of drawing the boundary liquid film upward, and therefore the quantitativeEquations (1, 2 and 3) for the flow velocities are exact, and not only for gas lifts. However, because of viscous friction at the interface, inversion of the boundary film does take place in the free ascent of bubbles in a liquid, but this is inversion of the gas film and not of the liquid film. It is known that liquid viscosities are hundreds of times greater than gas viscosities. When a bubble floats upward, the frictional forces acting on the interface create a return boundary flow of gas directed from the center of the bubble to its periphery, parallel to the surrounding flow of liquid. Because of this, the ascent of the bubble is accompanied by closed circulation of the gas, leading to a decrease of its resultant ascent velocity. The existence of closed circulation was demonstrated by Shabalin [6], who observed it when a jet of smoke was introduced into an ascending air bubble. His observations were confirmed by Garner and Hamerton [7]. It would be very interesting to determine the velocity of this circulation, since it would give an idea of the rate of renewal of the boundary gas film, but no method for theoretical or experimental determination of the circulation velocity of a gas is known at present.

In our opinion, the following method can be used for approximate estimation of this velocity.

If it is assumed that a gas bubble ascends in an ideal liquid, its upthrust is totally expended in producing the velocity. Here

$$V(\gamma_L - \gamma_G) = V\gamma_G \frac{w_G^2}{2g\delta},$$

and hence

$$w_G = \sqrt{2g\delta\left(\frac{\gamma_L}{\gamma_G} - 1\right)},$$

where V is the volume of the bubble, γ_L is the density of the liquid, γ_G is the density of the gas, w_G is the theoretical velocity of the gas, δ is the height of the gas bubble, and g is the acceleration due to gravity.

Further, on the assumption that the ascent velocity of a gas in a real liquid decreases because of the formation of a boundary return gas flow, resulting in closed circulation of the gas, the circulation rate (n) can be determined.

$$(1+n) = \frac{w_G}{w_s} = \sqrt{2g\left(\frac{\gamma_L}{\gamma_G} - 1\right)\frac{\delta}{w_s^2}},$$

where w_s is the experimental value of the ascent velocity of the bubble in the liquid, and n is the frequency of circulation per second.

The presence of an overflow weir in the apparatus alters only the quantitative ratio of the flows. The assertion [1] that "all the vertical pulsations of the liquid mutually cancel each other" is incorrect in relation to industrial equipment fitted with weirs or other overflow devices. We have seen that, when gas bubbles rise freely in a liquid layer without removal of the liquid, the amounts of liquid in the ascending and descending flows are indeed equal to each other, but if liquid is removed this equilibrium is disturbed. In industrial equipment liquid is generally fed in from below, and removed from above, through the overflow weir. In such cases the ascending flow of mixture takes up not only the amount of liquid which comes down with the descending flow, but also the amount removed from the top of the apparatus. The nature of the flows does not alter, but, in contrast to ordinary bubbling, there is a constant tendency to reach an equilibrium level of the gas-liquid mixture. However, equilibrium is unattainable, since in equipment with liquid removal the height of the overflow weir is below the equilibrium level of the gas-liquid mixture.

A definite quantitative relationship exists between the height of the overflow weir, the gas rate, the initial height of the liquid layer, and the amount of liquid removed.

This relationship follows from the fact that when a gas ascends in a liquid layer under equilibrium conditions the work of expansion of the gas is completely expended for raising the descending liquid [2], i.e.,

$$P_1 \cdot V_{sec} \cdot \ln\frac{P_1}{P_\tau} = \gamma \cdot F \int_h^H w_s \cdot d \cdot \Delta h. \tag{5}$$

If some of the liquid is removed from the apparatus in the process, the work of expansion of the gas must ensure the ascent of the removed as well as the descending liquid.

In this case the law of conservation of energy is expressed as follows:

$$P_1 V_{sec} \ln\frac{P_1}{P_\tau} = \gamma F \int_h^H w_s d\Delta h + \gamma Q (H - h), \tag{6}$$

where P_1 is the initial pressure of the gas, P_τ is the final pressure of the gas, V_{sec} is the volume of the gas fed in per second, Q is the volume of liquid removed per second, γ is the density of the liquid, F is the cross section of the vessel, H is the height of the gas-liquid mixture (overflow weir), and h is the initial height of the liquid.

For solution of the integral it is assumed that the ascent velocity in the given layer has a certain average constant value (w_s); we then have

$$P_1 V_{sec} \ln\frac{P_1}{P_\tau} = F\gamma (w_s)_{av} (H - h) + \gamma Q (H - h), \tag{7}$$

and hence

$$Q = \frac{P_1 V_{sec}}{\gamma (H - h)} \ln \frac{P_1}{P_2} - (w_s)_{av} \cdot F. \qquad (8)$$

Equation (8) can be used for calculation of the amount of liquid removed, both in gas lifts and in equipment fitted with overflow weirs, if the value of (w_s) is known.

It is clear from the foregoing that Pozin, Mukhlenov and Tarat give a wrong interpretation of the influence of the overflow weir on the hydrodynamics of the process.

Characteristics of the hydrodynamic regime of the process. Pozin, Mukhlenov and Tarat do not agree with our view that the flow velocities are the parameters which determine the hydrodynamic regime, and ask "what is determined in "the hydrodynamic regime of a gas-liquid layer in sieve apparatus" and give the answer: "The determinable parameters of the regime are usually considered to be . . . the height of the gas-liquid layer H (or its density γ, inversely proportional to H) and the hydraulic resistance ΔP."

As the "determining parameters" they give a whole series of quantities which are functionally related to H and ΔP.

$$H = f_1(w_G, i, h_O, s_O, \mu_L, \gamma_L, \sigma),$$

$$\Delta P = f_2(w_G, i, h_O, s_O, \mu_L, \gamma_L, \sigma),$$

where $\underline{w}$ is the velocity of the gas, $\underline{i}$ is the liquid rate, h_O is the height of the overflow weir, μ_L is the viscosity of the liquid, σ is the surface tension at the gas-liquid interface, γ_L is the density of the liquid, and s_O is the area of the overflow weir.

The authors cite determinations of these relationships "for certain bubbling regime conditions" and "in relation to the foam regime."

In the investigations cited a number of very valuable quantitative relationships were established, but they related to problems with which the present study is not concerned, as these quantitative relationships cannot reveal the hydrodynamics of the process under consideration or shed light on the mechanism and possible variations in its nature.

In our opinion, a hydrodynamic characterization of the ascent of gas bubbles in liquid layers in any type of equipment requires more or less exhaustive answers to the following questions: what are the processes which can take place and how are they interrelated; what is the hydrodynamics of each of these processes; what are the hydrodynamic quantities which characterize these processes, and how do these processes differ from each other?

Pozin, Mukhlenov and Tarat reject our hydrodynamic classification [2, 3], and propose the following definition for hydrodynamic regimes: "From our point of view, this regime is more correctly described as the foam regime, as foam is the accepted term for a disperse system consisting of a gas and a liquid, irrespective of its structure."

By this definition, any disperse system consisting of a gas and a liquid is a foam system. Since in all processes where gas ascends through a liquid layer we have "a disperse system consisting of a gas and a liquid," it follows that the foam regime is always present. It is hardly necessary to point out that this definition, by its vagueness, can confuse the problem of hydrodynamic classification of processes of gas ascent in liquid layers. The authors themselves admit the existence of a bubbling regime as distinct from the foam regime. How is bubbling to be distinguished from foaming?

The hydrodynamic regime in the ascent of gases through liquids in any apparatus depends on numerous factors. The problem is to select the minimum number of parameters for the most complete characterization of the given process. In our opinion the flow velocities are the required parameters.

If it is accepted in advance that the term "bubbling" represents free ascent of gas bubbles through a liquid layer, then, as we have shown, bubbling is characterized by the presence of three coexisting flows [2]. Because of the low viscosity of the gas, the flow of ascending bubbles is turbulent.

An idea of the hydrodynamics of the other coexisting flows can be obtained from the magnitude of the Reynolds number. This cannot be precisely defined for the downward flow of liquid. Its value can be approximately found by means of the following equation:

$$Re_f = \frac{h}{H-h} \cdot \delta \cdot \frac{\sqrt{2g\delta} \cdot \rho}{\mu}.$$

In this expression the equivalent diameter is replaced by the ratio $(h \cdot \delta)/(H - h)$, while the flow velocity is assumed to be $\sqrt{2g\delta}$, where δ is the average height of the gas bubbles; $h/(H - h)$ is the volume ratio of liquid to gas in the layer of mixture, and g is the acceleration due to gravity.

In all cases, including those in which the flow of the descending liquid around the bubble is laminar, renewal of the boundary liquid film during bubbling is inevitable. It is effected after the liquid has flowed around each bubble. Therefore, processes of diffusion and heat transfer are very intensive during bubbling.

It has been shown [3] that Equation (4), which connects the flow velocities, determines the extent of the bubbling regime, which lies in the range $0 > w_m/w_s > 1$, and that the critical gas velocity for the transition from bubbling to foaming or streaming is given by the equation

$$(w_m)_{cr} = [(F_G)_{max}/F]\, w_s.$$

On the first page of their paper, Pozin, Mukhlenov and Tarat [1] deny both the existence of the flows, and the determining significance of their velocities as hydrodynamic parameters. However, this does not prevent them from asserting, on the third page of their paper, what had been demonstrated by us by means of the above equation.

They present this equation in the form of the inequality

$$w_G > w_b \cdot \varphi_G,$$

where w_G is the velocity of the gas, equal to w_m; w_b is the velocity of bubble ascent, equal to w_s; φ_G is the fraction of the cross section occupied by the gas, equal to $(F_G)_{max}/F$.

They proceed similarly with the inequality (7)

$$H_{cr}/2 < h \text{ or } (H/H_{cr}) > 0.5.$$

[in the text [3] $(H_{cr}/2) < 2$ is printed instead of $(H_{cr}/2) < h$].

We used this inequality to show [3] that in the bubbling regime "the gas content of the liquid layer is always less than half of the layer." The authors state that $\varphi_G < 0.5$ is typical for the bubbling layer, and $\varphi_G > > 0.5$, for the foam layer. Here φ_G is the volume fraction of gas in the liquid layer.

The authors express φ_G in several ways ([1], Equations 3, 4 and 5), and give the same relationships as those given by us, but in different form.

It has already been shown [3] that the equation which expresses the functional relationship between the flow velocities not only determines the extent of the bubbling regime, but also indicates the possible directions of the transition which takes place.

We turn once again to Equation (4). It contains three variables, and represents the dependence of w_L on w_m and w_s. It is seen that, for a given liquid, only the velocity of the gas feed (w_m) can be varied, while w_s and w_L depend on w_m.

We see that when w_m is increased above $(w_m)_{cr}$ the descending liquid flow undergoes a sharp qualitative change. The equation shows that there are only two possibilities: a) the ratio w_m/w_s remains in the region $(w_m/w_s) < 1$ and w_L remains positive, and b) the ratio w_m/w_s passes into the region $(w_m/w_s) > 1$ and w_L becomes negative. Experience confirms this theoretical result; in the former case the bubbling regime passes into the streaming regime, and in the second, into the foam regime.

The mechanism of the transitions from bubbling to the streaming and foam regimes was briefly considered earlier [2]; a small additional explanation may be given here.

At the instant of transition the cross section of the vessel is physically capable of accomodating two flows simultaneously. Therefore, either the descending liquid flow must give up the fraction of the cross section which it occupies and turn upward, or the stream of ascending bubbles must become more closely packed, releasing part of the section occupied by it.

Inversion of the descending liquid flow is rare, as a necessary condition is that the liquid films surrounding the ascending bubbles must withstand the hydrostatic pressure in the layer, which is possible only in small layers of liquid, and only if the forces of surface tension predominate. Usually, and inevitably if the liquid layers are thick, the gas bubbles merge into a continuous stream under the action of the hydrostatic pressure. The velocity of ascent of a continuous stream is immeasurably greater than that of single bubbles, and therefore the bubbling and streaming regimes alternate in the same liquid layer over a wide range of velocities of the gas feed, from $(w_m)_{cr}$ to $(w_G)_{cr}$.

The streaming regime represents [2] the simultaneous action of three concentric flows: the center contains a continuous gas stream, surrounded by two liquid streams: an ascending stream resulting from the friction between the gas and liquid, and a descending stream resulting from the action of gravity. The second type of transition occurs in the region $(w_m/w_s) > 1$, and therefore w_L becomes negative, i.e., the stream of descending liquid is reversed upward.

Flows of ascending mixture, ascending bubbles, and ascending liquid may act after the transition. There is no doubt concerning the existence of flows of ascending mixture and ascending bubbles, as they were present under the bubbling regime, and persist under the new regime. It is not clear what forces could cause inversion of the descending liquid flow. It was shown above that the velocity of bubble ascent is such that the force of viscous friction between the ascending gas and the descending liquid flow is incapable of changing the direction of the liquid; therefore, other forces must cause the inversion. In this process the only force capable of causing inversion of the liquid flow and raising the liquid with the ascending gas stream is the force of surface tension.

Therefore, the liquid can ascend with the gas only in the form of foam films, and accordingly this is termed the foam regime. At the start of the transition foam can form only on the surface of the layer, as the amount of gas is insufficient to raise the whole liquid in the form of foam films. Therefore, two regimes must be operative in two different layers over a definite range of w_m. The transition is then completed, and the foam regime sets in throughout the layer if the amount of incoming gas is sufficient to carry away all the liquid in the form of foam films.

If the foam films are so stable as to resist renewal, the three above-mentioned flows must merge into one, into a flow of stable (immobile) foam.

In our opinion, further study of the hydrodynamics of gas emersion must be clearly differentiated, i.e., each hydrodynamic regime must be studied separately; the results should prove much more fruitful.

SUMMARY

1. In any type of apparatus, when a gas ascends through a layer of liquid, four different hydrodynamic regimes may arise, depending on the velocities of the acting streams: a) the bubbling regime, i.e., free ascent of gas bubbles through the liquid layer; b) the mixed regime, in which bubbling and streaming regimes alternate in the same liquid layer; c) the streaming regime; d) the foam regime, which may coexist with the mixed regime over a definite range of gas velocities.

2. The velocities of the acting flows are quite sufficient for hydrodynamic classification of the emersion effect in liquid layers, i.e., for determination of the regime of the process.

3. In any equipment, including sieve-plate apparatus, bubbling represents the action of three coexisting flows.

4. The design and dimensions of the apparatus do not determine the hydrodynamic regime of the process.

5. The presence of a weir or other overflow devices in the apparatus cannot alter the hydrodynamic character of the process, but influences the relative flows. In such cases the amount of liquid removed can be precisely defined by means of Equation (8).

LITERATURE CITED

[1] M.E. Pozin, L.P. Mukhlenov and E.Ia. Tarat, J. Appl. Chem. 30, 1, 45 (1957).*

[2] R.A. Melikian, J. Appl. Chem. 29, 12, 1792 (1956).*

[3] R.A. Melikian, J. Appl. Chem. 30, 1, 38 (1957).*

[4] L.S. Aksel'rod and V.V. Dil'man, J. Appl. Chem. 29, 12, 1803 (1956).*

[5] P.A. Semenov, J. Tech. Phys. (USSR) 14, 7-8 (1944).

[6] K.N. Shabalin, Friction Between Gas and Liquid in the Course of Absorption Processes (Metallurgy Press, 1945).**

[7] F.H. Garner and D. Hamerton, Chem. Eng. Sci. 3, 1, 1 (1954).

Received May 21, 1957

*Original Russian pagination. See C.B. translation.

**In Russian.

RESONANCE METHOD FOR INVESTIGATING THE RESISTANCE OF CONCRETE TO CORROSIVE MEDIA

V.V. Stol'nikov

The problem of the stability of concrete in corrosive media is one of great importance in various branches of building. A matter of special significance is correct evaluation of the degree of corrosion of concrete under the action of an aqueous medium containing dissolved salts, or having low hardness, in hydrotechnical constructions. This factor frequently determines the choice of the cement and the composition of the concrete, which plays an important part among the measures taken in the course of planning and construction of modern large hydrotechnical works. In such cases any unjustified raising of the specifications for cements and concretes introduces superfluous technical and economic difficulties in the provision of cements and other materials necessary for the production of concrete.

The existing standards and tests for the corrosiveness of water, given in the standard specification (N-114-54), are largely based on laboratory studies of the corrosion resistance of cements, performed by many investigators. Different methods were used in these studies, but the common feature of all of them is that they were performed not with specimens of concrete based on some particular cement, but with various "model" concretes, as they are described by some authors, or with cement pastes and hardened cement. Most of these investigations were carried out by the method described in GOST 4796-49, which was the standard procedure up to 1953. The concrete "models" used in this method are small porous specimens 1 x 1 x 3 cm, made with a monodisperse quartz sand fraction with a water-cement ratio of about 0.35. It is clear that such specimens cannot be used for simulation of the conditions for the action of corrosive waters, such as sulfate-containing waters, on concretes of definite composition and density. Neither does this method provide a criterion for estimating the influence of various ways of varying the structure of concrete on its stability in corrosive waters, or take into account the influence of certain cement characteristics which are significant in relation to the stability of real concretes, such as the water requirement, etc. The method takes no account of the possibility of increasing the density and therefore the stability of concrete based on a given cement by a decrease of the water-cement ratio.

In view of the extensive construction of large hydrotechnical works in the USSR, there is now a definite need for the development of a new method for assessing the corrosion resistance of concretes, in which the influence of the structural characteristics of a real concrete is taken into account by means of direct tests [1], in addition to the influence of the cement composition.

For this purpose we carried out an investigation, jointly with A.S. Gubar', in the Concrete Laboratory of the B.E. Vedeneev All-Union Scientific Research Institute of Hydraulic Engineering, on the sulfate resistance of concretes based on Portland cement; the structural changes in concrete under the action of the corrosive medium were characterized by the variations in the frequency of the natural vibrations of prismatic specimens of concrete.

The method based on determinations of the natural-vibration frequency of a system is one of the vibrational methods used for investigations of structural and mechanical changes which take place in structurized disperse systems under the influence of various factors. Vibrational methods differ significantly from static methods in that they largely give only an over-all, qualitative characterization of the system, just as measurement of the effective viscosity in steady flow of a structurized system provides an over-all, hydraulic characteristic of flow.

On the other hand, vibrational (dynamic) methods are usually fairly simple from the experimental standpoint, and avoid the difficulties associated with elimination of the influence of relaxation processes on the meas-

ured instantaneous deformations in cases when the relaxation time is fairly short.

The method based on determinations of the natural-vibration frequency of a system, if used with a homogeneous material, makes it possible to determine a most important property – Young's modulus. When applied to such polydisperse, heterogeneous systems as concrete, determination of Young's modulus by the resonance method is somewhat conventional, as the test conditions correspond to stresses close to zero. Our experiments showed that the natural-vibration frequency of concrete specimens, under equal conditions, depends on the temperature and the moisture content of the concrete. If the experiments are performed over a narrow temperature range (a few degrees), the influence of temperature may be disregarded. If the temperature of the specimen changes appreciably (by tens of degrees) during the test, the physicochemical and physicomechanical changes have a significant influence on the vibration frequency of the concrete specimens [2].

The elastic properties of concretes and mixes largely depend on the elastic properties of hardened cement, and possibly also on the elastic and structural properties of the cement in the region of contact with the aggregate. Variations of the elastic properties of hardened cement under the influence of temperature are the sum of the variations of the elasticity of individual crystals, superposed on which is an increase in the structural defects caused by irregularity of the thermal expansion of the individual crystals, and also by differences in the coefficient of linear expansion of the crystals in different directions.

The vibration frequency of a concrete specimen at constant temperature depends considerably on the moisture content, increasing with the latter within certain limits. This increase of the vibration frequency is associated with the formation of adsorption layers and solvate water films in the microcrevices, and these, as has been shown by Rebinder [3], hinder the rapid closing of the microcrevices during microdeformations owing to the viscous resistance of the water.

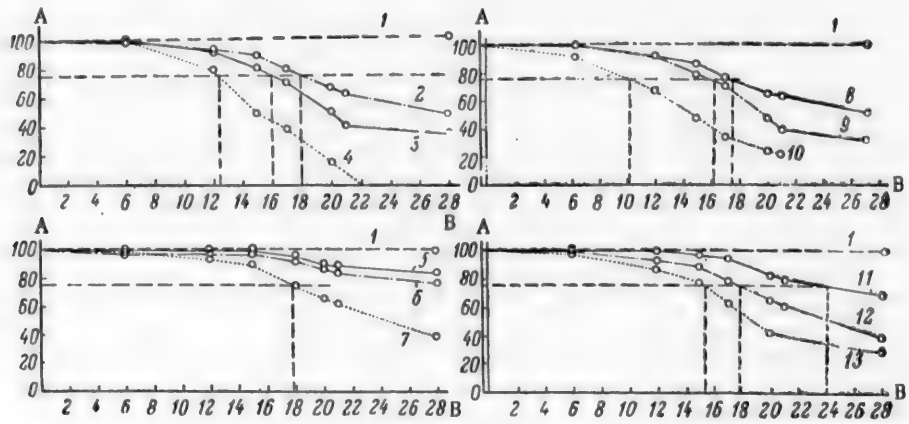

Variations of the dynamic elasticity modulus of concrete specimens: A) dynamic elasticity modulus E_d (%); B) time (months); 1) control specimens; 2) Code 7, without additives, W:C = 0.50; 3) Code 9, without additives, W:C = 0.60; 4) Code 16, without additives, W:C = = 0.70; 5) Code 3, without additives, W:C = 0.47; 6) Code 5, with SSB, W:C = 0.47; 7) Code 7, without additives, W:C = 0.50; 8) Code 12, with SNV, W:C = 0.54; 9) Code 9, without additives, W:C = = 0.60; 10) Code 10, with SSB, W:C = 0.54 (specimen broke down after 21 months); 11) Code 4, with SNV, W:C = 0.50; 12) Code 7, without additives, W:C = 0.50; 13) Code 6, with SSB, W:C = 0.50.

It is known that the sulfate corrosion of concrete consists of the reaction of $SO_4^{"}$ anions which penetrate into the concrete, with solid tetracalcium hydroaluminate; as a result, a double salt – calcium sulfoaluminate – is formed together with the $Ca^{"}$ cations of free lime. The formation of sulfoaluminate is accompanied by an increase of volume, relative to the initial volume of the hydroaluminate, so that the concrete structure is loos-

TABLE 1

Composition of Concrete Mixes Without Additives

Code No.	Composition	W/C*	Cement consumption (kg/m^3)
7	1:2.0:3.5	0.50	338
9	1:2.4:4.2	0.60	284
16	1:2.8:5.0	0.70	245

*Water-cement ratio

ened and numerous structural defects arise in it at the points where the sulfate anions have penetrated [4, 5]. It is likely that the region of contact between the cement and the aggregate is the first to be damaged [6]. At high concentrations of Na_2SO_4 the destruction of concrete is also known to be associated with formation and crystallization of gypsum in the concrete.

On the foregoing considerations it seems likely that the vibration frequency of concrete specimens should decrease rapidly with increasing corrosion.

Prismatic specimens 7 x 7 x 21 cm in size were made from cements of different compositions, and with different water-cement ratios, with ordinary sand. For evaluation of the structural changes, the specimens were kept in the corrosive media for different periods, after which their resonant vibration frequency was measured and the dynamic elasticity modulus calculated [2].

Up to an age of 15 days the specimens were hardened in tap water at 18°. They were then placed in the corrosive medium, which consisted of 5% sodium sulfate solution. The dynamic modulus was determined once a month for six months, and then once in two months during the following two years. Among the problems studied was the possibility or raising the sulfate resistance of concretes by the addition of surface-active substances.

The surface-active additives tested were the air-entraining SNV additive in the form of the abietic resin proposed by the Concrete Laboratory of the Scientific Research Institute of Hydraulic Engineering, and sulfite-alcohol waste liquor (SSB) from the Solikamsk plant.

The results of tests on concrete specimens with and without additions of surface-active substances were compared.

The compositions of the concrete mixes without additives are given in Table 1. The settling of a cone of the mix was 6 cm for all the composition. The maximum aggregate size was 25 mm.

A new characteristic was adopted for evaluation of the corrosion resistance of concrete specimens in corrosive media.

The corrosion resistance was expressed in terms of a coefficient calculated as follows:

$$C_c = \frac{1 - \frac{E_0 - E_n}{E_0}}{1 - \frac{a \cdot n}{N}} \qquad (1)^*$$

where C_c is the corrosion-resistance coefficient, E_0 is the dynamic elasticity modulus of control specimens kept in a noncorrosive aqueous medium, E_n is the dynamic elasticity modulus of the test specimens after n months of exposure to the corrosive medium, a is the permissible relative decrease of the dynamic elasticity modulus of the

*Equation (1) may be written in the form

$$C_c = \frac{E_n \cdot N}{(N - a \cdot n) \cdot E_0}.$$

TABLE 2

Corrosion-Resistance Coefficients of Concrete Specimens Without Additives

Code No.	W : C	Coefficient C_C after time (months)	
		10	20
7	0.50	1.00	0.73
9	0.60	0.99	0.52
16	0.70	0.91	0.15

TABLE 3

Concrete Compositions

Code No.	W : C	Surface-active additive	Cement consumption (kg/m^3)
		Series I	
		Concrete composition 1 : 2 : 3.5	
7	0.50	Without additive	338
3	0.47	SNV	334
5	0.47	SSB	334
		Series II	
		Concrete composition 1 : 2.4 : 4.2	
9	0.60	Without additive	284
12	0.54	SNV	284
10	0.54	SSB	284

TABLE 4

Corrosion-Resistance Coefficients

Code No. and additive	W : C	Coefficient C_C after time (months)		
		10	20	28
7, without additive	0.50	1.00	0.73	0.45
3, with SNV	0.47	1.04	0.98	0.95
5, with SSB	0.47	1.02	0.94	0.87

test specimens after N months of exposure to the corrosive medium, N is the time of exposure of the specimens to the corrosive medium during which the dynamic elasticity modulus decreases by $\underline{a}$.

This new characteristic not only provides a comparative evaluation of the corrosion resistance of concrete specimens, but gives an idea of the resistance of a concrete of real composition in a corrosive medium as a function of time. The permissible decrease of the modulus was taken as 25%; therefore, the value of $\underline{a}$ was 0.25. The time N was taken as five years, i.e., 60 months. Since the tests were performed with 5% Na_2SO_4 solution, which is a much higher concentration than that of the usual sulfate-containing waters met in building practice, and since the concrete specimens were relatively small (about 1 liter in volume), it seems likely that under these conditions it would be possible to predict the period of some tens of years during which the dynamic elasticity modulus of concrete in a construction would decrease by not more than 25%. Our observations showed that a decrease of the dynamic elasticity modulus by 25% is not accompanied by any appreciable changes in the appearance of the specimens.

TABLE 5

Corrosion-Resistance Coefficients

Code No. and additive	W : C	Coefficient C_c after time (months)		
		10	20	28
9, without additive	0.60	0.78	0.52	0.35
12, with SNV	0.54	0.98	0.73	0.59
10, with SSB	0.54	0.97	0.27	0

TABLE 6

Composition of Concretes of Series II With Initial Water-Cement Ratio 0.50

Code No.	Concrete composition	Surface-active additive	Cement consumption (kg/m^3)
7	1 : 2.0 : 3.5	Without additive	338
4	1 : 2.16 : 3.78	SNV	312
6	1 : 2.16 : 3.78	SSB	316

TABLE 7

Corrosion-Resistance Coefficients. Water-Cement Ratio 0.50

Code No. and additive	Coefficient C_c after time (months)		
	10	20	28
7, without additive	0.99	0.73	0.42
4, with SNV	1.00	0.91	0.79
6, with SSB	0.94	0.45	0.33

If the corrosion-resistance coefficient C_c was equal to 1, this meant that the behavior of the concrete specimen in the corrosive medium fully conformed to the specified condition. If $C_c > 1$, the specimen is more resistant than specified. If $C_c < 1$, the specimen has a corrosion resistance below the specification requirements.

Curves 2, 3 and 4 in the figure (plotted from average values) represent the variations of the dynamic elasticity modulus of the concrete specimens the composition of which is given in Table 1. These curves give an indication of the relative resistance of concretes in relation to the water-cement ratio.

Table 2 gives the corrosion-resistance coefficients C_c for concrete specimens without additives, kept in Na_2SO_4 solution for 10 and 20 months.

It is clear from Table 2 that in these experiments the resistance of the concrete after 20 months was almost five times as high if the water-cement ratio was decreased from 0.70 to 0.50, and 1.5 times as high on decrease of the water-cement ratio from 0.60 to 0.50. It follows that the corrosion resistance of concrete in 5% sodium sulfate solution decreases not linearly but in accordance with a parabolic law with increase of the water-cement ratio; the decrease of resistance is more rapid than the increase of the water-cement ratio, especially in the 0.60-0.70 range. On the other hand, the resistance of the concrete specimens did not conform to the specified conditions after 20 months of exposure in the concentrated corrosive solution, with any of the water-cement ratios used, although specimens with 0.50 water-cement ratio had relatively high resistance.

Two series of specimens were prepared for investigation of the sulfate resistance of concretes containing surface-active additives (Table 3).

Series I consisted of concrete of constant composition and consistency of the mix, equivalent to 6 cm (by cone settling). The water-cement ratio was decreased when additives were introduced in this series. Some in-

dividual results of this investigation are given below.

The results of tests, performed by the resonance method, of the sulfate resistance of concrete specimens of Series I are illustrated by Curves 5, 6, 7, 8, 9 and 10 in the figure.

The values of the corrosion-resistance coefficient C_c for specimens of Codes 7, 3 and 5 after exposure to Na_2SO_4 solution for 10, 20 and 28 months are given in Table 4.

It follows from Table 4 that the most stable specimens under the test conditions were specimens containing SNV; the deviation of the corrosion-resistance coefficient of these specimens from the specified value was only 0.05 after more than two years of exposure to 5% sodium sulfate solution.

These specimens proved twice as resistant as specimens without additives.

The corrosion-resistance coefficient of specimens of Codes 9, 12 and 10 are given in Table 5.

Table 5 shows that Code 12 concrete with addition of SNV was the most resistant of this group under the given test conditions. The least resistant was Code 10 concrete with added SSB; specimens of this concrete broke down completely after 21 months of exposure to the corrosive medium. The resistance of specimens with SNV after 28 months was approximately 1.5-2 times that of specimens with water-cement ratio 0.60 (without additives).

In Series II the cement consumption was decreased in concretes containing surface-active additives; the water-cement ratio and the cone settling were constant, as for the concrete compositions without additives, at 0.50 and 6 cm respectively (Table 6).

Variations of the dynamic elasticity modulus of specimens of Codes 7, 4 and 6 are shown in the figure by Curves 11, 12 and 13.

The corresponding values of the corrosion-resistance coefficient C_c, calculated for 10, 20 and 28 months, are given in Table 7.

It follows from Table 7 that, as in the preceding experiments, specimens with SNV added were the most stable in this group. After 28 months of exposure of the specimens to 5% Na_2SO_4 solution the corrosion-resistance coefficient of these specimens was almost double that of the specimens without additives, and over 2.5 times that of the specimens with SSB added.

The above results give an indication of the physicochemical factors which caused the increase of the corrosion resistance of the concretes when surface-active substances were added.

Whereas the results in Tables 4 and 5 might suggest that the increase of the corrosion resistance was largely the consequence of the decrease of the water-cement ratio on introduction of the additives (SNV and SSB), comparison of these results with the data in Table 7 shows that even when the water-cement ratio is kept constant and the cement content is decreased accordingly the specimens containing the air-entraining additive SNV had a higher resistance to corrosion. Specimens containing SSB, the principal effect of which is to "liquefy" the cement paste, did not give favorable results when the cement content was decreased, with retention of the original water-cement ratio.

This result is in full agreement with the results of our earlier investigations of the sulfate resistance of concrete specimens [7].

Hence it follows that an important factor, in addition to the decrease of the water-cement ratio, in increasing the corrosion resistance of concrete when surface-active substances are added is alteration of the structure of the material owing to the formation of a system of disconnected spheroidal pores by the action of emulsified air bubbles; these pores hinder capillary absorption and damp the local stresses which arise as the result of developing sulfate corrosion. Since the emulsifying action of SSB is slight, the corrosion resistance was not increased if the water-cement ratio was kept constant. The reason for the lower resistance of Code 6 specimens relative to specimens without additives was evidently the lower cement content.

In Code 4 specimens (with added SNV) not only was any possible decrease of the corrosion resistance caused by the decreased cement content compensated, but the resistance was even higher; it is easy to see that the only factor which could cause this was emulsified air.

SUMMARY

1. The resonance method for investigation of structural changes in concrete specimens can be used for estimation of the sulfate resistance of concrete.

2. This is a new method in relation to studies of the corrosion resistance of concretes and mixes, and it can be used for estimation of the resistance of actual concretes and mixes; the results can thus be extended to concrete in constructions, and the method can therefore be recommended for use for the appropriate practical purposes.

3. In contrast to other methods, the resonance method can be used to estimate the influence of the water-cement ratio in concrete on the sulfate resistance, and also to assess the influence of surface-active additives directly in concrete specimens.

4. It was found that the decrease of the sulfate resistance of concrete with increase of the water-cement ratio is nonlinear; under the experimental conditions used the sulfate resistance decreases more rapidly than the water-cement ratio increases, especially in the 0.60-0.70 range of water-cement ratios. The significance of specimen size was confirmed in the experiments.

5. The addition of air-entraining (SNV) and plastifying (SSB) surface-active substances to the mixture increases the sulfate resistance of concrete. The most favorable results were obtained with additions of SNV, which increased the resistance of the concrete severalfold. In view of the relatively small specimens used and the high concentration of the corrosive solution it seems likely that the favorable effect of this additive will be very considerable under practical conditions.

6. Emulsified, entrained air is an important factor in the increase of the corrosion resistance of concrete in sulfate waters under the experimental conditions used. With addition of SNV air-entraining additive, the corrosion resistance was increased both on decrease of the water-cement ratio and on decrease of the cement consumption; this is of great practical importance.

7. A new criterion for estimation of the corrosion resistance of concrete in corrosive media was used: the corrosion-resistance coefficient C_C, which can be used for evaluation of the corrosion resistance after any time of exposure, the resistance being related to a prescribed time during which a concrete of practical composition can remain in the given corrosive medium without significant damage. The quantity $A = (a \cdot n)/N$ may be determined more precisely as the result of further investigations.

8. Studies of the corrosion resistance of concretes of different composition, in different corrosive media (by means of the resonance method, with evaluation of the corrosion resistance in terms of the proposed new corrosion-resistance coefficient) should provide data for further refinement of the fundamental principles presented in this paper and for the formulation of recommended instructions for application of the method to the solution of practical problems in the construction industry.

In conclusion, the author expresses his deep gratitide to A.S. Gubar' and P.F. Poliakov for much help in the course of these investigations.

LITERATURE CITED

[1] V.V. Stol'nikov, in the book: Technology of Hydrotechnical Concrete (Gosenergoizdat, 1954), p. 9.*

[2] V.V. Stol'nikov, Proc. Acad. Sci. USSR 106, 6, 995 (1956).**

[3] P.A. Rebinder, L.A. Shreiner and K.F. Zhigach, Agents for Lowering Hardness in Drilling (Izd. AN SSSR, 1944).*

[4] V.M. Moskvin, Corrosion of Concrete (State Construction and Architecture Press, Moscow, 1952).*

[5] V.V. Kind, Corrosion of Cements and Concrete (Gosenergoizdat, 1955).*

[6] V.V. Stol'nikov, Proc. Conf. on Concrete Corrosion (Izd. AN SSSR, 1953), p. 52.

[7] V.V. Stol'nikov, Collected Papers on Silicate Chemistry and Technology (State Constructional Materials Press, 1956), p. 121.*

Received February 8, 1957

*In Russian.

**Original Russian pagination. See C.B. translation.

THE PROBLEM OF FORMATION OF A SEMICONDUCTING FILM IN LEAD–BISMUTH GLASSES DURING HYDROGEN TREATMENT

N.I. Ananich and L.A. Grechanik

Central Scientific Research Laboratory of Electrotechnical Glass

It is known that glass at low temperatures is a bad conductor of electricity, and is therefore often used as an insulating material in many branches of industry.

Sometimes materials of increased surface conductivity but high volume resistance are required for certain special purposes.* It is possible to obtain glass which conforms to these requirements. Numerous investigators have developed methods whereby glasses with high surface conductivity, electronic or ionic in nature, can be obtained [1-4].

The most reliable method for the production of a conducting film of the required resistance on glass surfaces is by high-temperature reduction, in hydrogen, of glasses containing the oxides of lead, bismuth, antimony, or combinations of these oxides. The oxides are reduced to the metals in the surface layers of the glass. Any desired resistance can be easily obtained because the surface resistance of the glass can be measured directly during the hydrogen treatment.

The easy reduction of the oxides of lead, bismuth and antimony in glass to the metallic state was initially used for decorative purposes only [5]. It is only recently that this property has been used for the formation of semiconducting films on glass.

There have been very few investigations of the formation of surface semiconducting films on glass containing these oxides, by the reduction of the latter in hydrogen [6, 7]. It is noted in these papers that the resultant conductivity depends in a complex manner on the glass composition. In purely lead glasses, even with very high PbO contents (up to 45 molar %), surface resistances of less than 10^9 ohms per cm square could not be obtained. It was found, however, that the surface resistance of reduced glass could be lowered considerably by the introduction of Bi_2O_3. Unfortunately, no systematic studies of the influence of Bi_2O_3 on the surface resistance of glasses treated in hydrogen have been reported.

Considerable interest attaches also to studies of the relationship between the surface resistance of glasses treated in hydrogen and the contents of nonreducible oxides, including sodium oxide, which is an essential component of almost all industrial glasses.

Because of the importance of these questions, the present investigation was concerned with a study of the influence of additions of Bi_2O_3 and Na_2O on the surface resistance of lead silicate glasses reduced in hydrogen. The hydrogen treatment was carried out at different constant temperatures.

Glass is subjected to repeated heating in air in the production of electrical vacuum apparatus; it was therefore necessary to test the stability of the surface resistance of reduced glasses to repeated heating in an oxidizing atmosphere. A series of experiments was performed for this purpose, in which previously reduced glasses were kept at 380° for several hours.

*For example, in certain high-voltage equipment semiconducting films allow surface charges to leak away without dangerous local overcharging.

EXPERIMENTAL

The glass specimens used were in the form of polished plates 14 x 10 x 3 mm. The specimens were thoroughly washed and then rubbed with alcohol before the hydrogen treatment. Graphite strips (electrodes) were attached to both sides of the plate in such a way that the direction of the current was parallel to the width of the specimen. This made it possible to disregard the volume conductivity of the glass in measurements of surface conductivity at room temperature. The resistance was measured by means of the "MOM-2m" megohmmeter.

A special apparatus was used for the treatment of the glass. The glass specimen was placed by means of a special holder into a quartz tube 18 mm in diameter, which was inserted in a horizontal tubular electric furnace. The holder was so arranged that the resistance of the specimen could be measured during the treatment. The specimen was placed in the region of the quartz tube which was in the constant-temperature zone of the furnace. The furnace was then switched on and heated to the required temperature. The furnace temperature was then kept constant by means of a three-position astatic control of the EPD-17 electronic potentiometer.

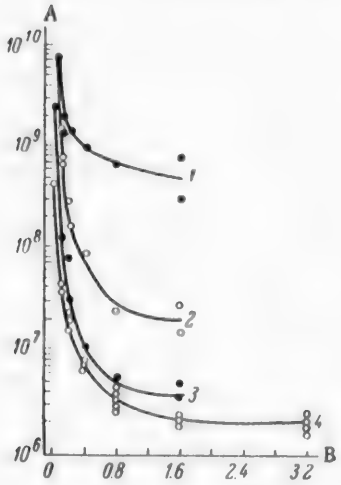

Fig. 1. Effect of Bi_2O_3 content on the surface resistance of glasses reduced in hydrogen at various constant temperatures: A) specific surface resistance (in ohms per cm square); B) Bi_2O_3 content (molar %). Temperature of hydrogen treatment (°C): 1) 480; 2) 440; 3) 400; 4) 380.

The initial resistance of the specimen was measured and hydrogen was then passed through the tube. The resistance was determined at intervals during the treatment. The reduction in hydrogen was continued until the resistance of the glass specimen became constant. The treated specimen was then extracted from the furnace and cooled. When it reached room temperature, the final specific surface resistance of the glass was measured.

Effect of additions of bismuth oxide on the surface resistance of high-lead glass after hydrogen treatment. The glass used for investigation of the effect of bismuth oxide on the surface resistance had the composition 32.26% PbO, 67.74% SiO_2 (the glass compositions are all given in molar percentages).

Increasing amounts of PbO were replaced by Bi_2O_3 in this glass in such a way that the total contents of the reducible oxides, PbO and Bi_2O_3, remained constant. Glasses containing from 0.1 to 3.2% Bi_2O_3 were investigated.

The hydrogen treatment was performed at 380, 400, 440, 480°.

The variations of the surface resistance of glass with the percentage content of Bi_2O_3 are plotted in Fig. 1. It is seen that the first additions of Bi_2O_3 (up to 0.4%) decrease the surface resistance of glass more sharply than the subsequent additions. Thus, whereas the introduction of 0.4% Bi_2O_3 into a pure lead glass lowers the surface resistance of hydrogen-treated glass from 10^9 to 10^7 ohms per cm square (i.e., by two orders of magnitude), further increase of the Bi_2O_3 content to 0.8% only reduced the resistance to $5 \cdot 10^6$ ohms per cm square.

The same graph also shows that the final value of the surface resistance of all the glasses studied depends on the treatment temperature, the surface resistance being lower with lower treatment temperatures. Films with resistances ranging from $2 \cdot 10^6$ to $2 \cdot 10^9$ ohms per cm square were obtained by hydrogen treatment of this series of glasses.

The variations of the surface resistance of the glasses in the course of treatment are plotted in Fig. 2. The resistance of the glass specimens are given for a treatment temperature of 380°.

In calculations of the specific surface resistance of the glass from the total resistance it was assumed that the volume conductivity of the glass remains constant during the experiment, and retains the same value as before the hydrogen treatment, when the surface conductivity is almost zero.

It follows from Fig. 2. that with increasing content of Bi_2O_3 in lead glass (from 0.1 to 3.2%) the rate of decrease of the surface resistance during hydrogen treatment increases with increasing Bi_2O_3 content; each Bi_2O_3

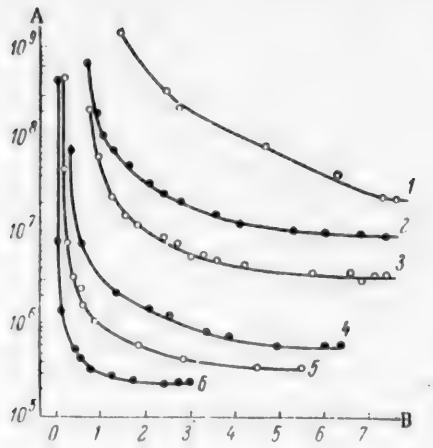

Fig. 2. Variations of the surface resistance of glasses with different Bi_2O_3 contents during hydrogen treatment at 380°: A) specific surface resistance of the glass (in ohms per cm square); B) duration of hydrogen treatment (hours). Bi_2O_3 contents (molar %): 1) 0.0; 2) 0.1; 3) 0.2; 4) 0.8; 5) 1.6; 6) 3.2.

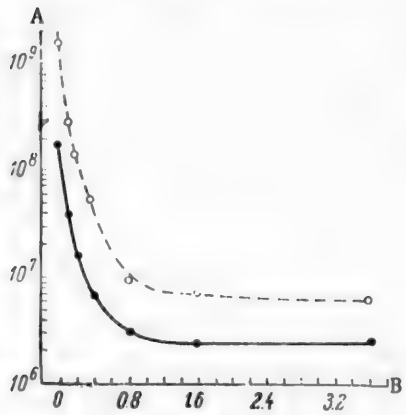

Fig. 3. Surface resistance of glasses with different Bi_2O_3 content after treatment in hydrogen only (continuous curve), and after additional exposure to air for 10 hours at 380° (dashed curve): A) specific surface resistance of the glass (in ohms per cm square); B) Bi_2O_3 content (molar %).

content corresponds to a quite definite minimum value of the surface resistance, which cannot be decreased further to any practical extent by further increase of the treatment time.

As already stated, it is impossible to obtain a surface resistance below 10^9 ohms in a glass in which the only reducible oxide is PbO. Since the introduction of only 0.2% Bi_2O_3 decreases the resistance of the glass after treatment under the same conditions by two orders of magnitude, it may be assumed that Bi_2O_3 favors the formation of glasses of lower resistance by preventing the aggregation of the reduced lead atoms.

Electrical vacuum apparatus, for which glasses with semiconducting films are often required, is subjected to the action of high temperatures during manufacture and even in service; we therefore studied the effects of repeated heating on the surface resistance of glasses reduced in hydrogen. Previously reduced specimens were held for a long time (5-10 hours) in an electric furnace at 380° in air. The specimens were then cooled to room temperature and their resistance was measured. It was found that the surface resistance of reduced glasses increases after such treatment, the increase being greater for lower Bi_2O_3 contents in the glass. With 0.1-0.2% Bi_2O_3 in the glass the resistance increased 10-fold after 10 hours of treatment, whereas with 0.8-3.2% Bi_2O_3 the increase was two- to threefold.

Variations of the surface resistance of glasses after additional heating are shown in Fig. 3, where the continuous curve represents the variation of surface resistance with the Bi_2O_3 content of glasses reduced at 380° in hydrogen, and the dash curve represents the resistance of the same glasses after they had been heated at the same temperature in air for ten hours.

It was also found that during the heating in air the resistance increases more rapidly at first, and the rate then diminishes. The resistance of specimens which had already been heated for ten hours at 380° increased only 1.2 to 1.5-fold during the subsequent 20 hours. The increase of the resistance of hydrogen-treated glasses after exposure to high temperatures in air can probably be attributed to the oxidation of part of the reduced lead. Additions of Bi_2O_3 have a favorable effect in this case also, by stabilizing the surface resistance of the glass.

Effect of Na_2O on the surface resistance of lead-bismuth glasses reduced in hydrogen. To determine the influence of Na_2O on the conductivity of the surface films formed by the reduction of lead-bismuth glasses, a series of glasses with gradually increasing contents of sodium oxide was investigated. The basic glass was one studied previously, of the following composition (%): 67.67 SiO_2, 31.56 PbO, 0.8 Bi_2O_3. Various amounts of Na_2O (from 0.5 to 4%) were introduced into this glass in place of SiO_2. The glasses with added Na_2O were treated in hydrogen at 380° as described above.

The variations of the surface resistance of the reduced glasses with the Na_2O content are plotted in Fig. 4. Addition of 0.5% Na_2O has a negligible effect, but further increases of the content of this oxide in the lead-bismuth glass produce a steady increase of the surface resistance. For example, the surface resistance is increased 100-fold by the introduction of 4% Na_2O into the original glass. Thus, even a relatively low content of Na_2O in

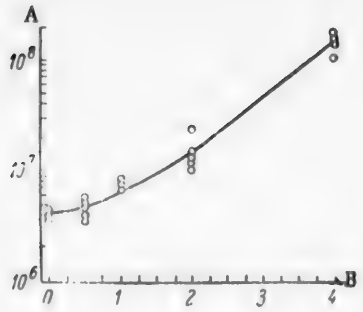

Fig. 4. Variation of the surface resistance of reduced glasses with the Na_2O content during hydrogen treatment at 380°: A) specific surface resistance of the glass (in ohms per cm square); B) Na_2O content of the glass (in molar %).

lead-bismuth glass prevents the formation of glasses of increased surface conductivity.

Glasses of increased surface conductivity cannot always be used for the direct production of complex glassware. In such cases the glass to be reduced can be used in the form of a coating, applied in powder form on the surface of the article while it is still being blown. The glass coating is then subjected to the usual hydrogen treatment. Our first experiments in this direction have yielded quite satisfactory results.

SUMMARY

1. Investigations of the effect of Bi_2O_3 content on the surface resistance of lead-bismuth glasses reduced in hydrogen showed that with additions of 0.1 to 3.2 molar % of Bi_2O_3 glasses with specific surface resistances from $2 \cdot 10^6$ to 10^9 ohms per cm square can be made.

2. The surface resistance of reduced lead-bismuth glasses is increased severalfold when the glass is subsequently heated in air. The surface resistance of the glass becomes more stable with increase of the Bi_2O_3 content.

3. Investigation of the influence of Na_2O on the surface resistance of lead-bismuth glasses reduced in hydrogen showed that additions of sodium oxide increase the resistance of the semiconducting film formed during reduction of the glass.

4. In some cases it is more appropriate to use the reducible glass in the form of a coating.

LITERATURE CITED

[1] H. Schulz, Glashütte 66, 685 (1936).

[2] I.C.M. Brentano and J.D. Richards, Phys. Rev. 95, 841 (1954).

[3] U.S. Patent 2636832, 2597562; J. Soc. Glass Techn. 38, 78A (1954).

[4] R. Gomer, Glastechn. Ber. 27, 301 (1954).

[5] W. Becker, Ceramic Abs. 29, 276 (1935).

[6] R.L. Green and K.B. Blodgett, J. Am. Ceramic Soc. 31, 89 (1948).

[7] K.B. Blodgett, J. Am. Ceramic Soc. 34, 14 (1951).

Received August 6, 1956

ANODE OVERVOLTAGE AND MECHANISM OF ANODIC DISCHARGE IN THE ELECTROLYSIS OF A CRYOLITE–ALUMINA MELT

V.P. Mashovets and A.A. Revazian

The All-Union Aluminum and Magnesium Institute

Different viewpoints have been held on the mechanism of the anode process in the electrolysis of cryolite-alumina melts.

It may be postulated that the potential-determining process is the direct discharge of oxygen-containing anions (O^{2-}, AlO_2^- or AlO_3^{3-}) on carbon, considered as an inert material, with liberation of oxygen, while the formation of CO and CO_2 is a secondary, purely chemical process. In this case the decomposition potential of alumina should be 2.12-2.17 v, and the back emf of 1.6-1.85 v observed in industrial cells must be attributed to a decrease of the partial pressure of oxygen as the result of its combination with carbon.

On the other hand, the direct participation of carbon in the anode process with formation of CO_2 or CO may be assumed:

$$2Al_2O_3 + 3C \rightarrow 4Al + 3CO_2$$

or

$$Al_2O_3 + 3C \rightarrow 2Al + 3CO.$$

The decomposition potential would then be 1.10 or 0.95 v respectively, and the higher back emf observed in practice must be attributed to overvoltage.

Frumkin and his associates [1] showed in a series of papers that the potential of the carbon electrode in aqueous solutions is determined by chemisorbed oxygen, combined in the form of intermediate oxides of carbon of the C_xO type. This concept is in full harmony with the modern theories of carbon combustion [2]. Rempel' and Khodak [3] explained the anode overvoltage in the electrolysis of cryolite-alumina melts by the retarded decomposition of such oxides.

Preliminary experiments showed that the anode overvoltage in cryolite-alumina melts consists of two components: the inertialess component f(i), which varies rapidly with change of current density, and the inertia component $\varphi(i)$, which varies very slowly. Fig. 1 shows the variation of the voltage of the electrolytic cell with increase of the anode current density from 0.1 to 0.7 amp/cm^2 and subsequent decrease to 0.1 amp/cm^2, under conditions in which cathodic polarization could be neglected. The increase of the voltage over the region ab and the corresponding decrease over the region cd are considerably greater than the change of voltage required to overcome ohmic resistance; they also include the inertialess overvoltage. Over the regions bc or de, however, the anode potential still changes slowly to a stable value corresponding to the new current strength.

It was shown by an oscillographic method that the inertialess component of the overvoltage changes almost instantaneously, in less than 0.0005 second.

Recently Haupin [4] also detected the existence of two polarizations – a rapidly-decreasing (in less than 0.001 second) and a slowly-decreasing, but, like ourselves, he was unable to separate them quantitatively by the oscillographic method.

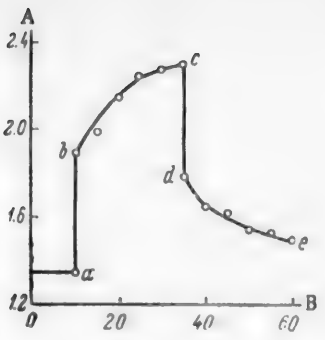

Fig. 1. Variation of cell voltage after increase of the anode current density from 0.1 to 0.7 amp/cm² and corresponding decrease: A) voltage (v); B) time (minutes).

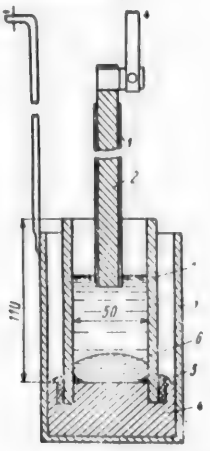

Fig. 2. Cell for measurement of decomposition potential: 1) sintered corundum tubes; 2) graphite anode; 3) steel beaker; 4) graphite plug; 5) carbonaceous packing; 6) aluminum cathode.

The long time, lasting tens of minutes, required for the electrode potential to become established after alteration of the current strength accounts for the fact, well known in the literature, that the measurements of the decomposition potential of cryolite-alumina melts with carbon anodes are not reproducible. We therefore changed the usual method for construction of the I–v curve.

In prolonged electrolysis at current strength I_1 (anode current density i_1) the voltage which becomes established in the cell is

$$U_1 = E_0 + f(i_1) + \varphi(i_1) - \eta_c + I_1 r, \qquad (1)$$

where E_0 is the reversible decomposition potential, $f(i_1)$ and $\varphi(i_1)$ are respectively the inertialess and the inertia components of anode overvoltage, η_c is the cathode overvoltage, and $\underline{r}$ is the ohmic resistance of the cell. If the current strength is then changed to I_1' (anode current density $j_1' \gtrless i_1$) and the new voltage U_1' is measured immediately (within 5-10 seconds), we have

$$U_1' = E_0 + f(i_1') + \varphi(i_1) - \eta_c' + I_1' r, \qquad (2)$$

when the inertia overvoltage $\varphi(i_1)$ has not yet undergone any appreciable change during the time of measurement. Thus, by prolonged electrolysis at current strength I_1, varied for brief intervals to I_1', I_1'', I_1''', etc., and then returned each time to I_1, we find a series of values for U_1', U_1'', U_1''', etc., for which the values of E_0 and $\varphi(i_1)$ are constant. Graphical extrapolation of U_1 to $I_1^0 = 0$ gives

$$U_1^0 = E_0 + \varphi(i_1) = \pi_1. \qquad (3)$$

This may be regarded as the quasiequilibrium potential to a disconnected graphite electrode the surface of which is saturated with C_xO oxides to a state corresponding to the current density i_1 of the prolonged electrolysis, measured relative to an aluminum electrode if the latter is not stably polarized.

Similarly, if prolonged electrolysis is performed at other current densities i_2, i_3, etc., and these are briefly changed to j_2', j_2'' . . . j_3', j_3'' . . . etc., we find a series of values π_2, π_3, etc. Extrapolation of the values of π_1, π_2, π_3 to $i = 0$ gives $\pi_0 = U_0^0 = E_0$. If the reversible decomposition potential E_0 is known, Equation (3) can be used to find the inertia components of the overvoltage, $\varphi(i_1)$, $\varphi(i_2)$, $\varphi(i_3)$ . . . at different current densities $\underline{i}$ of the prolonged electrolysis.

The electrolytic cell (Fig. 2) consisted of a piece of sintered corundum tube, plugged at the lower end with a graphite plug, sealed in with a carbonaceous mixture which was then baked. The cell was inserted in a steel beaker, which also served as the conductor to the cathode. A graphite anode 11 mm in diameter was closely inserted into the sintered corundum tube, so that only the end face of the anode was operative; this ensured a fairly uniform current density on the anode. The anode was placed at the requiredinterelectrode distance by means of a micrometer screw. Aluminum, which acted as the cathode, was introduced into the cell. The cathode area was 20.6 times the anode area; cathode polarization, which, as is known, is very low [5, 6], could thus be disregarded. The electrolyte was cryolite saturated with alumina. The temperature was 980-990°.

Data from several experiments with different current densities $\underline{i}$ in prolonged electrolysis are presented in Table 1; the cell voltages U measured during brief changes of the current density to $\underline{j}$ are given.

The results of all the experiments are plotted in Fig. 3 (the groups of curves are shifted along the U axis to

TABLE 1

Cell Voltages U During Brief Change of the Anode Current Density j, for Different Current Densities in Prolonged Electrolysis

Experiment No.	Interpolar distance (cm)	i (amp/cm²)	U (in v) at different j (amp/cm²)					
			0.1	0.2	0.4	0.6	0.8	1.0
3	5.5	0.1	1.55	1.85	2.44	2.75	3.65	—
4	3.0	0.1	1.35	1.45	1.62	1.71	1.98	2.16
8	0.3	0.5	1.62	1.70	1.90	2.10	2.32	2.56
9	6.0	0.5	1.72	1.94	2.45	2.91	3.33	3.73
10	7.7	0.8	1.75	1.90	2.26	2.65	3.05	3.45
11	3.0	0.8	1.68	1.80	2.05	2.30	2.53	2.78
13 *	3.0	0.8	1.23	1.35	1.60	1.87	2.15	—

* Anode saturated with hydrogen.

TABLE 2

Extrapolated Values of the Decomposition Potential U_x^0 and the Inertialess Overvoltage $\varphi(i)$ at Different Current Densities of Prolonged Electrolysis

Experiment No.	i_x, current density of prolonged electrolysis (amp/cm²)	Interelectrode distance (cm)	U_x^0 extrapolated (in v)	$\varphi(i) = U_x^0 - U_0^0$ (in v)	Back emf by Lozhkin's data [9] (in v)
1	0.05	2.7	1.15	0.04	1.10
2	0.05	7.2	1.14	0.03	1.10
3	0.1	5.5	1.23	0.12	1.24
4	0.1	3.0	1.25	0.14	1.24
5	0.2	2.5	1.34	0.23	1.34
6	0.2	3.7	1.30	0.19	1.34
7	0.4	2.0	1.46	0.35	1.46
8	0.5	0.3	1.52	0.41	1.49
9	0.5	6.0	1.50	0.39	1.49
10	0.8	7.7	1.56	0.45	1.565 *
11	0.8	3.0	1.54	0.43	1.565 *
12	1.0	5.5	1.59	0.48	1.59 *

* Interpolated values.

TABLE 3

Calculation of the Overvoltages f(i) and $\varphi(i)$

Experiment I				Experiment II			
Increments	Δi 0.0—0.1	Δi 0.1—0.2	Σ	Increments	Δi 0.0—0.2	Δi 0.2—0.3	Σ
$\Delta f(i)$	0.20	0.13	0.33	$\Delta f(i)$	0.35	0.17	0.52
$\Delta\varphi(i)$	0.18	0.11	0.29	$\Delta\varphi(i)$	0.27	0.06	0.33
Σ	0.38	0.24	0.62	Σ	0.62	0.23	0.85

TABLE 1

Inertialess and Inertia Overvoltages, f(i) and φ(i), Determined by Two Methods

Current density (amp/cm²)	Anode potential (in v)		Overvoltage		Ditto, from Table 3	
	graphite	graphite saturated with H_2	f (i)	φ (i)	f (i)	φ (i)
0.1	1.49	1.36	0.25	0.13	0.20	0.18
0.2	1.73	1.46	0.35	0.27	0.34	0.28
0.3	1.96	1.66	0.55	0.30	0.52	0.33
0.5	2.25	1.85	0.74	0.40	—	—
0.7	2.55	2.10	0.99	0.45	—	—
0.8	2.67	2.20	1.09	0.47	—	—
0.9	2.79	2.29	1.18	0.50	—	—

avoid overlapping). In most cases the plots are linear, so that extrapolation to $j = 0$ is easy; the resultant values of U^0 are summarized in Table 2. The values of U^0 for the same $\underline{i}$ are in good agreement in each pair of experiments. Thus, at a given current density i_x of prolonged electrolysis the anode enters into a certain stable state and acquires a stable quasiequilibrium potential $\pi_x = U^0_x$, which is determined by the composition of the adsorbed intermediate oxides of the C_xO type. It is interesting to note that the anode potential was unaffected even when the interelectrode distance was decreased to 0.3 cm. This confirms the view of Rempel' and Khodak [7] that a "metallic fog" has no "depolarizing" effect on the anode, and is in agreement with our observations in measurements of cell emf in cryolite-alumina melts [8].

The values found for U^0_x are in excellent agreement with the values of the back emf determined by Lozhkin in electrolysis [9], given in the last column.

Extrapolation of U^0_x to $i_x = 0$ (Fig. 4) gives $U^0_0 = 1.11$ v, in agreement with the theoretical decomposition potential E_0. The inertia component of the overvoltage $\varphi(i_x)$ for different current densities i_x of prolonged electrolysis is found as the difference $U^0_x - U^0_0$ (Table 2).

On the hypothesis that this part of the overvoltage is due to slow decomposition of the intermediate C_xO oxides at the anode, we attempted to eliminate these oxides, and hence the φ(i) component of the overvoltage, by saturating the anode with hydrogen. A channel 3 mm in diameter was drilled axially through the anode, and dried hydrogen was blown through it during the whole experiment. The results of one such experiment (No. 13) are given in Table 1. It was found that, irrespective of the current density $\underline{i}$ of the prolonged electrolysis, extrapolation of the $j-U$ curves to $j = 0$ always gives the constant value $U^0_0 = 1.12$ v, which is in good agreement with the thermodynamic value of the decomposition potential.

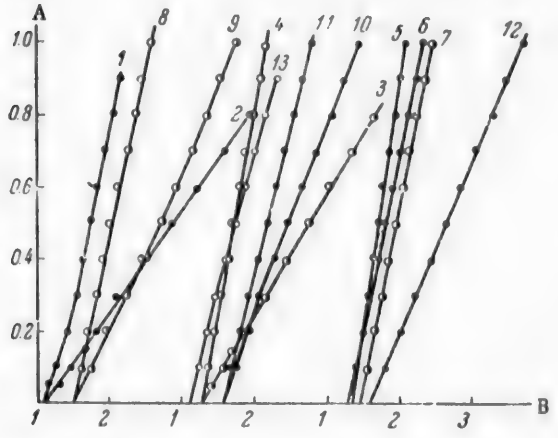

Fig. 3. Cell voltage U in relation to the briefly decreased current density $\underline{j}$, at different current densities $\underline{i}$ of prolonged electrolysis: A) current density $\underline{j}$ (amp/cm²); B) voltage U(v). The numbers on the curves correspond to the experiment numbers in Tables 1 and 2.

If, in Table 1, we compare Experiments 11 and 13, performed at the same current density and with the same interelectrode distance, we see that saturation of the anode with hydrogen decreases the voltage by 0.43-0.45 v, which corresponds to the φ(i) overvoltage for $i = 0.8$ amp/cm². This shows that saturation with hydrogen does in fact break down the C_xO oxides and eliminates the φ(i) overvoltage.

These experiments were followed by direct determinations of the anode potential on closed circuit, with separation of the overvoltage into the inertia component φ(i) and the inertialess component f(i).

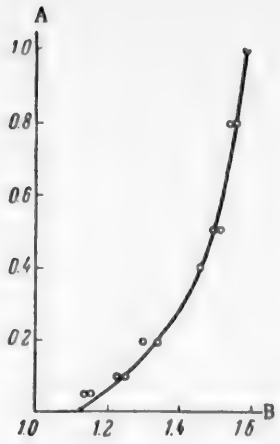

Fig. 4. Values of U_X^0 extrapolated from Fig. 3, and extrapolation to the decomposition potential U_0^0: A) current density $\underline{i}$ (amp/cm^2); B) voltage U (v).

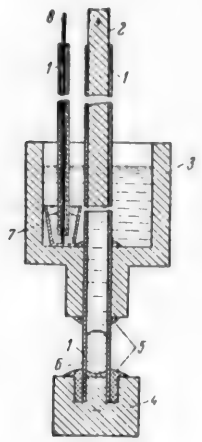

Fig. 5. Cell for measurement of anode potential: 1) sintered corundum tubes; 2) graphite anode; 3) graphite head; 4) graphite plug; 5) carbonaceous paste; 6) cathodic aluminum; 7) aluminum in sintered corundum crucible (reference electrode); 8) molybdenum wire.

The electrolytic cell (Fig. 5) consisted of a sintered corundum tube, 11 mm in internal diameter, closed from below with a graphite plug. A widened graphite head was fitted to the top end, the joints were packed with a carbonaceous paste, and the cell was baked in a Kryptol furnace.

The graphite anode was inserted firmly into the sintered corundum tube, and fixed at a distance of 2-3 mm from the top edge of the lower tube. The cathodic aluminum was put into the lower tube; the current passed to it through the graphite plug. This arrangement ensured that the current density at the electrodes was uniform. The upper wide head contained a small sintered corundum crucible containing aluminum, which served as the reference electrode. Its potential was measured by means of a molybdenum wire. Corrections were introduced for the drop of potential in the anode and in the electrolyte from the anode surface to the top edge of the lower tube. The latter correction is $\Delta = il\rho$; if the specific resistance of the electrolyte $\rho = 0.5$ ohm/cm, and the width of the gap between the anode and the tube edge $l = 0.2$ cm, we have $\Delta = 0.1\ \underline{i}$, where $\underline{i}$ is the current density.

The experiment with a fresh anode was commenced by electrolysis at current density 0.7-0.8 amp/cm^2 for 30-40 minutes. The current was then switched off until a steady anode potential $\pi_0 = 1.11$ v was reached. This ensured that the state of the anode was constant. The current was then switched on at a density of 0.1 amp/cm^2, and the potential (1.31 v) was measured immediately; the potential then increased during 20-25 minutes and reached a steady value of 1.49 v; the current density was raised to 0.2 amp/cm^2, the potential of 1.62 v was recorded, and the potential then rose gradually to 1.73 v.

In a second similar experiment $\pi_0 = 1.11$ v; current was passed at 0.2 amp/cm^2; the potential at the first instant was 1.46 v, and then rose to 1.73 v; the current density was raised to 0.3 amp/cm^2; the initial potential was 1.90 v, and the value then rose to 1.96 v.

These results were used to find, by subtraction, the increments of the inertialess $\Delta f(i)$ and the inertia $\Delta\varphi(i)$ components of the overvoltage; and by summation of the increments, the overvoltages themselves, $f(i)$ and $\varphi(i)$, for each current density; the results are given in Table 3.

At higher current densities, the overvoltages $f(i)$ and $\varphi(i)$ were determined by measurements of the anode potential with and without saturation of the graphite with hydrogen. The difference between the measured potentials gave the overvoltage $\varphi(i)$, and the inertialess overvoltage $f(i)$ was given by subtraction of 1.1 v from the potential of the hydrogen-saturated anode.

The results are given in Table 4, which also includes average results from Table 3 for comparison.

Comparison of the last two methods, and also of the values of $\varphi(i)$ in Table 4 with the values obtained from j−U curves (Table 2), shows good agreement.

The inertia overvoltage can be represented by the equation

$$\varphi(i) = 0.50 + 0.37 \log i, \qquad (4)$$

as is clear from Fig. 6. We shall return to this equation later.

The inertialess overvoltage corresponds to the empirical equation

$$f(i) = 1.3i^{0.8}, \qquad (5)$$

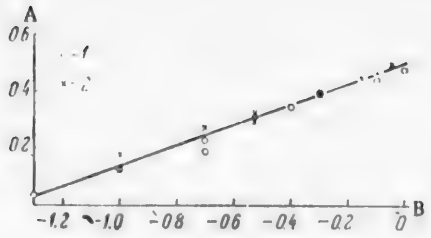

Fig. 6. Inertia component $\varphi(i)$ of the overvoltage as a function of log current density: A) inertia component of overvoltage $\varphi(i)$ (v); B) log i. Experimental points: 1) from Table 2; 2) from Table 4; straight line based on Equation (4).

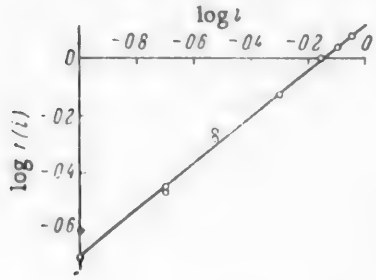

Fig. 7. Inertialess component f(i) of the overvoltage, in logarithmic coordinates. Points from Table 4; straight line based on Equation (5) or $\log f(i) = 0.114 + 0.8 \log i$.

as is evident from Fig. 7, which is plotted in logarithmic coordinates for greater clarity. Theoretical interpretation of Equation (5) is difficult.

The direct participation of carbon in the electrode process may be assumed from the results of our emf measurements of galvanic cells in cryolite-alumina melts [8]. In the same way, discharge of oxygen-containing ions in electrolysis takes place with the participation of carbon as an electromotoractive material.

At very low current densities the discharge proceeds at the most active regions of the graphite surface, with formation of carbon dioxide only. Depending on the composition of the oxygen-containing ions, this process can be represented by the equations:

$$2O^{2-} + C \rightarrow CO_2 + 4e,$$

$$4AlO_2^- + C \rightarrow CO_2 + 2Al_2O_3 + 4e$$

or

$$^4/_3AlO_3^{3-} + C \rightarrow CO_2 + {}^2/_3Al_2O_3 + 4e.$$

The anode potential is close to the value of the reversible potential, 1.11 v.

Two types of overvoltage arise with increase of current density. One of these, the inertialess f(i), we attribute to processes in the liquid part of the electric double layer. Whatever the nature of the dissociation of the cryolite and alumina, the melt has a higher concentration of fluorine-containing than of oxygen-containing anions. The mobilities of the former are probably also higher; therefore, they play the principal role in the transfer of current. Anodic discharge is effected by the oxygen-containing anions. Because of this, the negative layer of the double layer at the anode consists predominantly of fluorine-containing ions. To be discharged, the oxygen-containing ions must break through the screen of fluorine-containing ions. They must receive additional activation energy for this; they obtain it from the overvoltage f(i). Since the double layer is formed or changed almost instantaneously, this part of the overvoltage is inertialess. Incidentally, this shows that it must not be identified with concentration polarization.

The second, inertia part of the overvoltage $\varphi(i)$ is caused by the fact that carbon dioxide, initially formed at the most active regions of the carbon, is adsorbed and blocks these regions. Since the desorption of CO_2 is slow, as the current density increases the discharge is transferred to less active, more perfectly crystallized regions, where intermediate chemisorption oxides are formed as primary products:

$$O^{2-} + xC \rightarrow C_xO + 2e$$

or

$$2AlO_2^- + xC \rightarrow C_xO + Al_2O_3 + 2e.$$

These oxides are adsorbed on the graphite and make it passive; the discharge extends to increasingly less active regions with formation of progressively less stable oxides, and the overvoltage $\varphi(i)$ increases.

Equation (4) is characteristic of processes associated with activation

$$\varphi(i) = a + \frac{3}{2}\frac{RT}{F}\ln i = 0.50 + 0.37i.$$

The fractional valence $^2/_3$ in the denominator of the prelogarithmic coefficient is evidently due to the intermediate character of the C_xO oxides.

These oxides subsequently decompose, with liberation of CO_2 and formation of even lower oxides C_yO ($y > x$), which are held in the adsorbed state. It is thus possible that the only primary gaseous product is CO_2. It is possible, however, that the decomposition proceeds according to the equation

$$C_xO \rightarrow (2x-1)CO + (1-x)CO_2$$

when $0.5 < x < 1$, or even

$$C_xO \rightarrow yCO + 0.5(1-y)CO_2 + [x - 0.5(y+1)]C$$

when $x > 1$.

Since the decomposition of the sorption complexes is slow, the overvoltage $\varphi(i)$ is of the inertia type and is retained for a long time on the electrode, even after the current is switched off. Hence the potential $\pi_x = \pi_0 + \varphi(i)$ may be regarded as the quasistable potential of an anode the surface state of which corresponds to the current density i_x of the preceding prolonged electrolysis. This state is determined by the composition and stability of the adsorbed C_xO oxides.

The overvoltage $\varphi(i)$ cannot be ascribed to concentration polarization, since it would in that case be destroyed by the passage of hydrogen. It appears that hydrogen catalytically decomposes the intermediate oxides with liberation of active carbon:

$$C_xO + H_2 \rightarrow xC + H_2O), \quad (x > 0.5)$$
$$H_2O + \frac{1}{2}C \rightarrow H_2 + \frac{1}{2}CO_2.$$

The discharge proceeds on this activated carbon with direct formation of CO_2 without the overvoltage $\varphi(i)$, which is itself destroyed thereby. The inertialess overvoltage $f(i)$, associated with processes in the liquid part of the double layer, is not removed by the passage of hydrogen.

Adsorption of the intermediate oxides passivates the anode, and at a certain current density a potential is reached which is sufficient for discharge of fluorine-containing ions. At this stage there begins the discharge

$$4F^- + C \rightarrow CF_4 + 4e$$

or

$$4AlF_6^{3-} + 3C \rightarrow 4AlF_3 + 3CF_4 + 12e.$$

During the anode effect over 20% of carbon tetrafluoride appears in the anode gases [10]. The formation of CF_4 is the consequence and not the cause of anode passivation.

In former theories of the electrolysis of cryolite-alumina melts the possible participation of carbon, as an electromotoractive substance, in the anode process was not considered, as carbon ions are unknown both in solutions and in melts.

In the suggested mechanism the direct participation of carbon in the electrochemical process is postulated, but it is nevertheless unnecessary to assume the presence of free carbon ions.

Carbon, like silicon or germanium, should be regarded as a semiconductor, with extrinsic electronic or hole-type conductivity at low temperatures [11]. Impurities of group V, such as phosphorus or arsenic, having more than four valence electrons, may act as electron donors and confer electronic conductivity to graphite. Impurities with small numbers of valence electrons (aluminum, magnesium, iron) may act as electron acceptors and confer hole-type conductivity to the semiconductor. It is therefore understandable that at low temperatures there are no carbon ions in the graphite lattice, and graphite behaves as an inert, insoluble anode.

At 700-800° electrons in semiconductors may pass from the space charge region into the conductance region; the semiconductor acquires its own electronic productivity. At this stage certain carbon atoms are converted into ions, while retaining their position in the crystal lattice. Participation of these ions in the electrochemical process does not require their transition from the graphite lattice into the melt.

The total anode process

$$2O^{2-} + C \rightarrow CO_2 + 4e$$

(or the process with participation of AlO_2^- or AlO_3^{3-} anions) occurs in the following stages:

$$1)\ C \rightarrow C^{4+}_{\text{(ion in lattice)}} + 4e$$

$$2)\ C^{4+} + 2O^{2-} \rightarrow CO_2$$

or, in more general form

$$1)\ xC \rightarrow xC^{2/x+} + 2e$$

$$2)\ xC^{2/x+} + O^{2-} \rightarrow C_xO$$

with subsequent purely chemical decomposition of the intermediate oxides.

Thus, the discharge of oxygen-containing ions occurs precisely at the active regions of the graphite surface which are occupied by ionized carbon. The ionization of carbon takes place in the most defective zones of the crystal lattice.

SUMMARY

1. The overvoltage at the graphite anode in the electrolysis of cryolite-alumina melt is composed of two quantities: the inertia overvoltage $\varphi(i)$ and the inertialess overvoltage $f(i)$.

2. The thermodynamic decomposition voltage of alumina and the inertia component $\varphi(i)$ of the overvoltage were determined by means of a modified method of plotting I–v curves. It is shown that the inertia component of the overvoltage is eliminated when the anode is saturated with hydrogen.

3. The inertialess component $f(i)$ of the overvoltage was determined by direct measurements of the anode potential with and without saturation with hydrogen.

4. Both quantities, $f(i)$ and $\varphi(i)$, are expressed as functions of current density. The inertialess overvoltage is attributed to processes involved in the formation of the liquid part of the electric double layer, and the inertia component is attributed to adsorption and retarded decomposition of intermediate carbon oxides of the type C_xO at the anode surface.

5. A mechanism is suggested for the discharge of oxygen-containing anions on graphite with participation of carbon ions contained in the graphite crystal lattice in the electrochemical process.

LITERATURE CITED

[1] A.N. Frumkin, J. Phys. Chem. 5, 240 (1934); S.D. Levina, A.N. Frumkin and A. Lunev, J. Phys. Chem. 7, 664 (1936); E.M. Kuchinskii, R.Kh. Burshtein and A.N. Frumkin, J. Phys. Chem. 14, 441 (1940); A.N. Frumkin, Progr. Chem. 18, 9 (1949); B.P. Bruns and A.N. Frumkin, J. Phys. Chem. 1, 219 (1930); S.D. Levina, Progr. Chem. 9, 196 (1940).

[2] O.A. Esin and P.V. Gel'd, Physical Chemistry of Pyrometallurgical Processes, 1 (Metallurgy Press, 1950),* p. 167; A.S. Predvoditelev, L.N. Khitrin, O.A. Tsukhanova, Kh.I. Kolodtsev and M.K. Grodzovskii, Combustion of Carbon (Izd. AN SSSR, 1949).*

[3] S.I. Rempel' and L.P. Khodak, Proc. Acad. Sci. USSR 75, 833 (1950).

[4] W.E. Haupin, J. Electroch. Soc. 103, 174 (1956).

*In Russian.

[5] R. Piontelli and G. Montanelli, Aluminio 22 [6], 672 (1953).

[6] B. Feinleib and B. Porter, J. Electroch. Soc. 103, 231 (1956).

[7] S.I. Rempel' and L.P. Khodak, Nonferrous Metals 2, 37 (1951).

[8] V.P. Mashovets and A.A. Revazian, J. Appl. Chem. 30, 7, 1006 (1957).*

[9] G.A. Abramov, M.M. Vetiukov, I.P. Gupalo, A.A. Kostiukov and L.N. Lozhkin, Theoretical Principles of the Electrometallurgy of Aluminum (Metallurgy Press, 1953), p. 273.**

[10] V.P. Mashovets and E.L. Zakharov, J. Appl. Chem. 29, 1512 (1956).*

[11] A.F. Ioffe, Semiconductors in Modern Physics (Izd. AN SSSR, 1955).**

Received February 4, 1957

*Original Russian pagination. See C.B. translation.
**In Russian.

THE EFFECT OF A COMBINED ADDITION OF GLUE, β-NAPHTHOL AND ANTIMONY ON THE ELECTRODEPOSITION OF ZINC

A.I. Levin, A.V. Pomosov, E.E. Krymakova and V.I. Falicheva

The S.M. Kirov Urals Polytechnic Institute

Numerous investigations of the mechanism of action of surface-active substances in the electrodeposition of metals have revealed some very close and diverse relationships between the adsorption effects, which depend on the charge of the metal surface, and the effectiveness of the additive.

The additive normally used in electrolytic zinc plants, operating the low-acid (standard) process, for the production of good compact zinc deposits is glue. Its optimum concentration is 10-15 mg/liter, which may be raised to 25 mg/liter if the content of harmful impurities in the solution is increased.

However, later investigations have shown that there are surface-active substances which are considerably superior to glue in their effectiveness [1]. A combined additive consisting of glue, β-naphthol, and antimony is an agent of this type.

The present investigation was an attempt to determine electrode polarization, adsorption conditions, and nature of the adsorption layers in presence of the combined additive and of its individual components.

EXPERIMENTAL

The action of the combined additive was studied both in laboratory and in plant conditions.

The laboratory experiments were confined to a study of polarization in the electrodeposition of zinc in presence of the combined additive and of its individual components. The polarization was investigated in "standard" zinc electrolyte solutions containing (in g/liter): Zn 50 (as $ZnSO_4$), H_2SO_4 100.

The amounts of surface-active substances were varied in different combinations and concentrations.

The electrolyte was prepared from distilled water and chemically pure zinc sulfate and sulfuric acid. Carpenter's glue was used, and was added in colloidal form to the electrolyte. The β-naphthol was previously dissolved in caustic soda. Antimony was added in the form of a readily soluble salt, namely $K(SbO)C_4H_4O_6$ (tartar emetic).

All the experiments were performed in a thermostat with automatic temperature control. Polarization curves were plotted at 32 and 42°. The cathode used in the cell for the study of polarization was a smooth platinum plate 6 cm^2 in area; before the experiments the platinum was thoroughly cleaned and coated with electrolytic zinc (at $D_c = 2$ amps/dm^2). To maintain the electrolyte composition constant, the platinum anodes were also coated with thick, compact layers of zinc. The potential of the polarized cathode was measured relative to a saturated calomel electrode (0.248 v on the hydrogen scale). The emf was measured by means of a mirror galvanometer and a RAPS potentiometer.

The electrolytes were used only once in the experiments on the action of additives; fresh solutions were prepared for subsequent experiments. Certain difficulties arose in the determinations of the equilibrium potentials in acid solutions, owing to the rapid dissolution of zinc. In such cases the determinations of the polarization curves were commenced at I = 50-100 ma. The potential of the zinc electrode in absence of current had

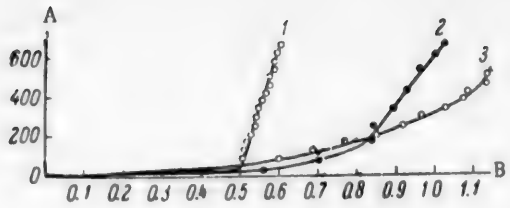

Fig. 1. Variations of cathode polarization with current density and additions of glue to a zinc electrolyte containing 50 g Zn (as $ZnSO_4$) per liter: A) current density D_C (amps/m^2); B) cathode polarization $\Delta\varphi$ (v). Curves: 1) without additions; 2) 20 mg glue per liter; 3) 20 mg glue and 100 mg H_2SO_4 per liter.

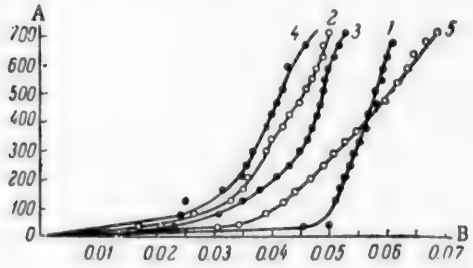

Fig. 2. Variations of cathode polarization with current density and the presence of various additives in a zinc electrolyte containing 50 g Zn (as $ZnSO_4$) per liter: A) current density D_C (amps/m^2); B) polarization $\Delta\varphi$ (v). Additions (in mg/liter): 1) no addition; 2) 10 of β-naphthol; 3) 20 of β-naphthol; 4) 10 of β-naphthol, 0.4 of Sb; 5) 20 of β-naphthol, 0.04 of Sb, 20 of glue.

to be measured immediately after determination of the polarization curve; this could not fail to affect the reproducibility of the results.

The influence of additives was studied not only in pure solutions of zinc sulfate, but also in presence of impurities most likely to be found in the process (cobalt and manganese ions).

In plant conditions, the influence of the combined additive was studied directly in the commercial cells. The results were compared with data obtained in neighboring cells – "standards."

Variations of the electrode potential and cathode polarization with temperature and current density in pure solutions containing 50 g of Zn and 100 g of H_2SO_4 per liter are given in Table 1.

Comparison of the values of electrode polarization at different temperatures shows that at 45° the zinc electrode potentials were more electropositive than at 35°.

This shift of the electrode potential in the positive direction with increase of temperature may be attributed to increased activity of the zinc ions.

The addition of glue both to acid and to neutral zinc electrolytes produces a considerable increase of the cathode polarization (Fig. 1). It is seen that the addition of glue produces a particularly large increase of polarization in solutions containing free acid.

The influence of β-naphthol on cathodic polarization of zinc is shown in Fig. 2; it is seen that the electrode polarization changes very little on addition of β-naphthol. In neutral solutions, this additive even has a depolarizing effect.

Since a combined additive consisting of glue, antimony and β-naphthol is usually recommended for the electrolysis of zinc sulfate solutions containing cobalt as an impurity, it was of considerable interest to determine the cathodic polarization in presence of β-naphthol in an electrolyte deliberately contaminated with cobalt. The results of these determinations are presented in Fig. 3.

The results show that the electrode potential of zinc in neutral solutions containing β-naphthol is shifted in presence of cobalt ions in the negative direction relative to the corresponding potentials in zinc sulfate solutions free from cobalt. However, the depolarizing effect of β-naphthol decreases with increasing current density and cobalt content.

The addition of 20 mg of β-naphthol per liter to an acid "standard" electrolyte containing 15 mg cobalt per liter leads, even at relatively high current densities, to a slight shift of the cathode potential in the positive direction.

Thus, in all cases β-naphthol has a depolarizing action in zinc sulfate solutions (see Curve 6, Fig. 3).

The action of additions of antimony in the cathode process of zinc deposition requires special consideration. It was long believed that antimony is a particularly dangerous impurity in zinc electrolytes [2]. However, it has recently been shown experimentally that additions of readily soluble compounds of antimony in definite, very low concentrations, facilitates the stripping of cathodic zinc from aluminum starting sheets [3]. Because of

TABLE 1

Cathode Polarization in the Deposition of Zinc from a Solution Containing 50 g of Zn and 100 g of H_2SO_4 per Liter, as a Function of Current Density and Temperature

D_c (amps/m²)	t = 35°		t = 45°	
	φ_i	(polarization) $\Delta\varphi$	φ_i	(polarization) $\Delta\varphi$
0	—0.808	—	—0.808	—
84	—0.864	0.056	—0.849	0.041
125	—0.869	0.061	—	—
167	—0.871	0.063	—0.862	0.054
251	—0.877	0.069	—0.870	0.062
335	—0.880	0.072	—0.876	0.068
418	—0.882	0.074	—0.880	0.072
502	—0.884	0.076	—0.884	0.076
585	—0.887	0.079	—0.889	0.081
670	—0.891	0.083	—0.893	0.085
752	—0.893	0.085	—0.896	0.088
835	—0.898	0.090	—0.897	0.089

this effect, antimony is now specially added in the form of a solution of tartar emetic to the electrolyte in all our national plants, in order to produce the so-called "separating layer" and to prevent difficult stripping. Moreover, antimony added together with glue and β-naphthol ensures the formation of especially good quality zinc deposits at high current efficiencies [1].

All these facts emphasize the importance of studies of the mechanism whereby antimony influences the electrodeposition of zinc.

The results of a study of the electrode polarization of zinc in presence of antimony are plotted in Figs 4 and 5.

Examination of Fig. 4 shows that under certain conditions antimony has a depolarizing effect in the discharge of zinc ions. A very important fact is that the depolarizing effect increases with increasing content of tartar emetic in the solution. At the same time, visual observations show that the presence of antimony in very small and strictly limited amounts favors the formation of particularly dense microcrystalline deposits.

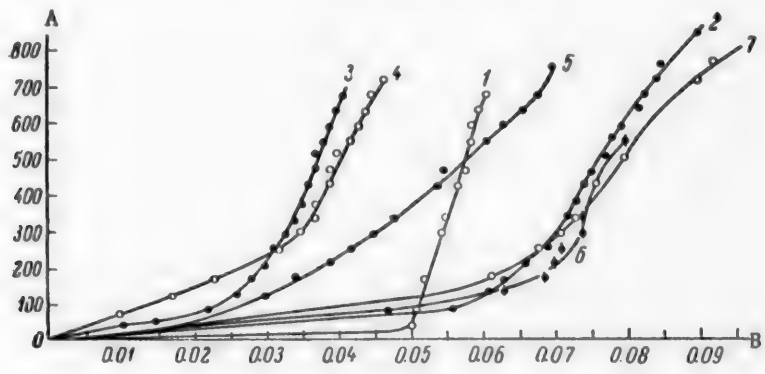

Fig. 3. Variations of cathode polarization in an electrolyte containing 50 g Zn (as $ZnSO_4$) per liter, and contaminated with cobalt: A) current density (amps/m²); B) cathode polarization $\Delta\varphi$ (v). Additions (in g/liter): 1) no addition; 2) 100 H_2SO_4; 3) 5 Co; 4) 15 Co; 5) 15 Co, 20 β-naphthol; 6) 100 H_2SO_4, 15 Co, 20 β-naphthol; 7) 100 H_2SO_4, 20 β-naphthol.

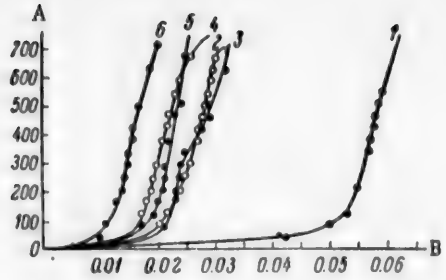

Fig. 4. Influence of the presence of antimony in the electrolyte on the cathodic polarization of zinc: A) current density D_c (amps/m^2); B) cathode polarization $\Delta\varphi$ (v). Solution contained 50 g $ZnSO_4$ per liter. Antimony added (in mg/liter): 1) no addition; 2) 0.02; 3) 0.05; 4) 0.075; 5) 0.1; 6) 0.2.

Before a discussion of the mechanism of the action of antimony, it was desirable to determine its influence when present together with glue and β-naphthol in the solution. The results of determinations of electrode potentials and polarization in presence of all these additives are plotted in Fig. 5. For comparison, the values of polarization and cathode potential in solutions without the additives, and in presence of glue only, are also given.

Considerations of the magnitude and nature of the shifts of the electrode potentials in the simultaneous presence of all three additives showed that their effects are not merely additive. It is evident that there is a more complex interaction between the components of the additive.

Experiments in Plant Conditions

Trials of the combined additive under plant conditions (in the electrolytic unit of the Cheliabinsk Zinc Plant) confirmed the results of the laboratory investigations and demonstrated the effectiveness of the additive. The quality of the cathodic deposits improved appreciably and the current efficiency with respect to zinc rose by 1.5-2.0% above the average value for the plant.

It was found that especially favorable results are obtained on addition of the combined additive of the following composition (in mg/liter): glue 10, β-naphthol 20, and antimony 0.02.

The following operating conditions were used in the experimental cells. In one of the cells (No. 2), the acidity, temperature, and additions of antimony and glue were the same as under ordinary production conditions. In cell No. 3 the conditions were the same, but 20 mg of β-naphthol per liter was added in alkaline solution every two hours (the amount was calculated on the volume of incoming electrolyte). In cell No. 4 the conditions were similar to those in No. 3, but 0.02 mg of antimony per liter, in the form of tartar emetic, was also added. To avoid an excess of antimony in the cell, it was added four hours after the stripping of the cathodic zinc. The temperature and acidity of the electrolyte were determined in all the experimental cells every two hours. The cathode deposits were weighed separately for each cell, after 24 hours of deposition.

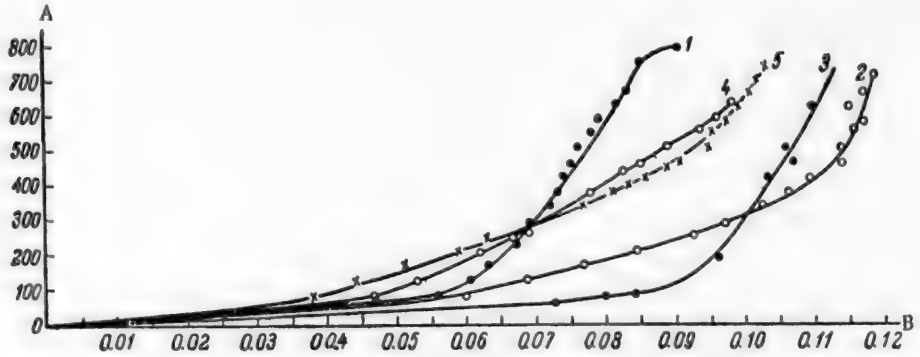

Fig. 5. Effect of the contents of various additives on the cathodic polarization in an electrolyte containing 50 g $ZnSO_4$ and 100 g H_2SO_4 per liter: A) current density D_c (amps/m^2); B) cathode polarization $\Delta\varphi$ (v). Additions (in mg/liter): 1) without addition; 2) 20 glue; 3) 20 glue, 20 β-naphthol; 4) 20 glue, 0.04 Sb; 5) 20 glue, 0.04 Sb; 20 β-naphthol.

The plant procedure for addition of antimony during this period was the following: 0.075 mg of antimony per liter (on the volume of electrolyte in the cell) was introduced at once before the stripping. In addition, 0.015-0.020 mg of antimony per liter was regularly introduced together with glue. Thus, actually 0.04 mg of antimony per liter was introduced every two hours.

The composition of the neutral electrolyte (in mg/liter) entering the electrolysis unit during the trials is given below.

Zn	Fe (total)	Fe^{++}	Co^{++}	Cd^{++}	Cu^{++}	As^{+++}	Sp. gr.
111.4	144	136	6.0	1.0	0.24	Traces	1.34

The spent electrolyte during the same period had the following characteristics: sp. gr. 1.24, zinc concentration 43.9 g/liter, acid concentration 99.5 g/liter. The cathode current density was 430 amps/m^2. The circulation rate of the electrolyte was maintained at 2.5 liters/minute.

TABLE 2

Effect of Composition of the Combined Additives on the Current Efficiency. Electrolyte Temperature 36°

Cell No.	Composition of additive (mg/liter)	Current efficiency (%)			
		1st day	2nd day	3rd day	4th day
2	Glue 16, antimony 0.015-0.020	90.6	90.9	89.6	87.0
3	Ditto + β-naphthol 10	89.0	92.8	91.5	–
4	Glue 16, β-naphthol 10, antimony 0.04	86.7*	90.9	94.0	93.0
Total in cascade	Glue 16, antimony 0.015-0.020	86.7	87.5	85.9	91.5

*Excess antimony had been introduced on the previous day; this caused external stripiness of the zinc deposit.

The results of the trials are presented in Table 2; it is seen that the presence of the combined additive in the electrolyte (Cell No. 4) has a very rapid effect on the cell performance.

The stripping of the zinc was very easy in all the cells. The cathode deposits formed in Cells Nos. 3 and 4 were particularly dense and microcrystalline, and were appreciably superior in external appearance to the deposits formed in the "standard" cells.

DISCUSSION OF RESULTS

The use of combined additives consisting of glue and β-naphthol (β–N), and especially of glue, β-naphthol, and antimony, results in a substantial improvement in the quality of the cathodic zinc deposits and increases the current efficiency. It must be noted that the combined additive is also effective in presence of considerable amounts of cobalt in the solution. However, an excess of antimony (above 0.08-0.1 mg/liter) results in partial dissolution of the previously-deposited zinc. In such cases a characteristic stripiness appears on the surface of the zinc deposits, mainly at the top ends of the sheets; this may affect either individual regions of the sheet or the whole sheet, according to the amount of excess antimony.

It was also noticed that a deficiency of readily soluble antimony compounds in the solution has an adverse effect on the structure of the cathodic zinc; this was seen especially clearly on examination of a fracture in the deposit.

No traces of "cobalt corrosion" on the zinc could be detected in presence of additives containing β-naphthol.

In our discussion of the mechanism of action of the combined additive, we first consider the influence of

β-naphthol, which has very little effect on the polarization in the discharge of zinc ions, either by itself or in presence of the other components.

This small influence of β-naphthol on the polarization with increase of current density is satisfactorily explained if it is taken into account that the zero-charge potential of zinc $\varphi_N = -0.63$ v. Since the metal is deposited at more negative potentials than $\varphi_N = -0.63$ v, the adsorption of β-naphthol (a molecular substance) should be very slight, and therefore its polarizing effect should be negligible.

It is probable that the favorable effect of β-naphthol depends on the fact that it forms a complex with cobalt ions and thus removes them from the reaction zone in the solution [4].

The following mechanism for the removal of cobalt impurities from zinc electrolytes by the action of β-naphthol may be postulated. The first stage is electrochemical oxidation to the trivalent state:

$$Co^{\cdot\cdot} - e \rightarrow Co^{\cdot\cdot\cdot}.$$

Trivalent cobalt can form complex compounds of the type $[Co(\beta\text{-}N)_6]Cl_3$ [5], which are very stable and are not hydrolyzed in aqueous solutions. It follows that the removal of cobalt from the electrolyte solution takes place mainly in the anolyte layers, where its oxidation to the trivalent state is most likely.

If the solution does not contain cobalt, β-naphthol may be omitted from the combined additive, as its influence on the polarization and electrocrystallization is very slight.

The main effective surface-active component of the combined additive is evidently glue, as it not only favors the formation of dense, microcrystalline zinc deposits, but also neutralizes the harmful effect of cobalt. This is because this additive is adsorbed mainly on the anodic regions of the microcells formed.

The explanation of the stronger effect of glue on the increase of polarization in acid than in neutral electrolytes is that at pH below 4.7 substances like gelatin and glue dissociate with formation of complex cations

$$R\begin{matrix}COOH\\NH_2\end{matrix} + H_2O \rightarrow \left[R\begin{matrix}COOH\\NH_2H\end{matrix}\right]^+ + OH^-.$$

Since zinc is deposited at potentials on the negative side of the zero-charge potential of zinc ($\varphi_N = -0.63$ v), cation-active additives should be particularly effective [6]. Therefore, organic compounds of high molecular weight which dissociate with the formation of surface-active cations (alkaloids, and organic derivatives of ammonia) are adsorbed on the cathode and produce very appreciable retardation of the cathode process. In such cases the Traube rule, according to which cathode polarization increases with increasing molecular size of the substance adsorbed on the cathode, is fully applicable.

The favorable effects of small amounts of antimony on the electrolyte on the structure of cathodic zinc deposits are also due to the adsorption of colloidal particles of antimony hydroxide on the cathode surface.

The nature of the salt added to the electrolyte is of considerable significance.

Not all antimony salts produce the same effect. For example, salts of oxy acids such as antimony sulfate $Sb(SO_4)_3$, etc., are only partially hydrolyzed when added to acid sulfate electrolytes, and form compounds such as antimonyl sulfate, $(SbO)_2SO_4$, which are not sufficiently surface-active. A particularly favorable effect on the formation of adsorption layers is produced by the readily soluble salt of trivalent antimony, $K(SbO)C_4H_4O_6$ (potassium antimonyl tartrate or tartar emetic). When added to a zinc electrolyte, a solution of tartar emetic reacts with sulfuric acid

$$K(SbO)C_4H_4O_6 + H_2SO_4 + 2H_2O \rightarrow Sb(OH)_3 + H_2C_4H_4O_6 + KHSO_4$$

with formation of a bulky white colloidal suspension of antimonious acid $Sb(OH)_3$, which forms a gel [7].

The colloidal suspension coagulates on the cathode surface to form islets and chains, which condense into a network structure. The spaces in the network then become filled with newly formed particles, and the film becomes continuous. If the film was impermeable, its thickness would then cease to increase. However, in presence of excess antimonious hydroxide the film continues to increase in thickness owing to the adhesion of large

flakes of the colloidal suspensions, continuously forming in the surface layers as the result of hydrolysis.

The presence of glue in the zinc sulfate electrolyte has a particularly favorable effect in the formation of denser adsorption layers. The dispersion of the colloidal system antimony + glue increases appreciably in presence of glue [8], and as a result the film on the zinc-electrolyte interface forms a particularly thin, nonporous, elastic layer [9]. An explanation of this action of the glue is that its micelles, being surface-active, are adsorbed and undergo denaturation in the process, with an increase of the film viscosity. The glue micelles are also adsorbed by the colloidal particles of antimony hydroxide, so that the combined film on the zinc surface acquires hydrophilic properties. Since metals have hydrophobic properties by virtue of their molecular structure, it is clear that the adsorption film results in a very appreciable change of the wettability of the cathode, both in magnitude and in sign, by the zinc sulfate electrolyte, and this leads to extensive changes in the chemical state of the metal surface.

The most favorable factor to influence the properties of the cathodic zinc deposit is the ability of glue to decrease the contact angle, so that the adhesion time of hydrogen bubbles to the cathode surface is decreased. In such cases zinc is deposited in smooth, compact form, with very faint traces of hydrogen liberation [10].

Hence, it may be concluded that introduction of the combined additive of glue and antimony alters the crystal structure of the cathodic zinc, which depends entirely on the formation and properties of the adsorption layer.

The foregoing results show that there is a quite definite optimum for the antimony content in the electrolyte. Excess tartar emetic causes appreciable brittleness and stripiness of the cathode deposit; these effects are usually attributed to excess colloids in the electrolyte.

In conclusion, it must be pointed out that antimony cations, not present as the hydroxide or basic salt, can also take part in the cathode process. At a certain instant the concentration ratio of antimony and zinc ions becomes such that both metals are liberated simultaneously at the cathode. Such simultaneous discharge is usually accompanied by depolarization [11]; this was confirmed experimentally in the study of the effect of antimony on cathodic polarization (see Fig. 4).

SUMMARY

1. In a study of the behavior of a combined additive consisting of antimony, β-naphthol, and glue in acid zinc sulfate electrolytes it was found that the favorable effect of β-naphthol is due to the formation of complex compounds with cobalt cations, which are thereby removed from the reaction zone.

2. It was found that the adsorption processes depend both on the charge of the metal and on the nature of the surface-active substances and colloidal suspensions formed in the course of electrolysis in the acid zinc electrolyte.

3. The combined colloidal system (antimony hydroxide and glue) has high dispersibility, and gives rise to a particularly thin, dense, and elastic film with a high contact area on the metal surface. This film not only has separating properties, but it also protects the aluminum and zinc against corrosion and favors the formation of more finely crystalline, dense, and smooth cathodic zinc deposits.

4. The depolarizing action of antimony cations, not present as the hydroxide or basic salt, may be ascribed to their effect in facilitating the crystallization of zinc in the simultaneous liberation of the two metals.

LITERATURE CITED

[1] A.I. Levin, "Corrosion and Metal Coatings" Coll. Trans. S.M. Kirov Urals Polytech. Inst. 43 (1953).*

[2] A.I. Gaev and O.A. Esin, Electrolysis of Zinc Compounds (ONTI, Sverdlovsk, 1937).*

[3] T.M. Shteingart, Nonferrous Metals 5, 32 (1954).

[4] I.N. Plaksin and D.M. Iukhtanov, Hydrometallurgy [in Russian] (Metallurgy Press, 1949).

[5] B.V. Nekrasov, General Chemistry [in Russian] (Goskhimizdat, 1948).

[6] V. Naumov, Colloid Chemistry [in Russian] (Goskhimizdat, Leningrad, 1932); A.I. Levin and A.V. Pomosov, Proc. Conf. on Electrochemistry [in Russian] (Izd. AN SSSR, Moscow, 1953).

* In Russian.

[7] H. Remy, Inorganic Chemistry [Russian translation] (Goskhimizdat, 1934).

[8] S.G. Mokrushin, Proc. Acad. Sci. USSR 46, 113 (1945); Colloid J. 15, 212 (1953);• 16, 372 (1954).•

[9] A.I. Levin and V.S. Kolevatova, Nonferrous Metals 9 (1956).

[10] A.I. Levin, V.S. Kolevatova and S.G. Mokrushin, Colloid J. 15, 252 (1953).•

[11] A.I. Levin, Coll. Trans. Urals Industr. Inst. 27, 130 (1947).

Received August 6, 1956

•Original Russian translation. See C.B. translation.

KINETICS OF THE PHOTOCHEMICAL CHLORINATION OF BENZENE*

F.F. Krivonos

The literature contains contradictory information on the kinetics of the photochemical chlorination of benzene. The reason is the great complexity of such reactions [1].

Slator [2] showed that this reaction conforms to a second-order law, and that its rate is directly proportional to the square of the chlorine concentration; the temperature coefficient of the reaction rate is 1.5. Unfortunately, the description of the experimental work is very brief and general, so that it is difficult to reproduce the experiments and therefore to confirm the conclusions.

Luther and Goldberg [3] stated that Slator's work was superficial and his conclusions were hasty. In their opinion, the principal factor which hinders investigations of the photochemical chlorination of benzene is the inhibiting effect of oxygen and therefore of traces of air; neither the reaction order nor the temperature coefficient are given in their paper, but it contains valuable experimental data on the variations of the reaction rate with the amount of oxygen present.

Lane and Noyes [4] studied the kinetics of the photochemical chlorination of benzene in the gas phase. They found that the reaction conforms to the first-order law, and that its rate is directly proportional to the chlorine concentration. The temperature coefficient is not given. Since they studied the reaction in the gas phase only, it is difficult to use their results in relation to the technological processes of hexachloran production. A defect common to both the papers cited is that the reaction kinetics was studied over a narrow range of chlorine concentrations.

The purpose of our investigation was to elucidate a number of questions of practical importance: to determine the reaction order, to derive the rate constant of the reaction and the temperature coefficient, to distinguish between the reaction rates in liquid and gas phases, to study the effect of air and light, and to utilize the results obtained for clarification of the technological processes.

EXPERIMENTAL

The apparatus used for determinations of the solubility of chlorine in benzene [5] was also used for the studies of the kinetics of photochemical chlorination of benzene.

Example. A round-bottomed flask 725 ml in capacity was weighed at 12° and barometric pressure 759.8 mm Hg. The weight increase after the flask had been filled with chlorine was 1.15 g. Calculations show that the flask contained 12.2% air and 87.8% chlorine (by volume). In terms of partial pressures this corresponds to 95 mm of air and 685 mm of chlorine at 20°. The flask was carefully darkened and 10 ml of benzene was introduced. The manometer reading was −250 mm Hg at equilibrium. Calculations show that this corresponds to an absorption coefficient of about 70. The flask was then illuminated by two electric lamps of 500 watts each, placed 25 cm from the reaction vessel. The manometer readings were taken at 5-minute intervals.

The results of this experiment are given in the table.

The value of K for the point corresponding to five minutes reaction time is calculated as follows. The manometer reading at that instant was −340 mm Hg. Therefore, the pressure in the vessel was 759.8 − 340 =

*Communication II in the series on the production of hexachloran.

Results of an Experiment on the Photochemical Chlorination of Benzene

Time (min)	Manometer readings (mm Hg)	Chlorine concentration (mm Hg)	K
0	−250	685	–
5	−340	499	0.064
15	−464	242	0.069
35	−528	124	0.048
45	−544	92	0.045

= 419.8 mm Hg. Subtraction of the pressure of air (95 mm) and benzene vapor (74.7 mm) gives 419.8 − (95 + + 74.7) = 250.1 mm Hg for the partial pressure of chlorine. The coefficient of absorption of chlorine in benzene at 20° is 69. The amount of benzene remaining in liquid form (after subtraction of the evaporated benzene) was 9.74 ml. This gives the amount of chlorine dissolved, the volume of the vessel being 725 ml

$$\frac{69 \cdot 9.74 \cdot 293 \cdot 250.1 \cdot 759.8}{760 \cdot 273 \cdot 725} = 249 \text{ mm Hg}$$

The total chlorine in the vessel was 250.1 + 249 = 499.1 mm Hg.

These data give $K = \frac{2.3}{5} \log \frac{685}{499.1} = 0.064$.

It is important to note that in the conditions of this experiment about half the chlorine was in the form of gas, and an equal amount was dissolved in benzene; therefore, the reaction proceeded 50% in the liquid and 50% in the vapor phase.

It follows from the data in the table that the reaction conforms to the first-order law, but as the reaction proceeds, and especially near the end, the reaction rate constant decreases appreciably. It is possible that the reason for the decrease of the reaction rate near the end is the presence of air, the amount of which (relative to the chlorine) increases during the reaction.

To test the validity of this method for determination of the reaction rate constant, in some experiments the free, undissolved chlorine was determined by addition of potassium iodide solution, as in the determinations of the solubility of chlorine in benzene.

Effect of temperature. To determine the effect of temperature on the rate of photochemical chlorination of benzene, experiments were performed at 10, 20, 30, 40, and 50°. The results are given below.

Effect of Temperature on the Rate of Photochemical Chlorination of Benzene

Temperature (°C)	10	20	30	40	50
Value of K	0.060	0.066	0.065	0.057	0.059

These results show that variations of temperature do not influence the reaction rate; the differences between the values of K in the different experiments are within the limits of experimental error. Hence, the temperature coefficient of the reaction rate is close to unity, which is characteristic of photochemical reactions in general [6]. The usual experimental errors are eliminated in the wide temperature range used (from 10 to 50°). For example, if the temperature coefficient was 1.5 (as given by Slator), the reaction rate constant at 50° should be five times that at 10°.

Since the temperature does not affect the reaction rate, it might appear at first sight that in the practical production of hexachloran the reaction temperature is immaterial. In fact, this is not the case. As was shown earlier [5], the solubility of chlorine in benzene falls rapidly with increasing temperature. Therefore, if the reaction occurs mainly in the liquid phase, increase of temperature should decrease the rate of reaction. It is

therefore more advantageous in practice to carry out the reaction at a low temperature. The losses of benzene due to evaporation are then also less. It is true that at low temperatures crystals of hexachloran begin to form more rapidly. However, as our experiments showed, the crystals do not greatly influence the illumination of the reaction mass provided that certain conditions (illumination from below, shallow reaction vessel, etc.) are satisfied. Under such conditions we were able to convert almost all the benzene into a continuous crystalline mass of hexachloran in a shorter time. It was then merely necessary to remove the finished product, without any need for the usual laborious operations involved in separation of the finished product from benzene solution. Moreover, the product formed at low temperatures is purer, with a lower content of the oily substance formed by substitution of hydrogen by chlorine in the benzene nucleus.

Effect of illumination intensity. It is known that the rate of a photochemical reaction is directly proportional to the square root of the illumination intensity. Under the influence of direct sunlight the reaction is approximately 5-6 times as rapid as under illumination from a 750-watt electric lamp placed 13 cm from the reaction vessel. The question of illumination is the most important and difficult in studies of the reaction kinetics, and also in the practical production of hexachloran. Many variables are significant in this respect: transparency of the apparatus, the presence of reflecting surfaces, the volume and shape of the vessel, voltage fluctuations in the electricity supply, etc. It is therefore difficult to study the individual influence of any single factor.

Example. An experiment was performed under conditions such that side effects associated with the reflection of light were eliminated (the apparatus was placed in a box lined inside with black fabric); illumination by two neighboring lamps of 200 watts each, at a distance of 25 cm, gave results corresponding to $K = 0.0147$. In another experiment, under the same conditions, but with two 500-watt lamps, the results gave $K = 0.0219$. Theoretically, a 2.5-fold increase of the illumination should give a reaction rate constant of $\sqrt{2.5} = 0.0232$. This experiment therefore confirms the general theory (the discrepancy is within the limits of experimental error).

The reaction rate constant can be increased two- to threefold by the use of a white paper screen. Even better results are obtained by the use of mirror reflectors.

Effect of admixtures of air. Luther and Goldberg [3] reported that all the difficulties which arise in studies of the photochemical chlorination of benzene are due to the inhibiting action of admixtures of air (oxygen). They did not derive any definite mathematical relationship, but noted that the inhibiting effect of oxygen increases with increasing content of air (and therefore with decrease of the initial condentration of chlorine).

Amount of Air (%) Remaining in the Flask Filled with Chlorine	K
6.8	0.0264
18.7	0.0232
48	0.0127
57	0.123

If the initial concentration of chlorine is increased, the following effect was observed: the reaction rate was somewhat lower at first, but increased considerably near the end. Our experiments have not, as yet, confirmed this "self-acceleration" of the reaction on increase of the initial chlorine concentration. It is true that we did not use such low concentrations of chlorine.

Our experiments on this subject were performed by the method described above, with the use of initial mixtures with different contents of air and chlorine, the filling of the flask with chlorine being stopped at different weight increases. The results of the experiments are given in the small table.

These results show that the reaction rate decreases with increasing air content of the reaction mixture. The decrease is specially noticeable at higher air contents. Thus, an increase of the air content from 18 to 50% produces an approximately 2-fold decrease of the reaction rate. Therefore, with the small fluctuations (of the order of 10%) in the composition of the gaseous mixture which occur in the production of hexachloran, the amount of air impurity can be disregarded.

In some experiments we succeeded in raising the amount of air present to 3%; this had an appreciable influence on the reaction rate constant. In general, however, there is no sense in practice in aiming at complete removal of air from the reaction mixture, as even chlorine obtained from cylinders may, as is known [7], contain up to 10% air.

We now return to a question touched upon earlier – the decrease of K as the reaction proceeds. If our hy-

pothesis that a 50% increase of the amount of air roughly halves the reaction rate is correct, this would account for the observed decrease of K. In the experiment detailed in the table the amount of air at the start of the reaction was 95 mm Hg. We now find the value of K separately for the time interval when there was as much chlorine as air in the reaction vessel. This corresponds to the time interval roughly between the 35th and 45th minutes. The rate constant calculated for this interval is about 0.0298, or approximately half of the initial value (0.064). Therefore, there is reason to believe that the decrease of K near the end of the reaction is caused by the presence of air.

Comparison of the reaction rates in the liquid and gas phases. A specific feature of our experiments is that the reaction took place in the liquid and gas phases simultaneously, as it is only under such conditions that the reaction rate constant can be determined from measurements of the pressure in the vessel. Experiments were therefore performed in such a way that the reaction occurred predominantly in the liquid phase in one case, and in the gas phase in the other. The reaction rate constant had the same value in both cases.

Example. In the experiment detailed in the table, when 10 ml of benzene was introduced into the flask the chlorine was divided equally between the liquid and gas phases (50% in each). In another experiment, when 1.5 ml of benzene was taken, calculations showed that 95% of the chlorine was in the gas phase, and only 5% in the liquid phase. The reaction rate constant was the same in both cases.

In practice, however, it is much more advantageous to perform the reaction in the liquid phase, as the volume of the equipment is thereby reduced approximately 100-fold.

For example, the solubility of chlorine at 10° is 3.97 moles/liter. The volume of this amount of chlorine in the gaseous state is $3.97 \cdot 22.06 = 90$ liters, and about 30 liters of benzene vapor is also required. Hence, the volume of the equipment is increased 120-fold in this case.

Laboratory preparation of hexachloran.* A simplified method for the laboratory preparation of hexachloran may be recommended on the basis of our results.

It seems at first sight that it is easy to obtain hexachloran in high yields under laboratory conditions: it is merely necessary to pass a stream of chlorine through an illuminated flask containing benzene until all the benzene crystallizes. Our experiments showed, however, that under these conditions the reaction is very lengthy and low yields are obtained (not greater than 30% of the yield calculated on the benzene taken). For example, Travkin [8] passed chlorine through 500 ml of benzene for 11 hours and obtained 420 g of hexachloran crystals, which is only 25% of the theoretical yield. No suitable methods for the laboratory preparation of hexachloran are described in the foreign literature either. Our experiments by Meunier's method [9], in which hexachloran is prepared by the passage of a stream of chlorine through boiling benzene, gave yields of only about 4% of the theoretical in reactions lasting about twelve hours (7 g of crystals were obtained after evaporation from 80 g of benzene).

Even worse results were obtained by the chlorination of benzene in presence of 1% alkali [10].

Our method for the laboratory preparation of hexachloran is described below.

Enough benzene is put into a conical flask to cover the bottom in a thin layer. The flask is closed by a cork with two holes. Through one of these passes a long glass tube, reaching nearly to the bottom, for the supply of chlorine. Through the other hole there is passed an exit tube, to the end of which is attached a widened tube immersed to a small depth in water in such a way that the liquid cannot be sucked back into the reaction vessel. The flask is placed in a flat-bottomed glass vessel containing circulating cold water to cool the reaction mixture. The reaction vessel is illuminated on all sides if possible, but especially from below, by electric lamps of total power of 500-1000 watts. Considerable amounts of hexachloran crystals appear after about an hour. About two to four hours is required for completion of the reaction (depending on the light intensity and the chlorine rate). The chlorine rate may be regulated so that the chlorine is absorbed completely without any excess escaping through the outlet tube. However, air is initially present in the reaction vessel, and chlorine from cylinders also contains air; therefore large amounts of air accumulate in the vessel as the reaction proceeds and the reaction may stop completely as a result. A certain excess of chlorine must therefore be supplied. About 35-40 g of hexachloran may be obtained from 20 ml of benzene; this is about 75% of the theoretical yield.

*A.A. Denisov took part in the experimental work.

SUMMARY

1. It is shown that the rate constant of the photochemical chlorination of benzene can be determined by means of pressure measurements in the vessel.

2. The photochemical chlorination of benzene is a reaction of the first order if the inhibiting effect of admixtures of air is taken into account.

3. The temperature coefficient of the reaction rate is close to unity.

4. The reaction proceeds at equal rates in the liquid and the gas phase.

5. The influence of various factors on the rate of photochemical chlorination of benzene can be studied if the value of K is used as a criterion.

LITERATURE CITED

[1] F. Getman and F. Daniels, Outlines of Physical Chemistry (Goskhimizdat, 1941).*

[2] Slator, Z. phys. Chem. 45, 540 (1903).

[3] Luther and Goldberg, Z. phys. Chem. 56, 43 (1906).

[4] Lane and Noyes, J. Am. Chem. Soc. 161 (1932).

[5] F.F. Krivonos, J. Appl. Chem. 31, 3, 503 (1958).**

[6] A.I. Brodskii, Physical Chemistry [in Russian] (Goskhimizdat, 1948).

[7] K.F. Pavlov and P.R. Romankov (Editors), Essays on General Chemical Technology [in Russian] (Goskhimizdat, 1947).

[8] I.S. Travkin, Doctorate Dissertation [in Russian] (Moscow, 1943).

[9] Meunier, Ann. Chim. [6], 10, 226 (1884).

[10] Matthews, J. Chem. Soc. 59, 166 (1891).

Received August 3, 1956

*Russian translation.

**Original Russian pagination. See C.B. translation.

HYDROGENATION OF GLUCOSE IN PRESENCE OF GRANULATED RANEY NICKEL CATALYST UNDER FLOW CONDITIONS*

E.M. Adaskin, N.I. Ziminova, B.L. Lebedev and S.V. Pavlov

The All-Union Scientific Research Institute of the Hydrolytic and Sulfite Alcohol Industry (Moscow Section)

The hydrogenation of sugars, including glucose, with formation of the polyhydric alcohol sorbitol has become a particularly important problem at the present time. This is shown by the interest aroused by this problem both in the USSR and abroad.

Sorbitol and its derivatives are becoming increasingly widely used in various industries: in the tobacco, food, paper, textile, pharmaceutical, and varnish and paint industries, in the production of glues, artificial cork, resins, cosmetics, etc.

The literature contains numerous papers dealing with the catalytic reduction of sugars under static conditions (in batch autoclaves). These papers contain a great variety of data on the use of various catalysts, the influence of temperature, agitation, pH of the medium, pressure, grain size, etc.

In 1912 Ipatieff [1] performed the first experiments on the catalytic reduction of sugars. Sorbitol was obtained in quantitative yield by the hydrogenation of glucose in alcoholic solution in presence of nickel at 100 atm and 130°.

Covert, Connor and Adkins [2] performed experiments using nickel on kieselguhr, or copper chromite under pressure.

Ioshikawa [3] also performed experiments with the use of nickel and iron-nickel catalysts under pressure.

An English patent [4] describes the hydrogenation of glucose in presence of metallic catalysts such as Ni, Co, or Cu, or of their oxides with the oxides of chromium, cerium, titanium, molybdenum, tungsten, thorium, or aluminum as promoters; it is recommended to carry out the process at 90 atm and pH 7-9.

Szewczyk et al. [5] studied the effects of agitation, pressure, temperature, and pH on the yield and quality of the sorbitol obtained by catalytic hydrogenation of glucose over $NiAl_2O_3$.

In their opinion, agitation and a pH value of 8.5 are necessary to avoid caramelization; variations of pressure in the range of 70-133 atm and temperature in the range of 97-200° do not influence the reaction product.

Maksimov [6] was the first to propose the use of Raney nickel as a catalyst for the hydrogenation of glucose.

The hydrogenation of glucose under various conditions (of temperature, pressure, reaction medium, etc.) in presence of Raney nickel catalyst was later described by Borisoglebskii [7], Ivanov [8], Tettamanzi and Arnaldi [9], Kanbinos and Ballun [10], Hefti and Kolb [11] and others.

*Communication I.

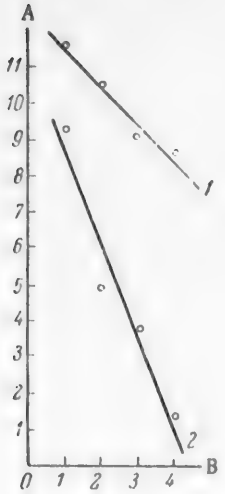

Fig. 1. Investigation of the comparative activities of Raney catalysts containing 46 and 27% nickel: A) amount of glucose hydrogenated over 1 g of nickel (in g); B) experiment numbers. Nickel content (%): 1) 46; 2) 27.

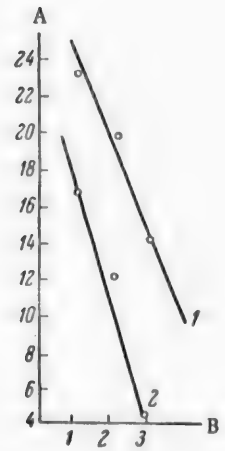

Fig. 2. Investigation of the comparative activities of Raney catalysts containing 46 and 50% nickel: A) amount of glucose hydrogenated over 1 g of nickel (in g); B) experiment numbers. Nickel content (%): 1) 46; 2) 50.

Thus, most of the investigations were concerned with the hydrogenation of glucose in batch equipment.

No information is available in the general literature on the continuous hydrogenation of glucose with the use of static catalysts. The very limited patent data are predominantly of a descriptive and advertizing character.

Zardalishvili, Tursin and Tsyplakov [12] were the first, in 1943, to obtain a patent for a process for the continuous hydrogenation of glucose to sorbitol. The catalyst was Raney nickel (1:1). The mixture of glucose solution and hydrogen was fed into the reactor from below. Later, de Nooijer and Koome [13] described a process in which the components were fed into the reactor from above.

It was of interest to study the continuous hydrogenation of glucose in a flow unit in presence of a stationary Raney nickel catalyst.

Studies of the Relative Activity of Raney Nickel Catalysts

Before the investigations of the continuous hydrogenation of glucose in the flow unit it was necessary to compare the relative activities of different Raney catalysts. The relative activities of Raney nickel (Ni 50%), a Raney-type nickel catalyst (Ni 27%), and a Raney-type nickel catalyst (Ni 46%) activated with chromium in the hydrogenation of glucose were studied.

The experiments were performed in a rotating autoclave 250 ml in capacity. Commercial anhydrous glucose was used as the starting material. The amount of catalyst taken was 5% of the weight of the glucose (calculated as nickel).

A sample of powdered alloy was treated with 20% caustic soda solution on warming until evolution of hydrogen ceased completely. The catalyst was then washed with distilled water to a weak alkaline reaction.

The prepared catalyst was stirred into 100 ml of glucose solution. Milk of lime was added to the solution to pH 8.5, and the solution was put into the autoclave. The autoclave was then closed, hydrogen was blown through, the required hydrogen pressure was obtained, and the heating was turned on. The time of heating to the required temperature was the same in all the experiments.

At the end of the experiment the autoclave was rapidly cooled in water to 20-30°, the gas was released, and the contents of the autoclave removed. When it was required to study the decrease of catalyst activity in the hydrogenation of several portions of glucose in presence of one portion of catalyst, the catalyst was immediately mixed with the next portion of glucose solution.

The concentration of the unreacted sugar in the filtrate was determined by Bertrand's method [14], and the dry solids content was found refractometrically. The concentration of hydrogenated sugars per 1 g of nickel was used as a measure of the catalyst activity, and also of the decrease of activity in repeated hydrogenation with the same portion of catalyst.

The results of determinations of the relative activity of Raney nickel catalysts are given in Table 1 and Figs. 1 and 2. A single portion of each of the catalysts was used in the experiments.

The data in Table 1 show that the catalyst promoted with chromium is more active than the catalysts without additions, and is deactivated more slowly.

Experiments with the continuous apparatus. The experiments were performed in presence of a stationary granulated Raney nickel catalyst, activated with chromium, at 130° and 75 atm hydrogen pressure; 35% glucose solution was made alkaline to pH 8.5-9.

TABLE 1

Tests of Raney Nickel Catalysts in the Hydrogenation of Glucose

Expt. No.	Nickel content (%) of Ni-Al catalyst	Residual sugars (%)	Am't glucose hydrogenated (g/l g N)	Experimental conditions
1	46	42.2	11.6	Hydrogenation time 1 hour, solution concentration 49%, temperature 130°, hydrogen pressure 75 atm, amount of solution 100 ml
2		47.3	10.5	
3		55.1	9.0	
4		57.3	8.5	
1	27	52.7	9.3	
2		73.7	4.9	
3		81.6	3.7	
4		93.1	1.4	
1	46	43.9	23.2	Hydrogenation time 30 min, solution concentration 19%, temperature 100°, hydrogen pressure 60 atm
2		52.1	19.8	
3		65.9	14.1	
1	50	56.1	16.7	
2		68.0	12.2	
3		87.2	4.9	

The experiments on the continuous hydrogenation of glucose were carried out in the laboratory unit of the All-Union Scientific Research Institute of the Hydrolytic and Sulfite Alcohol Industry; they are shown schematically in Fig. 3.

Hydrogen from the cylinders 1 passed into the hydrogen duct 2, and then into the gas holder 3 through a reducing valve. From the gas holder, the hydrogen entered the compressor 4, where it was compressed to 300 atm, then the buffer vessel 5 and the preheater 6.

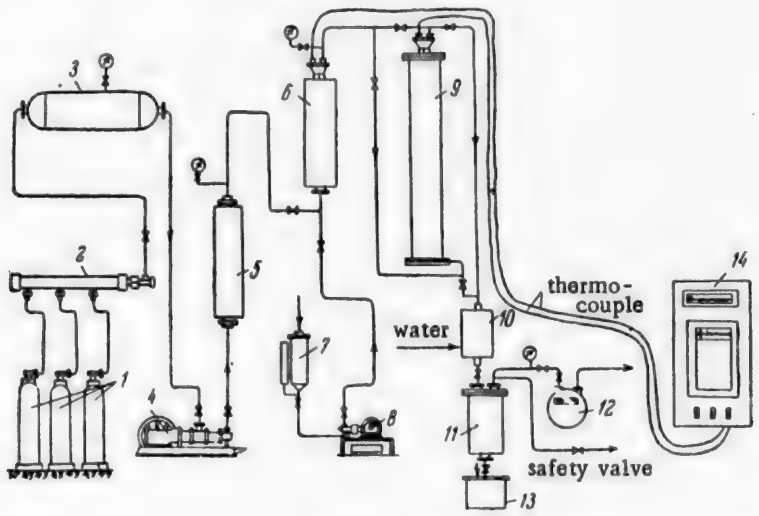

Fig. 3. Apparatus for continuous hydrogenation in presence of a stationary catalyst.

The glucose solution was put into the vessel 7, and fed into the preheater by means of the liquid pump 8. The mixture of hydrogen and glucose solution was heated to 80-90°, entered the reactor 9, passed through the layer of catalyst, and then entered the condenser 10, where it was cooled to 20-30°. The cooled mixture of hydrogen and solution then passed to the separator 11 where the hydrogen was separated from the solution.

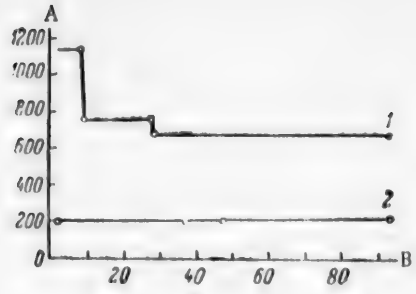

Fig. 4. Effect of feeding procedure on the catalyst activity: A) feed rate of solution (ml/hour); B) time (hours). Feed: 1) downward; 2) upward.

The hydrogen passed through the gas meter 12 and was released into the atmosphere. As the liquid accumulated in the separator it was led off through a throttle valve into the receiver 13, connected with the atmosphere.

The temperature in the reactor and preheater was measured by means of chromel-copel thermocouples, connected to the control panel 14, to an accuracy of ±0.5%.

The pressures of the liquid pump, the buffer vessel, preheater, and separator were measured by means of MT-150 manometers.

Activation of the alloy. The catalysts were prepared as follows. The alloy, crushed to the required grain size, was weighed and put into a round-bottomed flask fitted with a reflux condenser; the condenser was connected to a gas meter for recording the volume of hydrogen liberated in the reaction. 200 ml of 20% NaOH solution per 50 ml of alloy was introduced into the flask.

During the first few minutes hydrogen was evolved vigorously even without application of heat owing to the exothermic reaction between the aluminum and alkali; after 10-15 minutes the evolution of hydrogen died down somewhat, and the flask was then warmed.

The reaction was stopped when the volume of hydrogen liberated corresponded to the removal of 40% of aluminum from the alloy. The catalyst was then washed with distilled water to a weak alkaline reaction.

500 ml of catalyst so prepared (400 ml of catalyst with 2-3 mm grains, and 100 ml with 3-5 mm grains) was put into the reactor.

Evaluation of the hydrogenation process. For estimation of the degree of hydrogenation of the glucose solutions, the residual sugar (RS) was determined once or twice every hour by the Bertrand method. In addition, the dry solids content of each sample was determined refractometrically, and the pH of the medium potentiometrically. The permissible RS level was taken to be 1% of the dry solids.

The hydrogenation process was investigated both with downward and with upward feeding of the mixture of solution and hydrogen through the catalyst.

For comparison of the relative efficiency with downward and upward feeding, it was important to estimate the activity of the catalyst, in terms of hours of service life, and the amount of substance hydrogenated in terms of dry solids.

Downward feed of the components. The results of the experiments are given below and in Fig. 4.

Feed rate of glucose solution (in ml/hour)	Operating time at this feed rate (hours)	Residual sugar content in the last hour (%)
1140	8	0.9
760	19	0.83
690	66	1.0

When the glucose solution was fed at 1140 ml/hour the conversion was almost complete for seven hours.

However, after the eighth hour the percentage of residual sugars in the sorbitol almost reached the permissible level (0.9%). Therefore, the feed rate of the solution was lowered to 760 ml/hour, and from the 9th to the 27th hour of operation the residual sugar content rose from 0.5 to 0.83%.

Because of the increase in the residual sugars, the feed rate of the glucose solution was again lowered to 690 ml/hour; the loss of catalyst activity during the subsequent 66 hours was very small. With downward feeding of the glucose solution-hydrogen mixture through the catalyst, 27.8 kg of glucose was hydrogenated in 93 hours.

The average rate of hydrogenation was therefore 300 g of glucose per hour; i.e., 0.65 g of glucose was hydrogenated, on the average, per 1 g of nickel per hour.

Upward feed of the components. It was interesting to compare the results obtained with downward and upward feeding of the components in the same unit.

A fresh portion of catalyst, prepared as described above, was used for the study of hydrogenation with upward feeding of the components.

The results of the experiments are given below and in Fig. 4.

Feed rate of glucose solution (in ml/hour)	Operating time at this feed rate (hours)	Residual sugar content in the last hour (%)
190	36	0.23
200	11	0.5
220	46	0.54

A total of 7.7 kg of glucose was hydrogenated in 93 hours with upward feeding of the components. The average rate of hydrogenation in this case was 83 g of glucose per hour, or an average of 0.18 g of glucose per 1 g of nickel per hour.

Comparison of the results obtained by the two different feeding methods shows that the hydrogenation rate is more than three times as high with downward feeding of the mixture.

At the end of the experiments the activity of catalysts used for 93 hours in the autoclave* was tested in the unit.

The activity of fresh catalyst was tested for comparison. The experimental conditions and results are given in Table 2.

If the amount of glucose hydrogenated in one hour per 1 g of nickel in the fresh catalyst (I) is taken as 100%, then after 93 hours catalyst (II) lost 34% of its activity, and catalyst III, 58.5%.

However, having lost 34% of its activity in 93 hours, catalyst II gave an average hourly hydrogenation of 0.18 g of glucose per 1 g of nickel. Catalyst III, which lost 58.5% of its activity in 93 hours, gave an average hourly hydrogenation of 0.65 g of glucose per 1 g of nickel.

TABLE 2

Studies of Comparative Catalyst Activity (Time 1 hour, concentration of glucose solution 24.5%, temperature 120°, p = 60 atm, pH = 9.5, 25 ml of catalyst, grain size 2-3 mm)

Amount of glucose	Fresh catalyst I	Catalyst used with downward feeding	Catalyst used with upward feeding
Residual in solution (%)	11.6	41.8	63.7
Hydrogenated in 1 hour (%)	88.4	58.2	36.3
Hydrogenated in 1 hour (g)	21.7	14.3	8.9
Per 1 g of nickel per hour (g)	0.94	0.62	0.39

The catalyst efficiency mainly depends on the hydrogenation rate and the corresponding rate of decrease of catalyst activity, and therefore the catalyst efficiency Q may be expressed in grams of glucose hydrogenated per 1 g of nickel for a decrease of 1% in the activity, by the following formula:

$$Q = (K \cdot T)/f,$$

*As in original – Publisher's note.

where K is the amount of glucose hydrogenated (in g per 1 g of nickel per hour), T is the hydrogenation time (hours), and f is the decrease of catalyst activity in time T (%).

The experimental results are substituted into this formula.

In hydrogenation with downward feeding (III) we have

$$Q = \frac{0.65 \cdot 93}{58.5} = 1.03 \text{ g},$$

and in hydrogenation with upward feeding (II) we have

$$Q = \frac{0.18 \cdot 93}{34} = 0.49 \text{ g}.$$

Thus, the catalyst efficiency in operation by procedure (III) is double that in procedure (II).

SUMMARY

1. Chromium-promoted Raney nickel catalyst is more active than Raney nickel without promoters in the hydrogenation of glucose and has higher stability.

2. Experiments on the continuous hydrogenation of aqueous glucose solutions with different feed procedures showed that when the components are fed downward into the reactor (III), the hydrogenation rate is three times that obtained with upward feeding (II).

3. Calculations based on residual activities show that in the continuous process the specific consumption of catalyst in the hydrogenation of glucose is twice as high in procedure (II) as in procedure (III).

4. The lower hydrogenation rate in feeding by procedure (II) is due to difficulties in transport of hydrogen to the catalyst surface.

LITERATURE CITED

[1] W. Ipatieff, Ber. 45, 3218 (1912).

[2] L.W. Covert, R. Connor and H. Adkins, J. Am. Chem. Soc. 54, 1651 (1932).

[3] K. Ioshikawa, Bull. Inst. Phys. Chem. Research 13, 1045 (1934).

[4] British Patent 354,196.

[5] I. Szewczyk, E. Treszczanowicz and I. Chmielewska, Chem.Abs. 47, 3235 d (1953).

[6] V. Maksimov, J. Gen. Chem. 9, 936 (1939).

[7] D. Borisoglebskii, J. Appl. Chem. 13, 571 (1940).

[8] A. Ivanov, Food Industry 1, 3, 30 (1941).

[9] A. Tettamanzi and N. Arnaldi, Chem. Abs. 38, 3841 (1944).

[10] I.V. Kanbinos and A.T. Ballun, J. Am. Chem. Soc. 75, 4501 (1953).

[11] H.R. Hefti and W. Kolb, Swiss Patent 261,359.

[12] Ia.I. Zardalishvili, V.M. Tursin and V.M. Tsyplakov, Soviet Patent 62562.

[13] C.N.S. de Nooijer and I. Koome, Dutch Patent 72054.

[14] Tollens and Elsner, Short Handbook of Carbohydrate Chemistry [Russian translation] (Moscow, 1938).

Received January 25, 1957

AGING AND THERMOOXIDATIVE DECOMPOSITION OF ETHYLCELLULOSE*

O.P. Koz'mina and V.I. Kurliankina

Institute of High-Molecular Compounds, Academy of Sciences USSR

Like ordinary ethers – ethyl [1], isopropyl [2], benzyl [3] and others, cellulose ethers can also be oxidized by molecular oxygen.

The oxidative conversion of allylcellulose under the action of oxygen was studied earlier [4] by one of us. The oxidation of ethylcellulose (EC) has been studied by McBurney [5].

The present paper deals with the mechanism of aging and thermal degradation of cellulose ethers.

Ethylcellulose is unchanged when heated to 140-160° in an oxygen-free medium (Fig. 1), whereas in presence of oxygen degradation begins even at lower temperatures – the molecular weight, mechanical strength, and film elasticity decrease sharply [6], the minimum constant viscosity of concentrated solutions falls [7], and ethoxyl groups are split off while carbonyl and carboxyl groups form in the ethylcellulose molecule. The reaction is characterized by induction periods (Fig. 2), which are followed by periods of acceleration; heat is evolved, oxygen is rapidly absorbed, and volatile oxidation products such as acetaldehyde, ethyl alcohol, formic acid, ethyl formate, CO_2, etc. are split off.

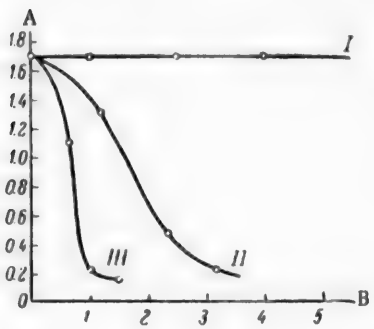

Fig. 1. Thermooxidative decomposition of ethylcellulose: A) intrinsic viscosity [η] of ethylcellulose in acetone; B) time (hours); I) [η] of ethylcellulose at 140° (in nitrogen); II) variation of [η] of ethylcellulose at 140° (in air); III) the same (in oxygen).

The length of the induction periods depends not only on the temperature, but also on the time of previous aging, and is determined by the formation of peroxide groups in the ether molecule. If the peroxide groups are removed (destroyed) under mild conditions, the induction periods in the oxidation reaction on heating are increased again [8].

The oxidation of ethylcellulose by oxygen under the influence of ultraviolet radiation is analogous to the oxidative decomposition of ethylcellulose in the dark.

EXPERIMENTAL

Apparatus and experimental conditions. The oxidation of ethylcellulose was performed in a vessel with a porous bottom, through which oxygen, nitrogen, or carbon dioxide was introduced from below through a long tube coiled in the form of a spiral (to heat the gas) (Fig. 3).

To determine the oxygen absorption, the reaction vessel 1 was connected to an oxygen buret. The oxidation was performed in a closed system, with continuous circulation of the gas phase through absorbents for removal of volatile reaction products from the oxygen. The circulation was effected by means of the electromagnetic pump 2 and glass valves 3, at a constant gas rate. The contaminated oxygen from the reaction vessel 1

*Communication III in the series on the oxidation of cellulose ethers by molecular oxygen.

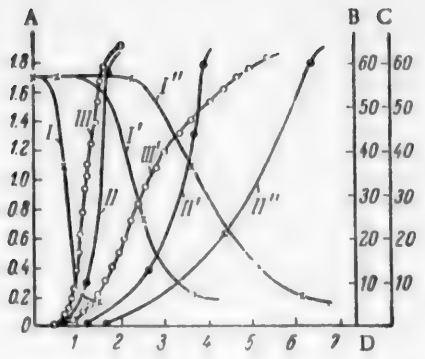

Fig. 2. Effect of temperature on the rate of thermooxidative decomposition of ethylcellulose: A) $[\eta]$ of ethylcellulose; B) amount of acetaldehyde (in mg per g of EC); C) amount of oxygen absorbed (in cc per g of EC); D) time (hours); I, I', I'') decrease of $[\eta]$ of ethylcellulose at 140, 130, and 125°; II, II', II") evolution of acetaldehyde at 140, 130, and 125°; III, III') absorption of oxygen at 140 and 130°.

was drawn through the absorption flasks containing chromic mixture 4, askanite, and a drying agent 5. The buret 6, containing water as the measuring liquid, was connected in the system along the path of the contaminated oxygen, which was therefore dried in the absorption flasks and entered the reaction vessel from below. The system was maintained at atmospheric pressure by means of the mercury circuit closer 7, connected through the relay 8 to the electrolytic cell 9. The latter was connected to the bulb 10 of the buret. The cell was automatically put into circuit as the pressure in the system fell, and under the pressure of the carbon dioxide liberated in the electrolysis of sodium oxalate the water in the buret rose until the pressure became equal to atmospheric; the system contained a pressure compensator 11, the volume of which was equal to the total volume of the heated parts of the apparatus.

If the reaction is performed without removal of the volatile products, as in McBurney's experiments [5], the oxidation proceeds irregularly, the volatile products must be blown out at intervals, and the oxygen consumption increases as the result of secondary processes. McBurney's procedure has other defects: if the oxidation is performed in a flask with a stirrer, the mixing is not uniform, because the dry ethylcellulose is readily electrified and adheres to the walls of the vessel and the stirrer, while the mercury seal is not safe, because mercury vapor which accelerates oxidation may enter the flask; the use of dibutyl phthalate in the measuring buret is also a bad choice. These defects are eliminated in our method.

Aging of ethylcellulose. When ethylcellulose is kept at room temperature, oxygen is slowly absorbed; after some time (three to four months after preparation) the ethylcellulose gives a positive reaction for peroxides and acetaldehyde can be detected.

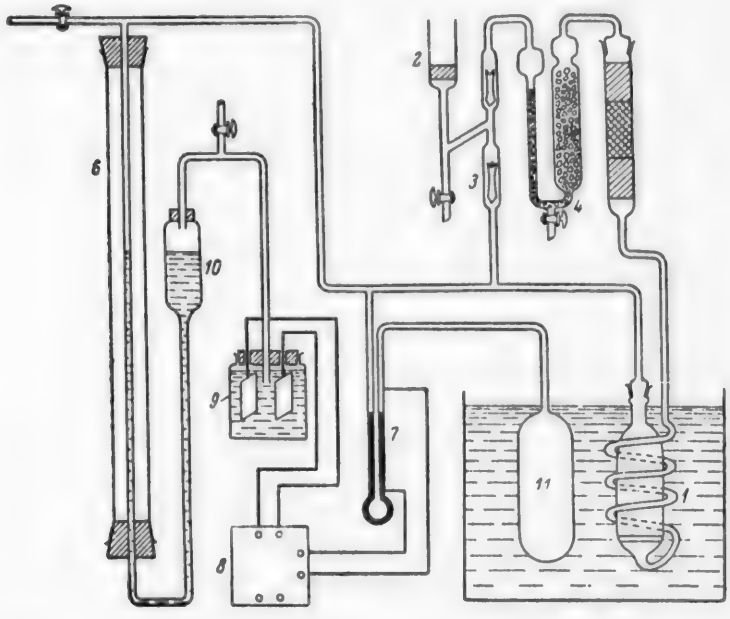

Fig. 3. Apparatus for oxidation of ethylcellulose. Explanations in text.

TABLE 1

Composition of the Liquid Oxidation Products of Ethylcellulose

Fractions	Boiling point (°C)	Amounts of fraction (%) under different experimental conditions	Composition	Characteristics**
I	21	50-60	Acetaldehyde	Boiling point 21°; 2,4-dinitrophenylhydrazone m.p. 167-168°; condensation product with dimedon, m.p. 139-140° (no m.p. depression with mixed samples)
II	51-54	10-25	Ethyl formate (with admixture of I)	B.p. 54°, $n^{20}D$ 1.3598, difficultly soluble in water, ester number 0.53 g NaOH per 1 g of substance; saponification gives C_2H_5OH and HCOOH
III*	65-76	0-4	Mixture of II and IV with admixture of methylglyoxal	Greenish, polymerizes readily; dioxime gives a red complex with Ni^{++} salts
IV	76-78	10-20	Ethyl alcohol (with admixture of II and III)	B.p. 78°, $n^{20}D$ 1.3620, forms iodoform, iodine number of xanthate 796 mg iodine per 1 g of xanthate; m.p. of diethylxanthide ~30°
V	Residue, not distilled 97-100	10-20	Water, ethyl alcohol, traces of aldehydes, peroxides, and unsaturated compounds	Reaction with the Fischer reagent, formation of esters and iodoform
Acids	105-110	0-25	Formic acid (~80% of the total). Acetic acid	Reduction of Ag^+ salt solutions, quantitative oxidation by $KMNO_4$, $Pb(HCOO)_2$ formed as characteristic needles (% Pb found 69.60, calculated 69.71); characteristic crystals of $AgOOCCH_3$

*Methylglyoxal is formed only in the oxidation of unpurified ethylcelluloses, containing ~0.5% ash, at 140°.
**The data refer to individual substances isolated from the primary fractions (Column 4).

TABLE 2

Oxidation of Ethylcellulose for Five Hours at 150°

Weight loss of EC (%)	Ethoxyl content after oxidation (%)	Volatile reaction products (mg per g of EC)			CH_3CHO content (as % of ethoxyl loss)	O_2 consumption (in ml per g of EC) at 20°, 760 mm
		CH_3CHO	Acids converted to HCOOH	CO_2		
7.48	39.92	59.2	35.5	15.1	59.3	60

There can be no doubt that peroxides of ethylcellulose are formed: the peroxide number is not changed either by vacuum treatment of the specimens or by dialysis of ethylcellulose solutions. For example, when sample 808-N had been stored for a long time its peroxide number was 6.4 ml of 0.01 N $Na_2S_2O_3$ solution per 5 g of ethylcellulose; after vacuum treatment it was 6.32 ml and after dialysis of an alcoholic solution, 6.30 ml. The peroxide and acetaldehyde contents increase so little during further storage that for many months the

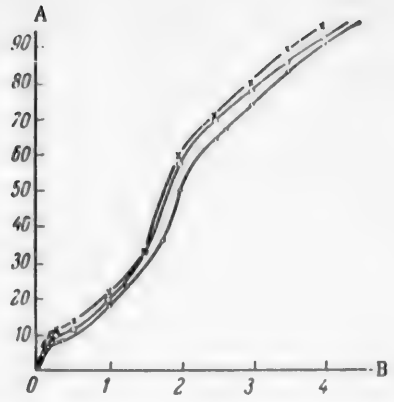

Fig. 4. Absorption of oxygen by ethylcellulose at 130°, with O_2 circulated at 3 liters/hour (duplicate experiments): A) amount of O_2 absorbed (per 1.5 g of EC); B) time (hours).

oxidation does not influence either the ethoxyl content or the degree of polymerization, and only affects the rate of thermo-oxidative decomposition. Whereas sample 808-N initially required ten hours of oxidation in oxygen at 130° to attain a certain degree of degradation, after three months the oxidation time became five hours, and after six months, three hours. Samples kept for a long time, containing peroxide groups, are characterized by a jump on the oxygen-absorption curve at the start of heating (Fig. 4), while the curve for freshly prepared ethylcellulose ascends smoothly (Fig. 2).

Oxidation of ethylcellulose on heating. The material used was technical ethylcellulose with ethoxyl contents from 47 to 49%, freed from mineral impurities down to 0.01% ash content by filtration of dilute solutions through columns with activated carbon, and reprecipitated in the form of a loose mass. If the precipitation conditions, the amount of ethylcellulose taken for the reaction, oxygen rate, and temperature were kept constant, reproducible results were obtained both for the amount of oxygen absorbed (Fig. 4), and for the percentage decrease of ethoxyl content

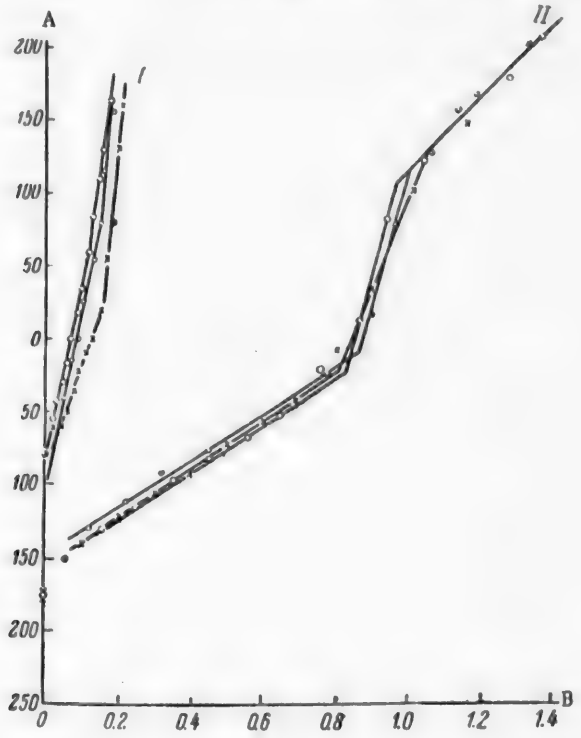

Fig. 5. Potentiometric titration curves of ethylcellulose with alkali, before and after oxidation (parallel determinations): A) potential (mv); B) volume of 0.0926 N NaOH (ml). Ethylcellulose: I) original; II) oxidized.

and the liberation of volatile oxidation products. Oxidation was studied at various temperatures (70, 90, 125, 130 and 140°); the only observed differences were in the reaction rate, while the composition of the volatile products remained similar.

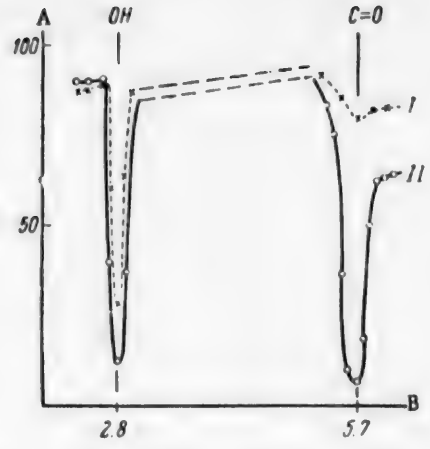

Fig. 6. Transmission spectrum of ethylcellulose in the infrared region: A) transmission (%); B) wavelength λ. Ethylcellulose: I) original; II) oxidized.

For accumulation of the volatile reaction products, large amounts of purified and unpurified factory samples of various grades of ethylcellulose were oxidized. One kilogram of ethylcellulose yielded from 70 to 150 ml, according to the degree of oxidation, of condensed volatile products collected in traps cooled to −80°. The composition of the condensate did not depend on the degree of substitution in the range studied, but the proportions of the components varied with the oxidation conditions. Under milder conditions the reaction products contained up to 3% of peroxides; the peroxide content decreased with increase of temperature and of the thickness of the ethylcellulose layer, and with decrease of the oxygen rate. The highest acid content was obtained at 125°; if the temperature was raised to 140° and the oxygen was passed slowly, there were no acids in the volatile products. The condensate was fractionated at a very low vapor rate in an empty column; this gave sharp separation of the fractions. If the condensates contained acids, these were previously removed as the barium or calcium salts (by neutralization with calcium or barium carbonates).

The composition of the fractions obtained after oxidation of ethylcellulose under various conditions is given in Table 1.

A more detailed investigation, with quantitative evaluation of the course of oxidation and analysis of the oxidized product, was performed with a sample of ethylcellulose 808-N, containing 47.23% ethoxyl and 0.008% ash. Similar amounts (1-1.5 g) of ethylcellulose were oxidized under the same conditions: at 130°, oxygen blown through at 3 liters per hour for five hours (until the substance began to liquefy).

In one series of experiments the weight changes of the ethylcellulose during oxidation, ethoxyl loss, amount of oxygen absorbed, and the volatile products formed were determined (Table 2 and Fig. 4), and in the other series the oxidized ethylcellulose was analyzed (Table 3, Figs. 5 and 6).

TABLE 3

Characteristics of Original and Oxidized Ethylcellulose

Ethylcellulose	Melting point (°C)	[η]	Molecular wt.* $1 \cdot 10^3$	Ethoxyl (%)	Carboxyl (%)		Aldehyde groups (%)	Carboxylic ester groups (%)
					total	uronic		
Original	185	2.20	50	47.23	0.10	0.04	Nil	Nil
Oxidized:								
a) water-insoluble fraction (after dialysis)	135	0.12	2	38.2	1.40	0.95	2.6	0.2
b) water-soluble fraction	80	–	–	31.3	6.2	2.0	6.7	0.3

*The molecular weight was determined by sedimentation in the ultracentrifuge; [η] is the intrinsic viscosity in alcohol-benzene mixture.

Acetaldehyde was determined quantitatively by means of the dimedon reaction [9] and by the hydroxylamine method, which also gave the volatile acids formed in the reaction (by difference of the pH during titration).

The errors in the determinations of aldehyde and acids under dynamic conditions were determined by means of control experiments on synthetic mixtures, and allowed for in the calculations.

The average results of ten parallel experiments are given in Table 2.

The acetaldehyde corresponds to about 60% of the ethoxyl groups split off, while the remaining 40% is distributed between ethyl alcohol in the free state and as ethyl formate.

The oxidized ethylcellulose was greatly degraded and heterogeneous; a considerable amount of it was soluble in water, whereas the original material was completely insoluble.

Elementary Composition of Ethylcellulose (%)

Original	C 56.77,	H 9.09,	O 34.14.
Oxidized	C 54.47,	H 8.63,	O 37.16.

The water-soluble portion (20% of the total) was extracted, dried, and obtained in the form of a brittle mass, readily ground to powder. The insoluble (main) fraction was dialyzed in alcoholic solution to remove low-molecular impurities. About 3% of the substance was dialyzed out; the composition of this was similar to that of the substance obtained from the aqueous extract.

The characteristics of the oxidized and original ethylcelluloses are compared in Table 3.

The carboxyl group content (total) was determined by potentiometric titration in alcoholic solution in a nitrogen atmosphere (Fig. 5). The potential changes abruptly at pH = 7.5-9.5. Alkali continues to be absorbed in the alkaline region as the result of a side reaction, probably with aldehyde groups.

Carboxylic ester groups were determined by saponification by cold 1% NaOH solution, by the method of Kaverzneva, Ivanov and Salova [10].

Carbonyl groups were determined by the hydroxylamine [11] and iodine methods. However, in the reaction of ethylcellulose with hydroxylamine in alcoholic solution the pH change is slight, and reliable results cannot be obtained by titration of the liberated acid. The carbonyl group content can be estimated from the amount of combined nitrogen in the ethylcellulose; this was 0.95%, corresponding to 0.7 millimole of carbonyl groups per 1 g of ethylcellulose (the excess hydroxylamine was first removed by dialysis of the solution to a negative Bamberger reaction).

The determination by the iodine method was performed in a carbonate buffer solution at pH 9.5. A weighed sample of oxidized ethylcellulose was dissolved in 5 ml of pure dioxan; when the carbonate buffer was added, the ethylcellulose remained in the form of a fine suspension which did not settle or adsorb iodine. The subsequent analysis followed the usual procedure. A blank experiment was also performed. Iodine was not adsorbed during a second treatment with iodine under the same conditions. The iodine number of the original ethylcellulose was determined by the usual method in heterogeneous conditions, with addition of alcohol (after acidification) to dissolve the ethylcellulose.

Determination of functional groups by infrared spectroscopy (from V.N. Nikitin's experiments). The total contents of carbonyl, carboxyl, and other groups containing the $-C=O-$ bond, and of hydroxyl groups, were determined in the original and oxidized ethylcellulose. 5% solutions in chloroform were used. The absorption maxima were found at 5.7μ for the carbonyl group and 2.8μ for the hydroxyl group (Fig. 6).

SUMMARY

1. The degradation of ethylcellulose on heating (at 100-150°) is caused by oxidation by atmospheric oxygen. Under the same conditions,but in absence of oxygen, ethylcellulose is stable when heated.

2. The oxidation of ethylcellulose by oxygen is characterized by an induction period the length of which depends on the temperature and the aging time.

3. Degradation is the consequence of decomposition of peroxides formed by the addition of oxygen molecules to the ether groups. Peroxide groups are formed even at room temperature during aging of ethylcellulose.

4. Thermooxidative decomposition decreases the molecular weight of ethylcellulose, ethoxyl groups are split off in the form of ethyl alcohol and acetaldehyde, and formic acid, ethyl formate, and carbon dioxide are formed; carboxyl and carbonyl groups are formed in the ethylcellulose molecule as a result.

LITERATURE CITED

[1] A.M. Clover, J. Am. Chem. Soc. 44, 1107 (1922).

[2] K.I. Ivanov, V.K. Savinova and E. Mikhailova, J. Gen. Chem. 16, 65, 103, 1015 (1946).

[3] A.M. Clover, J. Am. Chem.Soc. 46, 419 (1924); N.A. Milas, J. Am. Chem. Soc. 53, 221 (1931).

[4] S.N. Danilov and O.P. Koz'mina, J. Gen. Chem. 28, 1823 (1948).

[5] L.F. McBurney, Ind. Eng. Chem. 41, 1251 (1949).

[6] T.I. Samsonova and S.Ia. Frenkel', Colloid J. 20, 1 (1958).•

[7] T.I. Samsonova and L.V. Ivanova-Chumakova, Colloid J. 19, 3, 343 (1957).•

[8] O.P. Koz'mina, V.I. Kurilankina and E.N. Matveeva, Proc. Acad. Sci. USSR 144, 4, 789 (1957).•

[9] D. Vorländer, C. Ible and H. Volkholz, Z. Anal. Ch. 77, 789, 301 (1929).

[10] E.D. Kaverzneva, V.I. Ivanov and A.S. Salova, Bull. Acad. Sci. USSR, Div. Chem.Sci. 1, 185 (1952).•

[11] E.D. Kaverzneva and A.S. Salova, J. Anal. Chem. 8, 365 (1953).•

Received March 30, 1957

•Original Russian pagination. See C.B. translation.

ISOLATION OF PURE DEXTROPIMARIC ACID FROM P. SILVESTRIS OLEORESIN

I.I. Bardyshev, A.G. Sokolov and O.I. Cherniaeva

The purpose of the present work was isolation of pure dextropimaric acid from domestic P. silvestris oleoresin and determination of its physical constants which, as is seen from the data below, show considerable variations.

Dextropimaric acid was first isolated by Cailliot [1] from the oleoresin of P. maritima by crystallization of the resin acids from alcohol. The acid obtained had m.p. above 200°, $[\alpha]_D$ + 56°, and crystallized in the form of plates.

Vesterberg [2] isolated "pimaric" acid with m.p. 130-140° and $[\alpha]_D$ −58.6° from the oleoresin of P. maritima by crystallization from alcohol. After treatment of this acid with 3% aqueous caustic soda and recrystallization of the salt from hot water, the sodium salt was decomposed by hydrochloric acid and recrystallized repeatedly from alcohol. This gave dextropimaric acid with m.p. 210-211° and $[\alpha]_D$ +72.5°.

Tschugaeff and Theary [3] treated galipot by Vesterberg's method and isolated dextropimaric acid with m.p. 211-212° and $[\alpha]_D$ +75.5°.

Dupont [4], in isolating dextropimaric acid by Vesterberg's method, used strong acetic acid, which isomerized levopimaric acid into abietic acid. The following constants are given by Dupont for dextropimaric acid: m.p. 211-212° and $[\alpha]_D$ +63.5° (in alcohol).

Ruzicka and Balas [5] used Vesterberg's method to prepare dextropimaric acid from the oleoresin of Picea excelsa. Their dextropimaric acid had the following constants: m.p. 211-212°, $[\alpha]_D$ +57.7° (0.48% solution in absolute alcohol) and $[\alpha]_D$ +59.7° (2.9% solution in absolute alcohol).

Balas [6] isolated dextropimaric acid with m.p. 211-212° and $[\alpha]_D$ +79.3° from the oleoresin of P. maritima. He obtained well-defined crystalline salts of dextropimaric acid with various organic bases – propylamine, dipropylamine, etc.

Kraft [7] isolated dextropimaric acid with m.p. 211° and $[\alpha]_D$ +52.9° from the oleoresin of P. palustris by successive crystallization first of the ammonium and then of the sodium salts of the resin acids.

Shkatelev [8] was the first to isolate dextropimaric acid from the common pine (P. silvestris), which is very widespread in our country, by the following method. He isomerized the resin acids by means of strong hydrochloric acid, and crystallized the resultant mixture of acids from alcohol. After separation of abietic acid, dextropimaric acid was precipitated from the mother liquor; after several recrystallizations from alcohol it had m.p. 210° and $[\alpha]_D$ +69.7°.

Krestinskii et al. [9] separated the resin acids from P. silvestris by Vesterberg's method, by crystallization of the sodium salts of pimaric acid from hot water. From the more difficultly soluble sodium salt dextropimaric acid with m.p. 211-212° and $[\alpha]_D$ +71.25° (in alcohol) was obtained.

Sandermann [10] prepared dextropimaric acid as follows. A boiling solution of the resin acids in methyl alcohol was treated with p-quinone. After separation of the addition compound of p-quinone and levopimaric acid, the mother liquor was concentrated and crystals of dextropimaric acid separated out. After recrystallization from acetone, and then from glacial acetic acid and methanol, dextropimaric acid was obtained with m.p. 210-211° and $[\alpha]_D$ +75° (in chloroform).

It is seen from this survey that most authors give the following constants for "dextropimaric" acid: m.p. 210-212°, and $[\alpha]_D$ +63.5° to +75.5° (in alcohol).

However, the most recent work shows that this acid is not the pure substance but a mixture of isomers: dextropimaric acid (I) and isodextropimaric acid (II). These acids differ only by the spatial positions of the methyl and vinyl radicals at the seventh carbon atom.

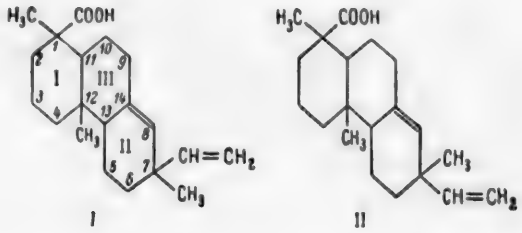

Harris and Sanderson [11] succeeded in separating these two isomeric acids and obtaining them in relatively pure form.

To separate these acids from accompanying substances, these authors prepared their amine salts, a method first used by Balas, and later by Palkin and Harris [12] and by Bardyshev [13]. Harris and Sanderson [14] used crystallization of the amine salts, and also the addition reaction of maleic anhydride with resin acids containing conjugated double bonds, to isolate from P. palustris oleoresin, and from the wood and gum rosins, dextropimaric acid of a high degree of purity, with m.p. 217-219° and $[\alpha]^{24}_D$ +79° (1% solution in absolute alcohol).

Our aim in the present investigation was to obtain pure dextropimaric acid from the oleoresin of P. silvestris.

To remove isodextropimaric acid, which is difficult to separate from dextropimaric acid, we recrystallized bornylamine pimarates from alcohol. As already reported [13], this method was used with success for the preparation of pure abietic acid. This method fully justified itself in the present instance also. Our dextropimaric acid melted within 1° at 219°, and had $[\alpha]^{24}_D$ +82.5° (1% solution in absolute alcohol), so that it was the purest sample of dextropimaric acid described so far in the literature.

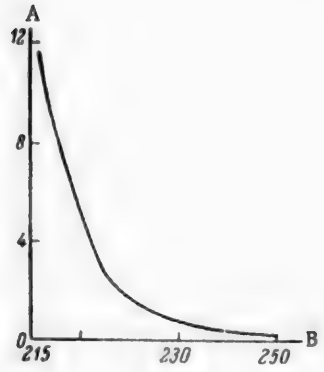

Ultraviolet absorption spectrum of dextropimaric acid: A) specific absorption coefficient α; B) wavelength (mλ).

The ultraviolet absorption spectrum of the dextropimaric acid• (see figure) has no maximum; this indicates an absence of conjugated double bonds, and is a characteristic feature of resin acids of this type.

EXPERIMENTAL

Isolation of the mixture of crystalline resin acids from the oleoresin. A weighed sample of the oleoresin was ground in a porcelain mortar with a small quantity of light-boiling ligroine (b.p. up to 100°) until a homogeneous mobile mass was obtained, and the liquid portion was separated by suction on a Buchner funnel. The mixture of resin acids was recrystallized twice from acetone. The filtered solution was cooled rapidly, the precipitated crystals were pressed out again on a Buchner funnel, and recrystallized from acetone, but this time slowly. The mixture of crystalline resin acids so obtained had m.p. 139.5-143°.

Preparation and recrystallization of the crystalline sodium salts. The resin acids were converted into their sodium salts. The resin acids were ground to a powder and transferred in portions to 1.5% aqueous caustic soda. The amount of caustic soda was taken in slight excess (2%) above the calculated amount. The resin acids were saponified with the solution heated to 40°. The transparent solution of the sodium salts of the resin acids was left to crystallize slowly. The

•1% solution in 95% ethyl alcohol.

sodium salts, which separated out in the form of white nacreous plates, were filtered off and recrystallized from hot water (not above 50°). The experimental results are presented in Table 1.

Fraction No. 1, which was the richest in the sodium salts of dextropimaric acid, was crystallized stepwise from hot water. The results of the crystallizations are given in Table 2.

TABLE 1

Experiments on the Preparation of Sodium Salts of Resin Acids

Fraction	Temperature conditions	Specific rotation*	
		expt. No. 1	expt. No. 2
Fraction No. 1	Cooled to 32°	− 78.8°	− 70.4°
Fraction No. 2	Cooled from 32 to 27°		− 82.3°
Fraction No. 3	Cooled from 27 to 15°	−164.8°	−127.5°

*The specific rotation was always determined for 1% solutions of the salts in 96% alcohol.

TABLE 2

Recrystallization of Fraction No. 1

Fraction	Specific rotation $[\alpha]_D$	Change of specific rotation on recrystallization				
		1	2	3	4	5
Fraction No. 1 from Expt. No. 1	−78.8°	−58.3°	−24.03°	+ 1°*	+9.3°	+38.3°
Fraction No. 1 from Expt. No. 2	−70.4°	−51.52°	−34.3°	+ 2.76°	−	−
Fraction No. 1** from Expt. No. 2	−70.4°	−33.15°	− 8.10°	+17.8°	−	−

*The crystal fraction was divided into two parts, one of which was recrystallized further, but the other was not.
**Fraction No. 1 from Experiment No. 2 was divided into two portions.

Recrystallization of free resin acids. The solubility in water of the sodium salts of the resin acids fell sharply as the fractions became richer in dextropimaric acid, and also as the result of hydrolysis. Therefore, further purification of the dextropimaric acid was effected by crystallization of the acids from alcohol.

The sodium salts were decomposed by shaking in a separating funnel with 0.5 N hydrochloric acid in presence of ethyl ether. This treatment was repeated three times, 1, 0.5, and 0.25 of the calculated amount of hydrochloric acid being added. The ether extracts were combined, washed with distilled water until the wash waters were neutral to methyl orange, dried over calcined sodium sulfate, and the ether was evaporated off on a water bath. The free resin acids were recrystallized several times from alcohol. The results of the recrystallization are given in Table 3.

Further recrystallization did not give the desired result, but merely led to loss of the substance.

Recrystallization of bornylamine dextropimarate and preparation of pure dextropimaric acid. Further purification of dextropimaric acid was effected by recrystallization of bornylamine dextropimarate. Acid fractions with $[\alpha]_D$ + 62.9, 64, 69.6° were dissolved in ethyl ether, and the calculated quantity (1 mole : 1 mole) of a saturated solution of bornylamine in ether was added. Because of the formation of bornylamine dextropimarate ($C_{19}H_{29}COOH \cdot NH_2C_{10}H_{17}$), which is almost insoluble in cold ether, the solution gradually set to a white compact mass.

TABLE 3

Recrystallization of Free Resin Acids

Fraction	Specific rotation $[\alpha]_D$ of fractions enriched with sodium dextropimarate	Change of specific rotation on recrystallization of free resin acids		
		1	2	3
Fraction No. 1 from Expt. No. 1	+38.3°	+50°	+60.5°	+62.9°
Fraction No. 1 from Expt. No. 1 (after 3rd recrystallization)	+ 1.0°	+35.1°	+55.1°	+69.6°
Fraction No. 1 (combined) from Expt. No. 2	+ 2.76° +17.8°	+47.2°	+59.4°	+54.5°

The ether was removed by suction through a No. 3 Schott funnel, and the salt was washed with a small quantity of ether in order to remove any accidental excess of either of the reagents. Bornylamine dextropimarate was then recrystallized three times from ethyl alcohol.

After the first recrystallization the salt had $[\alpha]_D$ +47.5°, after the second, +48.5°, and after the third, +49.0°. The dextropimaric acid isolated from this salt had m.p. 218.5-219° and $[\alpha]_D$ +77.5°.

The bornylamine dextropimarate was decomposed in a separating funnel by treatment with the calculated quantity of 0.5 N hydrochloric acid in presence of ether. This treatment was repeated three times. The combined ether extracts were washed with distilled water to a neutral reaction with methyl orange, dried over calcined sodium sulfate, and the ether was evaporated off on a water bath. The crystals so formed were recrystallized three times from alcohol to give dextropimaric acid with m.p. 219° and $[\alpha]_D$ +82.5° (1% solution in absolute alcohol).

SUMMARY

The dextropimaric acid isolated by the proposed method from the oleoresin of P. silvestris had m.p. 219° (uncorrected, in sealed capillary), and $[\alpha]^{24}_D$ +82.5° (1% solution in 99.2% ethyl alcohol).

LITERATURE CITED

[1] Cailliot, Bull. Soc. Chem. 21, 387 (1874).

[2] A. Vesterberg, Ber. 18, 3331 (1885); 20, 3248 (1887).

[3] L.A. Tschugaeff and P.I. Theary, Ber. 46, 1769 (1913).

[4] G. Dupont, Zntrbl. II, 348 (1921).

[5] L. Ruzicka and Balas, Zntrbl. III, 1462 (1923).

[6] Fr. Balas, Casopis Ceskoslovenskcho Lecarnictva 7, 320 (1927).

[7] K. Kraft, Ann. 520, 133 (1935).

[8] V.V. Shkatelov, The Composition of the Solid Part of Natural Resin and Colophony [in Russian] (Acad. Sci. Belorussian SSR Press, Minsk, 1939).

[9] V.N. Krestinskii, S.S. Malevskaia, N.F. Komshilov and E.V. Kazeeva, J. Appl. Chem. 12, 1939 (1939).

[10] W. Sandermann, Ber. 75, 174 (1942).

[11] G.C. Harris and T.F. Sanderson, J. Am. Chem. Soc. 55, 3677 (1933).

[12] S. Palkin and T.H. Harris, J. Am. Chem. Soc. 56, 1935 (1934).

[13] I.I. Bardyshev, J. Gen. Chem. 11, 996 (1941).

[14] G.C. Harris and T.F. Sanderson, J. Am. Chem. Soc. 70, 2079 (1948).

Received July 16, 1956

SOME PECULIARITIES OF THE REACTION OF FORMATION OF ETHYLENE OXIDE FROM ETHYLENE CHLOROHYDRIN*

P.V. Zimakov and L.M. Kogan

Ethylene oxide is a very reactive substance and is of great importance in the production of glycols, their ethers, and a number of other substances [1].

During the postwar years the field of application of ethylene oxide has widened further, mainly in the production of nonionic surface-active substances [2], in the synthesis of intermediates for synthetic fibers, and in certain other processes. Despite the ever-increasing importance of the direct oxidation of ethylene as a method for the production of ethylene oxide, the decomposition of ethylene chlorohydrin is still a method of considerable significance. This is due to the simplicity of the chlorohydrin process, the possibility of using ethylene at almost any concentration, the possibility of the simultaneous production of propylene oxide, and certain other causes.

In the light of the foregoing, and also because large amounts of ethylene and chlorine are now used in the production of ethylene oxide, it is necessary to carry out further studies and improvements of the production of ethylene oxide through ethylene chlorohydrin.

The preparation of ethylene oxide was first described by Würtz [3]. He performed the reaction between ethylene chlorohydrin and caustic alkalies in an aqueous medium at 90-100°

$$\begin{matrix} HO{-}CH_2 \\ | \\ Cl{-}CH_2 \end{matrix} + MeOH \rightarrow \begin{matrix} H_2C{-}CH_2 \\ \diagdown\ \diagup \\ O \end{matrix} + H_2O + MeCl.$$

Smith [4] carried out a similar decomposition of ethylene chlorohydrin by calcium and barium hydroxides [4]. In Russia, the properties of ethylene oxide were studied by Kashirskii [5], El'tekov [6], and Krasuskii [7]. Several papers have been published on the kinetics of formation of ethylene oxide from ethylene chlorohydrin. It has been shown that this reaction is a reaction of the second order [4, 8]. There are numerous patents in which different methods and apparatus for the technical utilization of this reaction are described [9, 10]. The technology of ethylene oxide has been developed in a number of scientific research organizations of the USSR by Dyment, Beschastnyi, Maiorov, Telitsina, et al. [11], Kedrinskii and his associates [12], and others.

In modern industrial processes the yield of ethylene oxide is 85-96%; the rest of the ethylene chlorohydrin is converted into ethylene glycol [13-18].

There are very few published papers on the mechanism and the characteristics of this reaction (apart from the kinetic studies already mentioned). This also applies to the monographs by Doroganevskaia and Churakov [19], Zimakov [1], and Kogan [13], which deal specifically with ethylene oxide. Papers published after these monographs [14-18] give only technical details of the process.

This situation has led to the publication of confusing or contradictory communications relating to the decomposition of ethylene chlorohydrin to give ethylene oxide. For example, it is known that when caustic soda is used the alkali solution must be added to the chlorohydrin solution, and not the other way about. If calcium

*A.V. Kaliadova took part in the experimental work.

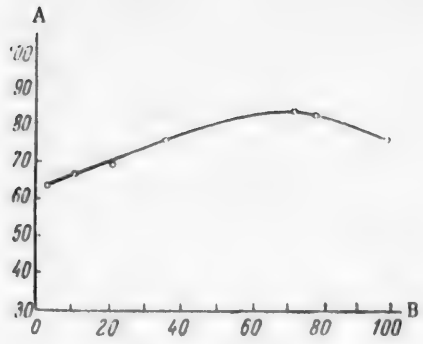

Fig. 1. Effect of the initial content of ethylene chlorohydrin in solution on the yield of ethylene oxide in the decomposition of ethylene chlorohydrin by caustic soda: A) yield (%); B) ethylene chlorohydrin content of original solution (wt. %). Batch process; concentration of the NaOH solution was increased from 5 to 40% with increase of the ethylene chlorohydrin concentration.

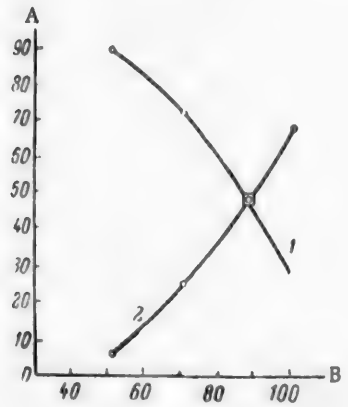

Fig. 2. Effect of temperature in the decomposition of ethylene chlorohydrin by caustic soda on the yields of ethylene oxide (1) and ethylene glycol (2): A) yield (%); B) temperature (°C). Batch process; amount of undecomposed ethylene chlorohydrin did not exceed 1% in any of the experiments.

hydroxide is used, the sequence of addition is immaterial. For higher yields of ethylene oxide it is recommended to use concentrated solutions of ethylene chlorohydrin for the reaction with metal hydroxides. Therefore, it has been proposed to use a packed tower as the reactor, in which rectification of the original dilute chlorohydrin solution was to be performed in conjunction with the reaction between the concentrated chlorohydrin and the base. This is in contradiction to the designs which have been described for modern reactors, which consist of simple hollow reaction vessels.

The present paper contains results obtained several years ago [19] in a study of the chemistry of the reaction between ethylene chlorohydrin and bases.

EXPERIMENTAL

Ethylene chlorohydrin was prepared from ethylene oxide and hydrogen chloride; after purification it contained 99.0-99.5% of the substance. Its constants were: b.p. 127-128°, d^{20}_4 1.915; $n^{26.5}_D$ 1.4390. The reaction was performed batchwise in a three-necked flask 3 liters in capacity. The duration of each experiment was 1.5 hours. Subsequent experiments were performed by a continuous process, which will be described later. The ethylene oxide passed through a water-cooled reflux condenser, and then condensed at −5°. The condensate was collected in a receiver, and the residual gas was bubbled through a definite volume of common salt solution in hydrochloric acid to absorb uncondensed ethylene oxide. Ethylene oxide was determined by absorption in a standard solution of common salt in hydrochloric acid [1]. Acetaldehyde was determined in the same sample by means of hydroxylamine hydrochloride [20]. Ethylene chlorohydrin was determined by saponification with standard caustic potash solution. The amount of glycols formed was found by neutralization of the reaction liquid with hydrochloric acid with phenolphthalein indicator, distillation of the liquid until a dry residue was obtained, treatment of the residue with alcohol, filtration of the residue, and fractionation of the alcoholic solution, first under atmospheric pressure to remove alcohol, and then under vacuum, with collection of the glycol fractions. The mono- and diethylene glycol contents of the fractions were determined from the boiling points and refractive indices [21]. The aqueous distillate was analyzed for ethylene chlorohydrin as described above, and for ethylene glycol by dichromate oxidation. In experiments in which little ethylene glycol was formed and the reaction liquid had a very low content of diethylene glycol, dichromate oxidation was used for the determination of ethylene glycol.

DISCUSSION OF RESULTS

In experiments on the decomposition of ethylene chlorohydrin by caustic soda, by the addition of 10-20% alkali solution to a boiling 10-20% solution of ethylene chlorohydrin, the yield of ethylene oxide did not exceed 65-69%, and the principal by-product was ethylene glycol, obtained in 26-30% yield. Small amounts of acetaldehyde (yield about 1%) and of diethylene glycol (yield 0.9-1.3%) were obtained. In experiments performed under the same conditions, but with the addition procedure reversed, the yield of ethylene oxide was

only 21-27%, while the yield of ethylene glycol rose sharply to over 50%. The yield of diethylene glycol reached 15-30%, and triethylene glycol was also formed. For a more detailed study of the alkaline decomposition of ethylene chlorohydrin, experiments were performed in which the concentrations of the starting substances were varied, and also at low temperatures. In these and all subsequent experiments the alkali solution was added to the ethylene chlorohydrin solution. The results of experiments on the decomposition of ethylene chlorohydrin with different concentrations of the reactants are given in Fig. 1.

It follows from these results that the yield of ethylene oxide increases continuously with increasing concentrations of the reactants, but when the water content of the solutions becomes low the yield falls somewhat.

The effect of reaction temperature on the yields of ethylene oxide and ethylene glycol is shown in Fig. 2.

It is seen that the decrease of the yield of ethylene oxide at lower reaction temperatures does not lead to a decrease in the conversion of ethylene chlorohydrin, and that the alkaline decomposition of ethylene chlorohydrin is of the same character at low temperatures as at the boil.

In the next series of experiments ethylene chlorohydrin was decomposed by calcium hydroxide. In these experiments the ethylene chlorohydrin solution was added to the hydroxide suspension in some cases, and the suspension was added to the ethylene chlorohydrin solution in others.

It was found that the yield of ethylene oxide in the decomposition of ethylene chlorohydrin by calcium hydroxide was 73-76%, or about 7-8% higher than in the decomposition by caustic soda under the same conditions, and that the addition sequence does not influence the yield of ethylene oxide, in contrast to the decomposition of ethylene chlorohydrin by caustic soda. The acetaldehyde yield in the decomposition of ethylene chlorohydrin by calcium hydroxide was 1.5%, i.e., somewhat higher than with the use of caustic soda. These experiments on the decomposition of ethylene chlorohydrin show that ethylene oxide is always formed, despite the differences in the experimental conditions. The only difference lies in the amount of oxide formed.

It follows from the experimental data that the main substance competing with ethylene oxide is ethylene glycol; this may be formed either by direct saponification of ethylene chlorohydrin

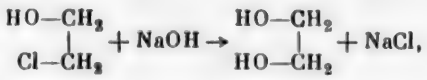

or by hydration of ethylene oxide

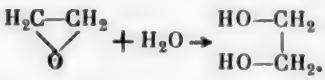

For clarification of this question, experiments were performed on the alkaline decomposition of ethylene chlorohydrin in presence of ethylene glycol, under the same conditions as before. From 180 to 215% of ethylene glycol was added to the ethylene chlorohydrin solution. The ethylene glycol had the following constants: b.p. 98° at 15 mm Hg, d^{20}_4 1.0854, $n^{26.5}_D$ 1.4330. It was found that addition of ethylene glycol results in an appreciable decrease of the ethylene oxide yield, down to 50-55%, and a proportionate increase of the diethylene glycol yield, to 10-12%, with small amounts of triethylene glycol.

In our opinion, diethylene glycol is formed by the reaction of ethylene oxide with ethylene glycol, as follows

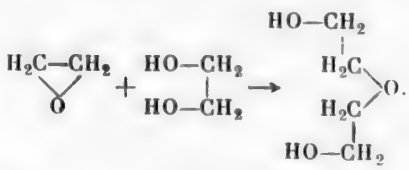

Special experiments showed that diethylene glycol is not formed to any appreciable extent directly from ethylene chlorohydrin and ethylene glycol.

The fact that appreciable amounts of diethylene glycol are formed with a decrease of the ethylene oxide

yield indicates that the reactivity of ethylene oxide at the instant of its formation is high. This justifies the view that even without addition of ethylene glycol the ethylene oxide is highly reactive, and this reactivity then results in hydration with formation of ethylene glycol.

However, this does not exclude the possibility that direct saponification of ethylene chlorohydrin may occur, without intermediate formation of ethylene oxide. In such a reaction water would not be consumed, and the reaction could be effected, for example, in alcohol. It is known that the chemical conversion of ethylene chlorohydrin in alcohol proceeds at an appreciable rate, as indicated by kinetic data and our preliminary experiments. To test this hypothesis, we carried out a series of experiments on the reaction of ethylene chlorohydrin with caustic potash in ethyl, n-propyl, and butyl alcohol solutions. The alcohols contained 5-10% water. The experimental conditions were as before. It was found that in the alkaline decomposition of ethylene chlorohydrin in alcohol the yield of ethylene oxide was 65-70%, i.e., roughly the same as in an aqueous medium, and that ethylene glycol is not formed under these conditions. The corresponding alkyl ethers of ethylene glycol were formed in these experiments; the yield of these ethers, about 25%, corresponds to the yield of ethylene glycol in the alkaline decomposition of ethylene chlorohydrin in an aqueous medium; small amounts of ethers of diethylene glycol were also formed.

As in the experiments discussed earlier, the formation of alkyl glycols from ethylene chlorohydrin and the corresponding alcohols, without the participation of ethylene oxide, does not take place here.

The formation of alkyl glycols should occur as follows:

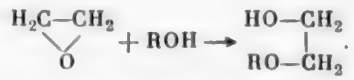

The diethylene glycol ethers are formed by the reaction

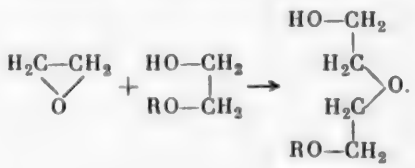

These experiments suggest that the formation of ethylene glycol in the decomposition of ethylene chlorohydrin occurs as the result of hydration of ethylene oxide; direct conversion of ethylene chlorohydrin into ethylene glycol does not occur under the experimental conditions used. These conclusions were confirmed by means of special experiments in which the ethylene oxide was removed from the reaction zone as soon as it formed. The apparatus had a relatively small reaction volume and a considerably larger evaporation section. The original liquids were fed continuously from header vessels into the reactor section, into which large amounts of steam were blown. The ethylene oxide formed was thus blown out and then condensed as described above. The remaining liquid passed through an overflow tube into the lower part of the apparatus, where it was boiled vigorously and then transferred into a receiver through a siphon tube. The vapors of ethylene chlorohydrin and ethylene oxide from the lower part of the apparatus avoided the reaction zone and were added to the main mass of ethylene oxide vapor. The experiments were performed at the boil, with 6% ethylene chlorohydrin solution and 10% suspension of the hydroxide.

The yield of ethylene oxide was 96-98%, and there was virtually no formation of ethylene glycol.

The subsequent experiments were performed in order to investigate the conditions and characteristic features of the hydration of ethylene oxide at the instant of its formation. In these experiments ethylene chlorohydrin was decomposed by caustic soda and calcium hydroxide under the conditions described above (in a continuous process), with different amounts of the bases. The starting substances were cooled to 0°, mixed at that temperature and then fed into the reactor. Reaction of the substances on mixing was avoided by the use of the low temperature. This ensured that the reactants were present in exact and predetermined proportions. The degree of hydration of ethylene oxide was estimated from changes in its yield.

A 6% solution of ethylene chlorohydrin and 10% solution or suspension of the base was used. The reaction was performed at the boil. The results of the experiments are given in Fig. 3. The graphs show that the yield of

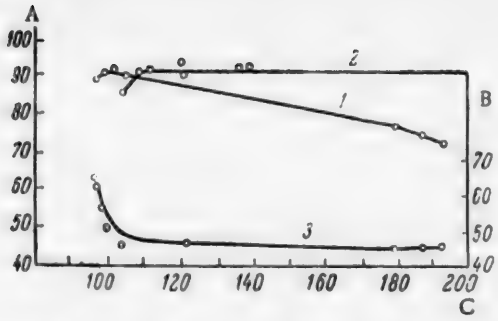

Fig. 3. Effect of the relative content of metal hydroxide on the yield of ethylene oxide (1 and 2) and on the amount of unreacted ethylene chlorohydrin (3) in the decomposition of ethylene chlorohydrin by caustic alkali (1 and 3) and by calcium hydroxide (2): A) yield calculated on the ethylene chlorohydrin decomposed (%); B) amount of unreacted ethylene chlorohydrin (% of original); C) relative content of metal hydroxide (%).

ethylene oxide depends on the amount of caustic soda taken; the yield decreases with increasing excess of caustic soda, while if less than the stoichiometric amount of caustic soda is used the yield of ethylene oxide, calculated on the amount of ethylene chlorohydrin decomposed, decreases very little. The maximum yield of ethylene oxide calculated on the ethylene chlorohydrin decomposed, is obtained when the relative content of caustic soda does not exceed 104% of the stoichiometric amount.

The yield of ethylene oxide, calculated on the ethylene chlorohydrin decomposed, remains almost constant over a wide range of relative contents of calcium hydroxide. With a small excess of the base, up to 5% over the stoichiometric amount, there is some decrease of the ethylene oxide yield. This decrease is fortuitous, and the probable explanation is that it is impossible to obtain an absolutely homogeneous suspension of the hydroxide, so that when the excess is small local zones are formed with a deficiency of the base.

The decomposition of ethylene chlorohydrin by calcium hydroxide differs in principle from the analogous reaction with the use of caustic alkalies, in that the reaction system is heterogeneous because of the low solubility of the hydroxide. Without considering the processes associated with the presence of a solid phase in the reaction zone (adsorption, surface reactions, etc.), we may note that the system is maintained at a definite and very low level of alkalinity, irrespective of the amount of hydroxide taken for the reaction.

It follows from the results of these experiments that the base used for decomposition of ethylene chlorohydrin is involved in a side reaction – hydration of ethylene oxide at the instant of its formation. The concentration of the base has a direct influence on the amount of ethylene glycol formed. The results of our experiments provide a satisfactory explanation for the definite addition procedure required in the decomposition of ethylene chlorohydrin by caustic alkalies. If ethylene chlorohydrin solution is added to the alkali solution, the reaction medium has a higher concentration of the base, and this leads to intensified hydration of the oxide and decrease of its yield. When calcium hydroxide suspension is used, the content of the base in solution always corresponds to the saturation concentration, and therefore the sequence in which the starting substances are added is immaterial.

We found that the hydration rate of ethylene oxide at the instant of its formation is higher than the hydration rate of ethylene oxide prepared previously and studied separately, as reported by Lichtenstein and Twigg [22].

The above results explain why packed-tower reactors have recently been replaced in industry by ordinary empty reactors. In a tower there is good contact between the rising vapor of the ethylene oxide formed and the sprayed alkaline liquid. It is clear that the conditions are favorable for hydration of ethylene oxide, leading to its loss in the form of ethylene glycol. In volume reactors of considerable diameter and small height the evaporation surface is large. This leads to rapid evacuation of the ethylene oxide from the reaction zone and, which is most important, prevents its contact with the alkaline liquid added for the decomposition of the ethylene chlorohydrin.

SUMMARY

1. In the production of ethylene oxide by decomposition of ethylene chlorohydrin by means of caustic soda or calcium hydroxide in an aqueous medium at 90-100° the yield of by-product ethylene glycol varies from a few percent to 50%, according to the process conditions. Small amounts of diethylene glycol and acetaldehyde (0.9-1.5% of each) are formed in the reaction.

2. The formation of ethylene glycol in the production of ethylene oxide from ethylene chlorohydrin is the consequence of a further reaction, the hydration of ethylene oxide, and not of the direct saponification of the original ethylene chlorohydrin.

3. In the production of ethylene oxide from ethylene chlorohydrin with the use of caustic alkalies, the relative amount of the alkali taken for the reaction has a significant effect on the yield. The maximum yield of ethylene oxide, 93% on the ethylene chlorohydrin taken for the reaction, was obtained when the amount of caustic soda did not exceed 104% of the stoichiometric quantity. This corresponds to a yield of 95% on the amount of ethylene chlorohydrin decomposed.

If calcium hydroxide is used in the production of ethylene oxide, the excess of the base does not influence the yield. The use of a suspension of calcium hydroxide, which is sparingly soluble in water, ensures that a constant and low concentration of the base is present in the reaction solution. A yield of over 90% of ethylene oxide, calculated on the ethylene chlorohydrin taken, was obtained under these conditions. This corresponds to a yield of 96% on the amount of ethylene chlorohydrin decomposed.

4. The hydration of ethylene oxide at the instant of its formation from ethylene chlorohydrin is much more rapid than the hydration of previously prepared ethylene oxide.

High yields of ethylene oxide are obtained if its vapor is immediately removed from the reaction zone, with the least possible contact with the base used for decomposition of the ethylene chlorohydrin. Therefore, packed towers are unsuitable as industrial reactors for the production of ethylene oxide; ordinary hollow reactors with small reaction layers and large evaporation surfaces, are more suitable for the process.

LITERATURE CITED

[1] P.V. Zimakov, Ethylene Oxide [in Russian] (Goskhimizdat, Moscow, 1946).

[2] L.M. Kogan, J. Chem. Ind. 2, 105 (1954).

[3] A. Würtz, Ann. Chim. phys. 55, 400 (1859); 69, 317 (1863).

[4] L. Smith, Z. phys. Ch. 81, 339 (1913).

[5] M. Kashirskii, J. Russ. Phys. Chem. Soc. 13, 76 (1881).

[6] A.P. El'tekov, J. Russ. Phys. Chem. Soc. 5, 81 (1873); 14, 355 (1882).

[7] K. Krasuskii, Dissertation (St. Petersburg, 1902).*

[8] P. Petrenko-Kritchenko and A.Iu. Konshina, J. Russ. Phys. Chem. Soc. 37, 1127 (1905); P. Evans, Z. phys. Ch. 7, 337 (1891); L. Smith, Z. phys. Ch. 101, 77 (1918); L.O. Wistrom and J.C. Warner, J. Am. Chem. Soc. 61, 1205 (1939); D. Porret, Helv. Chim. Acta 27, 1321 (1944); C.L. McCabe and J.C. Warner, J. Am. Chem. Soc. 70, 4031 (1948); J.E. Stevens, C.L. McCabe and J.C. Warner, J. Am. Chem. Soc. 70, 2449 (1948).

[9] German Patent 299682 (1920), C, IV, 16 (1920); U.S. Patent 1,446,872 (1923); Brit. Patent 236,379; Fr. Patent 583,851, C, I, 490 (1926); Brit. Patent 286,850 (1927); U.S. Patent 1,737,545; Fr. Patent 648,157, C, I, 2750 (1928); Fr. Patent 656,996 (1929), C, II, 648 (1929); Brit. Patent 292,066 (1927), Chem. Abs. 23, 1415 (1929), C, I, 2004 (1930); Brit. Patent 374,864 (1931), C, II, 2723 (1932); German Patent 541,769 (1927); Can. Patent 285920 (1928); C, I, 1153 (1932); U.S. Patent 1,996, 638 (1934); U.S. Patent 2,103,849 (1936), etc.; W. Dominik and J. Bartkiewczowna, C, I, 2810 (1935).

[10] German Patent 403,643 (1924); Fr. Patent 728,849 (1931), C, II, 2532 (1932).

[11] A.E. Beschastnov and O.N. Dyment, Sci. Tech. Bull. Experimental Plant "B," 25, 3 (1935); A.E. Beschastnov, A.E. Bairamov and E.I. Telitsina, ibid, 25, 32 (1935); A.E. Beschastnov and O.N. Dyment, ibid, 25, 25 (1935); E.V. Dmitrieva and O.P. Tikhomirova, ibid, 25, 34 (1935).

[12] V.V. Kedrinskii, Trans. All-Union Sci. Res. Inst. Chem. Conversion of Gases (Khimgaz) 4, 2, 98 (1949).

[13] L.M. Kogan, Production and Conversion of Ethylene Oxide in Germany (Goskhimizdat, Moscow, 1947).*

[14] P.P. McClellan, Ind. Eng. Ch. 42, 2402 (1950).

* In Russian.

[15] P.W. Scherwood, Petr. Refiner. 28, 97 (1949).

[16] P.W. Scherwood, Erdöl Kohle 8, 166 (1955).

[17] J. Plant, Industrial Chemist 28, 259 (1952).

[18] T. Urbanski, Przemyse Chemiczny 6, 288 (1952).

[19] E.A. Doroganevskaia and A.V. Churakov, Ethylene Oxide, Ethylene Glycol, Ethylene Chlorohydrin [in Russian] (ONTI, Peoples Commissariat of the Heavy Industry USSR, Moscow, 1935).

[20] L. Palfray and S. Tolland, Compt. Rend. Acad. Sci. Paris 199, 296 (1934).

[21] C. Matignon, H. Moureu and M. Dode, Bull. Soc. Chim. Fr. 5, 10, 1308 (1934); H. Moureu and M. Dode, Bull. Soc. Chim. Fr. 5, 4, 697 (1937).

[22] H.J. Lichtenstein and G.H. Twigg, Trans. Faraday Soc. 44, 905 (1948).

Received October 22, 1956

PRODUCTION OF β-CHLOROETHYL ISOPROPYL, β-CHLOROETHYL ISOAMYL, β-CHLOROETHYL HEXYL, AND β-CHLOROISOPROPYL ISOBUTYL ETHERS FROM UNSATURATED HYDROCARBONS

A.K. Seleznev

Organic Chemistry Laboratory, the Groznyi Petroleum Institute

Several methods for the preparation of β-chloro ethers directly from olefins are described in the literature: by the action of chlorine on olefins in presence of alcoholic alkali [1], the ammonia method for chloroalkoxylation of olefins [2], the vapor-phase method for chloroalkoxylation of olefins [3], and the chloroamide method for the synthesis of β-chloro ethers. Benzenesulfodichloramide (dichlorobenzenesulfonamide) has been used with success as the chloroalkoxylation agent [4, 5]. Skliarov used this agent for the synthesis of a series of β-chloro ethers from ethylene and propylene. The experiments were performed in a rotary autoclave with the use of liquefied olefins, alcohols, and the chloroamide. The synthesis of β-chloroethyl isopropyl ether with the use of isopropyl alcohol was unsuccessful owing to the very violent reaction between isopropyl alcohol and benzenesulfodichloroamide.

The aim in the present investigation was to prepare certain β-chloro ethers by the liquid-phase method, without cooling, from synthetic ethylene and propane-propylene cracking fraction. In one experiment on the synthesis of β-chloroethyl isopropyl ether, water was used as a cooling agent.

EXPERIMENTAL

A glass tube 3.5 cm in diameter and 120 cm long was used for the reactions. The tube was half filled with marble and the alcohol was introduced. Two narrow glass tubes, reaching almost to the bottom, were inserted into the reaction tube from above for the chlorine and olefin feeds. A thermometer was inserted in the lower end of the reaction tube, for measurement of the reaction temperature.

β-Chloroethyl isopropyl ether. 46.3 liters of ethylene and 300 ml of isopropyl alcohol (b.p. 81-82°, $n^{20}D$ 1.3773) was used in the experiment. 69 liters of chlorine was passed. The experiments were continued for 7 hours 40 minutes. The average rate of ethylene absorption was 6 liters per hour. The reaction tube was cooled by means of running water during the experiment. The thermometer reading in the lower part of the reaction tube was 15-16°. At the end of the experiment the reaction product was treated with water to wash out the alcohol, dried over calcium chloride, and the product (198.4 g) was fractionated.

The following fractions were obtained: 1) up to 84°, 19 g, 2) 84-120°, 143.4 g, and 3) residue 34 g. The 84-120° fraction (d^{20}_4 1.178, $n^{20}D$ 1.4342) was analyzed for chlorine by the Carius method:

0.1234 g substance: 0.305 g AgCl; 0.0304 g (24.63%) chloro ether.
0.1112 g substance: 0.274 g AgCl; 0.0278 g (25%) chloro ether.

The contents of chloro ether and dichloride in the 84-120° fraction were calculated from the weight of silver chloride formed in the Carius determination

$$\underset{(0.1234-y)-x}{Cl-CH_2-CH_2-O-C_3H_7-AgCl} \qquad \underset{y-(0.305-x)}{C_2H_4Cl_2-2AgCl}$$

These analytical data show that the 84-120° fraction consists of 25% chloro ether and 75% dichloride. The yield of chloro ether was 35.8 g, 14% of the theoretical calculated on the ethylene used.

The pure ether was isolated from the 84-120° fraction, consisting of 25% chloro ether and 75% dichloride. Sulfuric acid was used to separate the dichloride from the chloro ether [7].

40 ml of 87% sulfuric acid was added to 90 ml of the 84-120° fraction, cooled in ice. The dichloride which separated out in the top layer was removed. The dichloride was removed more completely from the sulfuric acid containing the chloro ether, by means of ligroine. The sulfuric acid was diluted with water and cooled, the chloro ether was extracted in ligroine, the extract was washed and dried over calcium chloride. The ligroine was distilled off and the residue was treated with caustic soda to remove the dichloride. After the alkali treatment the ether was washed, dried over calcium chloride, and distilled through a laboratory rectification column. A 120-120.3° fraction (11.5 g) was obtained, with the following constants: d^{20}_4 0.955, $n^{20}D$ 1.4117, MR_D 31.90. $C_5H_{11}OCl$. Calculated 31.80.

Analysis of 120-120.3° fraction (Carius)

0.1212 g substance: 0.1422 g AgCl. 0.1148 g substance: 0.1348 g AgCl

Found %: Cl 29.0, 29.05. $C_5H_{11}OCl$. Calculated %: Cl 28.92.

Elementary analysis

5.232 mg substance: 9.412 mg CO_2; 4.232 mg H_2O. 8.346 mg substance: 14.992 mg CO_2; 6.758 mg H_2O.

Found %: C 49.08, 49.02; H 9.05, 9.06. $C_5H_{11}OCl$. Calculated %: C 48.98; H 9.04.

The 120-120.3° fraction was pure β-chloroethyl isopropyl ether. It is a colorless liquid with a pleasant odor; it is not described in the literature.

This β-chloro ether mixed with the dichloride is being tested as a solvent for the deparaffinization of aviation oil.

β-Chloroethyl isoamyl ether.* 60 liters of ethylene and 300 ml of isoamyl alcohol (b.p. 128-131°) was used in the experiment. 85 liters of chlorine was passed. The experiment was continued for 10 hours. The average rate of ethylene absorption was 6 liters per hour. The reaction tube was not cooled. Heat was evolved in the reaction. The thermometer reading in the lower part of the reaction tube was 48-52°. At the end of the experiment the reaction product was diluted with water, the upper layer was washed, dried over K_2CO_3, and distilled. The fraction up to 136° was distilled off. The residue (127 g) was used for isolation of the chloro ether. Isoamyl alcohol was not driven off completely in the distillation; part remained mixed with the β-chloro ether.

Likhosherstov [8] removed residual higher alcohols either by large amounts of water, or by separation from the distilled β-chloro ethers by prolonged shaking with concentrated calcium chloride solution. We used sulfuric acid to remove residual isoamyl alcohol from the β-chloro ether. Sulfuric acid forms compounds of the oxonium type with β-chloro ethers. It is known that sulfuric acid reacts with alcohols to form acid esters, which separate out as salts after neutralization. Aschan [9] converted alcohols (menthol, borneol and others) into sulfates by means of diethyloxonium sulfate. The sulfate esters of all these alcohols are formed much more readily from the oxonium sulfates than by the direct action of sulfuric acid.

The residual product (127 g) was cooled in ice, and 45 ml of chemically pure sulfuric acid (sp. gr. 1.84) was added in small portions. After 24 hours the acid ester and excess sulfuric acid were neutralized, on cooling, with concentrated caustic soda solution, and water was then added to dissolve the salt formed. The chloro ether which separated out was extracted in ligroine (boiling up to 52°). The ligroine was distilled off, and the residue (81.2 g) was treated with caustic soda and warmed gently to remove the dichloride mixed with the chloro ether. After the alkali treatment the product was diluted with water to dissolve the precipitate, and the chloro ether was extracted in ligroine. The 58.5 g of residue after removal of ligroine was distilled under vacuum through a laboratory rectification column.

*V.V. Balashova took part in the experimental work.

TABLE 1

Fractionation Data and Constants of the Fractions Obtained

Boiling range (°C)	Weight of fraction (g)	$n^{20}D$	d^{20}_4	MR_D	
				found	calculated
59-79.5 (35 mm)	1.76	1.4215	–	–	–
79.5-80 (35 mm)	29.28	1.4250	0.9370	41.11	41.04
80-81 (35 mm)	20.80	1.4250	0.9386	41.04	41.04
Residue	5.60	–	–	–	–

TABLE 2

Fractionation Data and Constants of the Fractions Obtained

Boiling range (°C)	Weight of fraction (g)	$n^{20}D$	d^{20}_4	MR_D	
				found	calculated
57-79 (10 mm)	4.0	1.4320	–	–	–
79-79.5 (10 mm)	8.9	1.4310	0.932	45.74	45.65
79.5-80 (10 mm)	10.1	1.4310	0.934	45.64	45.65
Residue	3.8	–	–	–	–

The fractionation data are given in Table 1.

The yield of β-chloro ether was 50 g, 12.4% of the theoretical calculated on the ethylene used.

80-81° fraction (35 mm). Chlorine content (Carius)

0.1876 g substance: 0.179 g AgCl. 0.1782 g substance: 0.1702 g AgCl.

Found %: Cl 23.60; 23.62. $C_7H_{15}OCl$. Calculated %: Cl 23.53.

Elementary analysis

7.888 mg substance: 16.170 mg CO_2; 7.094 mg H_2O. 4.778 mg substance: 9.798 mg CO_2; 4.308 mg H_2O.

Found %: C 55.94, 55.96; H 10.06, 10.08. $C_7H_{15}OCl$. Calculated %: C 55.81; H 10.04.

The 80-81° fraction (35 mm) was pure β-chloroethyl isoamyl ether. It is a colorless liquid with a pleasant odor; it is not described in the literature.

β-Chloroethyl hexyl ether. 58 liters of ethylene and 300 ml of n-hexyl alcohol (b.p. 154-156°) was used in the experiment. 82 liters of chlorine was passed. The experiment was continued for 10 hours. The average rate of ethylene absorption was 5.8 liters per hour. The thermometer reading in the lower part of the reaction tube was 47-55°. At the end of the experiment the reaction product was diluted with water, the upper layer was washed, dried over Na_2SO_4, and distilled. The fraction up to 160° was driven off, and the β-chloro ether was obtained from the residue (113.2 g) by the method described for β-chloroethyl isoamyl ether. After the treatment 27.6 g of the product was distilled under vacuum through a laboratory rectification column.

The fractionation data are given in Table 2.

79.5-80° fraction (10 mm). Chlorine content (Carius)

0.1308 g substance: 0.1146 g AgCl. 0.1512 g substance: 0.1322 g AgCl.

Found %: Cl 21.68, 21.63. $C_8H_{17}OCl$. Calculated %: Cl 21.53.

Elementary analysis

3.820 mg substance: 8.182 mg CO_2; 3.593 mg H_2O. 7.830 mg substance: 16.760 mg CO_2; 7.340 mg H_2O.

Found %: C 58.45, 58.43; H 10.52, 10.49. $C_8H_{17}OCl$. Calculated %: C 58.35; H 10.40.

The 79.5-80° (10 mm) fraction was pure β-chloroethyl hexyl ether. It is a colorless liquid with a pleasant odor; it is not described in the literature.

β-Chloroisopropyl isobutyl ether $\begin{matrix} CH_3-CH-CH_2Cl \\ | \\ O-CH_2-CH-CH_3 \\ | \\ CH_3 \end{matrix}$. 128 liters of a propane-propylene cracking fraction, containing 38 liters (29.8%) of propylene, 300 ml of isobutyl alcohol (b.p. 106-108°), and 43 liters of chlorine was used in the experiment. The experiment was continued for 6 hours 20 minutes. 31 liters (24.3%) of propylene was absorbed. The thermometer reading in the lower part of the reaction tube was 39-51°. At the end of the experiment the reaction product was diluted with water, the upper layer was washed, dried over Na_2SO_4, and fractionated.

The following fractions were obtained: 1) up to 148°, 0; 2) from 148-151°, 16.8 g; 3) from 151-155°, 29.9 g; 4) residue 37.8 g.

The β-chloro ether was isolated from the 148-151° and 151-155° fractions (46.7 g) by the method described for β-chloroethyl isoamyl ether. After the treatment the product was distilled under vacuum through a laboratory rectification column. The 151.6-152.2° fraction (19 g) was isolated; it had the following constants: $n^{20}D$ 1.4165, d^{20}_4 0.9233, MR_D 40.99. $C_7H_{15}OCl$. Calculated 41.04.

Chlorine content (Carius)

0.1194 g substance: 0.1132 g AgCl. 0.1544 g substance: 0.1462 g AgCl.

Found %: Cl 23.45, 23.42. $C_7H_{15}OCl$. Calculated %: Cl 23.53.

0.1984 g substance: 13.561 g benzene: Δt 0.50. 0.2362 g substance: 14.503 g benzene: Δt 0.56.

Found: M 149.81, 148.90. $C_7H_{15}OCl$. Calculated: M 150.65.

Elementary analysis

4.899 mg substance: 10.037 mg CO_2, 4.372 mg H_2O. 8.657 mg substance: 17.740 mg CO_2, 7.752 mg H_2O.

Found %: C 55.91, 55.92; H 9.986, 10.02. $C_7H_{15}OCl$. Calculated %: C 55.81; H 10.04.

The 151.6-152.2° fraction was pure β-chloroisopropyl isobutyl ether. It is a colorless liquid with a pleasant odor; it is not described in the literature.

LITERATURE CITED

[1] M.V. Likhosherstov and A.A. Petrov, J. Gen. Chem. 5, 10, 1348 (1935).

[2] A.A. Petrov and G.E. Morgun, Trans. Voronezh State Univ. 8, 2 (1935).

[3] A.A. Petrov, Trans. Voronezh State Univ. 8, 2 (1935).

[4] M.V. Likhosherstov and T.V. Shalaeva, J. Gen. Chem. 8, 4, 370 (1938).

[5] M.V. Likhosherstov and V.A. Skliarov, Trans. Voronezh State Univ. 8, 2 (1935).

[6] V.A. Skliarov, J. Gen. Chem. 9, 23, 2121 (1939).

[7] A.K. Seleznev, J. Appl. Chem. 27, 650 (1954).*

[8] M.V. Likhosherstov and S.V. Alekseev, J. Gen. Chem. 9, 1279 (1934).

[9] O. Aschan and A. Schwalbe, Finska Kem. Medd. 40, 133; 41, 98 (1932).

Received December 6, 1956

*Original Russian pagination. See C.B. translation.

INFLUENCE OF IRON SALTS ON THE KINETICS OF THE REACTION BETWEEN POLYETHYLENE POLYAMINES AND HYDROPEROXIDES, AND THE USE OF THIS REACTION FOR INITIATION OF POLYMERIZATION*

B.A. Dolgoplosk and D.Sh. Korotkina

In a number of recent investigations the reaction between polyamines and hydroperoxides has been used for initiation of polymerization in emulsion [1-3].

In 1950 Whitby [1] made a detailed study of the influence of polyamine structure on the activity of the initiation system. He noted that diethylenetriamine, triethylenetetramine, and tetraethylenepentamine are most effective. In the same paper it is reported that the activity of the system may be increased on replacement of cumene hydroperoxide by diisopropylbenzene hydroperoxide.

Spolsky and Williams [2] and Neclutin and Westerhoff [3] reported that iron salts have a strong influence on polymerization kinetics in polyamine systems. According to their data, the reaction proceeds at a high rate in presence of traces of iron. Increase of the iron concentration in the system retards the process; in the authors' view, this is the consequence of rapid consumption of the components of the system (hydroperoxide and polyamine). To weaken the action of iron salts, they recommend the addition of complex-forming agents such as potassium or sodium ethylenedinitriletetraacetates. Other authors [4] drew similar conclusions concerning the influence of iron salts.

In our investigations in the All-Union Scientific Research Institute of Synthetic Rubber in 1951-1952 it was shown that small amounts of iron salts accelerate the emulsion polymerization of divinyl-styrene mixtures when the process is initiated by an oxidation-reduction system consisting of di(tert-butyl)isopropylbenzene hydroperoxide and tetraethylenepentamine. The yield of polymer reached 60% in two hours with the use of this system.

In 1953 Howland and Neclutin [5] published a paper in which they recommended the use of a polyamine system containing small amounts of iron salts for the emulsion polymerization of divinyl-styrene mixtures at temperatures below 0°.

The present paper reports a study of the influence of iron salts on the rate of reaction between hydroperoxides and polyamines, in connection with the possible use of this reaction for the initiation of polymerization at low temperatures.

EXPERIMENTAL AND DISCUSSION OF RESULTS

We studied the kinetics of the interaction of polyamines with cumene hydroperoxide (CHP) in hydrocarbon and aqueous media in conditions simulating emulsion polymerization. The reaction with tert-butylisopropylbenzene hydroperoxide (alkyl hydroperoxide) was studied under model conditions only, because of the low solubility of this hydroperoxide in water.

The course of the reaction was followed by the consumption of hydroperoxide, which was determined iodometrically. The polyamines were synthesized by the method of Alphen and Hofmann [6].

Interaction of hydroperoxides with polyamines in a hydrocarbon medium. The reaction between triethylene-

*Communication VII in the series on oxidation-reduction systems for initiation of radical processes.

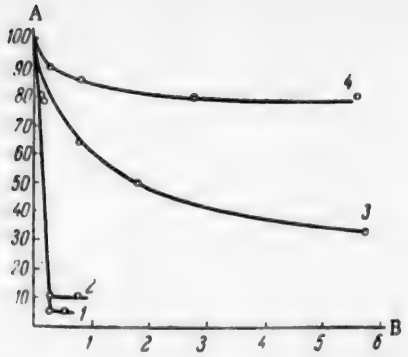

Fig. 1. Reaction of CHP with triethylenetetramine in ethylbenzene. Iron naphthenate content, 0.005 wt. %: A) amount of hydroperoxide (%); B) time (hours). Temperature (°C): 1) 50; 2) 0; 3) −15; 4) −30.

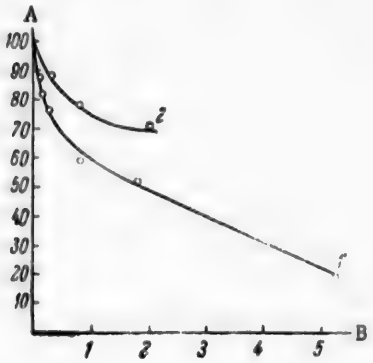

Fig. 2. Reaction of alkyl hydroperoxide with triethylenetetramine in ethylbenzene. Iron naphthenate content, 0.005 wt. %: A) amount of hydroperoxide (%); B) time (hours). Temperature (°C): 1) −15; 2) −30.

tetramine and hydroperoxides was performed in ethylbenzene and styrene at various temperatures. The solutions contained 0.5% of cumene hydroperoxide and 0.5% of the polyamine by weight.

In the experiments with tert-butylisopropylbenzene hydroperoxide, the solution contained 0.62% of the hydroperoxide and 0.5% of the polyamine by weight. The experiments were performed in nitrogen free from traces of oxygen [7].

The experimental data on the reaction rate of CHP with triethylenetetramine in presence of iron salts at various temperatures are plotted in Fig. 1.

It is seen that in presence of 0.005% of iron naphthenate the reaction at 0 and 50° is extremely rapid. At lower temperatures the reaction rate falls appreciably, although it is still very considerable at −15°. The reaction is somewhat more rapid if tert-butylisopropylbenzene hydroperoxide is used instead of CHP (Fig. 2).

The amount of iron naphthenate present has a significant influence on the rate of reaction between polyamines and hydroperoxides (Figs. 3 and 4).

It follows from these results that the rate of the reaction between the components of the system at −30° can be varied within wide limits by variation of the iron naphthenate concentration.

Reaction of hydroperoxides with polyamines in water, emulsifier solutions, and under conditions simulating emulsion polymerization. In absence of iron salts the rate of reaction between hydroperoxides and polyamines in water* at 0° is not high. The rate increases with increasing molecular weight of the amine; this is probably related to the number of secondary amino groups in the chain (Fig. 5).

The introduction of very small amounts of iron salts, such as ammonium ferric alum, results in a sharp acceleration of the reaction between the hydroperoxide and the polyamine; as in the preceding case, the rate is proportional to the amount of iron introduced into the system, and can be varied within wide limits (Fig. 6).

It is interesting to note that the amount of ammonium ferric alum introduced into the system is very small, from 0.2 to 0.001 part to 1 part of hydroperoxide.

The presence of emulsifier in the aqueous solution has a significant effect on the rate of the reaction between hydroperoxides and polyamines.

The aqueous phase contained 2.9% emulsifier, 0.05% caustic soda, 0.5% triethylenetetramine, 0.15% CHP, and 0.0002% ammonium ferric alum.

The reactions in aqueous solution were studied at 0° (Fig. 7).

The results show that the highest reaction rates are obtained with the use of sodium laurate or a technical mixture of the sodium salts of other paraffinic acids as emulsifier.

*In an aqueous solution containing 0.17% CHP and 0.17% polyamine by weight.

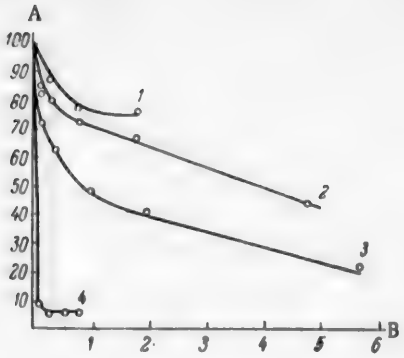

Fig. 3. Reaction of alkyl hydroperoxide with triethylenetetramine in ethylbenzene in presence of various amounts of iron naphthenate at −30°: A) amount of hydroperoxide (%); B) time (hours). Amount of iron naphthenate (wt. %): 1) 0.005; 2) 0.01; 3) 0.025; 4) 0.05.

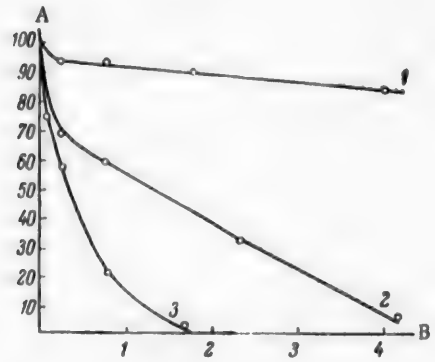

Fig. 4. Reaction of alkyl hydroperoxide with tetraethylenepentamine in styrene at +5°: A) amount of hydroperoxide (%); B) time (hours). Amount of iron naphthenate (wt. %): 1) 0; 2) 0.0002; 3) 0.001.

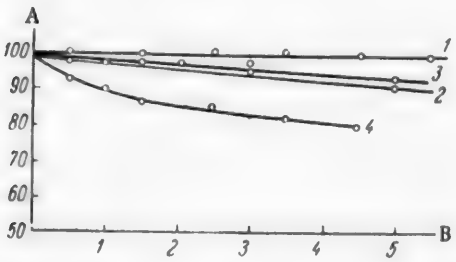

Fig. 5. Reaction of CHP with polyamines in water: A) amount of hydroperoxide (%); B) time (hours). Polyamines: 1) diethylenetriamine; 2) triethylenetetramine, pH 10.2; 3) triethylenetetramine, pH 11.9; 4) tetraethylenepentamine.

The reaction between triethylenetetramine and alkyl hydroperoxide under conditions simulating emulsion polymerization is considerably slower than the same reaction in water and aqueous solutions. The experiments were performed at 0° with an emulsion of ethylbenzene containing 0.3% hydroperoxide and 0.5% triethylenetetramine in 5.8% aqueous Nekal solution, consisting mainly of sodium di(sec-butyl)naphthalene sulfonate (Fig. 8).

Thus studies of the reaction between hydroperoxide and polyamines under various conditions showed that the rate of the reaction can be greatly increased by the addition of very small amounts of ferric iron salts in the form of ammonium ferric alum or ferric naphthenate.

The role of iron salts in reversible oxidation-reduction systems consists of alternate transfer of electrons between the reducing and the oxidizing agent. This concept is hardly applicable to polyamine systems, as in the conditions used the latter do not reduce ferric iron to ferrous.

Emulsion polymerization in presence of hydroperoxides and polyamines. In the experiments on the efficiency of polyamine systems for initiation of the polymerization of divinyl-styrene mixtures at +2°, the following hydroperoxides were tested: cumene hydroperoxide, diisopropylbenzene monohydroperoxide, and tert-butylisopropylbenzene hydroperoxide.

The most suitable emulsifier for this system proved to be potassium paraffinate; this is in harmony with the results obtained on the influence of the nature of the emulsifier on the kinetics of the hydroperoxide-polyamine reactions (Fig. 7). The nature of the hydroperoxide, especially in presence of iron salts, has a considerable influence on the polymerization rate (Fig. 9). The most effective is found to be tert-butylisopropylbenzene hydroperoxide.

The chemical nature of the iron compound has only a slight effect on the polymerization rate (see Table).

Thus, 60% yield can be obtained in two hours at 2° in polymerization in the presence of a system consisting of polyamines, tert-butylisopropylbenzene hydroperoxide, and iron salts.

METHOD

In the kinetic studies of the reaction between hydroperoxides and polyamines, the reaction was performed in a vessel fitted with a stirrer and two burets with stopcocks for supply of hydroperoxide and polyamines. Before each experiment the reaction vessel was blown through with nitrogen freed from oxygen by passage through a column packed with copper turnings and ammoniacal ammonium chloride solution [7]. The weighed quantities of hydroperoxide, ferric naphthenate, and ethylbenzene or styrene (freshly distilled) were introduced in a current of nitrogen. After the mixture had reached the required experimental temperature, nitrogen

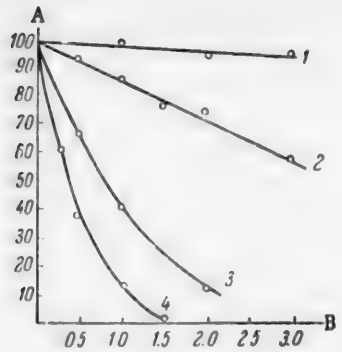

Fig. 6. Reaction of triethylenetetramine with CHP in water in presence of Fe^{+++}: A) amount of hydroperoxide (%); B) time (hours). Amount of ammonium ferric alum (wt. %): 1) none; 2) 0.00017; 3) 0.0017; 4) 0.0034.

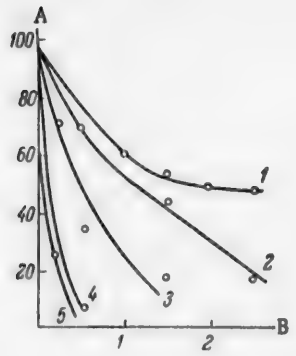

Fig. 7. Reaction of triethylenetetramine with CHP in aqueous solutions of various emulsifiers: A) amount of hydroperoxide (%); B) time (hours). Emulsifiers: 1) none; 2) Nekal; 3) sodium oleate; 4) sodium laurate; 5) sodium salts of paraffinic acids.

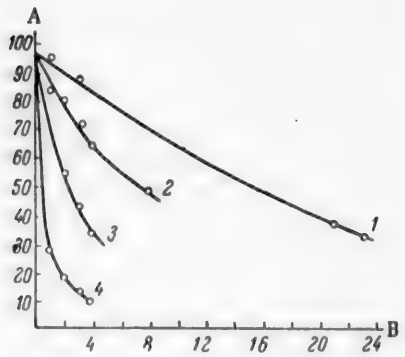

Fig. 8. Reaction of triethylenetetramine with CHP in a model emulsion in presence of Fe^{+++}: A) amount of hydroperoxide (%); B) time (hours). Additions to hydrocarbon phase (wt. %): 1) 0.0026 ammonium ferric alum; 2) ditto + 0.33 sodium stearate; 3) 0.0026 ferric naphthenate; 4) 0.007 ferric naphthenate.

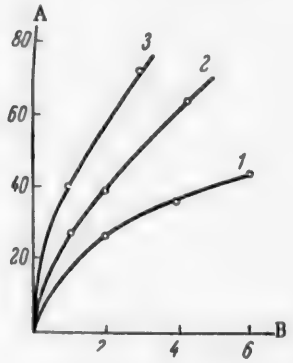

Fig. 9. Effect of the nature of the hydroperoxide on the polymerization rate in presence of 0.005% of ferric naphthenate: A) yield of polymer (%); B) time (hours); 1) isopropylbenzene (cumene) hydroperoxide; 2) diisopropylbenzene monohydroperoxide; 3) tert-butylisopropylbenzene hydroperoxide.

Effect of Different Iron Compounds on the Polymerization Rate at +2°

Activator	Activator concentration (wt. %)	Polymer yield (%) in time (hours)			
		1	2	3	4
Ammonium ferric alum	0.002	–	62.5	61.4	62.5
Ferrous sulfate	0.002	44.6	56.6	62.0	61.7
Iron-pyrophosphate complex (1 : 1.2 ratio)	0.002	47.6	50.0	–	55.8

was blown through again for 15 minutes, and the polyamine was introduced into the system. Samples were taken for analysis, in a current of nitrogen, at definite intervals.

The amount of unreacted hydroperoxide was determined iodometrically in presence of glacial acetic acid.

Emulsion polymerization was performed in a somewhat-modified hydrogenation apparatus [8]. The emulsifier solution and polyamine were put into the reactor, followed by the necessary amount of styrene with ferric naphthenate dissolved in it. The polymerization mixture was cooled to 0° and the apparatus was filled with purified nitrogen. The system was blown through with nitrogen, and divinyl was then added to the mixture. The reactor was placed in a thermostat. The apparatus was shaken vigorously by mechanical means, for agitation of the reaction mixture. After half an hour a solution of the hydroperoxide in 5 ml of styrene was introduced into the reactor. Samples were taken during the process through a special side tube with a stopcock.

SUMMARY

1. The reactions of triethylenetetramine and tetraethylenepentamine with hydroperoxides in various media at 0° proceed at a low rate.

2. These reactions can be effected at any desired rate at low temperatures (down to −35°) by the addition of very small amounts of iron salts.

3. The oxidation-reduction system consisting of polyethylene polyamines, hydroperoxides, and iron salts is very effective for initiation of emulsion polymerization at temperatures of about 0°.

LITERATURE CITED

[1] C.S. Whitby, N. Wellman and V. Floutz, Ind. Eng. Ch. 42, 3, 455 (1950).

[2] R. Spolsky and H.L. Williams, Ind. Eng. Ch. 42, 9, 1847 (1950).

[3] N. Neclutin, C. Westerhoff and L. Howland, Ind. Eng. Ch. 43, 5, 1246 (1951).

[4] W. Embree, R. Spolsky and H. Williams, Ind. Eng. Ch. 43, 11, 2553 (1951).

[5] L.H. Howland, N.C. Neclutin, R.L. Provost and F. Manger, Ind. Eng. Ch. 45, 6, 1304 (1953).

[6] Van Alphen, Rec. Trav. Chim. Payspas 155, 413 (1936); A.W. Hofmann, Ber. 23, 2972.

[7] K. Ihrig, F. Roberts and H. Levin, Ind. Eng. Ch. Anal. Ed. 17, 1, 31 (1945).

[8] S.V. Lebedev, Life and Works [in Russian] (ONTI, 1938), p. 283.

Received April 8, 1956

BRIEF COMMUNICATIONS

MINIMUM EQUIVALENT PACKING HEIGHT (HTU) IN PACKED ABSORPTION, RECTIFICATION AND EXTRACTION COLUMNS

V.V. Kafarov and Iu.I. Dytnerskii

It has been shown [1] that various operating regimes may exist in packed columns; these may be represented as relationships between the Nusselt number Nu and the Reynolds number Re, illustrated in Fig. 1; here the Nusselt number is

$$Nu \simeq \frac{D + \epsilon_d}{D},$$

and the Reynolds number is

$$Re = \frac{4w_0\gamma_v}{g\mu_v\sigma},$$

where D and ϵ_d are the coefficients of molecular and turbulent diffusion (in m^2/second), σ is the specific surface of the packing (in m^2/m^3), γ_v is the density of the vapor (in kg/m^3), w_0 is the linear velocity of the vapor (in m/second), μ_v is the viscosity of the vapor (in $kg \cdot sec/m^2$), and g is the acceleration due to gravity (in m/sec^2).

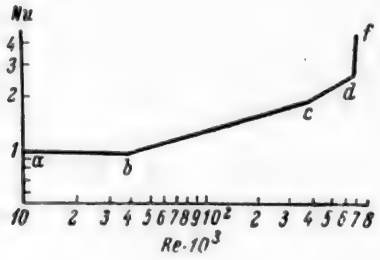

Fig. 1. Variations of transfer regime in a packed tower.

The different sections of the broken line in Fig. 1 represent the following regimes: ab is the laminary regime (molecular transfer), bc is the intermediate regime, cd is the turbulent regime, and df is the free-turbulence or emulsification regime. The point d represents the point of phase inversion (formerly this was defined as the flooding point), above which the liquid fills the whole free space of the packing which is not occupied by gas or vapor, and becomes a continuous phase. The liquid becomes permeated with gas or vapor vortices. Above the point d (section df) the whole layer of packing becomes filled with gas-liquid or vapor-liquid emulsion, and the phase contact area reaches its maximum while its renewal time is at a minimum. It is clear (Fig. 1) that at this stage the maximum separating power of the column is reached, with a corresponding minimum equivalent packing height (HTU).

Earlier [2] we derived an equation for the calculation of flow rates under free turbulence conditions in packed absorption, rectification, and extraction columns.

$$y = 1.2e^{-4.0x}, \tag{1}$$

where

$$y = \frac{w_l^2\sigma}{gF_s^3} \cdot \frac{\gamma_l}{\Delta\gamma}\left(\frac{\mu}{\mu_w}\right)^{0.16}\left(\frac{S_{cd}}{S_{ca} + S_{da}}\right)^{0.2}, \tag{2}$$

$$x = \left(\frac{L}{G}\right)^{\frac{1}{4}} \left(\frac{\gamma_l}{\Delta\gamma}\right)^{\frac{1}{8}}, \tag{3}$$

e is the base on natural logarithms; w_l is the velocity of the light phase (m/sec); μ is the viscosity of the liquid in gas-liquid and vapor-liquid systems (kg·sec/m²) or the viscosity of the continuous phase for liquid-liquid systems (kg·sec/m²); μ_w is the viscosity of water at 20°; γ_l and γ_h are the densities of the light and heavy phase respectively (kg/m³); $\Delta\gamma = (\gamma_h - \gamma_l)$ is the density difference between the heavy and the light phases (kg/m³); S_{cd}, S_{ca}, and S_{da} are the surface tensions at the boundaries between the continuous and disperse phase, continuous phase and air, and disperse phase and air respectively (dynes/cm); L and G are the gravimetric liquid and gas (vapor) rates (in kg/m²·hour) for gas-liquid and vapor-liquid systems, and the volume rates of the heavy and light phases (in m³/m²·hour) for liquid-liquid systems; F_s is the open section of the packing (in m²/m²).

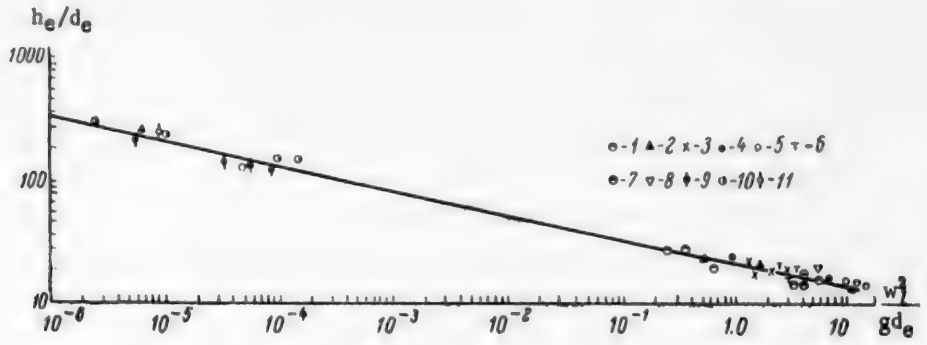

Fig. 2. Variation of packing efficiency in the emulsification regime with the light-phase velocity w_l and the geometrical dimensions of the packing, in absorption, rectification, and extraction processes. Gas-liquid system: 1) porcelain rings 8 x 8 x 2 mm; 2) ditto, 12 x 12 x 2 mm; 3) ditto, 16 x 16 x 3 mm; 4) ditto, 20 x 20 x 3 mm; 5) metal shavings 8 x 8 x 0.2 mm (our data). Vapor-liquid system: 6) porcelain rings 8 x 8 x 2 mm, ceramic rings 10.9 x 11.5 x 2 mm, glass rings 5.7 x 5.9 x x 0.6 mm (data of Kafarov and Bliakhman [8]); 7) porcelain rings 8 x 8 x 2 mm (Luk'ianov's data [4]; 8) ditto (Kirschbaum's data [5]). Liquid-liquid system: 9) glass rings 6.62 x 6.7 x 0.6 mm (data of Kafarov and Planovskaia [9]); 10) porcelain rings 25 x 25 x 3, 16 x 16 x 3, 12 x 12 x 2, 8 x 8 x 2 mm (Ellis' data [6]); 11) porcelain rings 12 x 12 x 2 mm (data of Sherwood, Evans and Longcor [7]).

Above the point f liquid begins to accumulate above the packing [3], the efficiency of the packing decreases as the result of bubbling and mixing, and "flooding" occurs. The point f can therefore be defined as the flooding point.

Special experiments were performed to determine the separating efficiency of the packing in the emulsification regime, for gas-liquid systems (absorption), vapor-liquid systems (rectification), and liquid-liquid systems (extraction); analysis of the results yielded an equation for determination of the minimum HTU. The experimental results of a number of workers [4-7], obtained for regimes with minimum HTU at velocities corresponding to, or close to the inversion point, were also analyzed. The experimental data were plotted (Fig. 2) as the following relationship:

$$h_e/d_e \text{ against } w^2/gd_e, \tag{4}$$

where h_e is the minimum HTU (m), and $d_e = 4F_s/\sigma$ is the equivalent packing diameter (m).

It is clear from the graph that the experimental data for different systems and packings fit satisfactorily around a straight line represented by the equation:

$$h_e/d_e = 24(w_l^2/gd_e)^{-0.2} \quad (5)$$

It follows from Equation (5) that HTU depends only on the velocity of the light phase and the dimensions of the packing. It must be remembered, however, that, in accordance with Equation (1), the velocity of the light phase depends on the value of (L/G), the densities of the liquid and gas phases, and to a small extent on their viscosities and surface tensions.

Thus, the physical properties of the system are indirectly taken into account in calculations of the minimum HTU. Numerous experimental results obtained by different workers for packed columns with different systems and different packings, at flow rates corresponding to or close to the inversion point were used in the analysis; hence the generalized result may be regarded as fairly reliable, so that Equation (5) can be recommended for calculations of equivalent packing heights under the conditions of the greatest free turbulence – the emulsification regime. Under other operating conditions in the packed columns, at and below the inversion point, the efficiency of the packing should be lower and the HTU greater than that given by Equation (5). An equation for calculation of the equivalent packing height at the inversion point was derived earlier [10]. It must also be noted that these results are in full agreement with earlier data on absorption under the free-turbulence regime [11], whereby it was shown that the absorption coefficients for different systems conform to the same law, if differences in the gas solubilities (Henry coefficients) are taken into account, and they are not determined by the characteristics of molecular transfer (molecular viscosity and molecular diffusion coefficients).

SUMMARY

1. An equation has been derived for calculation of HTU for absorption, rectification and extraction processes in packed columns under emulsification conditions.

2. The HTU's obtained under emulsification conditions are the lowest possible.

LITERATURE CITED

[1] V.V. Kafarov, Processes and Equipment of Chemical Technology, *collected papers (Goskhimizdat, 1953).

[2] V.V. Kafarov and Iu.I. Dytnerskii, J. Appl. Chem. 30, 11, 1698 (1957).**

[3] B.J. Lerner and C.S. Grove, Ind. Eng. Chem. 1, 216 (1951).

[4] B.G. Luk'ianov, Dissertation, D.I. Mendeleev MKhTI (1950).*

[5] E. Kirschbaum and A. David, Chem. Eng. Techn. 25, 10, 592 (1953).

[6] S.R.M. Ellis, Ind. Chemist 334, 483 (1952).

[7] T.K. Sherwood, J.E. Evans and L.V. Longcor, Ind. Eng. Chem. 31, 144 (1939).

[8] V.V. Kafarov and L.L Bliakhman, J. Appl. Chem. 23, 3, 244 (1950).**

[9] V.V. Kafarov and M.A. Planovskaia, J. Appl. Chem. 24, 6, 624 (1951).**

[10] V.V. Kafarov J. Chem. Ind. 5 (1953).

[11] V.V. Kafarov and V.I. Trofimov, J. Appl. Chem. 30, 2, 211 (1957).**

Received April 4, 1957

*In Russian.

**Original Russian pagination. See C.B. translation.

REGULATION OF THE FLOW OF GRANULAR MATERIALS BY THE INJECTING ACTION OF A GAS STREAM

A.R. Brun-Tsekhovoi

The action of devices for regulation of the flow of granular materials in chemical processes involving their continuous circulation depends on variations of the cross section of the pipe along which the solid is conveyed. Among such devices are gate valves and other types of valve. Their common defect is the rapid erosion of the parts which come in contact with the solid particles. It is therefore desirable to develop a regulating device without throttling parts, which are subject to the most rapid wear.

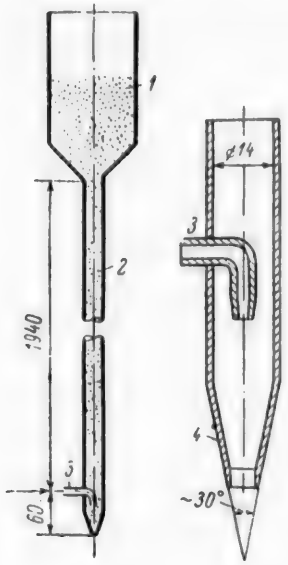

Fig. 1. Diagram of laboratory device, and design of the lower end of the stand pipe.

Such a device may be based on the principle of injection of a stream of gas into the granular material. The experiments described below were performed to test this idea. The apparatus is shown schematically in Fig. 1. The principal parts of the device are the hopper 1 and the stand pipe 2, fitted with a gas-injection inlet 3 and terminating in a conical nozzle 4. The apparatus also included a cylinder with compressed air, fitted with a reducing valve for regulation of the air rate, which was measured by means of a rheometer (not shown in the diagram).

The main object of these experiments was to determine the relationship between the flow rates of the solid material and of the injected air. The experiments were performed by the following method. The hopper 1 and the stand pipe 2 were filled with the granular material. The lower end of the stand pipe was closed by a fine gauze before the start of the determination. After the hopper and stand pipe had been filled, air was admitted through the inlet 3; after the air rate had reached the required value the gauze was removed and the solid material began to emerge from the nozzle. The results were used to plot the flow rate of the solid Q_s against the air rate Q_a.

A glass stand pipe 2 m high and 14 mm in internal diameter was used in these experiments. The solid consisted of silica gel particles of average diameter 0.53 mm and bulk density 0.45 g/cm^3.

The relationship was determined for four different diameters of the exit nozzle (d_1 = 2, 3.7, 8 and 9.5 mm).

The experimental results are plotted in Fig. 2. These curves confirm that there is a relationship between the flow rate of the solid material and the flow rate of the injected air. The nature of this relationship is influenced by the ratio of the diameters of the stand pipe and exit nozzle. As this ratio decreases, the $Q_s = f(Q_a)$ curves become increasingly steep, and the relationship becomes more nearly linear. The smooth nature of the curves shows that a regulator designed on this principle may have high sensitivity.

The maximum flow rate of the solid material is determined by the cross section of the exit nozzle. This maximum rate corresponds to a certain limiting value of the air rate. Above this rate the continuous column of the granular material in the stand pipe is disrupted, because the rate of flow from the pipe exceeds the rate of supply of the solid from the hopper into the pipe. After the column has been disrupted, the level of solid in the

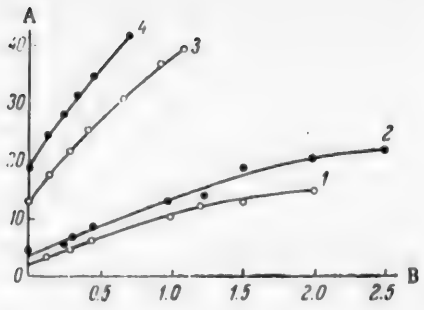

Fig. 2. Variation of the flow rate of the solid material with the flow rate of injected air: A) flow rate of solid material (kg/hr); B) flow rate of injected air (liters/min). Diameter of exit nozzle d_1 (mm): 1) 2; 2) 3.7; 3) 8; 4) 9.5.

pipe falls continuously, the dense layer of solid particles disappears, and the solid particles begin to fall freely from the hopper into the pipe. The maximum flow rate probably depends to a considerable extent on the design of the inlet from the hopper into the stand pipe.

The regulation range, expressed as the ratio of the maximum to the minimum flow rate of the solid, decreases with increase of the diameter of the nozzle exit. When $d_1 = 2$ mm, the regulation range is 8.45, and when $d_1 = 9.5$ mm it falls to 2.22. The maximum linear air velocity in the nozzle exit varies from 11.1 to 0.16 m/sec over this range of nozzle diameters.

These results show that it is possible to design a device for the regulation of the flow rate of solid materials, based on the principle of an injected gas stream.

It is seen that the experiments were performed with the solid material moving along the pipe in a continuous (and not a "fluidized") layer. The solid left the stand pipe to enter the atmosphere and not a "fluidized" layer. It seems likely that the action of the regulator should not change qualitatively if the material moves along the pipe in a fluidized state and then enters a fluidized layer. However, the quantitative results would be different as the density of the layer in the pipe would change, and the resistance at the exit nozzle would increase.

Received December 18, 1956

DETERMINATION OF THE SOFTENING TEMPERATURE OF GLASS BY THE METHOD OF DRAWING A HORIZONTAL THREAD

V.L. Indenbom and V.I. Sheliubskii

All the diverse methods for the shaping of glass, which give rise to a variety of applications of glass in modern technology, are based on the use of the specific characteristics of the hardening of glass. The transition from the liquid to the solid state in glass is gradual, and may be characterized by the so-called softening range, which corresponds to variations of the glass viscosity between 10^9 and 10^{13} poises [1]. At the top limit of this range glass is very plastic and is easily drawn into threads, whereas at the lower limit it becomes brittle.

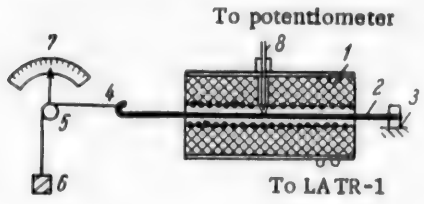

Fig. 1. Diagram of apparatus.

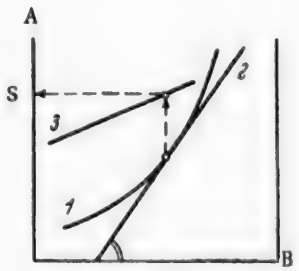

Fig. 2. Graphical determination of the "softening point": A) temperature (°C); B) time (sec); 1) angle of rotation vs. time, $\varphi = \varphi(\tau)$; 2) tangent $d\varphi/d\tau = 0.1$ °/sec; 3) glass temperature as a function of time, $t = t(\tau)$.

In any actual method used for glass shaping, the behavior of the glass over a relatively narrow viscosity range is usually of determining significance, and therefore we may use the concept of "softening temperature." For example, in the production of optical and coated glasses the softening temperature is taken to be the temperature at which the glass articles stick together [2, 3]. In glass-blowing operations, which are of great industrial importance, such as in the production of laboratory glass ware and of electrical vacuum apparatus, the softening point is characterized by the ability of the glass to change its shape under external load [4-6] or under its own weight [7-9].

A method recommended by some authors is the estimation of the local plastic deformation, produced in a specimen in a state of heterogeneous stress, by the indentation of a metal rod into the specimen [4], by the bending of a glass rod [5, 6], etc. The results so obtained are difficult to correlate directly with the viscosity of the glass.

Another difficulty arises with the use of the method adopted in the U.S.A., based on the elongation of a vertical glass thread under its own weight [7-9]. This method is designed to determine the temperature corresponding to a viscosity of $10^{7.6}$ poises, but at such low viscosities the surface tension begins to have a significant effect on the elongation of the thread [10]. The surface tension is the main source of error in this method; according to Littleton [7] and Falter [9], the error is 4-6°.

The softening temperature is sometimes determined from the maximum of the dilatometric curve, reached at the point where the rate of plastic deformation of the glass by the measuring device balances the rate of thermal expansion of the glass. If an interference dilatometer is used, the temperature corresponding to a viscosity of $10^{11.3}$ poises can be determined by this method to an accuracy of about 8° [8].

The method described below for determination of the softening point of glass from the rate of elongation of a horizontal glass thread stretched by a constant load is free from a number of the defects named above, and is

also very simple. It is based on the method used by the Moscow Electric Lamp Factory [11]. The improved version of this method, as described in this paper, was adopted at our suggestion in the vacuum tube industry in 1952 (Specification of the Ministry of the Communications Equipment Industry 938-52), and has fully justified itself in practice.

The apparatus (Fig. 1) consists of a horizontal tubular furnace 1, with the glass thread 2 under test stretched along its axis. One end of the thread is fixed in the holder 3, and the other terminates in a hook, attached to a cotton thread 4 which passes over a balanced pulley 5 carrying a pointer. A load 6 is suspended from the free end of the thread. The rotation of the pulley is read off along the scale 7 graduated in 1° divisions. The temperature in the furnace is measured by means of a thin chromel-alumel or platinum thermocouple 8 in conjunction with a potentiometer of the PP or EPV-01 type. The hot junction of the thermocouple is placed in the middle of the furnace at a distance of 1-2 mm from the glass thread. The furnace temperature is regulated by means of a LATR-1 autotransformer.

Determination of the softening temperature consists essentially of consecutive measurements of the angle of rotation of the pulley and of the furnace temperature while the furnace is heated at a strictly constant rate, about 6° per minute. The apparatus parameters are so chosen that the "softening point" lies just in the middle of the softening range, and corresponds to a viscosity of 10^{11} poises. The following parameters may be recommended: diameter of the glass thread 0.6-0.7 mm, load 20 g, pulley diameter 6 mm, uniform temperature zone in furnace 140-160 mm long. Under these conditions, as will be shown below, the softening temperature corresponds to an angular rotation rate of the pulley of 0.1 °/sec.

To find the "instant of softening," it is convenient to plot the pulley rotation angle against the time in such a way that the scales of 10 seconds along the abscissa axis and 1° along the ordinate axis are numerically equal. To find the required point, a tangent with a slope factor of unity is drawn to touch the curve. The softening temperature is found from the temperature-time curve, plotted on the same graph (Fig. 2).

From the formula [12]

$$\eta = \frac{\sigma l}{3\frac{dl}{d\tau}}$$

(here η is the viscosity of the glass, σ is the tensile stress, l is the length of the softened portion of the thread, and $dl/d\tau$ is the rate of elongation of the thread) and the above parameters of the apparatus, the nonequilibrium viscosity of the glass at the instant of softening is found to be approximately $10^{10.8}$ poises.

The table shows, for a number of commercial glasses, a comparison of the softening temperature with the temperature at which the equilibrium viscosity, determined by Lillie's method [12], is 10^{11} poises. It is seen that the method described, despite its simplicity, can be used to find the temperature corresponding to an equilibrium viscosity of 10^{11} poises, to within 2-3°. Under factory conditions the error does not exceed 5-6°.

Experimental Results

Type of glass	Composition (wt. %)									Temperature corresponding to $\eta = 10^{11}$ poises (°C)	Softening temperature (°C)
	SiO_2	B_2O_3	Al_2O_3	PbO	BaO	CaO	MgO	Na_2O	K_2O		
ЗС-5	66.9	20.3	3.5	—	—	—	—	3.9	5.4	585	587
ЗС-4 (№ 12) .	55.3	—	1.7	30.0	—	—	—	3.8	5.4	491	493
№ 23 . . .	69.6	2.8	4.0	—	—	6.9	—	9.0	7.7	595	595
№ 2	71.9	—	—	—	2.0	5.5	3.5	16.1	1.0	552	549
С-88-13	69.5	2.0	–	—	2.0	5.5	3.5	11.0	6.5	577	578

The greatest difficulty in this method is the construction of a furnace with a uniform temperature zone of the required length, and a fairly rapid temperature drop at the ends of this zone. It was found that good results are obtained with a furnace with three-sectional nichrome winding (160 mm per section), shunted with specially adjusted resistances, and with an internal nickel tube 150 mm long and with walls 3-5 mm thick.

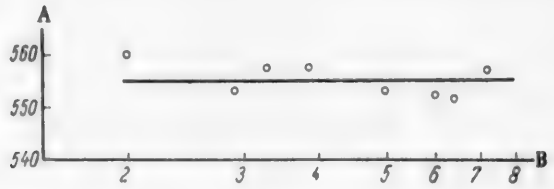

Fig. 3. Variation of softening temperature with the heating rate (BD-1 glass): A) softening temperature (°C); B) heating rate (°/min).

It is interesting to note that although this method is based on measurements of the nonequilibrium fluidity of glass, the results are virtually independent of the heating rate. Fig. 3 shows that the "softening temperature" remains constant to within 2-3° with variations of the heating rate from 1 to 10° per minute. It does not follow, of course, that the furnace may be heated at any random rate – the results may be completely distorted by the influence of delayed elastic deformation.

In view of the successful use of this method in the vacuum tube industry, it may be recommended as a standard rapid method, not only for laboratory purposes, but in production control.

LITERATURE CITED

[1] Glass Technology, edited by I.I. Kitaigorodskii (Industrial Construction Press, 1951).*

[2] E. Zschimmer, Silikat. Z. 2, 129 (1914).

[3] K.V. Struve, Ceramics and Glass 8, 10, 31 (1932).

[4] L.A. Manuilov, G.I. Kliukovskii and A.A. Gezburg, Laboratory Manual of Silicate Technology [in Russian] (Industrial Construction Press, 1955).

[5] L.K. Kovalev and R.L. Shuster, Bull. Acad. Sci. Kazakh SSR 1, 81 (1953).

[6] S.K. Dubrovo and Iu.A. Shmidt, J. Appl. Chem. 29, 557 (1956).**

[7] J.T. Littleton, J. Am. Ceram. Soc. 10, 259 (1927).

[8] J.T. Littleton, J. Soc. Glass Techn. 24, 176 (1940).

[9] A.H. Falter, J. Am. Ceram. Soc. 28, 5 (1945).

[10] M.V. Okhotin and R.I. Tsoi, Glass and Ceramics 7, 6, 13 (1950).

[11] M.G. Cherniak, Ceramics and Glass 7, 2, 18 (1931).

[12] H.R. Lillie, J. Am. Ceram. Soc. 14, 502 (1931).

Received March 25, 1957

*In Russian.

**Original Russian pagination. See C.B. translation.

THE SIMULTANEOUS ELECTRODEPOSITION OF METALS

B.I. Skirstymonskaia

The electrodeposition of two metals which form solid solutions or chemical compounds with each other is usually accompanied by changes in the discharge potentials of their ions. These changes are due to liberation of the energy of interaction between the alloy components. The relationship between these quantities is given by the well-known thermodynamic expression

$$\Delta\varphi = \frac{\Delta\Phi}{nF},$$

where, to calculate the shift of the deposition potential of a given component ($\Delta\varphi$) the change of its partial molar free energy ($\Delta\bar{\Phi}$) must be known. The latter depends on the composition of the alloy in the following way. The partial energy of solution of a given component decreases with increase of its content in the alloy, while the partial free energy of the other component increases, reaching its maximum value when atoms of the one component are mixed with the pure second component [1]. Fig. 1 shows a plot, based on various literature data, of the partial free energies of solution of solid zinc and copper in solid alloys [2].

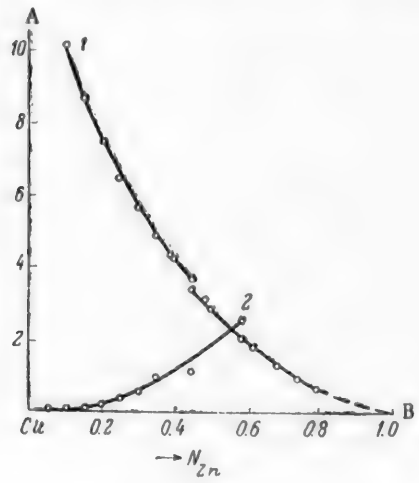

Fig. 1. Effect of alloy composition on the partial molar free energy: A) partial free energies of solution (kcal); B) composition of alloy. Curves: 1) Zn; 2) Cu.

It follows from the foregoing that in the simultaneous electrodeposition of two metals the deposition potential of each must become more positive; alternatively, the values of the partial current for the deposition of a given metal should increase at constant potential. The partial polarization curve for each component* should then be shifted in the direction of more positive potentials, and the degree of this displacement should vary with the composition of the alloy.

Some results obtained in a study of the simultaneous deposition of copper and zinc are presented in this paper.

The electrolyte was an oxalate solution [3] in which the total content of copper and zinc salts was constant (0.0256 mole/liter), while the contents of each (in moles/liter) were varied as follows:

$CuSO_4$	$ZnSO_4$	H_3BO_3	$K_2C_2O_4$**
0.020	0.0056	0.324	0.187
0.010	0.0156	0.324	0.187
0.0016	0.024	0.324	0.187

*The partial polarization curves characterize the rate of discharge of each of the simultaneously discharging ions.

**If a known large excess of $K_2C_2O_4$ is present, variations of the $\frac{[K_2C_2O_4]}{[Me^{++}]}$ ratio do not affect the positions of the polarization curves.

In parallel experiments each of the metals was deposited singly from solutions containing H_3BO_3, $K_2C_2O_4$ and a salt of the given metal at a concentration corresponding to its concentration in one of the mixed solutions. The experimental procedure was described earlier [4]. The electrolysis was performed at predetermined potentials, while the partial current densities were calculated from the results of chemical analysis of the alloys.

The partial polarization curves so obtained are shown in Fig. 2a and b.

The partial curves for Zn in its simultaneous deposition with copper are shifted by 0.25-0.5 v in the positive direction relative to the partial curves for zinc deposited singly.

The magnitude of the displacement of potential may depend on a number of factors, but it is seen that it primarily depends on the zinc content of the alloy. Thus, the Zn content of the alloy is 8-15% for Curve 1, 50-60% for Curve 2, and 85-90% for Curve 3.

Hence, we may conclude that the depolarization of zinc diminishes with increasing zinc content of the alloy; this is in agreement with the change of its partial free energy. The deposition of the second component, copper, together with the zinc is more difficult than its separate deposition; the partial curves for copper are shifted in the negative direction, and the additional polarization (overpolarization) increases with increasing copper content of the alloy.

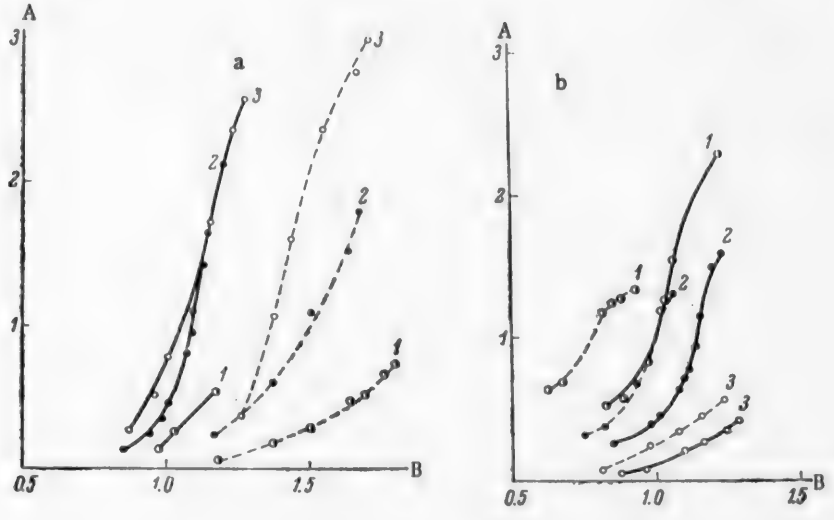

Fig. 2. Variation of the displacement of the partial polarization curves for zinc (a) and copper (b) with the alloy composition: A) partial current density; B) potential. Electrolytes: 1) 1; 2) 2; 3) 3. Separate deposition – dashed lines; simultaneous deposition – continuous lines.

A similar effect of depolarization of one component, with simultaneous difficulty in the deposition of the component deposited in the greater quantity, was observed in the simultaneous deposition of Co and Ni from sulfate solutions [5], and of Sn and Pb from fluoborate solutions [6]. The partial curves based on experimental data for the deposition of brass from cyanide solutions [7] also indicate depolarization of zinc and overpolarization of copper.

The causes of the overpolarization of one of the components are at present difficult to determine, because not enough information is available about the processes which take place in the simultaneous electrocrystallization of metals or about the thermodynamic properties of the components in the alloy. It may be suggested that this effect is caused by the expenditure of additional energy for the formation of the crystal lattice. It is also possible that, because of the different extent to which the partial curve for each component is displaced, a redistribution of current takes place in such a way that the partial current for the predominant metal in the alloy may become less than its value in individual deposition, and thus give rise to the idea of overpolarization of one of the components in the simultaneous deposition of the metals. Our results, in conjunction with literature

data on the displacement of the partial curves in the simultaneous deposition of metals, show that this effect is independent of the nature of the discharging ions (simple or complex ions) and of the phase diagram of the alloy.

SUMMARY

1. The relationship between the changes of partial free energy and the displacement of potentials in the simultaneous deposition of two metals with formation of solid solutions or chemical compounds has been considered.

2. When copper and zinc are deposited simultaneously, zinc is depolarized, and the polarization of copper is increased, relative to the polarizations of these metals when deposited individually. The relationship between the shift of potential and the content of a given component in the alloy has been demonstrated.

LITERATURE CITED

[1] C. Wagner, Thermodynamics of Alloys (USA, 1952).

[2] O. Kubaschewski and J.A. Catterall, Thermochemical Data on Alloys (London, 1956).

[3] A.I. Stabrovskii, J. Appl. Chem. 24, 5, 471 (1951).•

[4] B.I. Skirstymonskaia, J. Appl. Chem. 31, 3, 408 (1958).•

[5] V.M. Kochegarov, A.Ia. Rotinian and N.P. Fedot'ev, Trans. Leningrad Tech. Inst. 40, 112 (1957).

[6] V.M. Kochegarov, Trans. Leningrad Tech. Inst. 40, 124 (1957).

[7] F. Spitzer, Z. Elektroch. 23, 345 (1905).

Received November 5, 1957

•Original Russian pagination. See C.B. translation.

KINETICS OF THE LIBERATION OF COPPER BY THE DIAPHRAGM METHOD OF INTERNAL ELECTROLYSIS

A.K. Zhdanov, V.A. Khadeev and F. Mirzabekov

The V.I. Lenin State University of Central Asia

In the liberation of metals by internal electrolysis from solutions of fairly high concentrations, various semipermeable diaphragms must be placed between the anode and cathode spaces to prevent contact deposition on the anode. However, if such diaphragms are used the ohmic resistance of the cell is considerably increased, and the rate of metal deposition falls sharply. For this reason diaphragm methods have not been widely adopted as control methods in industrial practice.

We found that if a sintered glass, porosity 1, is used as a diaphragm to separate the anode and cathode spaces, the cell resistance is not excessive, while in presence of a slight excess of hydrostatic pressure in the anode compartment contact deposition on the anode is prevented.

It was of interest to study the kinetics of the liberation of copper by internal electrolysis with the use of a diaphragm made from sintered glass, porosity 1. The polarographic method was used, whereby the copper concentration of the solution could be determined fairly rapidly, accurately, and simply at any instant during the course of electrolysis.

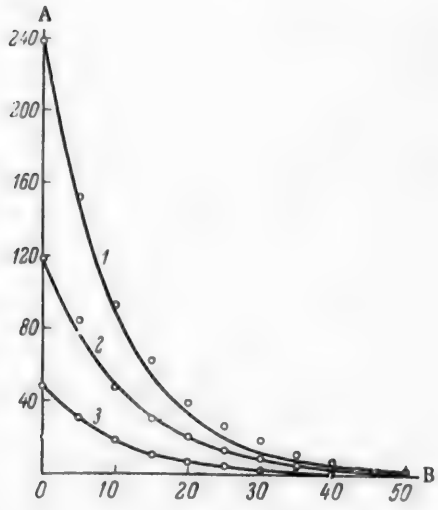

Fig. 1. Variation of the amount of copper present in solution with the time of deposition by internal electrolysis with a zinc anode. Copper content of original solution (mg): 1) 238.2; 2) 118.8; 3) 46.85.

The electrolytic cell was an ordinary chemical beaker, 300 ml in capacity; the cathode was made from platinum gauze. The anode, made from chemically pure zinc or aluminum, was placed inside a small beaker the bottom of which consisted of sintered glass, porosity 1 and served as the diaphragm. This beaker was made from a sintered glass filter, porosity 1, from which the lower part had been cut off. It was firmly closed at the top by a cork with two holes; a tube leading to a header vessel containing the anolyte passed through one, and the anode lead passed through the other. The cathode rod was fixed by a clamp to the end of the anode so that the upper end of the platinum gauze was at the level of the porous diaphragm. The header vessel consisted of a modified dropping funnel with a spherical bulb below the tap. The diaphragm beaker and the header vessel were completely filled with the anolyte. The tap of the header was slightly opened to allow the anolyte to flow slowly into the beaker and set up a pressure on the diaphragm, so that copper ions could not penetrate to the anode.

For the electrolysis, the assembled apparatus together with its fixed electrodes was placed in an electrolytic cell containing copper sulfate, in such a way that only the lower end of the diaphragm beaker was immersed in the solution. The electrolysis was performed at 75° in all the experiments.

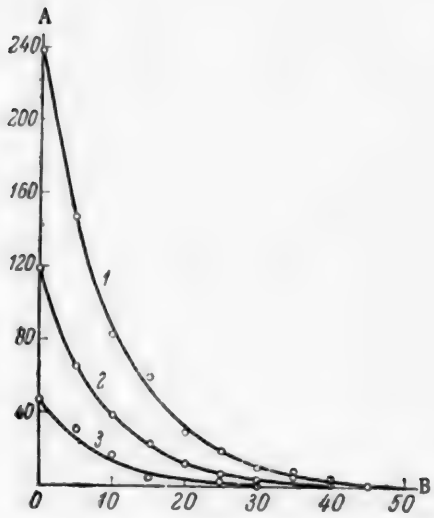

Fig. 2. Variation of the amount of copper present in solution with the time of deposition by internal electrolysis with an aluminum anode. Copper content of original solution (mg): 1) 238.2; 2) 118.8; 3) 46.85.

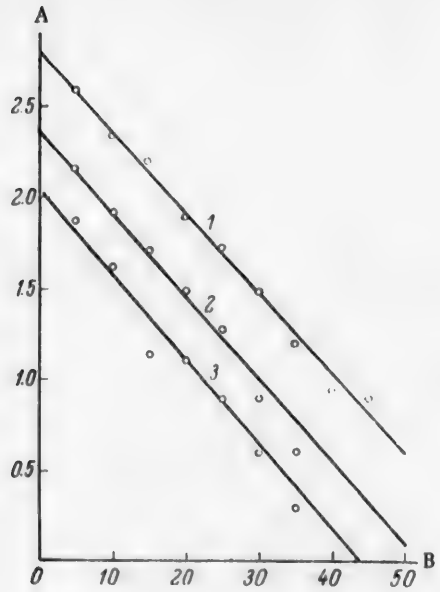

Fig. 3. Variation of the logarithm of the current strength with the time of deposition of copper by internal electrolysis with a zinc anode. Copper content of original solution (mg): 1) 238.2; 2) 118.8; 3) 46.85.

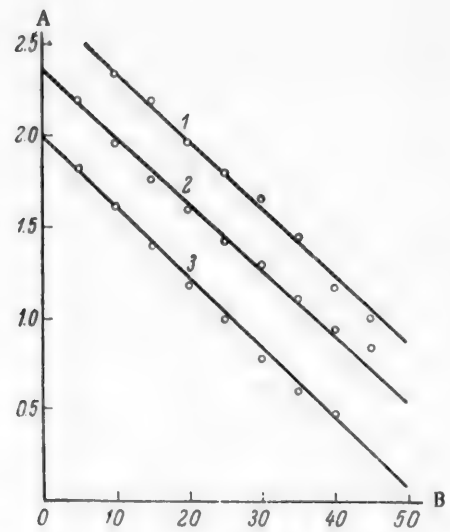

Fig. 4. Variation of the logarithm of the current strength with the time of deposition of copper by internal electrolysis with an aluminum anode. Copper content of original solution (mg): 1) 238.2; 2) 118.8; 3) 46.85.

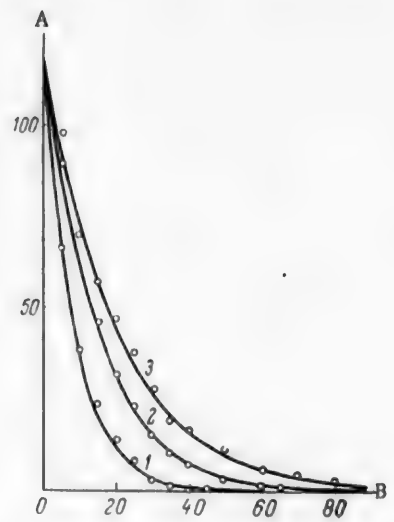

Fig. 5. Variation of the amount of copper present in solution with the time of deposition by internal electrolysis with a zinc anode, for different anolyte concentrations. Copper content of original solution 118.8 mg. Potassium chloride content of anolyte (%): 1) 30; 2) 10; 3) 5.

For the polarographic determination of copper, the capillary tube of the dropping electrode was immersed in the electrolytic cell. It was connected to a saturated calomel electrode by means of an electrolytic bridge with sintered glass plates, porosity 2, sealed in its ends, and an intermediate vessel containing saturated potassium chloride solution. The dropping and calomel electrodes were connected to a manual polarograph in the usual manner. The current strength was measured by means of a mirror galvanometer with a sensitivity shunt. The electrolytic bridge was filled with saturated potassium chloride solution from a reservoir through a tap sealed to the top of the bridge. The liquid levels in the electrolytic cell and the intermediate vessel were equal, to prevent siphoning of the solutions through the bridge.

The experiments on the kinetics of the liberation of copper by internal electrolysis were performed as follows. First, to determine the diffusion current constant of the copper ions, the diffusion current was measured in the original copper sulfate solution heated to 75°. This was followed by a series of determinations of the diffusion current during electrolysis (after 5, 10, 15, 20, 25 minutes, etc.) until a constant residual current was obtained, indicating that the liberation of copper was complete.

To avoid polarographic maxima, the diffusion current was measured at an increased external voltage of 0.8 v.

The results of the current strength determinations in the course of electrolysis were used to calculate the corresponding concentrations of copper, with the aid of the diffusion current constant previously determined.

Both zinc and aluminum anodes were used for studying the kinetics of internal electrolysis. A saturated solution of potassium chloride was the anolyte in all cases. The copper contents of the solutions (in mg) were: 238.2, 118.8, 46.85 and 23.42. The initial electrolyte volume was 100 ml in each experiment.

The results of the kinetic studies are presented graphically in the form of curves showing the variations of copper concentration with time: for the zinc anode in Fig. 1 and the aluminum anode in Fig. 2.

It is also clear from Figs. 1 and 2 that most of the copper (about 90%) is deposited within 20 minutes, both with the zinc and with the aluminum anode. The time required for the liberation of the remaining 10% of copper is 1.5-2 times that required for the main quantity. Thus, the complete liberation of moderate or large amounts of copper requires 50-60 minutes; for the liberation of small amounts of copper by this method, 30-40 minutes is required.

A plot of the logarithm of the current strength against time (Figs. 3 and 4) is satisfactorily linear. It follows that the current strength, and therefore the copper concentration, varies exponentially with time. We can therefore write $i = i_0 \cdot 10^{-k\tau}$, where i is the current strength, i_0 is the current strength before the start of electrolysis, τ is the time, and k is a constant.

An exponential relationship between the concentration of the electrolytically determined ions and the time, with constant cathode potential, has been reported by other authors [1, 2].

The slope of the linear plot of the log current strength against the time, and the intercept cut off along the abscissa axis, readily give the values of the constants i_0 and k; these may be used to calculate the theoretical current strength and therefore the copper concentration at any instant after the start of electrolysis; it is then possible to plot theoretical curves for the rate of liberation of copper by internal electrolysis. These theoretical curves for all the cases studied are shown in Figs. 1 and 2, together with the experimental results which are indicated by individual points. It is seen that these points fit satisfactorily on the theoretical curves.

A study was also made of the kinetics of internal electrolysis, with a zinc anode and the same amount of copper but different anolyte concentrations. The results of these experiments are shown in Fig. 5. It is seen that the rate of liberation of copper in internal electrolysis increases with the anolyte concentration, probably because the ohmic resistance of the cell decreases with increase of the latter.

LITERATURE CITED

[1] J.J. Lingane, J. Am. Chem. Soc. 67, 1916 (1945).

[2] P.N. Kovalenko, J. Appl. Chem. 23, 10, 1067 (1950).*

Received October 22, 1956

*Original Russian pagination. See C.B. translation.

STEAM–GAS ACTIVATION OF ANTHRACITE IN A FLUIDIZED LAYER*

K.E. Makhorin and V.M. Chertov

One effective method for purification of waste waters from the aniline dye industry is by adsorption of organic substances on active carbon. However, in view of the scarcity and high cost of carbon adsorbents, the adsorption method is not used at present for purification of industrial wastes. This method should be widely adopted when cheap activated carbon can be produced [1-3].

The results of a study of the activation of fine-grained Donets anthracite by steam-gas mixture in a fluidized layer are presented in this paper. The experiments were performed with the aid of a unit built at the Rubezhnoe Chemical Combine (Fig. 1).

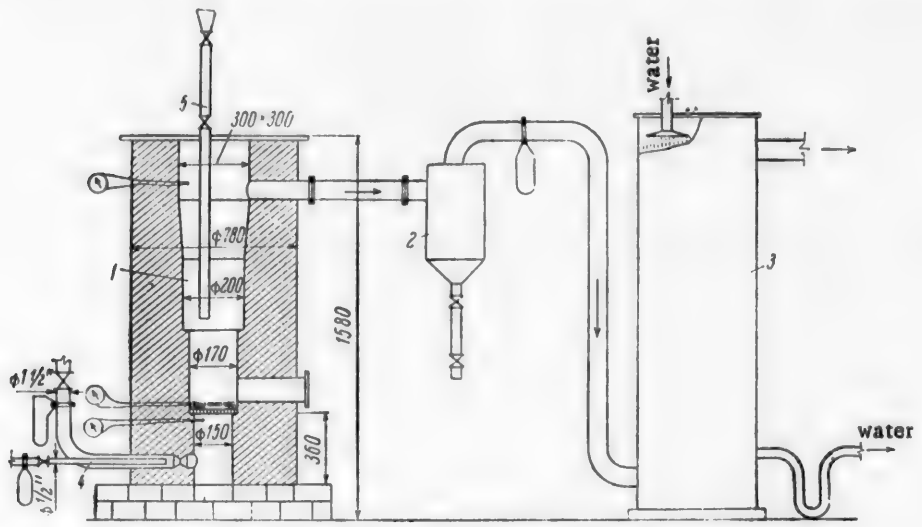

Fig. 1. Apparatus for activation of anthracite in a fluidized layer: 1) furnace; 2) cyclone; 3) scrubber; 4) burner; 5) feed.

Benzene vapor was burned in the combustion chamber of the furnace. The combustion products, diluted with steam at 1050-1250°, passed through a grating into the reactor charged with anthracite. The amount of steam-gas mixture was sufficient to fluidize the layer. The gases passed from the furnace into a cyclone, and then into the air through a scrubber.

The activation was performed batchwise. The furnace was charged with 5 kg of anthracite, which gave a static layer of 250-300 mm. The height of the fluidized layer varied between 700 and 950 mm. The particle size was 0.25-2.0 mm.

*This work was performed under the scientific guidance of V.F. Kopytov. A.M. Koganovskii, E.M. Kaliniichuk, E.I. Dikolenko, and V.V. Reznichenko took part in the investigations.

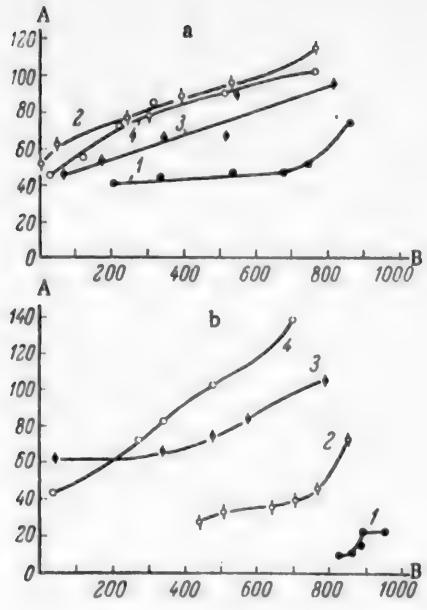

Fig. 2. Adsorption isotherms for phenol and methylene blue on activated anthracite, for different process temperatures. Activation time 1 hour 30 minutes: A) adsorption capacity (mg/g); B) equilibrium concentration (mg/liter); a) adsorption of phenol; b) adsorption of methylene blue. Temperature (°C): 1) 780; 2) 820; 3) 845; 4) 960.

EXPERIMENTAL

It was found in the course of the furnace trials that the gas must be entirely free from oxygen for the production of activated anthracite of good quality, with relatively little scorching. With 1-4% of O_2 the scorching of the anthracite increased, and the grating became choked with fused ash.

The subsequent experiments were performed in an oxygen-free atmosphere. This was ensured by the combustion of benzene with a deficiency of air.

Activation temperature. The influence of temperature on the scorching and adsorption capacity of the anthracite was studied. The furnace temperature was varied by variations of the relative amounts of steam, gas and air, the total flow rate of the activating gas being kept constant. In the first series of experiments the activation time was 1 hour 30 minutes. The process conditions and the adsorption capacities of the carbons are given in Table 1 and Fig. 2. The results show that scorching increased from 17 to 69% with variation of the temperature of the fluidized layer from 780 to 960°.

The adsorption capacity of the carbon for methylene blue increased continuously with increase of temperature, and was 140 mg/g at 960°. The adsorption of phenol increased to 115 mg/g at 820°, and then fell to 95-100 mg/g. The carbons had low capacity at low equilibrium concentration.

In the second series of experiments the activation time was 2-2.5 hours, and the temperature in the layer was varied from 755 to 920°. The results of the determinations are given in Table 2, and the adsorption isotherms for the experimental carbon samples are plotted in Fig. 3.

With increase of temperature of the fluidized layer from 755 to 920° the scorching increased from 30 to 69%, and the capacity of the carbon for phenol rose from 40 to 120-140 mg/g at an equilibrium concentration of 700-800 mg/liter. The best quality carbons were obtained at 830-885°.

TABLE 1

Process Conditions for Activation Time 1 Hour 30 Minutes

Temperature (°C)		% Content in gas of		Scorching (%)	Benzene test (°C)
furnace	layer	CO_2	H_2O		
1060	780	11.3	35.5	17	2.6
1160	820	12.0	31.5	28	3.7
1140	845	9.0	40.0	46	2.4
1170	885	9.4	41.3	50	2.5
1200	960	8.4	31.6	69	2.7

Activation time. The effects of activation time on the scorching of the anthracite and its capacity for phenol and methylene blue were studied.

The temperature of the fluidized layer was 765-800°, and of the combustion space, 1050-1060°. The activation time was varied from 1 hour 30 minutes to 4 hours 50 minutes. The process conditions and the adsorp-

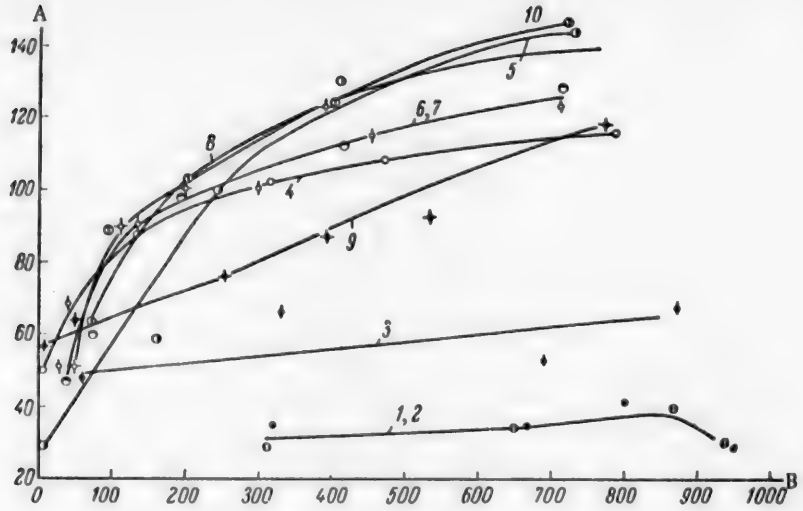

Fig. 3. Isotherms for the adsorption of phenol by activated anthracite, for different activation temperatures. Activation time 2-2.5 hours: A) adsorption capacity (mg/g); B) equilibrium concentration (mg/liter). Temperature (°C): 1) 755; 2 and 3) 775; 4) 830; 5) 860; 6) 870; 7) 880; 8) 885; 9) 920; 10) KAD carbon.

TABLE 2

Process Conditions for Activation Time 2-2.5 Hours

Temperature (°C)		% Content in gas of		Scorching (%)	Benzene test (°C)
furnace	layer	CO_2	H_2O		
980	755	9.0	43.9	30	2.5
1120	775	11.2	25.6	24	1.0
1060	775	12.0	32.6	31.4	3.0
1140	830	8.8	43.3	40.0	4.1
1150	860	11.2	38.1	57.2	4.0
1100	870	9.8	42.2	52.5	4.1
1190	880	10.1	32.7	54.0	3.0
—	885	9.9	37.8	54.0	3.6
1140	920	11.1	30.7	69.0	3.2

tion capacities of the carbon are given in Table 3 and Fig. 4, where it is seen that the scorching increased from 17 to 74%, and the maximum adsorption of phenol from 50 to 140 mg/g. The adsorption rate at low equilibrium concentrations increased together with the increase of maximum capacity.

The optimum activation time at the temperature used was four hours, when the scorching was about 50%, the maximum capacity for phenol was 140 mg/g, and for methylene blue, 70 mg/g. When the time was increased to 4 hours 50 minutes the scorching increased to 58-74%, and the adsorption of phenol fell to 100-120 mg/g.

In the experiments detailed in Table 4 the temperature of the fluidized layer was 820-875°, and the activation time was from 1 hour 30 minutes to 2 hours 45 minutes. The optimum time fell to 2-2.25 hours with increase of the process temperature from 765-800° to 820-875°. The adsorption of methylene blue was 100 mg/g, and of phenol, 110-140 mg/g, under these conditions (Fig. 5).

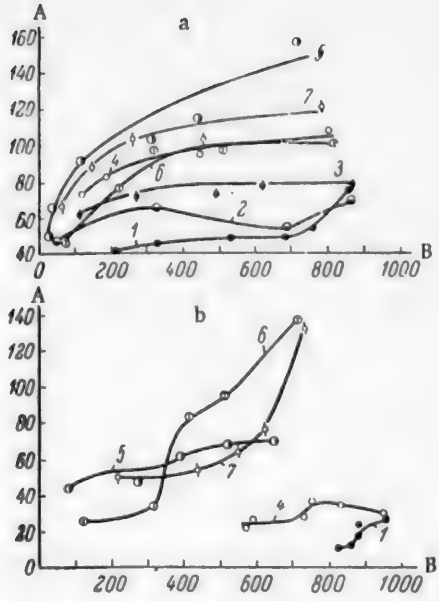

Fig. 4. Adsorption isotherms of phenol and methylene blue on activated anthracite, for different activation times. Activation temperature 765-800°: A) adsorption capacity (mg/g); B) equilibrium concentration (mg/liter); a) adsorption of phenol; b) adsorption of methylene blue. Time: 1) 1 hr 30 min; 2) 2 hr 15 min; 3) 3 hr; 4) 3 hr 25 min; 5) 4 hr; 6) 4 hr 50 min; 7) 4 hr 50 min.

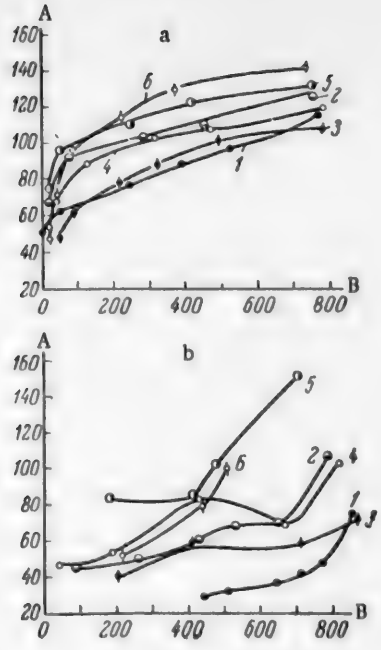

Fig. 5. Adsorption isotherms of phenol and methylene blue on activated anthracite, for different activation times. Activation temperature 820-875°: A) adsorption capacity (mg/g); B) equilibrium concentration (mg/liter); a) adsorption of phenol; b) adsorption of methylene blue. Time: 1) 1 hr 30 min; 2) 1 hr 50 min; 3) 2 hr; 4) 2 hr 15 min; 5) 2 hr 30 min; 6) 2 hr 45 min.

TABLE 3

Process Conditions for a Fluidized Layer at 765-800°

Activation time	Temperature (°C)		% Content in gas of		Scorching (%)	Benzene test (°C)
	furnace	layer	CO_2	H_2O		
1 hr 30 min	1060	780	11.3	35.5	17	2.6
2 hr 15 min	1060	775	12.0	32.6	31.4	3.0
3 hr 00 min	1060	770	10.9	35.8	28	3.0
3 hr 25 min	1050	775	9.8	44.0	40	3.8
4 hr 00 min	1060	770	10.4	40.6	49.6	3.5
4 hr 50 min	—	765	8.9	47.5	58.0	4.0
4 hr 50 min	1050	800	10.0	44.3	74	3.3

Therefore, a steam-gas mixture containing 35-40% H_2O and 9-11% CO_2 can be used for the production of activated anthracite in a fluidized layer, at layer temperature 830-885° and with activation time 2-2.5 hours; the adsorption capacity of the product, calculated on the weight of carbon, is 12-14% for phenol and 10-12% for methylene blue. This carbon is not inferior in quality to KAD commercial carbon (Fig. 3). Under static conditions

TABLE 4

Process Conditions for a Fluidized Layer at 820-875°

Activation time	Temperature (°C)		% Content in gas of		Scorching (%)	Benzene test (°C)
	furnace	layer	CO_2	H_2O		
1 hr 30 min	1160	820	12.0	31.5	28	3.7
1 hr 50 min	1150	825	10.2	41.5	42	4.3
2 hr 00 min	1000	875	8.7	35.3	48	2.6
2 hr 15 min	1140	830	8.8	43.3	40	4.1
2 hr 30 min	1160	830	11.6	32.4	65.4	2.7
2 hr 30 min	1150	860	11.2	38.1	57.2	4.0
2 hr 45 min	1145	830	9.5	36.7	53.0	3.0

the activated anthracite takes up to 24.2% benzene vapor, calculated on the weight of carbon; this corresponds to a microporosity of 0.275 cc/g. Its moisture capacity when boiled in water is 68.5% by weight.

The suitability of activated anthracite for purification of waste waters from the Rubezhnoe Chemical Combine was tested in experimental columns packed with the carbon, and in adsorbers with circulating beds. The waste waters from the factory tank were clarified and then passed through the carbon. According to the data of the Water Laboratory of the Institute of General and Inorganic Chemistry of the Academy of Sciences, Ukrainian SSR, the results were quite satisfactory; the wastes were decolorized by treatment with the activated anthracite, and its oxidizability fell to 90-95%. The absorption of chlorine and dissolved oxygen did not exceed the corresponding values for river water. The effluent was free from organic odor, and chlorination did not result in the formation of odors and tastes of chlorinated phenols or other "chemicals." Nitrophenols were absent from the purified effluent, and the amine content did not exceed 1 mg/liter. The amount of water purified by some samples of the activated anthracite was more than double the amount purified by KAD carbon under the same conditions.

LITERATURE CITED

[1] K. Lorenz, Gesundheits-Ing. 75, 11, 189 (1954).

[2] A. Godel, Chem. Eng. 55, 7, 110 (1948).

[3] F. Sabel, Chem. – Ing. – Technik 2, 93 (1952).

Received for the second time December 23, 1957

CHANGES IN THE INFRARED ABSORPTION SPECTRA DURING VULCANIZATION OF EBONITES

A.S. Kuz'minskii and L.V. Borkova

Scientific Research Institute of the Rubber Industry

The vulcanization process is based on reactions between rubber and sulfur. The sulfur bonds formed during vulcanization join the molecular chains of rubber into a continuous spatial three-dimensional network.

Soft vulcanizates are characterized by a low density of cross links. If the amount of sulfur reacting with the rubber is large, products known as ebonites, with a specific range of properties, are formed.

Whereas there have been many investigations performed on soft vulcanizates, the information of the vulcanization of ebonites is fragmentary and often contradictory [1-11]. For example, the concept has become firmly established according to which ebonite is the product of maximum saturation of rubber molecules with sulfur [1-4]. Doubts concerning the possibility of such extensive conversion of the polymers have been expressed in only a few papers [9, 10].

Very little is known about the properties of the bonds forming the spatial network in ebonites, and their influence on the mechanical and other properties.

This paper deals with a study of the infrared absorption spectra of ebonites at different stages of vulcanization.

EXPERIMENTAL

As the result of vulcanization, ebonite completely loses the ability to dissolve or even swell in organic solvents. Because of this, the use of ordinary chemical methods for investigation of the structural changes in rubbers during vulcanization of ebonites becomes very restricted and in some cases impossible.

Attempts to use infrared spectroscopy for studies of the vulcanization of soft rubbers have not yielded any significant results, as the degree of conversion of the rubber in such cases does not exceed a few percent, often less than the error limits of the method. However, this method gives reliable results and is therefore very effective in studies of the vulcanization of ebonites, which have dense spatial networks.

The UIKS-4 infrared spectrometer with photographic recording was used for the investigation. The spectra were measured in the wavelength region corresponding to the double bonds. The variation of unsaturation in the course of vulcanization was determined from changes in the absorption coefficient of ebonite films at different stages of vulcanization. The absorption coefficient $\underline{k}$ was calculated by means of the Bouguer–Lambert–Beer equation [12]

$$k = \frac{1}{d \cdot c} \ln \frac{I_0}{I},$$

where $\underline{d}$ is the thickness of the specimen (cm), $\underline{c}$ is the volume fraction of rubber in the ebonite, I_0 is the intensity of the incident light (taken as 100%), and I is the intensity of the transmitted light.

The unsaturation of the unvulcanized rubber was taken as 100%. The unsaturation of ebonite at different

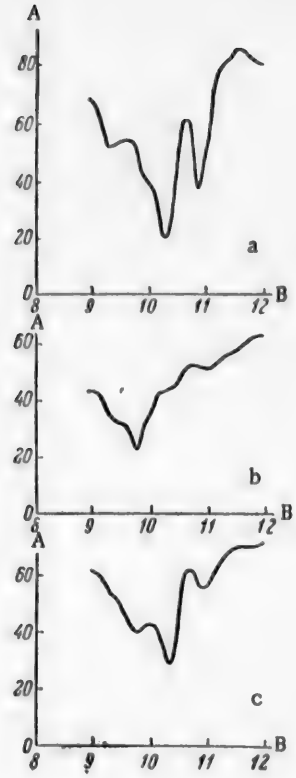

Fig. 1. Variations of the infrared spectrum of SKS-30 ebonite during vulcanization at 190°. Composition of ebonite (wt. parts): SKS-30, 100; sulfur, 40. A) Transmission of ebonite relative to air (%); B) wavelength (in μ). Vulcanization time (hours): a) unvulcanized; b) 3; c) 5.

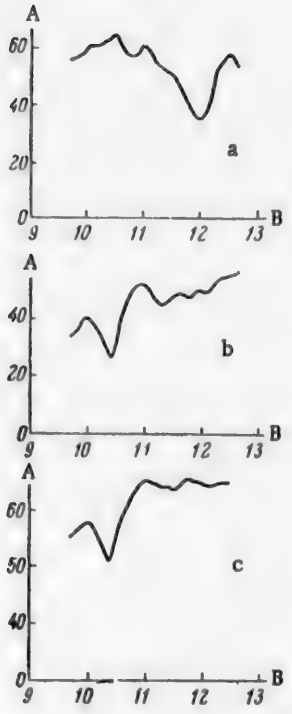

Fig. 2. Variation of the infrared spectrum of NR ebonite during vulcanization at 170°. Composition of ebonite (wt. parts): natural rubber, 100; sulfur, 47. A) Transmission (%); B) wavelength (in μ). Vulcanization time (hours): a) unvulcanized; b) 2; c) 4.

stages of vulcanization was expressed in percentages of the unsaturation of the original rubber. The relative changes of unsaturation were therefore determined. The thickness of the ebonite films was 30-70μ, and the thickness variations did not exceed 2-4%. The film thickness was measured by means of a mechanical micrometer.* The reproducibility of the results was in the range of 10-15%.

The ebonites studied were based on butadiene-styrene (SKS-30), sodium butadiene (SKB) and isoprene (NR) rubbers. Most of the experiments were with ebonites based on butadiene-styrene rubbers. The infrared spectra of ebonites vulcanized at different temperatures (150-190°) and containing various amounts of sulfur (from 30 to 50 weight parts per 100 parts of rubber) were studied.

DISCUSSION OF RESULTS

Considerable changes take place in the infrared spectra of ebonite during vulcanization. The higher the vulcanization temperature, the more pronounced these changes are. In illustration, Fig. 1 shows the infrared spectra of SKS-30 ebonites vulcanized at 190°. The absorption band at 10.3μ corresponds to the double bonds of the principal chain, and the 10.9μ band to double bonds in the vinyl side chains. Fig. 2 shows the infrared spectra of NR ebonites vulcanized at 170°. Changes in the infrared spectra were also observed in the course of vul-

*Ebonite is in the glassy state, and therefore does not undergo deformation during mechanical measurement of thickness.

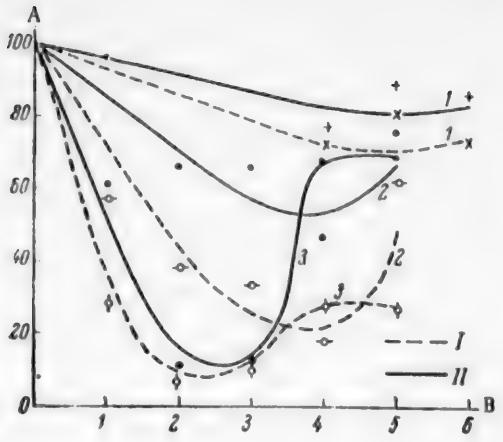

Fig. 3. Variation of unsaturation in the course of vulcanization of ebonite at different temperatures. Composition of ebonite (wt. parts): SKS-30, 100; sulfur, 40. A) Unsaturation of the ebonite (% of rubber unsaturation); B) vulcanization time (hours). Changes of unsaturation: I) at the double bonds of vinyl side chains; II) at the double bonds of the principal chain. Vulcanization temperature (°C): 1) 150; 2) 170; 3) 190.

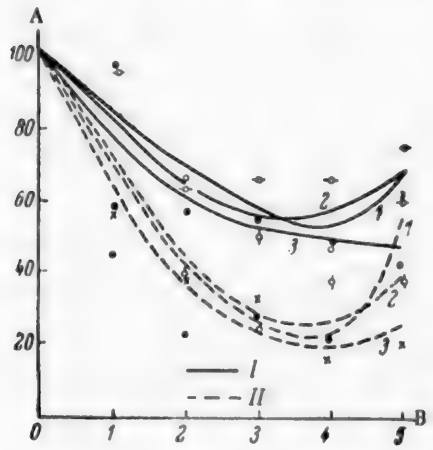

Fig.4. Variations of unsaturation in ebonites with different sulfur contents, during vulcanization at 170°: A) unsaturation of the ebonite (% of rubber unsaturation); B) vulcanization time (hours). Contents of SKS-30 and sulfur respectively (in wt. parts): 1) 100 and 40; 2) 100 and 50; 3) 100 and 30. Changes of unsaturation: I) at the double bonds of the principal chain; II) at the double bonds of the vinyl side chains.

canization of SKB ebonites. The variations of the unsaturation of rubbers in the course of vulcanization of ebonites are plotted in Figs. 3 and 4. All the kinetic curves are based on infrared data.

Examination of these results shows that when the sulfur has been completely combined, irrespective of its initial concentration, the ebonite has a considerable content of double bonds. The lower the vulcanization temperature, the more double bonds are retained for a given amount of bound sulfur. If the vulcanization temperature is 150°, up to 80% of the double bonds remains in the rubber, at 170°, up to 50%, while at 190° only 10% of the double bonds remains. The double bonds in the vinyl side chains are lost at a considerably higher rate than the double bonds in the principal chain. It is clear that no conclusions can be drawn from this concerning the influence of the positions of the double bonds in the rubber molecule on the reactivity.

The infrared absorption spectra represent the overall change in the unsaturation, as not only are double bonds consumed during vulcanization but new ones are formed. In fact, as is clear from Figs. 3 and 4, the unsaturation decreases only in the early stages of vulcanization, when free sulfur is still present in the system. Further vulcanization leads to a fairly considerable increase in the unsaturation of the ebonite. The increase of unsaturation becomes greater with increase of vulcanization temperature, and reaches the considerable value of 50% at 190°.

In the spectra of ebonites based on natural rubber (Fig. 2), the 11.9μ absorption band, corresponding to

the double bonds in the $-CH=CH-$ group, disappears during vulcanization, but a new absorption band, also characteristic of double bonds, appears at 10.4μ. It follows that there are two tendencies during vulcanization of ebonites based on different rubbers: loss of double bonds, and formation of new double bonds.

In experiments on the thermal vulcanization of ebonites in absence of sulfur it was found that double bonds are not formed. Therefore, an increase of unsaturation is specific for sulfur ebonites only. As is clear from Fig. 5, the increase of unsaturation during vulcanization coincides in time with the decrease of the equilibrium modulus and of the amount of bound sulfur. Free sulfur does not appear in the process. These effects are evidently interrelated. The partial cleavage of sulfur cross links, which results in a decrease of the equilibrium modulus, leads to the formation of sulfur in an active form. The free sulfur radicals remove the hydrogen atoms in the α-position to the double bonds, forming hydrogen sulfide and free radicals in the rubber

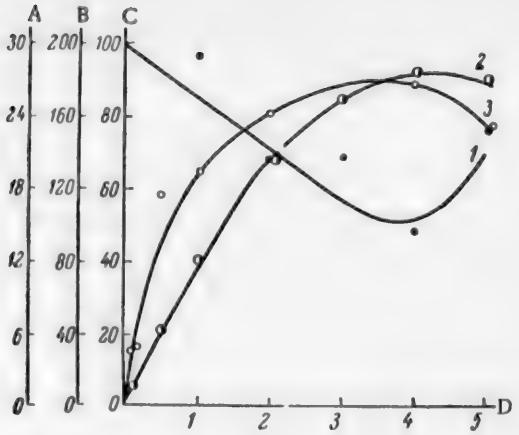

Fig. 5. Variations of the composition and structure of ebonite during vulcanization at 170°. Composition of ebonite (wt. parts): SKS-30, 100; sulfur, 40. A) Amount of bound sulfur (%); B) equilibrium modulus of elasticity (kg/cm^2); C) unsaturation of the ebonite (% of rubber unsaturation); D) vulcanization time (hours); 1) change of unsaturation during vulcanization; 2) change of equilibrium modulus during vulcanization; 3) change of the amount of bound sulfur during vulcanization.

chain. The free radicals in the chain are evidently the source of double bond formation. Thus, the formation and disappearance of double bonds during vulcanization of ebonites reflect two other tendencies: formation and breakdown of sulfur linkages which form the spatial network in ebonites. While the system contains free sulfur, the predominant process is formation of cross links (loss of unsaturation). When the sulfur has been consumed, breakdown of the sulfur "bridges" (formation of double bonds) becomes the dominant process.

Evidently, the denser the ebonite network, the more "bridges" break down, and the greater is the observed reversion effect. As is shown in Fig. 3, the rates and limits of the decrease and increase of unsaturation increase with temperature, and therefore the minima on the curves are shifted toward the coordinate origin. It is easy to see that these changes are caused by the increase in the rates of formation and breakdown of the sulfur bridges with increase of temperature. Similar results with regard to the behavior of sulfur bridges were found in the vulcanization of soft rubbers [13], so that the analogy is complete. As Fig. 4 shows, the initial sulfur concentration has no significant influence either on the rate of change of unsaturation during vulcanization, or on the nature of the kinetic curves. It must be noted that the solubility of sulfur in rubber at 150-190° is considerably below the amounts used for vulcanization (30-50 wt. part per 100 of rubber) [14]. Some of the sulfur is dispersed mechanically in the rubber. As the sulfur combines with the rubber, the solution is supplemented by the dispersed sulfur. Thus, a constant sulfur concentration is maintained during the vulcanization, and therefore the reaction rate is independent of the initial sulfur content.

The activation energy of ebonite vulcanization, calculated from the loss of unsaturation, is 23 kcal/mole, whereas the activation energy for the vulcanization of soft rubbers reaches 30 kcal/mole. The lowering of the energy barrier may be caused by the great relative significance of the secondary reactions of sulfur addition to sulfur bonds already formed; this has been demonstrated by Bresler [14]. It is known that these reactions proceed with much greater ease than the primary addition of sulfur to rubber. We showed with the aid of radioactive sulfur that polysulfide bonds are formed at the first stages of ebonite vulcanization, and the number of sulfur atoms in a "bridge" may reach 25.

SUMMARY

1. The infrared spectra of ebonites at different stages of vulcanization were studied, and it was shown that the changes of unsaturation, the amount of sulfur bound, and the density of the spatial network formed in vulcanization, as determined by different independent methods, are in good agreement.

2. Ebonite at optimum vulcanization is unsaturated. Its degree of unsaturation increases with decrease of vulcanization temperature.

3. There are two competing tendencies in the vulcanization of ebonite: formation and loss of double bonds. These tendencies are caused by the formation and breakdown of sulfur bridges in the ebonite. The formation and breakdown of sulfur bridges during vulcanization is a common feature not only of ebonites but also of soft rubbers.

4. The rate of loss of double bonds and the limiting decrease of unsaturation are independent of the amount of sulfur originally dispersed in the rubber, as vulcanization proceeds at constant concentration of dissolved sulfur.

LITERATURE CITED

[1] T. Midgley, Ind. Eng. Chem. 34, 7, 861 (1942).

[2] G.A. Blokh and A.F. Chuprina, Proc. Acad. Sci. USSR 99, 5 (1954).

[3] B.A. Dogadkin, Chemistry and Physics of Rubber [in Russian] (Goskhimizdat, 1947).

[4] F.F. Koshelev, Rubber Technology [in Russian] (Goskhimizdat, 1951).

[5] T. Alfrey, Mechanical Behavior of High Polymers [Russian translation] (IL, Moscow, 1952).

[6] B.A. Dogadkin and M.M. Reznikovskii, Progr. Chem. 24, 7 (1955).

[7] B.I. Gengrinovich, Colloid J. 17, 4, 270 (1955).*

[8] E.A. Hauser and M.C. Cze, J. Phys. Chem. 46, 118 (1942).

[9] N. Sheppard and G.B.M. Sutherland, Rubb. Chem. Techn. 19, 1 (1946).

[10] N. Sheppard and G.B.M. Sutherland, Rubb. Chem. Techn. 26, 4, 799 (1948).

[11] M.L. Selker and A.R. Kemp, Rubb. Chem. Techn. 1, 8 (1949).

[12] V.N. Nikitin, Bull. Acad. Sci. USSR, Ser. Phys. 17, 5, 644 (1953).

[13] A.S. Kuz'minskii and V.F. Chertkova, Proc. Acad. Sci. USSR 107, 428 (1956).*

[14] S.E. Bresler, V.I. Priadilova and V.Ia. Khainman, J. Tech. Phys. (USSR) 24, 4, 577 (1954).

Received August 13, 1956

*Original Russian pagination. See C.B. translation.

VARNISH FLAWS ("BITTINESS") IN ALKYD ENAMELS

I.A. Popova and R.D. Zamyslov

Central Works Laboratory, Cheliabinsk Paint and Varnish Works, Ministry of the Chemical Industry

The fault known as "bittiness" in enamels is a very serious defect. This effect has different causes. Mechanical impurities (foreign matter or pieces of badly-ground pigment) can be dealt with by greater care in purification, although this occasionally involves considerable difficulties. A much more difficult task is to prevent the so-called "varnish bittiness," caused by particles of the varnish base, which originates either in the manufacturing process or during storage of the finished product for various times. The latter is very characteristic of of alkyd enamels. There is no detailed information in the literature on the nature of this type of bittiness or methods for its prevention.

In Gurevich's paper [1] the view is put forward that the tendency of enamels to aggregation is due to the presence of difficultly soluble polymeric components of the varnish base in the system. These components are adsorbed on the pigment surface and make the adsorption layers mutually cohesive.

A number of other sources [2-5] refer to the heterogeneous and inconsistent character of alkyd bases, which is the result of the complexity of the processes used in their preparation, as the starting materials are diverse and differ in reactivity, and also of variations in the process conditions and equipment used. No practical hints for the prevention of bittiness are given.

The object of the present work was to determine the nature of the bittiness of alkyd enamels and to investigate possibilities of its prevention.

Our observations, made over a number of years, on the condition of alkyd enamels showed that deterioration of enamel quality, down to complete unserviceability, occurs because of the appearance or intensification of bittiness and thickening; these two effects are not always interrelated in time. Bittiness may appear after different periods, either during the first few months or even days after manufacture, or during the second or third year of storage.

Bittiness is most pronounced in enamels pigmented with carbon black, azure and red pigments; in a number of cases, an enamel, which was in itself free from the defect,formed a bitty film on drying.

For a deeper study of the condition of enamels, determinations of the purity by standard methods and visual evaluation of dried coatings were accompanied by systematic microscopical examinations. The undiluted enamel was smeared in a thin layer on a slide. The specimen was usually examined by transmitted light, under x120 magnification, directly after the application and when dry. The edge of the bitty rim of the enamel smear on the glass was sometimes examined. A total of about 120 samples of different enamels were investigated in this way, immediately after manufacture and after different storage times.

When microscope preparations of bitty enamels, or enamels which formed a bitty film after drying,were examined, in the great majority of cases the field of view contained, in addition to pigment particles, transparent colorless or yellowish particles of various shapes, sometimes with regular faces, around which the pigment particles seemed to cluster. This aggregation of the pigment, more pronounced at the particle surface, decreased with the distance from the particle. These "pigment zones" were especially prominent in enamels pigmented with carbon black or with red pigment. The particles of aggregation centers varied greatly in size, from the scarcely visible under the magnification used to 40-60μ along the greatest length. The particle sizes were de-

termined by means of an eyepiece scale calibrated against a micrometer objective. It proved impossible to use the ordinary micrometer method even with the very bitty enamels.

Such nonpigment particles were hardly ever seen in microscope preparations of clean enamels, which gave clean films even after drying. In some cases the particles (aggregation centers) were almost invisible in fresh smears but became numerous and distinct in dried specimens. Systematic microscopical analysis of enamels after different storage times generally revealed the appearance, or an increase in the number and size, of transparent nonpigment particles consistently with the appearance or intensification of bittiness. A different microscopic picture was observed only in rare cases.

Since the varnish base is not chemically homogeneous, it seems likely that the transparent particles are difficultly soluble components of the base. To investigate the thermal stability of these particles, a bitty enamel or an enamel which formed a bitty film on drying was sprayed onto black iron plates. One plate was dried at room temperature, and the other at 140-150° for 10-15 minutes. Generally the films of the same enamel dried under different conditions differed in external appearance. Coatings dried naturally showed the usual "bittiness" picture: a rough surface with bumps varying in height. The hot-dried coatings had a pitted surface, with crater-like depressions of different sizes; if the bittiness of the naturally-dried coating was fairly fine, the hot-dried coating was sometimes apparently smooth, without visible pits. This difference between the external appearances of coatings dried under different conditions was observed for different grades of alkyd and pentaalkyd enamels. In rare cases, usually in enamels which had been stored a long time and had thickened considerably, the hot-dried coating was bitty and without pits, like the naturally-dried coating.

These tests showed that the transparent particles, centers of pigment aggregation, which are seen under the microscope melt at a fairly high temperature, and thereby cause pitting of the coating; they are insoluble or relatively less soluble resinous components of the alkyd varnishes.

An attempt was made to isolate the "bittiness" in the form of the particles observed under the microscope. This attempt was successful with three samples of production pentaalkyd enamels. In enamel PF-61 based on varnish PFD-03 bittiness appeared during the second year of storage; enamels PF-67 and PF-68 based on PFL-03 varnish showed considerable bittiness on the first day after manufacture. The "bits" were separated from enamel PF-61 by washing with white spirit on a sieve of 10,000 mesh per cm^2. The largest particles remained on the sieve. The bits in enamels PF-67 and PF-68 (pigmented with red pigment and carbon black) were also separated by means of white spirit, but by repeated decantation rather than by sieving. The last washings were performed with aviation gasoline, residues of which were evaporated off at room temperature. It is obvious that only the coarsest fraction of the "bittiness" was isolated by this method.

When examined under the microscope, the bits were found to be rounded or angular "grains" of various sizes and shapes, with a few pigment particles adhering to them.

Considerable amounts (up to 12-15 kg) of enamels were treated in this way, to isolate enough of the particles for certain analysis. Solubility tests showed that they are almost insoluble in ethyl alcohol, and only slightly soluble in acetone and benzene. They could not be dissolved completely in mixed solvents on heating. It was also found that the solubility of the particles, exposed to air, generally deteriorates with time. The acid and hydroxyl numbers were not determined because of the poor solubility of the material in mixed solvents and in acetylation mixture. The saponification number was determined by the usual method. Phthalic anhydride was detected qualitatively by its liberation on heating, and estimated quantitatively by the volumetric method. Glycerol and pentaerythritol were determined quantitatively by the method used in the works laboratory, a combination of the dichromate and periodate methods. The ash content was determined by combustion, and the composition of the ash was found spectroscopically. The fatty acids were isolated by the usual method and their weight determined after they had been dried in a current of CO_2. During the analysis they were separated into two fractions: soluble in benzene, and insoluble in benzene but soluble in acetone and alcohol. For determination of certain constants the fatty acids were isolated separately from material which had not been dried in air, and all the operations were performed in an atmosphere of carbon dioxide. The following constants were determined for both fatty acid fractions: neutralization number by titration with 0.1 alcoholic alkali, iodine number by the Kaufmann method, and the hydroxyl number by the Verley and Bölsing method.

For comparison, similar analyses were performed on varnish bases from PF-67 and PF-68 enamels, centrifuged to remove pigments and some of the bittiness (Table 1).

TABLE 1

Analytical Results

Enamel	Material studied	Saponification number (mg KOH)	Phthalic anhydride (%)	Fatty acids		Glycerol (%)	Pentaerythritol (%)	Ash (%)
				soluble in benzene (%)	insoluble in benzene (%)			
PF-67	"Bits"	338	30.3	37.0	12.0	14.4	4.5	10.80
	Varnish base	266	13.6	76.3	1.6	–	–	1.52
PF-68	"Bits"	368	30.9	28.3	11.5	–	–	2.60
	Varnish base	242	13.8	74.3	4.1	–	–	0.41

Qualitative spectroscopic analysis of the ash showed the presence of very large relative amounts of lead in all the samples. The amount of manganese was less. Iron and zinc were also found.

Analytical data on the fatty acids isolated from the bits and varnish base in PF-67 varnish are given in Table 2.

TABLE 2

Analytical Data on Fatty Acids

Material studied	Solubility in benzene	Neutralization number (mg KOH)	Iodine number (%)	Hydroxyl number (mg KOH)	Consistency at room temperature
Fatty acids from "bits" in PF-67 enamel	Soluble	196	75.5	167	Pasty
	Insoluble	215	48.5	240	Solid
Fatty acids from varnish base of PF-67 enamel	Soluble	196	116.5	122	Liquid
	Insoluble	199	70.0	–	Solid

DISCUSSION OF RESULTS

In the great majority of cases "bittiness" in alkyd enamels is caused by acid particles of the varnish base; these react by their acid radicals with heavy metals (lead, manganese, iron, zinc) to give compounds insoluble in the common solvents. The formation of these particles begins during the production of the alkyd varnishes and continues during the production and storage of the enamels. These particles also act as centers around which pigment particles aggregate, with intensification of the physical nature of the bittiness.

The particles causing "varnish bittiness" are composed of alkyd resins with a high content of phthalic anhydride. The fatty acids in these resins are characterized by relatively lower iodine numbers and relatively higher hydroxyl numbers. Therefore these particles are less soluble on aliphatic or aromatic hydrocarbons, which form the constituents of the solvents used in the production of alkyd varnishes and enamels. Their solubility decreases still further as the result of formation of heavy-metal salts. The ash content of the particles is 6-7 times that of the base. This fact indicates that the catalysts and driers used in the production of alkyd resins and enamels favor the occurrence of varnish bittiness.

The time required for "ripening" of large grains, when the enamel becomes commercially valueless, depends on the following factors: the size and numbers of the particles formed initially, their reactivity, and the rates of the oxidation and polymerization processes occurring during the production of the varnish and enamel.

The formation of difficultly soluble or insoluble components in the varnish base must be largely attributed to unfavorable conditions of synthesis of alkyd resins in fired kettles of simplified design, resulting in local overheating at the kettle bottom and sides, and to the possible easy occurrence of oxidative polymerization processes which are not controllable.

SUMMARY

1. "Bittiness" in alkyd enamel coatings is caused by difficultly soluble or insoluble components of the varnish base, of definite chemical composition which differs from that of the base.

2. The main cause of formation of these bittiness centers lies in imperfections in the technology of alkyd base production, and especially local overheating.

LITERATURE CITED

[1] Ia.M. Gurevich, Bull. Exch. Exp. Varnish and Paint Ind. 3, 9 (Goskhimizdat, 1952).

[2] A.M. Lubman, Bull. Exch. Exp. Varnish and Paint Ind. 3, 19 (Goskhimizdat, 1952).

[3] B.M. Dubrova and L.I. Liskina, Bull. Exch. Exp. Varnish and Paint Ind. 4, 5 (Goskhimizdat, 1953).

[4] A.M. Lubman and L.I. Liskina, Bull. Exch. Exp. Varnish and Paint Ind. 5, 18 (Goskhimizdat, 1953).

[5] A.Ia. Drinberg, Technology of Film Formers [in Russian] (Goskhimizdat, 1955).

[6] V.S. Kiselev, Practical Manual of Film-Former Technology [in Russian] (Goskhimizdat, 1948).

Received March 12, 1957

EXCHANGE PROPERTIES OF "LIGNIN ACIDS"

I.V. Skrynnik, S.I. Sukhanovskii and M.I. Chudakov

All-Union Research Institute of the Hydrolysis and Sulfite Alcohol Industry

In the alkaline activation of hydrolytic lignin, a considerable proportion of it forms the so-called "lignin acids," the sodium salts of which are readily soluble in water. Alkaline activation of hydrolytic lignin is effected at 160-180° in an aqueous medium, the consumption of caustic soda being 25% on the weight of the lignin. In this case 90-95% of the lignin is dissolved, forming a complex mixture of lignin decomposition products and polysaccharide residues [1, 2].

When this mixture is acidified with mineral or organic acids or carbon dioxide, an amorphous brown precipitate of "lignin acids," with an enormous adsorption surface, is formed at pH 6.

We have shown [3] that "lignin acids," when added in excess, enter into exchange reactions with salts of 2- and 3-valent metals. These reactions in general proceed almost stoichiometrically; 1000 g of "lignin acids" can combine with about 3 g-equiv of metal.

Fig. 1. Effect of solution concentration on the amount of metal precipitated: A) relative amount of metal precipitated; B) concentration of solution (normality).

"Lignin acids" form insoluble salts with most multivalent metals; these salts can usually be separated from the solutions without difficulty.

The possibility of separating metals from solutions creates potentialities for the use of hydrolytic lignin (which has a low ash content) in industry for precipitation of valuable products from waste waters, pickling liquors, etc.

Data on the isolation of various multivalent metals from dilute solutions of their salts by means of "lignin acids" are presented in this paper.

Technical lignin from the Leningrad hydrolysis plant was used for the investigation.

The lignin had the following composition (%): ash 1.8, reducing substances (by Bertrand's method) 0.3, acids calculated as sulfuric 0.5, difficultly hydrolyzable polysaccharides 15.0, methoxyl groups 10.4. The dry lignin was ground for ten minutes in a vibratory mill before the alkaline activation. The alkaline activation was performed in an autoclave fitted with a stirrer, with 25% of caustic soda calculated on the lignin; the liquor ratio was 7.5, and the activation time was six hours at 180°. The alkaline solution was acidified with hydrochloric acid to pH 6.3, centrifuged to remove suspended particles, and used to precipitate metals from 0.01 N solutions of their salts.

To 100 ml of metal salt solution, 5-10 ml of the sodium salts of "lignin acids," containing 0.8-1 g of lignin per 100 ml (calculated on the lignin precipitated on acidification with hydrochloric acid) was added. The precipitant solution was added in some excess, and therefore the filtrate after removal of the precipitate was always colored yellow.

To ensure good coagulation of the precipitate, the mixture was heated on a water bath for ten minutes at 70°. The precipitate was then filtered off and washed with distilled water to remove traces of soluble salts. The precipitate was dried and ashed; the percentage of metal precipitated from the original salt solution was calculated from the weight of the ash.

The results for the precipitation of metals from 0.01 N solutions of their salts are given below.

Salt	Metal precipitated (%)	Salt	Metal precipitated (%)
$Pb(CH_3COO)_2$	99.75	$NiSO_4$	47.00
$BaCl_2$	97.30	$CuSO_4$	40.00
$Al_2(SO_4)_3$	95.40	$CaCl_2$	38.60
$Bi(NO_3)_2$	69.50	$MgCl_2$	35.00
$FeSO_4$	71.00	$CoSO_4$	25.00
$MnSO_4$	47.80		

These results show that "lignin acids" precipitate lead, aluminum and barium almost quantitatively from 0.01 N solutions. Bivalent and lighter metals are precipitated less effectively.

The precipitation of calcium from solutions of the chloride and acetate was studied in order to determine the influence of anions on the precipitation of cations. The amounts precipitated were 37.6 and 36.3% respectively, so that the nature of the anion has almost no effect on the cation precipitation. It was of interest to study the behavior of "lignin acids" when the amounts added are insufficient for the double-decomposition reaction with the salt solutions, i.e., to investigate the possibility of metal precipitation as the result of adsorption effects. For these experiments, 0.02, 0.04, 0.06, 0.08 and 0.1 N solutions of manganese sulfate were prepared. Equal amounts of the sodium salts of "lignin acids," known to be insufficient for complete precipitation of the metal, were added to these solutions. It was found that the double-decomposition reaction is accompanied by precipitation of the metal by the action of adsorption forces on the precipitate surface. The precipitation of metals is more complete from more highly concentrated solutions. As is clear from Fig. 1, the amounts of metal precipitated from different solutions are not proportional to their initial concentrations. For example, nearly 20 times as much manganese was precipitated from 0.1 N manganese sulfate solution as from 0.02 N solution.

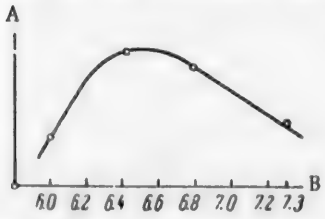

Fig. 2. Effect of pH on the precipitation of metals: A) relative amounts of metal precipitated; B) pH of lignin acids.

To confirm that metals can be precipitated on the surface of free "lignin acids," experiments were performed on the precipitation of iron from 0.01 N $FeSO_4$ solutions.

"Lignin acids" were isolated by the action of 20% hydrochloric acid on the sodium salts obtained by the alkaline activation of hydrolytic lignin. The precipitates were washed with water and dried at 105°. 1-3 g of the dry "lignin acids" was added to 100 ml of 0.01 N ferrous sulfate solution. The mixture was shaken for 30 minutes, and then heated for 30 minutes on the water bath. The solution was then left to settle for twelve hours, the precipitate was separated off, washed, dried and ashed. An average of 52-54% of the iron could be removed from the 0.01 N solution.

To determine the influence of pH, in the range of 6-7.3, on the degree of precipitation of the metal, we studied the precipitation of manganese from 0.01 N $MnSO_4$ solution. The results are given in Fig. 2. It is seen that the greatest amount of manganese is precipitated at pH 6.4.

SUMMARY

1. In a study of the exchange properties of sodium salts of "lignin acids" it was shown that they can be used for effective precipitation of metals from dilute solutions of their salts.

2. Free "lignin acids" can also be used to precipitate metals from solutions.

LITERATURE CITED

[1] S.I. Sukhanovskii and M.I. Chudakov, J. Appl. Chem. 28, 3, 410 (1956).*

*Original Russian pagination. See C.B. translation.

[2] S.I. Sukhanovskii and M.I. Chudakov, Trans. Kirov. Acad. Wood Technology 75 (1956).

[3] A.P. Krasnova, S.I. Sukhanovskii and M.I. Chudakov, J. Appl. Chem. 30, 12, 1827 (1957).*

Received November 5, 1957

*Original Russian pagination. See C.B. translation.

STUDY OF THE EFFECT OF INCREASED PRESSURE ON THE COURSE OF REACTIONS BETWEEN SOLID ANHYDRIDES AND AMINES*

M.Kh. Gluzman and D.G. Arlozorov

The influence of elevated pressures on the course of reactions between solid inorganic substances was studied by Spring [1, 2] and by Berg, Ianat'eva and Savitskii [3], who found a small increase in the yield in reactions between salts under a pressure of 6000 atmospheres. Budnikov and Berezhnoi [4] noted that the effects of pressure should be, on the one hand, to facilitate the reaction by bringing the reacting particles closer together, and on the other, to compress the grains of each component, reducing their active surface with an adverse effect on the reaction.

The influence of elevated pressures on the course of reactions involving organic solids has not previously been studied. We therefore studied a number of solid anhydride-amine systems from this standpoint; data obtained by one of us on their interaction at various temperatures without excess pressure were available [5].

EXPERIMENTAL

A special unit was designed for the experiments; compressed tablets consisting of equimolecular amounts of amine and anhydride could be held in it under pressure in isothermal conditions. The substances were thoroughly ground, sifted through screens of 900 and 3600 mesh/cm^2 and subjected to pressures of up to 1550 kg/cm^2 in the die of a hydraulic press surrounded by a jacket through which oil at the required temperature was circulated from a thermostat. The observations were made at temperatures not exceeding the melting points of the low-melting eutectics. The tablets were then powdered and the contents of N-arylamino acids determined; the isotherms were compared with the isotherms for the reactions of the same systems under normal pressures.

The following systems were investigated: 1) phthalic anhydride + anthranilic acid; 2) benzoic anhydride + + β-naphthylamine; 3) benzoic anhydride + p-chloroaniline; 4) succinic anhydride + anthranilic acid; 5) succinic anhydride + β-naphthylamine; 6) succinic anhydride + norsulfazole.

All the isotherms determined under high pressures lie considerably lower than the isotherms for the same systems under normal pressures.

An explanation of this result is that increase of pressure usually raises the melting point [6] and also the melting point of the eutectic [7]; it was shown by one of us earlier [8] that the closer the reaction temperature to the melting point of the eutectic, the better does a reaction between solids proceed. Another significant factor is that the vapor pressure decreases with increase of external pressure, and therefore the gas phase, which usually plays an important part in reactions between solids [9], takes less part in the reaction.

In our opinion, the explanation of the adverse effect of pressure on the course of reactions involving solids must be sought in these two causes, since the contact between the solid particles is a factor of much less importance than the simultaneous participation of the vapor and liquid phases.

*Communication IX in the series on reactions involving solid organic substances.

SUMMARY

The influence of increased pressures on the course of the acylation of amines in the solid phase was studied; it was found that the yield of N-arylamino acids decreases with increase of pressure, because of the shift of the melting points of the eutectics toward higher temperatures and the decreased vapor pressure of the components.

LITERATURE CITED

[1] W. Spring, Zbl. 897 (1885).

[2] W. Spring, Zbl. 1231 (1888).

[3] L.G. Berg, O.K. Ianat'eva and E.M. Savitskii, Proc. Acad. Sci. USSR 75, 383 (1950).

[4] P.P. Budnikov and A.S. Berezhnoi, J. Appl. Chem. 13, 1286 (1940).

[5] M.Kh. Gluzman and D.E. Plotkina, Trans. Chem. Faculty and Chem. Sci. Res. Inst. Khar'kov State Univ. 14, 188 (1956); 15, 158 (1956).

[6] Chemist's Reference Book,* I (Goskhimizdat, 1951), p. 670.

[7] N.K. Vorob'ev, V.A. Gol'tsshtein and M.Kh. Karapet'iants, Manual of Physical Chemistry [in Russian] (Goskhimizdat, 1951), p. 111.

[8] M.Kh. Gluzman and R.S. Mil'ner, Trans. Chem. Faculty and Chem. Sci. Res. Inst. Khar'kov State Univ. 17 (1957).

[9] M.Kh. Gluzman and R.S. Mil'ner, Trans. Chem. Faculty and Chem. Sci. Res. Inst. Khar'kov State Univ. 14, 211 (1956).

Received October 19, 1956

* In Russian.

SULFONATION OF 2- AND 4-NITROPHENANTHRENEQUINONES*

V.I. Sevast'ianov

Titkov [1] was the first to sulfonate unsubstituted phenanthrenequinone to the monosulfonic acid and to establish the structure of the phenanthrenequinone-2-sulfonic acid formed. A method for the preparation of phenanthrenequinone-2,7-disulfonic acid is described in our preceding communication [2].

The present communication deals with the sulfonation of nitro derivatives of phenanthrenequinone, and in particular of 2- and 4-nitrophenanthrenequinones. Experiments showed that nitrophenanthrenequinones are sulfonated by 15-16% oleum to form 2- and 4-nitrophenanthrenequinone-7-sulfonic acids. The presence of perhydrol during the sulfonation of the nitro isomers, in contrast to the sulfonation of unsubstituted phenanthrenequinone, has no appreciable influence on the reaction.

The structures of the sulfonic acids was confirmed by conversion of the latter into dihydroxyphenylcarboxylic acids by way of the amino- and hydroxyphenanthrenequinone-7-sulfonic acids. The following acids were isolated: 2- and 4-aminophenanthrenequinone-7-sulfonic acids, 2- and 4-hydroxyphenahthrenequinone-7-sulfonic acids, 4,4'-dihydroxydiphenyl-2-carboxylic acid (Product I), and 2,4'-dihydroxydiphenyl-6-(or 6')-carboxylic acid (Product II). The m.p. of Product I was 269.5-270°. A mixed sample with Product I obtained from phenanthrenequinone-2,7-disulfonic acid gave no m.p. depression. Decarboxylation of (I) gave 4,4'-dihydroxydiphenyl (III) with m.p. 273.5-274.5°. This gave no m.p. depression with (III) prepared from benzidine. Decarboxylation of (II) gave 2,4'-dihydroxydiphenyl (IV), m.p. 161.3-162.5°. This gave no depression with (IV) prepared from diphenylene.

EXPERIMENTAL

2-Nitrophenanthrenequinone-7-sulfonic acid (potassium salt). A solution of 25.3 g of 2-nitrophenanthrenequinone in 130 ml of 15% oleum was warmed and stirred on the water bath until a sample of the mass dissolved completely in water. The reaction mass was cooled and poured into saturated potassium chloride solution. The potassium salt of 2-nitrophenanthrenequinone-7-sulfonic acid was filtered off and washed with 10% potassium chloride solution and with water. Pale yellow needles were obtained after recrystallization from water. The yield was 28.5 g, about 77% of the theoretical.

Found %: S 8.67, 8.56; N 3.69, 3.78. $C_{14}H_6O_7NSK$. Calculated %: S 8.63; N 3.77.

To obtain the free 2-nitrophenanthrenequinone-7-sulfonic acid, the reaction mass was poured into concentrated hydrochloric acid. The liquid was filtered, the precipitate was washed with hydrochloric acid, and recrystallized from the latter; golden-yellow prisms of m.p. 237-238° were obtained. The substance is soluble in alcohol, water, and acetone.

4-Nitrophenanthrenequinone-7-sulfonic acid was prepared by sulfonation of 4-nitrophenanthrenequinone under the same conditions, and isolated either in the free state or as the barium salt. The latter crystallizes from water in the form of golden yellow plates. The yield was about 50% of the theoretical.

Found %: S 8.06, 8.07; N 3.39, 3.36. $(C_{14}H_6O_7NS)_2Ba$. Calculated %: S 8.00; N 3.49.

Free 4-nitrophenanthrenequinone-7-sulfonic acid crystallizes from concentrated hydrochloric acid in the

*Communication II in the series on the sulfonation of phenanthrenequinone-9,10.

form of golden yellow needles with m.p. 262.5-263.5°. It is readily soluble in alcohols, water, and acetone.

2-Aminophenanthrenequinone-7-sulfonic acid. A mixture of 18.6 g of finely powdered potassium salt of 2-nitrophenanthrenequinone-7-sulfonic acid, 40 g of granulated tin, and 200 ml of technical hydrochloric acid (sp.gr. 1.19) was warmed with stirring for 10-12 hours at 85-90°. At the end of the reduction the reaction mass was carefully decanted from the residual tin and filtered. The precipitate was washed with water and dissolved in 50 ml of 10% sodium carbonate solution; air was then blown through the solution for 1.5 hours to oxidize the leuco base to quinone, and the solution was filtered. The filtrate was acidified, and the precipitate was filtered off and washed with water to a neutral reaction. To remove impurities, the precipitate was reprecipitated twice from sodium carbonate solution by means of hydrochloric acid. An amorphous greenish powder, soluble with difficulty in hot water, was obtained. The yield of dry 2-aminophenanthrenequinone-7-sulfonic acid was 13.4 g, or about 88% of the theoretical.

Found %: S 10.67, 10.66; N 4.59, 4.61. $C_{14}H_9O_5NS$. Calculated %: S 10.57; N 4.62.

4-Aminophenanthrenequinone-7-sulfonic acid was prepared by the reduction of the barium salt of 4-nitrophenanthrene-7-sulfonic acid as described for the preceding experiment. The reduction product was filtered, washed with water to a neutral reaction, shaken with water, and air was blown through it for 0.5 hour. The precipitate was filtered and dried. The product is an amorphous powder, soluble in water with difficulty. The yield of dry 4-aminophenanthrenequinone-7-sulfonic acid was about 63%.

Found %: S 10.82, 10.82; N 4.59, 4.61. $C_{14}H_9O_5NS$. Calculated %: S 10.57; N 4.62.

2-Hydroxyphenanthrenequinone-7-sulfonic acid. 4 g of 2-aminophenanthrenequinone-7-sulfonic acid was dissolved in 20 ml of a 10% solution of soda ash. 100 ml of water and 40 ml of concentrated technical hydrochloric acid was added to the solution to separate the original substance in a finely divided state. The suspension was diazotized by the gradual addition of 0.9 g of sodium nitrite dissolved in 10 ml of water, at room temperature. The reaction mass was then boiled for 30 minutes. The liquid was cooled and filtered, the precipitate was washed with cold water to a neutral reaction, pressed out and dried.

2-Hydroxyphenanthrene-7-sulfonic acid is an amorphous red-brown powder. The yield was 3.4 g, or about 85% of the theoretical.

Found %: S 10.48, 10.53. $C_{14}H_8O_6S$. Calculated %: S 10.54.

4-Hydroxyphenanthrenequinone-7-sulfonic acid was obtained under the same conditions in approximately 65% yield. It is an amorphous dark red powder, slightly soluble in water.

Found %: S 10.47, 10.49. $C_{14}H_8O_6S$. Calculated %: S 10.54.

4,4'-Dihydroxydiphenyl-2-carboxylic acid. 8 g of caustic potash was melted with 0.5 ml of water in a nickel crucible on a sand bath. 2 g of 2-hydroxyphenanthrenequinone-7-sulfonic acid was added in small portions to the mixture at 190-200°, stirred with a metal spatula, the reaction mass was heated to 315-320° during 30 minutes, and held at that temperature for 15 minutes. The cooled melt was leached out with water. The precipitate which separated after acidification of the alkaline solution with hydrochloric acid was filtered off, washed, and dried. Two recrystallizations from alcohol yielded colorless crystals in the form of oval grains. The yield was 0.95 g, m.p. 269.5-270°. A mixed sample with 4,4'-dihydroxydiphenyl-2-carboxylic acid prepared previously by the alkaline fusion of phenanthrenequinone-2,7-disulfonic acid gave no m.p. depression. The substance is soluble in alcohol and water.

Found %: C 67.70, 67.77; H 4.31, 4.33. $C_{13}H_{10}O_4$. Calculated %: C 67.82; H 4.38.

2,4'-Dihydroxydiphenyl-6(or -6')-carboxylic acid was prepared as described above, by the alkaline fusion of 4-hydroxyphenanthrenequinone-7-sulfonic acid, the yield being about 70% of the theoretical. The position of the carboxyl group was not established.

Found %: C 67.73, 67.69; H 4.37, 4.34. $C_{13}H_{10}O_4$. Calculated %: C 67.82; H 4.38.

4,4'-Dihydroxydiphenyl. A thoroughly ground mixture of 3 g of 4,4'-dihydroxydiphenyl-2-carboxylic acid, 3 g of calcium hydroxide, and 5 g of river sand was heated in a glass tube at 325-330° until deposition of crystals on the inner walls of the projecting cold part of the tube ceased. The tube was cooled and the sublimate was collected. The yield was 0.18 g. The m.p. was 273.5-274.5° after recrystallization from alcohol.

The 4,4'-dihydroxydiphenyl was identified by a m.p. test on a mixed sample with 4,4'-dihydroxydiphenyl prepared from benzidine.

2,4'-Dihydroxydiphenyl was prepared by decarboxylation, as described above, of 2,4'-dihydroxydiphenyl-6-(or -6')-carboxylic acid. 3 g of the latter yielded 0.25 g of substance. The m.p. after recrystallization from alcohol was 161.3-162.5°. The compound was identified by a m.p. test on a mixed sample with 2,4'-dihydroxydiphenyl prepared from diphenylene.

LITERATURE CITED

[1] V.A. Titkov, Author's Certif. 76374.

[2] V.I. Sevast'ianov, J. Appl. Chem. 30, 12, 1858 (1957).*

Received February 28, 1957

*Original Russian pagination. See C.B. translation.

SYNTHESIS OF 3-CHLORODIPHENYLAMINE

S.V. Zhuravlev and A.N. Gritsenko

Institute of Pharmacology and Chemotherapy, Academy of Medical Sciences USSR

The high pharmacological activity of 10-(γ-dimethylaminopropyl)-2-chlorophenothiazine prompted us to prepare certain dialkylaminoacyl derivatives of 2-chlorophenothiazine; the results of preliminary pharmacological tests of these are given in one of our papers [1]. We wished to prepare other derivatives of 2-chlorophenothiazine, such as 10-(N-methylpiperidyl-3-methyl)-2-chlorophenothiazine, the analog of a pharmacologically active preparation known in the literature as pacatal, lacumin, etc. [2]. This compound does not contain a chlorine atom in the phenothiazine nucleus.

The synthesis of 3-chlorodiphenylamine, which is the main intermediate in the preparation of 2-chlorophenothiazine, is described in this paper.

There are various methods for the preparation of 3-chlorodiphenylamine. For example, from 2-chlorobenzoic acid and 3-nitroaniline, 3-nitrodiphenylamino-2'-carboxylic acid is prepared, and decarboxylated to give 3-nitrodiphenylamine [3]. The latter is reduced to 3-aminodiphenylamine [4], and the amino group is replaced by chlorine to yield 3-chlorodiphenylamine [5]. There is another and shorter route for the preparation of 3-chlorodiphenylamine from 2-chlorobenzoic acid and 3-chloroaniline. In this method 3-chlorodiphenylamino-2'-carboxylic acid is prepared, and the carboxyl group is split off to give 3-chlorodiphenylamine [6].

We have developed another method for the preparation of 3-chlorodiphenylamine, comprising the following reactions: diazotization of 3-nitroaniline and decomposition of the diazonium salt in hydrochloric acid solution by cuprous chloride to give 3-chloronitrobenzene [7] which is reduced by the Bechamp method to 3-chloroaniline in the same conditions as used for the production of aniline from nitrobenzene [8]. The 3-chloroaniline is acetylated, and 3-chloroacetanilide is condensed with bromobenzene in presence of Ullmann catalysts. Saponification of 3-chloro-N-acetyldiphenylamine gives 3-chlorodiphenylamine:

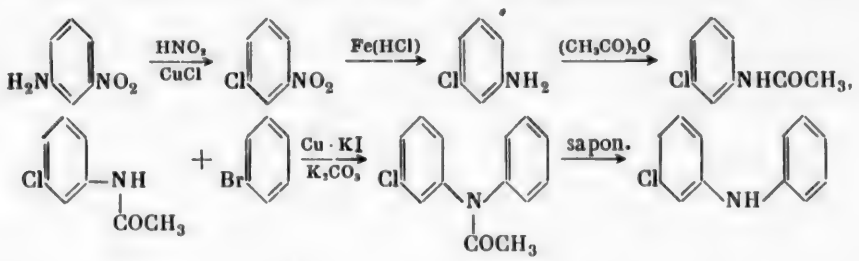

Preliminary experiments showed that when free 3-chloroaniline is treated with bromobenzene in absence of nitrobenzene, 3-chlorodiphenylamine is not formed. If the reaction takes place under the same conditions but in presence of nitrobenzene, 3-chlorodiphenylamine is obtained in approximately 20% yield. Most of the reaction mass is resinified in the process. Therefore all subsequent investigations were concerned with the conditions of reaction of acetylated m-chloroaniline with bromobenzene. The reaction between 3-chloroacetanilide and bromobenzene was carried out under the conditions described for the preparation of 3-nitrodiphenylamine from 3-nitroaniline and bromobenzene [9]. Nitrobenzene was used as the reaction medium in some of the experiments. The reagents were taken in the following proportions: 1 mole of m-chloroacetanilide to 2

moles of bromobenzene and 0.5 mole of calcined potash, and small amounts of potassium iodide and copper bronze. In the experiments in which nitrobenzene was used the yields of 3-chlorodiphenylamine reached 45-50%. A considerable proportion of the unreacted 3-chloroacetanilide was recovered as 3-chloroaniline on saponification. The total yield of 3-chlorodiphenylamine, if the 3-chloroaniline is used again, can be raised to 60-65%. When this procedure was used, the temperature of the reaction mixture was gradually raised from 180 to 210° during 18 hours. Lower yields of 3-chlorodiphenylamine were obtained if these conditions were changed. In experiments in which little or no nitrobenzene was used the yield of 3-chlorodiphenylamine was 68-76%. The reaction mixture was boiled for 40-44 hours.

EXPERIMENTAL

3-Chloronitrobenzene was prepared by the method of Hartman and Brethen [7]. 138 g (1.0 mole) of 3-nitroaniline yielded 112 g (71%) of 3-chloronitrobenzene of m.p. 43.5-45°; this was used without further purification for the preparation of 3-chloroaniline.

3-Chloroaniline. 142 g of iron filings, 15 ml of strong hydrochloric acid, and 213 ml of water was put into a three-necked round-bottomed flask, 1 liter in capacity, fitted with a mercury seal, a reflux condenser, and a powerful stirrer. The mixture was heated to boiling and 112 g (0.71 mole) of 3-chloronitrobenzene was introduced by portions during 1.5 hours with vigorous stirring through a side neck of the flask into the boiling mixture. The mixture was boiled and stirred for three hours after the addition. The reaction products were then distilled in steam. The colorless oily layer which separated from the distillate was removed and distilled under vacuum. The yield was 70 g (77.3%) of 3-chloroaniline, which distilled at 101-103° at 8-10 mm (literature data, 102° at 10 mm [10]).

3-Chloroacetanilide. 65 ml (0.64 mole) of acetic anhydride was added during ten minutes with stirring to 70 g (0.55 mole) of 3-chloroaniline. The hot solution was stirred for 30 minutes. The reaction mass was then diluted with 75 ml of water, cooled, and seeded with 3-chloroacetanilide. The solution rapidly crystallized to a dense mass. This was filtered on the following day. The residue was washed several times with ice-cold water and dried. The yield was 90 g (96.5%) of 3-chloroacetanilide melting at 71.5-73° (literature data, 72.5° [11]).

3-Chlorodiphenylamine. a) 85 g (0.5 mole) of 3-chloroacetanilide, 157 g (1.0 mole) of bromobenzene, 38.5 g (0.28 mole) of anhydrous potassium carbonate, 0.75 g of potassium iodide, 0.05 g of copper bronze, and 325 g of nitrobenzene was put into a one-liter round-bottomed flask fitted with a reflux condenser provided with a tube containing calcium chloride. The flask was kept at about 180° for ten hours. Then the temperature was raised to 210° during eight hours. The reaction mass was cooled and the nitrobenzene and excess bromobenzene were distilled off in steam. The oily residue in the distillation flask was separated from the water, mixed with 300 ml of alcohol and 180 ml of strong hydrochloric acid, and boiled under reflux for three hours. The reaction products were diluted with water. The oil which separated out was removed and distilled under vacuum. The yield was 47.5 g (46.5%) of 3-chlorodiphenylamine, which distilled at 175-180° at 7-8 mm (literature data, b.p. 335-336° at 724 mm [3], 340° at 766 mm [5]).

The acid aqueous solution remaining after separation of 3-chlorodiphenylamine was made alkaline, the oil was separated off and distilled under vacuum. This gave 25.2 g of 3-chloroaniline of b. p. 100-102° at 9 mm. b) 90.0 g (0.53 mole) of 3-chloroacetanilide, 164.1 g (1.06 mole) of bromobenzene, 41.3 g (0.3 mole) of anhydrous potassium carbonate, 0.85 g of potassium iodide, 0.05 g of copper bronze, and 5 ml of nitrobenzene was put into a round-bottomed flask and boiled for 44 hours on an oil bath under reflux. The mixture was then cooled, the solid residue was filtered off and washed with a small quantity of dichloroethane. The solvent and excess bromobenzene were distilled from the filtrate under vacuum. The oily substance remaining in the distillation flask was boiled for four hours with 420 ml of ethyl alcohol and 200 ml of strong hydrochloric acid. The reaction mass was diluted with water, and the oil was separated off and distilled under vacuum. The yield was 80.5 g (74.5%) of 3-chlorodiphenylamine which distilled at 180-185° at 10 mm. A second distillation yielded 71.4 g (66.5%) of 3-chlorodiphenylamine of b.p. 180-182° at 10 mm. The substance boiled at 322° at 743 mm.

Found %: N 6.94, 7.19. $C_{12}H_{10}NCl$. Calculated %: N 6.88.

LITERATURE CITED

[1] S.V. Zhuravlev and A.N. Gritsenko, J. Gen. Chem. 26, 3385 (1956).*

*Original Russian pagination. See C.B. translation.

[2] S.V. Zhuravlev, A.N. Gritsenko and M.I. Dorokhova, J. Gen. Chem. 27, 1668 (1957).*

[3] F. Ullmann, Ann. 355, 330 (1907).

[4] H. Wieland and W. Rheinheimer, Ann. 423, 28 (1921).

[5] H. Burton and Ch.S. Gibson, J. Chem. Soc. 2245 (1926).

[6] G.R. Sabatiny, J.J. Gulesich and R.F. Doerge, J. Am. Pharm. Assoc. 17, 454 (1956).

[7] Syntheses of Organic Preparations (IL, 1949) I, 485.**

[8] H.E. Fierz-David, Production of Organic Dyes [Russian translation] (Goskhimizdat, 1933), p. 70.

[9] J. Goldberg, Ber. 40, 4545 (1907).

[10] D.R. Stull, Vapor Pressures of Individual Substances [Russian translation] (IL, Moscow, 1949).

[11] Chemists Reference Book, II (Goskhimizdat, 1951).**

Received November 30, 1956

*Original Russian pagination. See C.B. translation.
**In Russian.

USE OF ETHYLENEDIAMINE FOR THE SYNTHESIS OF UNSATURATED NITRO COMPOUNDS OF THE AROMATIC SERIES

O. M. Lerner

Among the different methods for the preparation of β-nitrostyrenes, the condensation of aromatic aldehydes with primary nitro alkanes has acquired the greatest importance [1, 2].

The condensing agents used in the condensation with nitromethane are aqueous or alcoholic solutions of alkalies and sodium methylate. The aldol-condensation products initially formed readily lose water under the action of strong mineral acids and are converted into unsaturated nitro compounds.

Knovenagel and Walter [3] were the first to show that primary aliphatic amines – methylamine, ethylamine, and n-amylamine – catalyze reactions of the crotonaldehyde-condensation type, which lead directly to the synthesis of the compounds in question.

This discovery not only simplified the synthesis, but made it possible to introduce other primary nitro paraffins (nitroethane, n-nitropropane, phenylnitromethane, etc.) into the reaction.

The range of aliphatic amines used in this reaction has in fact been extended only by the use of n-butylamine [4].

In a study of the condensation of aromatic aldehydes with nitromethane and nitroethane we found that a new effective catalyst for the Knovenagel reaction is ethylenediamine; in many cases unsaturated nitro compounds could be obtained in high yields with its use.

The condensation products could not be separated completely owing to the easy solubility in the reaction mixture of most of the β-nitrostyrenes formed from aromatic aldehydes and nitroethane. It was found that the most convenient method of separation and purification of compounds (VI, VII, IX) is vacuum distillation – a method commonly used in the synthesis of aliphatic nitro olefins, but not used extensively for the aromatic series. It proved possible to recover some of the unreacted aldehyde by this method. To avoid additional drying before the distillation, calcined sodium sulfate was added to the reaction mixture before the condensation. The presence of a water-abstracting agent in the condensation process undoubtedly helped to shift the reaction equilibrium in the direction of β-nitrostyrene formation.

The appended table contains our results obtained with the use of ethylenediamine, which are compared with the best yields as reported in the literature, for evaluation of the new catalyst.

EXPERIMENTAL

Preparation of 4-methoxy-β-nitrostyrene (I). A solution of 5 g (0.0368 mole) of anisaldehyde, 2.9 g (0.0368 mole) of nitromethane, 5 ml of ethanol, and 2 drops of ethylenediamine was left to stand in a closed vessel in darkness at 8-10°. After ten days the nitro olefin was filtered off and washed with small portions of alcohol. The yield of (I) was 6.4 g, or 97.3% of the theoretical, m.p. 86°.

Preparation of 4-dimethylamino-β-nitrostyrene (II). A mixture of 5 g (0.0336 mole) of 4-dimethylaminobenzaldehyde, 2.05 g (0.336 mole) of nitromethane, 10 ml of ethanol, and 2 drops of ethylenediamine was left in darkness at 14-15°. The ruby-red crystals of the nitro olefin (II) formed after four days were filtered off and washed with alcohol. The yield of (II) was 6.2 g, or 96.7% of the theoretical, m.p. 184° (from acetone).

Yield of β-Nitrostyrenes

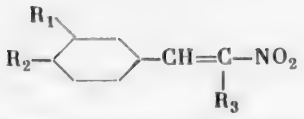

Serial No.	R_1	R_2	R_3	Yield with ethylenediamine (%)	Literature data: yield (%)	catalyst	lit. reference
I	H	OCH_3	H	97	86	Methylamine	[3]
II	H	$N(CH_3)_2$	H	96	87	n-Butylamine	[5]
III	OCH_3	OH	H	92	95	Methylamine	[6]
IV	H	CH_3	H	95	60	n-Amylamine	[7]
V	O—CH_2—O		H	93	93	Methylamine	[3]
VI	H	H	CH_3	76	86	n-Butylamine	[4]
VII	H	OCH_3	CH_3	100	80	n-Amylamine	[3]
VIII	H	$N(CH_3)_2$	CH_3	51	—	n-Butylamine	[8]
IX	H	CH_3	CH_3	86	50	n-Amylamine	[7]

Preparation of 4-hydroxy-3-methoxy-β-nitrostyrene (III). A mixture of 5 g (0.0329 mole) of vanillin, 2 g (0.0329 mole) of nitromethane, 5 ml of ethanol, and 2 drops of ethylenediamine was kept for a week in darkness at 15-20°. The yellow crystals of nitro olefin (III) were washed with small portions of alcohol. The yield of (III) was 5.9 g, or 92% of the theoretical, m.p. 164°.

Preparation of 4-methyl-β-nitrostyrene (IV). A solution of 5 g (0.0417 mole) of p-toluic aldehyde, 2.55 g (0.0417 mole) of nitromethane, 5 ml of ethanol, and 2 drops of ethylenediamine was kept in darkness at 8-10°. After ten days the slightly yellowish needles of nitro olefin (IV) were filtered off and washed with a small quantity of alcohol. The yield of (IV) was 6.5 g, or 95.7% of the theoretical, m.p. 101°.

Preparation of 3,4-methylenedioxy -β-nitrostyrene (V). A mixture of 5 g (0.0384 mole) of piperonal, 3.05 g (0.05 mole) of nitromethane, 10 ml of ethanol, and 3 drops of ethylenediamine was kept in darkness at 8-10°. The condensation was complete after one week. The precipitate of nitro olefin (V) was filtered off and washed with alcohol. The yield of (V) was 6.0 g, or 93% of the theoretical, m.p. 158°.

Preparation of β-methyl-β-nitrostyrene (VI). A mixture of 13.9 g (0.131 mole) of benzaldehyde, 11.3 g (0.15 mole) of nitroethene, 1 ml of ethanol, 10 g of calcined sodium sulfate, and 5 drops of ethylenediamine was heated for 18-20 hours in a sealed tube in a thermostat with periodic shaking. The red solution was distilled under vacuum (produced by a water-jet pump). The 1st fraction, 5 g, was unchanged benzaldehyde, b.p. 60-62° at 10 mm; the 2nd fraction, 11 g, was nitro olefin (VI) b.p. 137-139° at 10 mm, yield 75.8% of the theoretical, on the amount converted. A second distillation gave the pure substance of b.p. 135-136.5° at 9 mm, m.p. 63-64°.

Preparation of 4-methoxy-β-methyl-β-nitrostyrene (VII). A mixture of 15.5 g (0.114 mole) of anisaldehyde, 11 g (0.147 mole) of nitroethane, 1 ml of ethanol, 7 g of calcined sodium sulfate, and 5 drops of ethylenediamine was heated in a sealed tube for seven hours at 80°. The product was distilled under vacuum. The first fraction, 9.07 g, was unchanged anisaldehyde, b.p. 120° at 7 mm; the second fraction, 9.05 g, was nitro olefin (VII) b.p. 167-173° at 7 mm, quantitative yield on the amount reacted. A second distillation gave the pure substance with b.p. 176.2-178.8° at 9 mm, m.p. 43-44°.

Preparation of 4-dimethylamino-β-methyl-β-nitrostyrene (VIII). A mixture of 5 g (0.0336 mole) of 4-dimethylaminobenzaldehyde, 3 g (0.04 mole) of nitroethane, 10 ml of alcohol, and 3 drops of ethylenediamine was heated for 24 hours in a thermostat at 50°. The pale yellow precipitate of nitro olefin (VIII) was filtered off and washed with small portions of alcohol; the yield was 2.45 g, m.p. 123.5-124° (from ethanol). Evaporation of the mother liquor yielded a further 1.05 g of impure (VIII). The total yield was 3.5 g, or 51% of the theoretical.

Preparation of 4,β-dimethyl-β-nitrostyrene (IX). A mixture of 15 g (0.125 mole) of p-toluic aldehyde, 10 g (0.133 mole) of nitroethane, 1 ml of ethanol, 10 g of calcined sodium sulfate, and 5 drops of ethylenedi-

amine was heated for 20 hours in a sealed tube in a thermostat at 80°, and the reaction mass was then distilled under vacuum. The first fraction, 7 g, was unchanged p-toluic aldehyde; the second fraction, 10.25 g, was nitro olefin(IX) b.p. 137-143° at 7 mm, yield 86.6% of the theoretical on the amount reacted. A second distillation gave the pure substance with b.p. 150-150.7° at 8 mm, m.p. 52-53°.

LITERATURE CITED

[1] W. Emerson, Chem. Rev. 45, 183 (1949).

[2] W. Emerson, Chem. Rev. 45, 347 (1949).

[3] E. Knovenagel and L. Walter, Ber. 37, 4502 (1904).

[4] H. Hass et al., J. Org. Chem. 15, 8 (1950).

[5] F. Benington et al., J. Org. Chem. 21, 1470 (1956).

[6] K. Cairaud and C. Lappin, J. Org. Chem. 18, 1 (1953).

[7] D. Worrall, J. Am. Chem.Soc. 60, 2841 (1938).

[8] D. Worrall and L. Cohen, J. Am. Chem. Soc. 66, 842 (1944); Chem. Abs. 38, 3625 (1944).

Received July 24, 1957

IMPROVEMENT OF THE METHOD FOR THE PRODUCTION OF OCTESTROL ("OCTOFOLLIN")

G.I. Kiprianov and L.M. Kutsenko

The Ukrainian Institute of Experimental Endocrinology, Khar'kov

The first report of the high estrogenic activity and low toxicity of 2,4-di(p-hydroxyphenyl)-3-ethylhexane appeared in 1943 [1]. The valuable medicinal properties of this compound were revealed as the result of a systematic study of the alkyl derivatives of 1,3-di(p-hydroxyphenyl)propane. The monoalkyl [2] and dialkyl derivatives [3] of this compound did not have high activity. The trialkyl derivatives of 1,3-di(p-hydroxyphenyl)propane proved more effective; the highest estrogenic activity among these was found in one of the four possible racemic forms of 2,4-di(p-hydroxyphenyl)-3-ethylhexane, which melted at 161-163° (minimum active dose for rats 0.8 γ) [4]. This compound is known abroad under the names of "octofollin" and "benzestrol," and in the USSR as "octestrol."

Only one method for the synthesis of octestrol has been described [4]. The starting material is 1,3-di(p-anisyl)-2-ethylpentanone-1 (III), which may be prepared from α-ethyl-p,p'-dimethoxychalcone (I), or from the acid chloride of α-ethyl-β-anisylvaleric acid (II) by the Friedel-Crafts reaction with anisole [5]. Only one of two racemic forms, formed in equimolar propertions, of the pentanone (III) (m.p. 80-82°) is used for the synthesis of octestrol. This form reacts with methylmagnesium iodide to give the carbinol (IV). Dehydration of the latter, followed by hydrogenation of the hexene (V) formed over Raney nickel, gives 2,4-di(p-anisyl)-3-ethylhexane as a mixture of two racemic forms. One of these forms (m.p. 56°), which is obtained in yields of up to 80% by hydrogenation, yields octestrol (VII) on saponification of the methoxyl groups.

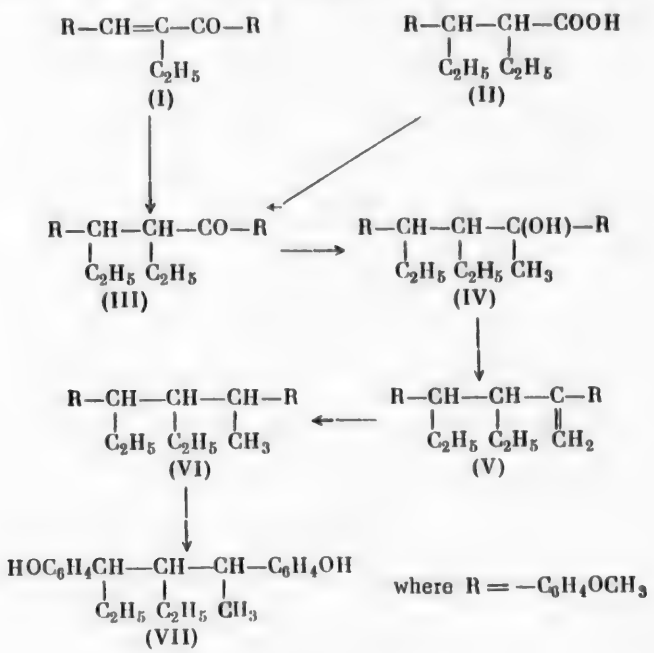

Exact data on the yields of the crystalline racemic form of (III) and of pure octestrol are not given in the papers cited [3, 4]. It is not stated whether the other (liquid) racemic form of (III) can be used.

In a test of the method for the synthesis of octestrol from α-ethyl-p,p'-dimethoxychalcone we found that the crystalline isomer of (III) can be obtained in a yield of only 37.5% of the theoretical. However, the liquid isomer remaining in the mother liquor is readily isomerized into the crystalline form when heated with alcoholic alkali, so that the yield of the required crystalline form can be raised to 73%, i.e., nearly doubled. The remaining stages of the synthesis gave high yields, in agreement with the results reported by the foreign authors. If the liquid form of (III) is used, the yield of octestrol reaches 41% calculated on the original α-ethyl-p,p'-dimethoxychalcone.

Clinical tests of the synthesized octestrol confirmed that it is nontoxic and has high estrogenic activity [6].

EXPERIMENTAL

α-Ethyl-p,p'-dimethoxychalcone (I) was prepared by condensation of anisaldehyde and p-methoxybutyrophenone in presence of dry hydrogen chloride, by the method of Bogert and Davidson [7]. Yield 85%, b.p. 230-235° at 4 mm.

1,3-Dianisyl-2-ethylpentanone-1 (III). A solution of ethylmagnesium bromide was prepared from 77 g of magnesium and 383 g (3.5 moles) ethyl bromide in 1800 ml of dry ether, and cooled to −10°; to this a solution of 317 g (0.68 mole) of α-ethyl-p,p'-dimethoxychalcone in 800 ml of ether was added with vigorous stirring, and the mixture was left at room temperature. On the next day the mixture was poured onto finely chopped ice, 400 ml of hydrochloric acid was added, the ether layer was separated off, and the aqueous layer was extracted with ether. The combined ether solutions were washed with 5% sodium carbonate solution and water, dried over calcium chloride, and the solvent was evaporated off. The residue (about 300 g) was recrystallized from 250 ml of alcohol. The yield of the crystalline form of 1,3-dianisyl-2-ethylpentanone-1 was 131 g or 37.5%, m.p. 80-82°.

Alcohol was distilled off from the mother liquor, and alcoholic caustic potash (36 g in 360 ml) was added to the residue; the solution was boiled for three hours under reflux. It was then diluted with 300 ml of water, the alcohol was distilled off under slightly reduced pressure, the oily isomerization product was extracted with ether, and the ether solution was washed with water and dried over $CaCl_2$. The ether was evaporated off, the residue was dissolved in alcohol (100 ml), and crystallized to yield a further 89 g (25.5%) of crystalline (III).

Two further treatments of the mother liquors with alcoholic potash gave an additional 34 g of the crystalline product. The total yield of the crystalline form of 1,3-dianisyl-2-ethylpentanone-1 (m.p. 80-82°) was 254 g, or 73%.

2,4-Di(p-anisyl)-3-ethylhexene-1 (V). An ether solution of 150 g of crystalline 1,3-dianisyl-3-ethylpentanone-1 (m.p. 80-82°) was added to a Grignard reagent prepared from 22.5 g of magnesium and 150 g of CH_3I in 750 ml of ether. After decomposition of the Grignard complex and evaporation of the solvent, the 2,4-dianisyl-3-ethylhexanol-1 (IV) (about 140 g) was dehydrated without further purification. Two to three drops of strong hydrochloric acid was added to the carbinol, and the liquid was heated under vacuum (40-60 mm) at 140-150° until liberation of water ceased. The dehydration product was diluted with 400 ml of alcohol and allowed to crystallize, yielding 128 g (86% of the theoretical) of crystalline 2,4-di(p-anisyl)-3-ethylhexene-1, m.p. 42-44° (the reported yield [4] was 80%, m.p. 44°).

2,4-Di(p-anisyl)-3-ethylhexane (VI). A solution of 93.5 g of 2,4-di(p-anisyl)-3-ethylhexene-1 in 850 ml of alcohol was hydrogenated in an autoclave at room temperature at an initial hydrogen pressure of 100 atmospheres over Raney nickel catalyst prepared as described [8] from 80 g of Raney alloy. The course of the hydrogenation was indicated by the decrease of hydrogen pressure; the process was completed in two hours. The catalyst was filtered off and washed with ether. Evaporation of the filtrate yielded 75 g (80%) of 2,4-di(p-anisyl)-3-ethylhexane, m.p. 56°.

2,4-Di(p-hydroxyphenyl)-3-ethylhexane (VII), (octestrol). 73.5 g of 2,4-di(p-anisyl)-3-ethylhexane, 198 g of caustic soda, and 800 ml of alcohol was heated in an autoclave at 200° for 18 hours. The alkaline solution was diluted with water and the alcohol was distilled off. Hydrochloric acid was added to the residue until acid to Congo Red, and the liberated phenol was filtered off, dried, and crystallized from dichloroethane (400 ml) with addition of activated charcoal. The yield was 55 g (82%) of 2,4-di(p-hydroxyphenyl)-3-ethylhexane, m.p. 160-162° (reported m.p. [4], 162°).

SUMMARY

It was found that the liquid racemic form of 1,3-di(p-anisyl)-2-ethylpentanone can be easily isomerized to the crystalline form required for synthesis of octestrol, whereby the yield of octestrol can be almost doubled.

LITERATURE CITED

[1] E.W. Blanchard, A.H. Stuart and R.C. Tallman, Endocrinology 32, 307 (1943).

[2] A.H. Stuart and R.C. Tallman, J. Am. Chem. Soc. 65, 1579 (1943).

[3] A.H. Stuart, A.I. Shukis and R.C. Tallman, J. Am. Chem. Soc. 67, 1475 (1945).

[4] A.H. Stuart, A.I. Shukis, R.C. Tallman, G. McCanvol and G.R. Treves, J. Am. Chem. Soc. 68, 729 (1946).

[5] A.I. Shukis and I. Ritter, J. Am. Chem. Soc. 72, 1488 (1950).

[6] L.I. Lobanovskaia, Obstetrics and Gynecology 1 (1950).*

[7] M.T. Bogert and D. Davidson, J. Am. Chem. Soc. 54, 334 (1932).

[8] Organic Syntheses, 3 [Russian translation] (IL, Moscow, 1952), p. 338.

Received May 3, 1957

*In Russian.

A NEW METHOD FOR THE SYNTHESIS OF NITRO KETONES

V.V. Perekalin and K. Baier

Nitro ketones are used with success as starting materials for the synthesis of various pharmaceuticals: spasmolytics [1], analogs of quinacrine [2], adrenalin [3], and chloromycetin [4, 5]. α-Nitro ketones have become available owing to the success achieved in the oxidation of α-nitro alcohols [4, 6], while nitro ketones of the γ series are readily obtained by condensation of nitro alkanes with vinyl ketones [7].

We have discovered a relatively simple general method for the synthesis of α,γ-dinitro ketones, by interaction of unsaturated nitro compounds with α-nitro ketones in organic solvents in presence of basic catalysts (triethylamine).

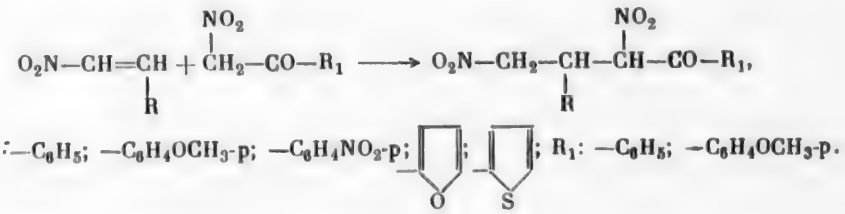

where R: —C_6H_5; —$C_6H_4OCH_3$-p; —$C_6H_4NO_2$-p; ; ; R_1: —C_6H_5; —$C_6H_4OCH_3$-p.

Examples of Syntheses

2,4-Dinitro-1,3-diphenylbutanone-1 (I). One drop of triethylamine was added to a boiling solution of 0.33 g (0.002 mole) of α-nitroacetophenone and 0.298 g (0.002 mole) of β-nitrostyrene in 8 ml of benzene, and the mixture was boiled for five minutes. The solvent was evaporated off and the residue was washed with methanol, to isolate the white condensation product (I); m.p. 106-112° (from n-hexane-benzene mixture), yield 0.44 g, or 75% of the theoretical.

Found %: N 9.02, 9.00. $C_{16}H_{14}O_5N_2$. Calculated %: N 8.91.

2,4-Dinitro-1-phenyl-3-(4'-nitrophenyl)-butanone-1 (II). 0.33 g (0.002 mole) of α-nitroacetophenone and 0.390 g (0.002 mole) of p-,β-dinitrostyrene in 8 ml of benzene, condensed by the method described in Example 1, gave the condensation product (II) with a yield of 0.72 g, or 80.5% of the theoretical; m.p. (decomposition) 155-156° (from 80% acetic acid).

Found %: C 53.63, 53.54; H 4.22, 4.04; N 11.90, 11.90. $C_{16}H_{13}O_7N_3$. Calculated %: C 53.48; H 3.65; N 11.70.

2,4-Dinitro-1-phenyl-3-(2-furyl)-butanone-1 (III). A mixture of 0.495 g (0.003 mole) of α-nitroacetophenone, 0.417 g (0.003 mole) of 2-furyl-nitroethylene, and one drop of triethylamine, in 8 ml of benzene, was kept for seven hours at room temperature and then boiled for two minutes. Evaporation of the solvent and washing of the residue with methanol yielded 0.49 g, or 54% of the theoretical yield, of the condensation product (III); m.p. 71-75° (from n-hexane-benzene mixture).

Found %: N 9.32, 9.45. $C_{14}H_{12}O_6N_2$. Calculated %: N 9.21.

2,4-Dinitro-1-phenyl-3-(2-thienyl)-butanone-1 (IV). A mixture of 0.33 g (0.002 mole) of α-nitroacetophenone, 0.31 g (0.002 mole) of 2-thienylnitroethylene, and one drop of triethylamine in 5 ml of methanol was boiled for five minutes.

The yield of the condensation product (IV) was 0.40 g, or 62.5% of the theoretical; m.p. 113-115° (from ethanol).

Found %: C 52.54, 52.49; H 4.36, 4.71; N 8.78, 8.91. $C_{14}H_{12}O_5N_2S$. Calculated %: C 52.16; H 4.38; N 8.70; S 9.95.

2,4-Dinitro-1-(4'-methoxyphenyl)-3-phenylbutanone-1 (V). A mixture of 0.298 g (0.002 mole) of β-nitrostyrene, 0.390 g (0.002 mole) of ω-nitroacetanisone, and one drop of triethylamine was boiled in 5 ml of methanol until the precipitate was completely dissolved. After the solvent was evaporated off a yellow oil separated out, which solidified on standing and crystallized when rubbed with a little methanol to the white crystalline condensation product (V); m.p. 113-116° (from n-hexane-benzene mixture). Yield 0.41 g, or 60% of the theoretical.

Found %: N 8.05, 8.14. $C_{17}H_{16}O_6N_2$. Calculated %: N 7.91.

LITERATURE CITED

[1] O. Eisleb, Ber. 74, 1433 (1941).

[2] D.S. Breslow, H.C. Walker, R.S. Yost and C.R. Hauser, J. Am. Chem. Soc. 67, 1472 (1945).

[3] B. Reichert and W. Koch, Ber. 68, 445 (1935).

[4] L.M. Long and H.D. Troutman, J. Am. Chem. Soc. 71, 2470 (1949).

[5] O. Dann, H. Ulrich and E.F. Möller, Z. Naturforsch. 7b, 344 (1952).

[6] L. Canonica, Gazz. chim. Ital. 79, 192 (1949); L. Canonica and C. Cardani, Gazz. chim. Ital. 79, 262 (1949).

[7] E.P. Kohler, J. Am. Chem. Soc. 38, 889 (1916).

Received July 12, 1957

SIGNIFICANCE OF ABBREVIATIONS MOST FREQUENTLY ENCOUNTERED IN SOVIET PERIODICALS

FIAN	Phys. Inst. Acad. Sci. USSR.
GDI	Water Power Inst.
GITI	State Sci.-Tech. Press
GITTL	State Tech. and Theor. Lit. Press
GONTI	State United Sci.-Tech. Press
Gosenergoizdat	State Power Press
Goskhimizdat	State Chem. Press
GOST	All-Union State Standard
GTTI	State Tech. and Theor. Lit. Press
IL	Foreign Lit. Press
ISN (Izd. Sov. Nauk)	Soviet Science Press
Izd. AN SSSR	Acad. Sci. USSR Press
Izd. MGU	Moscow State Univ. Press
LEIIZhT	Leningrad Power Inst. of Railroad Engineering
LET	Leningrad Elec. Engr. School
LETI	Leningrad Electrotechnical Inst.
LETIIZhT	Leningrad Electrical Engineering Research Inst. of Railroad Engr.
Mashgiz	State Sci.-Tech. Press for Machine Construction Lit.
MEP	Ministry of Electrical Industry
MES	Ministry of Electrical Power Plants
MESEP	Ministry of Electrical Power Plants and the Electrical Industry
MGU	Moscow State Univ.
MKhTI	Moscow Inst. Chem. Tech.
MOPI	Moscow Regional Pedagogical Inst.
MSP	Ministry of Industrial Construction
NII ZVUKSZAPIOI	Scientific Research Inst. of Sound Recording
NIKFI	Sci. Inst. of Modern Motion Picture Photography
ONTI	United Sci.-Tech. Press
OTI	Division of Technical Information
OTN	Div. Tech. Sci.
Stroiizdat	Construction Press
TOE	Association of Power Engineers
TsKTI	Central Research Inst. for Boilers and Turbines
TsNIEL	Central Scientific Research Elec. Engr. Lab.
TsNIEL-MES	Central Scientific Research Elec. Engr. Lab.–Ministry of Electric Power Plants
TsVTI	Central Office of Economic Information
UF	Ural Branch
VIESKh	All-Union Inst. of Rural Elec. Power Stations
VNIIM	All-Union Scientific Research Inst. of Meteorology
VNIIZhDT	All-Union Scientific Research Inst. of Railroad Engineering
VTI	All-Union Thermotech. Inst.
VZEI	All-Union Power Correspondence Inst.

Note: Abbreviations not on this list and not explained in the translation have been transliterated, no further information about their significance being available to us. – Publisher.